

Mechanism of **ABCE1** in Ribosome Recycling

PhD Thesis by **Milan Gerovac**
supervised by **Prof. Dr. Robert Tampé**

Goethe University Frankfurt, Institute of Biochemistry, Biocenter
Max-von-Laue-Str. 9, 60438 Frankfurt am Main, Germany

■ Institute of Biochemistry
BIOCENTER OF THE GOETHE UNIVERSITY



Mechanism of ABCE1 in Ribosome Recycling

Dissertation
zur Erlangung des Doktorgrades
der Naturwissenschaften



vorgelegt beim Fachbereich
Biochemie, Chemie und Pharmazie
der Johann Wolfgang Goethe - Universität
in Frankfurt am Main

von

Milan Gerovac

aus Osijek

Frankfurt am Main, 2018
(D30)

vom Fachbereich Biochemie, Chemie und Pharmazie der
Johann Wolfgang Goethe - Universität als Dissertation angenommen.

Dekan:

Prof. Dr. Clemens Glaubitz

1. Gutachter:

Prof. Dr. Robert Tampé

2. Gutachterin:

Jun. Prof. Dr. Michaela Müller-McNicoll

Datum der Disputation:

Menschen erschaffen zu gerne Neues
durch Verdrängen dessen was gerade ist.

Dabei übersehen sie, dass wahrhaftig
zeitlose Leistungen auf Bestand
und Zusammenarbeit gründen.



A. Abbreviations

A	absorption at indicated wavelength in the index	EF	elongation factor
Ab / α	antibody	el. / E	eluate
ABCE1 / Rli1	ATP-binding cassette protein family E1	eRF	eukaryotic release factor
AIEX	anion exchange chromatography	EtBr	ethidium bromide
ALEX	alternating-laser excitation	F _E	FRET efficiency
AMP-PNP	5'-adenylyl-imidodiphosphate	FeS	iron-sulfur
APS	ammonium persulfate	FT	flow through
ATP	adenosine-5'-triphosphate	FRET	Förster resonance energy transfer
AU	absorption unit	FSC	Fourier shell correlation
2-ME	2-mercaptoethanol	g	gravitation: 9.7 m/s ²
bp	base pair	GFP	green fluorescent protein
CIEX	cation exchange chromatography	GTP	guanosine-5'-triphosphate
CL	cantilever	Hbs1 / aEF1 α	paralogs of eRF3
cv	column volume	HEPES	4-(2-Hydroxyethyl)piperazine-1-ethanesulfonic acid
cysless / cl	cysteine-less	HLH	helix-loop-helix
Δ	deleted or lacking	HPLC	high performance liquid chromatography
Da	dalton	IB	immunoblot
DEPC	diethyl pyrocarbonate	eIF	eukaryotic initiation factors
DNA	deoxyribonucleic acid	IMAC	immobilized metal ion affinity chromatography
Dom34 / Pelota	paralog of eRF1	IPTG	isopropyl- β -D-thiogalacto-pyranoside
NTP	nucleoside triphosphate	LB	lysogeny broth
DTT	dithiothreitol	M	molar (mol/l)
ϵ	extinction coefficient	MS	mass spectrometry
EDTA	ethylenediaminetetraacetic acid		

NBD	nucleotide-binding domain	S	supernatant in protein purification
NBS	nucleotide-binding site	SDG	sucrose density gradient
NHS	<i>N</i> -hydroxysuccinimide	SDS	sodium dodecyl sulfate
NMD	nonsense-mediated decay	SEC	size exclusion chromatography
NGD	<i>no-go</i> decay	SLIC	sequence- and ligation-independent cloning
NSD	non-stop decay	sm	single-molecule
NTA	<i>N</i> -nitriilotriacetic acid	<i>S.c.</i> / <i>Sc</i>	<i>Saccharomyces cerevisiae</i>
nt	nucleotides	sCy3/-5	sulfo-Cyanin-3/-5
OD	optical density at indicated wavelength in the index	<i>S.s.</i> / <i>Ss</i>	<i>Sulfolobus solfataricus</i>
ORF	open reading frame	TCA	trichloroacetic acid
uORF	upstream ORF	TEMED	<i>N,N,N',N'</i> -tetramethyl- ethylenediamine
P	pellet	Tris	<i>tris</i> -(hydroxymethyl)- aminomethane
PAGE	polyacrylamide gel electrophoresis	TEV	Tobacco Etch Virus
PEG	polyethylene glycol	UV	ultraviolet
pH	<i>potentia hydrogenii</i>	v_e	elution volume
P _i	inorganic phosphate	v_t	total volume
pI	isoelectric point	v_0	void volume
PTC	peptidyl transfer center	(v/v)	volume per volume
Rli1	RNAse L inhibitor 1 (ABCE1)	(w/v)	weight per volume
RNA	ribonucleic acid	w/o	without
RNC	ribosome nascent chain complex	<i>wt</i>	wild-type
rt	room temperature		
S	Svedberg – sedimentation velocity		

B. Content

A	Abbreviations	1
B	Content	3
C	Deutsche Zusammenfassung	9
D	Abstract	15
E	Publications and contributions	17
F	Declaration	19
1	Introduction	25
1.1	From diversified, meandering functions to ribosome recycling – a brief history	29
1.2	The role of the recycling factor in translation termination	31
1.3	Mechanistic basis and structural insights into ribosome splitting	33
1.4	How does ABCE1 power ribosome splitting?	34
1.5	Scope & objectives	35
2	Methods and materials	36
2.1	General bioinformatics	36
2.1.1	Protein parameters	36
2.1.2	Sequence alignment	36
2.1.3	Model and density superposition	36
2.1.4	Model visualization	36
2.2	General cloning techniques	37
2.2.1	TOPO® cloning	38
2.2.2	Cloning of translation stalling constructs for <i>S. cerevisiae</i>	38
2.2.3	Single site-directed mutagenesis	40

2.2.4	Transformation into <i>E. coli</i>	40
2.2.5	Transformation into <i>S. cerevisiae</i>	41
2.2.6	Colony PCR	42
2.3	General biochemical techniques	42
2.3.1	Protein, RNA, and nucleotide concentration determination by absorption	42
2.3.2	Nucleotide preparation	43
2.3.3	SDS-PAGE	44
2.3.4	pH-neutral SDS-PAGE	45
2.3.5	Urea-PAGE	45
2.3.6	Coomassie staining	45
2.3.7	Silver staining	46
2.3.8	Immunoblotting	46
2.4	Protein production and purification	47
2.4.1	ABCE1 _{H6} from <i>S. cerevisiae</i>	47
2.4.2	Dom34 _{H6} from <i>E. coli</i>	48
2.4.3	eIF6 _{H6} from <i>E. coli</i>	49
2.4.4	Crude 80S ribosomes	50
2.4.5	Ribosomal subunits	50
2.4.5.1	Genetic labeling of the small ribosomal subunit by <i>GFP</i>	51
2.4.6	assembly of <i>vacant</i> ribosomes	52
2.4.7	<i>In vivo</i> stalling of 80S ribosomes	52
2.4.8	S100 extract and aminoacylation of tRNA ^{Phe}	53
2.4.9	80S–mRNA–tRNA ^{Phe}	54
2.5	<i>In vivo</i> functional assays	55

2.5.1	Plasmid shuffling assay in yeast	55
2.5.2	Growth studies by serial dilution	56
2.5.3	Ribosome profile analysis by SDG	58
2.5.3.1	Gradient preparation, harvesting, and profile visualization	57
2.6	<i>In vitro</i> functional assays	58
2.6.1	Ribosome profile analysis	58
2.6.2	Radioactive NTPase assay	58
2.6.3	Colorimetric NTPase assay	59
2.6.4	Anti-association assay and preparation of the 40S–ABCE1 complex	59
2.6.5	Ribosome pelleting assay	60
2.6.6	Native PAGE and ribosome splitting assay	60
2.7	Cryo-EM reconstruction	62
2.7.1	Electron microscopy and image processing of the 40S–ABCE1 complex	62
2.7.2	Model building of the 40S–ABCE1 complex	63
2.7.3	Preparation of the 30S–ABCE1 complex	64
2.7.4	Electron microscopy and image processing of the 30S–ABCE1 complex	64
2.7.5	Model building of the 30S–ABCE1 complex	65
2.7.6	Preparation of the native 40S–ABCE1 complex	65
2.7.7	Electron microscopy, image processing, and model building of the native 40S–ABCE1 complex	66
2.7.8	Data availability	67
2.8	smFRET studies	67
2.8.1	ABCE1 labeling with sCy3/sCy5	67
2.8.2	Surface preparation for immobilization	68

2.8.3	smFRET-ALEX setup	69
2.8.4	ABCE1 immobilization and smFRET analysis	70
2.8.5	Particle picking and FRET efficiency trace extraction	71
2.9	Style points and conventions	72
2.10	Materials	73
3	Results	86
3.1	<i>In vivo</i> ribosome stalling	86
3.1.1	Limits of present <i>in vitro</i> ribosome stalling approaches	87
3.1.2	<i>In vivo</i> ribosome stalling – approach, constructs, and challenges	88
3.1.2.1	Programming construct	88
3.1.2.2	Proof of principle - 80S–GFP–tRNA (RNC _{GFP})	90
3.1.2.3	40S–GFP (R _{GFP}) labeling for the third generation splitting assay	92
3.1.2.4	Purification and validation of R _{GFP} NC _{GFP} constructs	93
3.2	<i>In vitro</i> programming of ribosomes	97
3.2.1	Aminoacylation of Phe–tRNA ^{Phe}	98
3.2.2	Preparation of ribosomal subunits	100
3.2.3	Assembly of 80S–mRNA–tRNA complexes	101
3.3	Production and purification of yeast translation factors	102
3.3.1	ABCE1 _{H6}	102
3.3.2	Dom34 _{H6}	105
3.3.3	eIF6 _{H6}	106
3.4	In gel splitting assay	108
3.5	Structure of the eukaryotic 40S–ABCE1 post-splitting complex	111
3.5.1	AMP–PNP dependent binding of ABCE1 to 40S	112

3.5.2	Anti-association activity of ABCE1	112
3.5.3	Preparation of the 40S–ABCE1 post-splitting complex	113
3.5.4	3D classification of particles	114
3.5.5	Structure of the 40S–ABCE1 post-splitting complex	119
3.5.6	Structure of an asymmetric ABC system in a fully closed conformation	120
3.5.7	Repositioning of the FeS cluster domain	122
3.5.8	The post-splitting state is essential for cellular homeostasis	124
3.5.9	NTPase activity of ABCE1 in the post-splitting complex	127
3.5.10	Post-splitting complex in Archaea	129
3.5.11	Catalytic mutants of ABCE1	131
3.6	ABCE1 in initiation complexes	133
3.7	Conformational dynamics of ABCE1 probed by smFRET	136
3.7.1	Engineering of a cysteine-less ABCE1 variant	137
3.7.2	Double-cysteine variants of ABCE1 for smFRET	139
3.7.3	Viability and purification of cysteine-less and double-cysteine ABCE1 variants	140
3.7.4	Labeling of ABCE1 and immobilization	141
3.7.5	Conformational dynamics	143
4	Discussion	153
4.1	How does ABCE1 split the ribosome?	153
4.2	What is the role of the recycling factor in translation (re-)initiation?	157
4.3	Conformational dynamics and elastic NBD dimerization	164
4.4	Impact on ribosome homeostasis and ribosomopathies	165
4.5	Ribosome remodeling by the fungal ABC-type elongation factor eEF3	166

4.6	Antibiotic resistance and translational control	168
4.7	Outlook	169
5	Acknowledgements	171
6	References	173
G	Erklärung und Versicherung – Declaration and author’s declaration	188
H	<i>Curriculum vitae</i>	189

C. Deutsche Zusammenfassung

Genetische Information wird von Desoxyribonukleinsäuren (DNS) in Boten-Ribonukleinsäuren (mRNS) kopiert (Transkription), welche wiederum am Ribosom in Proteine übersetzt wird (Translation). Das Ribosom setzt sich aus einer großen und kleinen Untereinheit zusammen, bestehend aus ribosomaler RNS (rRNS) und Proteinen. Im Zwischenraum der beiden Untereinheiten wird die mRNS gebunden und mittels aminoacylierter Transfer-RNS (tRNS) übersetzt. Die Aminosäuren im Protein werden durch Tripletts von Nukleobasen in der mRNS (Codons) und Anti-Codons auf der tRNS dekodiert. Im Peptidyl-Transfer-Zentrum der großen Untereinheit wird dabei das naszierende Peptid um jeweils eine weitere Aminosäure kovalent erweitert (Elongation) und bleibt während der gesamten Übersetzung an der tRNS gebunden. Am Ende der Translation wird das Protein von der tRNS abgelöst. Dazu wird das Stop-Codon durch proteinogene Entlassungsfaktoren (*release factor*, eRF1 und -3) erkannt und die Peptid-tRNS-Bindung hydrolysiert (Termination). Im Anschluss bindet das *ATP-binding cassette* (ABC) Protein E1 (ABCE1) an den Entlassungsfaktor im terminierten Ribosom (Prä-Spaltungskomplex) und katalysiert die Spaltung der ribosomalen Untereinheiten, die für eine weitere Translationsrunde zur Verfügung stehen. ABCE1 ist aus zwei Nukleotid-Bindedomänen (NBD1 und -2) aufgebaut, die komplementär zwei Nukleotid-Bindestellen (NBS I und II) formen. ABCE1 enthält eine N-terminale Eisen-Schwefel (FeS)-Cluster-Domäne. Durch Dimerisierung der beiden NBDs werden zwei Nukleosidtriphosphate eingeschlossen. Die dabei entstehende mechanische Energie aus der Dimerisierung wird an assoziierte Domänen übertragen, die mit dem Ribosom wechselwirken. Wenn die mRNS vor dem Stop-Codon geschnitten wird oder eine stabile Sekundärstruktur aufweist, führt dies zu einem mechanischen Anhalten der mRNS-Translation und es werden Kontrollprozesse des *no-go decay* eingeleitet zum Abbau von fehlerhafter mRNS, naszierendem Protein oder sogar assoziierter Faktoren. Der nicht-kanonische Entlassungsfaktor Pelota erkennt die angehaltenen ribosomalen Komplexe. ABCE1 kann analog zum Entlassungsfaktor auch an Pelota binden und spaltet das Ribosom. Die Peptid-tRNS wird bei den Kontrollprozessen nicht hydrolysiert, bleibt nach dem Spalten

des Ribosoms in der großen Untereinheit verankert, und dient als Erkennungsmarker für die Markierung des naszierenden Peptids mit Ubiquitin für den proteasomalen Abbau.

Für die Rekonstitution von *in vitro* Spaltungsexperimenten wurden in der Bäckerhefe spaltungskompetente Ribosomen als Substrat für ABCE1 *in vivo* programmiert angehalten und gereinigt. Durch Expression einer Reporter-mRNS mit selbst-prozessierenden 3'-Ribozym wurde die mRNS *in vivo* geschnitten und translatierende Ribosomen an dieser angehalten. Das Recycling der angehaltenen Ribosomen konnte durch das genetische Entfernen des Entlassungsfaktors Pelota (Dom34) verhindert und der angehaltene Zustand angereichert werden. N-terminal kodierte die mRNS für eine Polyhistidin-Markierung zur Affinitätsreinigung der angehaltenen ribosomalen Komplexe. Als Reporter für das kodierte Protein auf der mRNS wurde das grün fluoreszierende Protein (GFP) genutzt, welches zugleich als fluoreszierender Marker im naszierenden Protein diente. Das Spaltungsexperiment selbst war im Green Labor etabliert worden und gründet auf der Analyse von ribosomalen Untereinheiten durch native Gelelektrophorese. Hierbei beruhte die Detektion auf radioaktiv markiertem Peptid an der tRNS. Dieser Ansatz wurde genutzt für die Analyse der *in vivo* angehaltenen Ribosomen mittels Fluoreszenzdetektion *via* GFP-Reporter am naszierenden Protein und an der kleinen ribosomalen Untereinheit im nativen Polyacrylamid-Gel. Das *in vitro* rekonstituierte Spalten der angehaltenen Ribosomen erfordert neben dem Spaltungsfaktor ABCE1, den nicht-kanonischen Entlassungsfaktor Dom34 (in der Bäckerhefe) und den Antiassoziationsfaktor eIF6, der die Reassoziations der ribosomalen Untereinheiten nach dem Spalten verhindert. Das Spalten der *in vivo* angehaltenen Ribosomen wurde durch Zugabe von ABCE1/Dom34/eIF6 und Adenosintriphosphat (ATP) etabliert. Das naszierende Protein GFP verblieb dabei an der tRNS gebunden und in der großen ribosomalen Untereinheit verankert.

Die Funktion von eIF6 wurde in einem Anti-/Reassoziationsansatz überprüft, in welchem die ribosomalen Untereinheiten dissoziieren und wieder assoziieren abhängig von der Kalium- und Magnesium-Konzentration. Bindet jedoch der Antiassoziationsfaktor eIF6 an die große Untereinheit, wird das Reassoziieren verhindert und die resultierenden ribosomalen Untereinheiten können mittels Sukrose-Dichtegradientenzentrifugation getrennt werden.

Der Anti-/Reassoziationsansatz wurde benutzt zur Überprüfung der Interaktion von ABCE1 mit der kleinen ribosomalen Untereinheit. Die ATP abhängige Interaktion wurde durch Verwenden des nicht-hydrolysierbaren ATP-Analogons AMP-PNP stabilisiert. Mithilfe diesen Ansatzes konnte der Komplex zwischen ABCE1 und der kleinen ribosomalen Untereinheit *in vitro* rekonstituiert werden, der formal den Post-Spaltungskomplex darstellt.

Die Struktur des Post-Spaltungskomplexes aus der Bäckerhefe wurde mit Hilfe der Kryoelektronenmikroskopie (EM) in Zusammenarbeit mit der Beckmann Gruppe (Genzentrum, LMU, München) rekonstruiert. Die Präparationsmethode des Post-Spaltungskomplexes mittels Anti-/Reassoziaton der Ribosomen erlaubte eine starke Anreicherung von ABCE1 an der kleinen ribosomalen Untereinheit und ermöglichte das Erzielen einer Auflösung von 3,9 Å in der Rekonstruktion. Zum ersten Mal konnte die Position der FeS-Cluster-Domäne an der kleinen ribosomalen Untereinheit nach dem Spalten lokalisiert werden, welche in eine Tasche zwischen Helix 44 und uS12 bindet. Die Domäne muss zwischen dem Prä- und Post-Spaltungskomplex eine deutliche Drehung um ca. 150° vollziehen. Die NBDs von ABCE1 liegen als geschlossenes dimerisiertes ABC-System vor, das in den beiden NBS jeweils ein Nukleotid aufweist. Neben der veröffentlichten offenen Konformation des ABC-Systems im freien Zustand und der halb-geschlossenen Konformation im Prä-Spaltungskomplex ist die Konformation von ABCE1 im Post-spaltungskomplex voll-geschlossen mit zwei gebundenen Nukleotiden in den NBS. Insgesamt konnten zahlreiche Interaktionen identifiziert werden, die den Post-Spaltungskomplex stabilisieren. So wird der Arm zwischen der NBD1 und der FeS-Cluster-Domäne über Arginin 7 an der Helix 5 der rRNS fixiert. Prolin 30 der FeS-Cluster-Domäne bildet eine Interaktionsbrücke zu Isoleucin 52 von uS12 aus, Serin 150 stabilisiert die Helix-Loop-Helix-Domäne der NBD1 an der rRNS Helix 15. Arginin 573, sowie Serin 588 interagieren mit der rRNS Helix-Verbindung 8/14. Weiterhin konnte eine Brücke zwischen Glutamin 262 zum C-Terminus von eS24 identifiziert werden.

In Zusammenarbeit mit Peter Kötter (Institut für Molekulare Biowissenschaften, Goethe-Universität, Frankfurt/M.) wurde ein *Plasmid Shuffling Assay* entwickelt, der es erlaubt das essenzielle Wildtyp-Gen von *ABCE1* durch ein mutiertes *ABCE1**-Gen zu ersetzen. Die Überlebensfähigkeit des Stammes konnte so in Abhängigkeit des mutierten Gens bestimmt

werden. *In vivo* wurde mithilfe des *Shuffling Assays* bestätigt, dass die interagierenden Reste Arginin 7 und Tyrosin 301 bei einer Doppelmutation letal sind.

Die hier gewonnenen Erkenntnisse erlauben Rückschlüsse auf den Spaltungsmechanismus von ABCE1. So muss die FeS-Cluster-Domäne zwangsläufig auf ihrer Rotationstrajektorie mit dem Entlassungsfaktor kollidieren und diesen wie einen Keil zwischen die beiden ribosomalen Untereinheiten drücken, der dabei das Ribosom spaltet. In der finalen Position konnte eine mutmaßliche Kollision der FeS-Cluster-Domäne mit uL6 der großen ribosomalen Untereinheit identifiziert werden, die das Blockieren der Reassoziaton der beiden Untereinheiten in der Präparation und nach dem Spalten durch ABCE1 erklärt.

Weiterhin konnte in Zusammenarbeit mit der Beckmann Gruppe eine niedrig-aufgelöste Dichtekarte des Post-Spaltungskomplexes in Archaeen rekonstruiert werden. Diese zeigt die FeS-Cluster-Domäne in der gleichen Position wie in der Bäckerhefe. Zur Rekonstitution wurden katalytisch inhibierte Varianten von ABCE1 benutzt, die von Elina Nürnberg-Goloub (Institut für Biochemie, Goethe-Universität, Frankfurt/M.) charakterisiert wurden. Diese nehmen den geschlossenen Zustand ohne Zugabe von AMP-PNP ein und das Aufheizen auf 80-100 °C entfällt, was der physiologischen Temperatur des Organismus *S. solfataricus* entspricht. In *Plasmid Shuffling* Studien in *S. cerevisiae* konnte gezeigt werden, dass Mutationen katalytischer Reste der NBS II größtenteils letal sind, wohingegen Mutationen in der NBS I toleriert werden. Dies spricht für einen regulatorischen Prozess in ABCE1, in dem die NBS II eine Kontrollfunktion und die NBS I die Spaltungsfunktion übernimmt. Dies steht auch in Übereinstimmung mit der Struktur des Post-Spaltungskomplexes, in der die Position der FeS-Cluster-Domäne über die NBS I stabilisiert wird.

Die Spaltung des Ribosoms durch ABCE1 ist in der Literatur als ATP-Hydrolyse abhängig beschrieben. Nicht-hydrolysiertes AMP-PNP konnte jedoch im Post-Spaltungskomplex identifiziert werden, der die Momentaufnahme der Spaltung selbst darstellt. Diese Diskrepanz kann in Übereinstimmung gebracht werden, wenn angenommen wird, dass ABCE1 mehrmals schließt bis eine Spaltung des Ribosoms stattfindet. Diese Annahme deckt sich auch mit den Beobachtungen der Stimulation der ATPase beim Spalten. Folglich muss es in ABCE1 einen regulatorischen Mechanismus geben, der möglicherweise durch das

Ribosom geschaltet wird und dabei die ATPase der NBS I stimuliert. Voraussetzung ist dabei das Schließen der NBS II.

Mithilfe der 3,9 Å-Struktur des Post-Spaltungskomplexes wurde eine niedrig-aufgelöste Dichtekarte von ribosomalen Initiationskomplexen mit gebundenem ABCE1 rekonstruiert. ABCE1 nimmt hier die gleiche Konformation wie im Post-Spaltungskomplex an. Zusätzlich war die kleine ribosomale Untereinheit mit Initiationsfaktoren (eIF) und einer Initiator-tRNS besetzt. Diese Beobachtung erlaubt es zum ersten Mal den Zyklus der Translation strukturell zu schließen. Bisher konnte noch keine direkte Interaktion zwischen ABCE1 und den Initiationsfaktoren identifiziert werden. Diskutiert wird eine Interaktion zu eIF3 und dessen b-g-i Untereinheit. Die FeS-Cluster-Domäne könnte dabei eine Brücke zwischen eIF3 und der kleinen ribosomalen Untereinheit bilden. Interessanterweise bindet die FeS-Cluster-Domäne aber an eine Position der Helix 44, die auf der gegenüberliegenden Seite einen Knick aufweist. Vor kurzem wurde publiziert, dass genau an dieser Stelle die γ -Untereinheit von eIF2 beim Erkennungsvorgang des Start-Codons durch Initiator-tRNS bindet. Zusammengefasst ergibt dies, dass ABCE1 in der Post-Spaltungskonformation Initiationsfaktoren auch über die Wechselwirkung mit der rRNS beeinflussen könnte, insbesondere im Bereich der Helix 44. Ein weiterer Ansatz sieht vor, dass ABCE1 die Re-Initiation durch Kollision der FeS-Cluster-Domäne an der Helix 44 mit der WH-Domäne des Re-Initiationsfaktors eIF2D blockiert. Es ergeben sich folglich zahlreiche Szenarien, in denen ABCE1 unterstützend oder unterdrückend auf die Initiation wirken könnte, oder sogar beides, und damit die Funktion einer ATP-hydrolyse bestimmten Zeitschaltuhr übernimmt.

Zur Bestimmung der konformationellen Dynamik von ABCE1 in Echtzeit wurde ein System auf Einzelmolekül-basiertem Förster-Resonanzenergietransfer (smFRET) etabliert. Das Bäckerhefe ABCE1 wurde zur Detektion von FRET mit fluoreszierenden Proben an Cystein-Paaren markiert. Die zusätzlich vorhandenen Cysteine außerhalb der FeS-Cluster-Domäne mussten dazu ersetzt werden durch Aminosäuren ohne freie Thiolgruppen. Nachträglich wurden Cystein-Paare für die Fluoreszenzmarkierung mittels Maleimid-Kupplung eingesetzt. Die Positionen der Cystein-Paare für die Abstandsbestimmungen zwischen den NBS I und II waren bereits von Kristin Kiosze-Becker (Institut für Biochemie, Goethe-Universität,

Frankfurt/M.) im archealen System charakterisiert worden. Zusätzlich wurde eine weitere Variante benutzt für die Abstandsbestimmung zwischen der FeS-Cluster-Domäne und der NBD1. Die Zell-Viabilität dieser Varianten wurde in *Plasmid Shuffling* Studien belegt und Bindungsstudien an der kleinen ribosomalen Untereinheit bestätigten die Aktivität und Nutzbarkeit der fluoreszenzmarkierten Varianten. In Kollaboration mit Philipp Höllthaler (Institut für Biochemie, Goethe-Universität, Frankfurt/M.) wurden die Doppel-Cysteinvarianten mit Fluoreszenz-Donor (sCy3)- und -Akzeptor (sCy5)-Proben markiert und an einer Glasoberfläche immobilisiert. In einem alternierenden Laseranregungs-smFRET-Aufbau konnte die Donor- und Akzeptor-Fluoreszenz ausgelesen und die FRET-Effizienz bestimmt werden. Die FRET-Effizienz ist zum relativen Abstand der Donor- und Akzeptor-Proben anti-korreliert. Mithilfe der summierten Abstandsverteilung wurden konformationelle Populationen identifiziert. In Abhängigkeit der kleinen ribosomalen Untereinheit sowie verschiedener Nukleotide wurde dynamisches Verhalten für alle drei Varianten beobachtet. Es konnte bestätigt werden, dass die beiden NBS durch Zugabe von ATP und AMP-PNP schließen und die FeS-Cluster-Domäne rotiert, wie in der Struktur des Post-Spaltungskomplexes beobachtet. Dieses System erlaubt die Bestimmung der Verweildauer und der konformationellen Dynamiken von ABCE1 mit Substraten bei Raumtemperatur. Hierbei können Rückschlüsse auf die zeitliche Abfolge der inneren Bewegungstrajektorien des ABC-Systems geschlossen werden. Interaktionspartner für ABCE1 könnten in Zukunft spaltungskompetente Ribosomen oder Initiationskomplexe sein. Weiterhin konnte gezeigt werden, dass die beiden NBS in Anwesenheit von AMP-PNP und der kleinen ribosomalen Untereinheit öffnen und schließen. Zudem konnte deutlich schnelleres Öffnen und Schließen der beiden NBS beobachtet werden, als dies die bestimmte ATPase Rate vorgab. Dies erlaubt das Aufstellen der Hypothese einer *elastischen konformationellen Dynamik* und Dimerisierung der NBDs in ABC-Systemen, die abhängig ist von Interaktionspartnern und Nukleotiden, aber nicht unmittelbar zur ATP-Hydrolyse führt.

D. Abstract

Translation is a universal process in all kingdoms of life and organized in a cycle that requires ribosomal subunits (40S and 60S), messenger RNA (mRNA), aminoacylated transfer RNAs (tRNAs), and a myriad of regulatory factors. As soon as translation reaches a stop codon or stalls, a termination or surveillance process is launched *via* release factors eRF1 or Pelota (Dom34), respectively. The ATP-binding cassette (ABC) protein ABCE1 interacts with release factors at the ribosomal A-site and coordinates the recycling process in Eukarya and Archaea. Two asymmetric nucleotide-binding sites (NBSs) control and execute the ribosome splitting upon dimerization and closure of the two nucleotide-binding domains (NBDs).

Ribosome nascent chain complexes (RNCs), ABCE1, and Dom34 from *S. cerevisiae* were produced for the reconstitution of splitting assays in order to probe for ABCE1's actions in the splitting process with its native substrate. Translating ribosomes were stalled *in vivo* in a *no-go* situation on truncated mRNAs by a 3'-ribozyme motif that generates truncated mRNAs. The initiated decay mechanisms were circumvented by genomic deletion of the release factor Dom34 (Pelota) of the *no-go* decay machinery. The mRNA coded for an N-terminal affinity purification tag (His-tag) and the green fluorescent protein (GFP) as a reporter of the translated nascent chain in the ribosomal complexes. RNCs were successfully *in vivo* stalled, enriched, and purified. In native gels, the reconstituted splitting experiments were analyzed by separation of RNCs, ribosomal subunits, and nascent chain-tRNA complexes based on the fluorescence readout of the GFP reporter. In addition, the anti-association factor eIF6 was added in the splitting reaction because it blocks the immediate re-association of ribosomal subunits after splitting. The anti-association activity of eIF6 was probed by an anti-/re-association assay, in which ribosomes are anti-associated by high salt and low magnesium conditions and in a second step re-associated. The re-association can be blocked by binding of eIF6 and other anti-associating factors to the ribosomal intersubunit sites. This approach allowed for the discovery of an anti-association activity of ABCE1 that was dependent on the non-hydrolysable ATP analog AMP-PNP. In addition, the formed complex between 40S and ABCE1 represented formally a post-splitting intermediate.

In collaboration with the Beckmann lab, the structure of the post-splitting complex was reconstructed at 3.9 Å. The ABC system of ABCE1 is fully closed and its N-terminal iron-sulfur (FeS) cluster domain is rotated by 150-degree to a cleft at helix 44 and uS12. The FeS cluster domain is stabilized by interactions of Pro30 to uS12, Arg7 to helix 5, and the cantilever arm that links it to NBD1. Tyr301 of NBD1 stabilizes the FeS cluster domain in the rotated position by interaction to the backbone of the cantilever arm. Upon transition to the post-splitting state, the FeS cluster domain must clash with the release factor and push it in-between the ribosomal subunits like a wedge and split the ribosome. In addition, in the post-splitting state, the FeS cluster domain would putatively clash with uL14 of the large ribosomal subunit, and this is the structural explanation for the anti-association effect of ABCE1. In Archaea, a similar conformation of the post-splitting complex was reconstructed in collaboration with the Beck and Beckmann labs and Kristin Kiosze-Becker and Elina Nürenberg-Goloub. Based on the high-resolution structure of the post-splitting complex, the post-splitting state of ABCE1 was identified in the 43S initiation complex 40S-ABCE1-tRNA-eIF2-eIF3. Subsequently, we proposed the post-splitting complex as a platform for initiation.

In the quest to elucidate conformational dynamics of ABCE1, a reconstituted system was established to study conformational dynamics in real-time. Single-molecule Förster resonance energy transfer (smFRET) was used for the relative distance detection between a donor and acceptor fluorophore. A cysteine-less ABCE1 variant was engineered with additional cysteines for fluorescent labeling by thiol-maleimide-coupling. In collaboration with Philipp Höllthaler, the double-cysteine variants were labeled for smFRET studies and alternating-laser excitation (ALEX) smFRET measurements were performed with ABCE1 and the small ribosomal subunit. ABCE1's nucleotide-dependent NBD dimerization and FeS cluster domain rotation was determined in real-time. Finally, a higher opening and closing frequency of the NBDs was discovered than the determined ATPase rate. This observation could be explained by the hypothesis of *elastic dimerization* that is not immediately connected to ATP hydrolysis.

E. Publications and contributions

Parts of this thesis were published in the following papers with indicated contributions.

Gerovac M, Tampé R (2018)

Control of mRNA translation by versatile ATP-driven machines.

Trends Biochem Sci, in press

Contributions: M.G. and R.T. wrote the manuscript.

Nürenberg-Goloub E, Heinemann H, **Gerovac M**, Tampé R (2018)

Ribosome recycling is coordinated by processive events

in two asymmetric ATP sites of ABCE1.

Life Sci Alliance 1: 3 e201800095

Contributions: E.N.-G.: Conceptualization, methodology, investigation, formal analysis, validation, visualization, writing–original draft, review and editing. H.P.: Investigation, formal analysis, and validation of 30S binding (Figs. 5 and EV5). M.G.: Investigation, formal analysis, validation, visualization of yeast viability (Fig. 1E and S2), and review. R.T.: Conceptualization, resources, formal analysis, supervision, funding acquisition, investigation, methodology, project administration, writing–original draft, review and editing.

Heuer A* & **Gerovac M***, Schmidt C, Trowitzsch S, Preis A,

Kötter P, Berninghausen O, Becker T, Beckmann R, Tampé R (2017)

Structure of the 40S–ABCE1 post-splitting complex

in ribosome recycling and translation initiation.

Nat Struct Mol Biol 24: 453–60

*both authors contributed equally to this work.

Contributions: M.G., A.H., T.B., R.B. and R.T. designed the study. M.G. developed the preparation of the post-splitting complex and performed all functional assays. M.G. and P.K. conducted the plasmid shuffling experiment. M.G. and S.T. designed the NTPase assays. M.G.

and A.H. prepared the EM samples. A.P. and A.H. prepared the initiation complex. A.H. and O.B. collected and A.H. processed the cryo-EM data. C.S., A.H. and T.B. built and refined the model. C.S., T.B., A.H. and M.G. analyzed and interpreted the structures. M.G., T.B., A.H., S.T., R.B. and R.T. wrote the manuscript. R.T. initiated and R.B. and R.T. conceived the project.

Kiosze-Becker K, Ori A, **Gerovac M**, Heuer A, Nürnberg-Goloub E, Rashid UJ, Becker T, Beckmann R, Beck M, Tampé R (2016)

Structure of the ribosome post-recycling complex probed by chemical cross-linking and mass spectrometry.

Nat Commun 7: 13248

Contributions: K.K.-B. conducted the biochemical and cross-linking experiments. A.O. and M.B. performed the MS analysis and interpreted the MS data. U.J.R. supported the project in its initial phase. M.G., A.H., E.N.-G., T.B. and R.B. carried out the cryo-EM analysis. K.K.-B., A.O., M.B. and R.T. wrote the manuscript, and R.T. conceived the experiments. All authors reviewed the manuscript.

F. Declaration

Except where stated otherwise by reference or acknowledgment, the here presented work was generated by myself under the supervision of Prof. Dr. Robert Tampé in my doctoral studies. All contributions from colleagues are explicitly referenced in the thesis.

The material listed below was obtained in the context of collaborative research:

Affiliations: ¹Goethe University Frankfurt/M., ²Howard Hughes Medical Institute (HHMI) and Johns Hopkins University and Johns Hopkins Medical Institutions (JHMI), ³Gene Center and Ludwig-Maximilians University (LMU) Munich

Figure 4 I Plasmid shuffling assay development. P. Kötter¹ supervised me in the development of the plasmid shuffling assay and performed with S. Lamberth¹ the tetrad analysis for the generation of the strain CEN.MG1-9B. My own contribution was the generation of the constructs and conductance of all cloning steps.

Figure 5 I smFRET-ALEX microscope setup. P. Höllthaler¹ created the figure and granted permission for reprint.

Figure 6a I Immobilized samples and data processing. P. Höllthaler¹ produced microscopy images. I assembled the figure.

Figure 9a I GFP-Rz-tRNA co-localized in SDG with 80S ribosomes in *dom34Δski2Δ*. A. Klein¹ contributed by taking images of yeast cells at the confocal fluorescence laser scanning microscope. My own contribution was the generation of the construct, initial strain, selection process, preparation, and fixation of the cells for imaging.

Figure 10b,c I 40S(Asc1-GFP-HA) production in the *dom34Δski2Δ* background. P. Kötter¹ and S. Lamberth¹ performed the tetrad analysis for generation of the strain MG004. A. Klein¹ contributed by taking images of yeast cells. My own contribution was the generation of the construct, initial strains, selection process, preparation, and fixation of the cells for imaging.

Figure 12b I Quality control of 80S-GFP-Rz. A. Heuer³ contributed by negative staining and EM imaging. My own contribution was sample preparation for negative staining.

Figure 20a | Splitting assay development. A. Schuller² supervised me in the in gel splitting assay. My contribution was the production and purification of Dom34 and ABCE1, and the conductance and analysis of the assay.

Figure 22 | AMP-PNP stimulated binding of ABCE1 to 40S. 40S ribosomes were provided by A. Schuller². I purified ABCE1 and conducted the experiment.

Figure 23c | Preparation of the 40S–ABCE1 post-splitting complex. Sample preparation for cryo-EM was conducted in collaboration with A. Heuer³; the same sample was used for reconstruction. My own contribution was the development of the preparation assay and analysis *via* SDS-PAGE and silver staining.

Figure 24 | Raw cryo-EM data and classification of the reconstituted 40S–ABCE1 complex. A. Heuer³, T. Becker³, O. Berninghausen³ recorded, classified the data, and reconstructed the density map of the particle.

Figure 25 | Cryo-EM structure of the reconstituted 40S–ABCE1 complex and assessment of resolution. A. Heuer³ and T. Becker³ produced all data.

Table 11 | EM data collection and refinement statistics. A. Heuer³ and T. Becker³ produced all data.

Figure 26 | Overall structure of the 40S–ABCE1 post-splitting complex. A. Heuer³, C. Schmidt³, T. Becker³, and I modelled the structure of the post-splitting complex. Structures and color codes were assembled in collaboration with the Beckmann lab³. My own contribution was the generation of images and the assembly of the figure.

Figure 27 | Conformational transition of NBSs of ABCE1 from pre- to post-splitting state. A. Heuer³ generated the motion bar diagram based on a structure assembly that I provided. My own contribution was the analysis of the closure of the ABC system, generation of images and assembly of the figure.

Figure 28a,b | NBS are occluded with ATP. T. Becker³ generated images of density maps with structures. My own contribution was the analysis of the ABC system and figure generation.

Figure 29 I Interactions between the 40S subunit and ABCE1 in the post-splitting state.

T. Becker³ generated images of density maps with structures. In collaboration with the Beckmann lab³ we evaluated interactions. My own contribution was the generation of the figure.

Figure 30d I NBD1 stabilizes the FeS cluster domain in post-splitting state by an essential cantilever arm interaction.

P. Kötter¹ supervised me in the generation of the plasmid shuffling assay and performed with S. Lamberth¹ the tetrad analysis for the strain CEN.MG1-9B. My own contribution was the generation of the constructs, transformation, and assay execution.

Figure 31 I Dynamic conformation of the cantilever. T. Becker³ generated images of density maps with structures. My own contribution was the figure generation.

Figure 33 I NTPase stimulation of ABCE1 by the 40S subunit. S. Trowitzsch¹ executed the NTPase experiment in the radioactive lab. My own contribution was the design of the study, preparation of all components for the assay, supervision of S. Trowitzsch¹, data analysis, and figure design. S. Trowitzsch¹, R. Tampé¹, and I verified the data analysis. The Beckmann lab³ provided 40S. The justifications for this division of work were legal guidelines in radioactive working.

Figure 35 I Low-resolution cryo-EM structure of the 30S–ABCE1 post-splitting complex.

K. Kiosze-Becker¹ provided the 30S subunit. E. Nürnberg-Goloub¹ provided the ABCE1 mutant. A. Heuer³ and I conducted sample preparation at the Gene Center and LMU Munich. A. Heuer³ and I performed screening of conditions for cryo-EM. Heuer³ and O. Berninghausen³ recorded the micrographs. A. Heuer³ and T. Becker³ reconstructed the low-resolution density map of the post-splitting 30S–ABCE1 complex. My own contribution was the analysis, visualization, and evaluation of the low-resolution density map for publication. T. Becker³ prepared the image of the density map. I prepared the figure and included data by K. Kiosze-Becker¹.

Figure 36b I Catalytic mutants show a strong growth defect. I provided the plasmids and E. Nürnberg-Goloub¹ introduced mutations. I conducted the assay, analyzed the data, and generated the figure.

Figure 37 I Preparation and cryo-EM of the native 40S–ABCE1 complex. A. Heuer³, A. Preis³, O. Berninghausen³, T. Becker³, and R. Beckmann³ produced all data.

Figure 38 I Native 40S–ABCE1 initiation complex. A. Heuer³, A. Preis³, O. Berninghausen³, T. Becker³, and R. Beckmann³ produced all data.

Figure 40d I Fluorophore probe positions and immobilization setup. P. Höllthaler created graphical elements and granted permission for reprint. My contribution was the assembly of the figure.

Figure 42a I Labeling of ABCE1 by sCy3/sCy5. In collaboration with P. Höllthaler¹, ABCE1 was labeled. P. Höllthaler¹ recorded the SEC profiles. My own contribution was the supervision of these experiments.

Figure 44 I Dynamic FRET efficiency trace of the sCy3/sCy5 labeled NBS II variant with 40S and AMP-PNP. P. Höllthaler¹ analyzed and exported the data. My own contribution was the supervision of these experiments and assembly of the figure.

Figure 45 I Conformational populations of the FeS-NBD1 variant. P. Höllthaler¹ and I analyzed the data and generated the figures. My own contribution was the supervision of these experiments.

Figure 46 I Conformational populations of the NBS I variant. P. Höllthaler¹ and I analyzed the data and generated the figures. My own contribution was the supervision of these experiments.

Figure 47 I FRET efficiency population shifts of FeS-NBD1 and NBS I variants. P. Höllthaler¹ and I analyzed the data and generated the figures. My own contribution was the supervision of these experiments.

Figure 48 I Conformational populations of the NBS II variant. P. Höllthaler¹ and I analyzed the data and generated the figures. My own contribution was the supervision of these experiments.

Figure 49 I FRET efficiency population shifts of the NBS II variant with 40S. P. Höllthaler¹ and I analyzed the data and generated the figures. My own contribution was the supervision of these experiments.

Figure 50 | Integration time dependency of populations in the case of the NBS II variant. P. Höllthaler¹ and I analyzed the data and generated the figures. My own contribution was the supervision of these experiments.

Figure 51 | Dynamic F_E-traces of ABCE1 variants with 40S & AMP-PNP. P. Höllthaler¹ and I analyzed the data and generated the figures. My own contribution was the supervision of these experiments.

Figure 52 | FeS cluster domain rotation and implications on ribosome splitting. My contribution was the identification of the FeS cluster domain clash with uL14. The Beckmann lab³ verified this observation. I generated the figure.

Figure 55 | Cryo-EM structures of the 40S–ABCE1 post-splitting complex and the 48S initiation complex. T. Becker³ created the images with density maps. I created the figure in collaboration with T. Becker³.

Whenever a figure, table, or text is identical to a previous publication, it is cited and stated explicitly after the relevant section in the thesis that copyright permission and/or co-author agreement has been obtained. The following parts of the thesis have been previously published, see **Table 1**:

Table 1 | Previous publication of elements in this thesis

publication	sections	figures and tables
(Gerovac & Tampé, 2018)	D, 1, 1.1., 1.2, 1.3, 1.4, 4.1, 4.2, 4.4, 4.5, 4.6, 4.7	Figure 3, Figure 53, Figure 54, Figure 56, Figure 58
(Nürnberg-Goloub <i>et al.</i> , 2018)	-	Figure 36b
(Heuer & Gerovac <i>et al.</i> , 2017)	2.4.4, 2.5.1, 2.6.2, 2.6.4, 2.7, 3.5 f., 3.6 f., 4.1, 4.2	Figure 23, Figure 24, Figure 25, Figure 26, Figure 27, Figure 28, Figure 29, Figure 30, Figure 31, Figure 32, Figure 33, Figure 37, Figure 38, Figure 52, Table 11
(Kiosze-Becker <i>et al.</i> , 2016)	2.7.5, 2.7.7, 2.7.8	Figure 35

f.: and following sub-sections

1 Introduction

Genetic information is transcribed into messenger ribonucleic acids (mRNAs). These mRNAs are translated into proteins *via* adaptors, called transfer RNAs (tRNA), which decipher consecutive mRNA triplet codes into a covalently linked polypeptide chain. The fundamental process of translation is catalyzed by universally conserved ribosomal RNAs (rRNAs) and ribosomal proteins that collectively form the small (40S in Eukarya; 30S in Archaea and Bacteria) and large ribosomal subunits (60S in Eukarya; 50S in Archaea and Bacteria) (**Figure 1**). During translation initiation, numerous initiation factors (eIFs) assist the assembly of an elongation competent ribosomal complex (80S in Eukarya; 70S in Archaea and Bacteria) consisting of the small and the large subunit, mRNA, and methionylated initiator tRNA. The conserved rRNA core and ribosomal proteins recruit elongation factors (eEFs) that coordinate tRNA binding and its transposition along the subunit interface. The ribosomal tRNA-binding sites are subdivided into the aminoacyl-tRNA carrying A-site, the peptidyl-tRNA carrying P-site, and the exit E-site harboring deacylated tRNA. In a cyclic process, the GTPase elongation factor eEF1A guides the consecutive aminoacylated tRNA to the A-site. The nucleophilic attack of the A-site tRNA's α -amino group on the carbonyl of the P-site's peptidyl-tRNA is coordinated in the ribosomal peptidyl transferase center (PTC) (Nissen & Hansen *et al.*, 2000, Polikanov *et al.* 2014). Subsequently, the GTPase eEF2 translocates the elongated peptidyl-tRNA from the A-site to the P-site. GTPase activation of elongation factors is universally triggered by the sarcin-ricin loop of the large ribosomal subunit (Voorhees *et al.*, 2010). Canonically, protein elongation terminates at a stop codon, which is not recognized by a tRNA, but *via* the NIKS-motif of the eukaryotic class I release factor eRF1 (Bertram *et al.*, 2000) that is delivered in complex with the GTPase class II release factor eRF3 (Frolova *et al.*, 1996, Frolova & Seit-Nebi *et al.*, 2002, Stansfield *et al.*, 1995, Zhouravleva *et al.*, 1995) (**Figure 1**). A swing-out of the middle (M) domain in eRF1 positions a conserved GGQ motif in the P-site of the PTC that catalyzes the hydrolysis of the peptidyl-tRNA (**Figure 3a,b**) (Frolova *et al.*, 1999, Preis *et al.*, 2014, Shaw & Green, 2007, Song *et al.*, 2000).

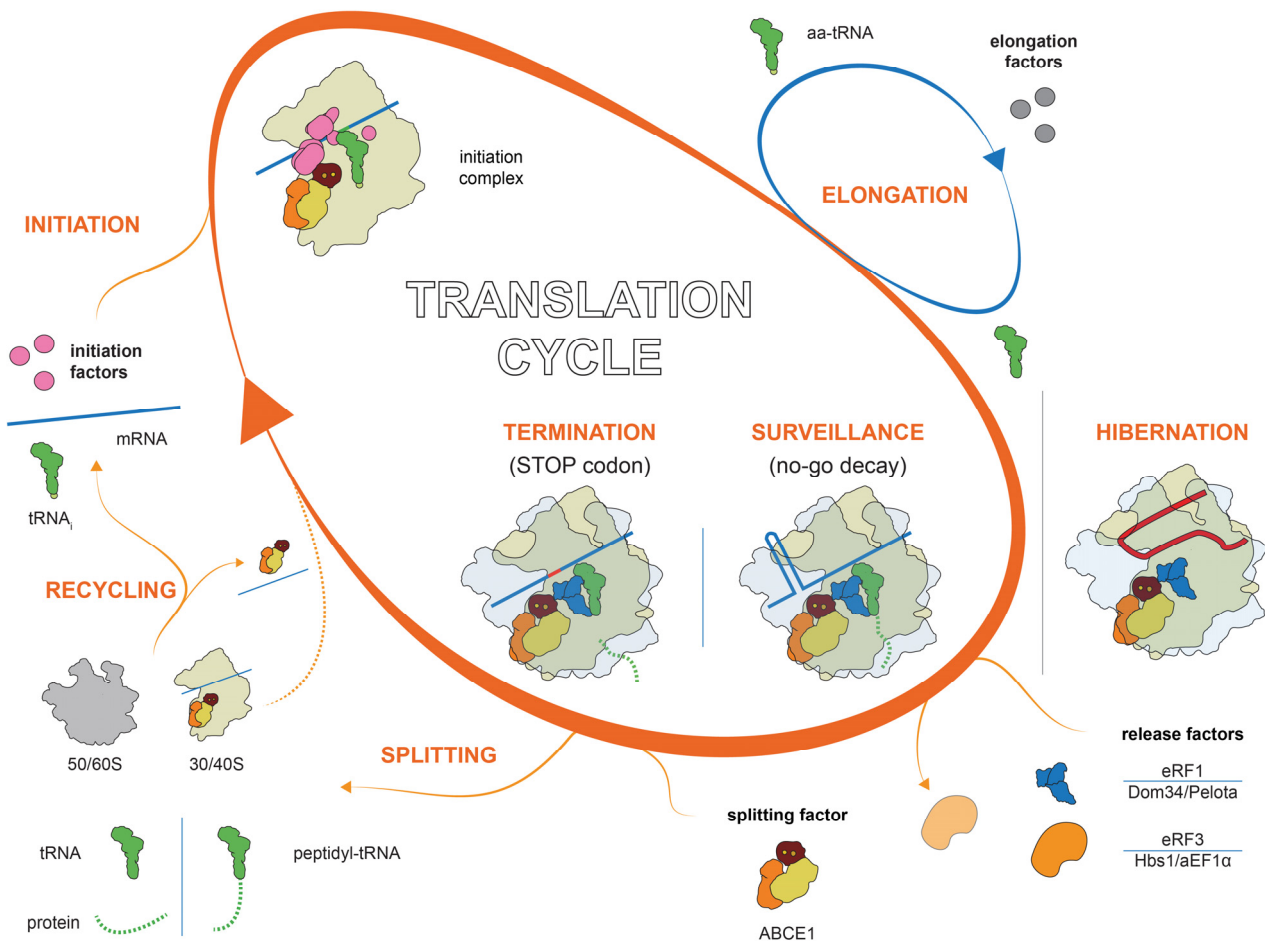


Figure 1 | Overview of the translation cycle. Translation is initiated upon formation of the initiation complex by the small ribosomal subunit (30/40S), mRNA, initiator tRNA_i, and initiation factors. The large ribosomal subunit (50/60S) joins the initiation complex and elongation starts upon delivery of aminoacylated-tRNA by elongation factors. Upon stop codon recognition by eukaryotic release factor 1 (eRF1) that is delivered by eRF3, the complex is terminated and peptide released. In the case of *no-go* decay surveillance mechanisms Dom34/Pelota delivered by Hbs1/aEF1α recognize the complex. In surveillance, no peptide is released. In addition, hibernating and *vacant* ribosomes can also be substrate for *no-go* decay mechanisms that lack mRNA or are locked by Stm1. ABCE1 is the universal splitting factor of these complexes. After splitting, ABCE1 may remain bound to the small ribosomal subunit and facilitate initiation or re-initiation on the same mRNA. Graphical elements were adapted from (Heuer & Gerovac *et al.* 2017), reprinted with permission.

The prokaryotic release factors (RF1 and RF2) use the same mechanism of GGQ motif driven termination, but do not require a delivery factor and recognize diverse stop-codons (Korostelev & Asahara & Lancaster *et al.*, 2008, Laurberg & Asahara & Korostelev *et al.*, 2008, Svidritskiy & Korostelev, 2018, Weixlbaumer & Jin *et al.*, 2008). After release of the

hydrolyzed peptide, the ribosomal complex is formally (post-)terminated with a bound tRNA in the P-site and the release factor in the A-site.

Still, evolution responded to critical situations in mRNA surveillance with new mechanistic solutions and non-canonical players. Translation may be stalled at stable secondary structures or 3' truncated mRNAs, called a *no-go* stall (Doma & Parker, 2006). In *vacant* ribosomes, the ribosomal subunits can be loosely associated if no mRNA is bound. In a hibernation mode, after starvation, the mRNA channel can be arrested by the suppressor protein Stm1 (Ben-Shem & Garreau de Loubresse & Melnikov *et al.*, 2011, Pisareva & Skabkin *et al.*, 2011). All stalled and arrested ribosomes have in common that the cell launches surveillance mechanisms, in all these cases the *no-go* decay pathway for ribosome recycling (**Figure 1**) (Jackson *et al.*, 2012, Shoemaker & Green, 2012). The eukaryotic class I release factor Pelota (Dom34 in yeast) is recruited to the stalled complexes (Graille *et al.*, 2008, Guydosh & Green, 2014, Kobayashi *et al.*, 2010, Lee *et al.*, 2007, Passos *et al.*, 2009, Pisareva & Skabkin *et al.*, 2011, Saito & Hosoda *et al.*, 2013, Shoemaker & Green, 2011, van den Elzen *et al.*, 2014). Pelota is neither engaged in codon recognition nor able to hydrolyze the peptidyl-tRNA bond owing to a lack of NIKS and GGQ motifs, respectively, and thus acts in a distinct manner than the termination factor eRF1 (Graille *et al.*, 2008, Kobayashi *et al.*, 2013). Consequently, peptide release does not occur in the *no-go* decay pathway. In Eukarya and Archaea, ribosomal complexes that are stalled in *no-go* decay, including complexes after canonical termination and hibernation, are resolved by splitting of the ribosome into its large and small subunits. Splitting is facilitated by the ATP-binding cassette (ABC) protein of family E 1 (ABCE1, **Figure 2**) in cooperation with class I eRFs (eRF1 or Pelota) (Barthelme *et al.*, 2011, Pisarev *et al.*, 2010, Pisareva & Skabkin *et al.*, 2011, Shoemaker & Green, 2011). By closing and opening its two head-to-tail oriented nucleotide-binding domains (NBDs) elicited by ATP binding and hydrolysis, ABCE1 performs a tweezer-like motion (Chen *et al.*, 2003). The engagement of the two NBDs transmits mechanical power to associated domains and motifs (Becker & Franckenberg *et al.*, 2012, Brown & Shao *et al.*, 2015, Heuer & Gerovac *et al.*, 2017, Preis *et al.*, 2014, Shao & Murray & Brown *et al.*, 2016). ABCE1 harbors an N-terminal iron-sulfur (FeS) cluster domain, which interacts with class I eRFs (Barthelme *et al.*, 2011, Barthelme *et al.*, 2007, Becker & Franckenberg *et al.*, 2012, Brown & Shao *et al.*,

2015, Karcher *et al.*, 2008, Pisarev *et al.*, 2010, Preis *et al.*, 2014, Shao & Murray & Brown *et al.*, 2016). In contrast to canonical termination, during *no-go* decay, the polypeptide-tRNA remains in the exit tunnel of the large ribosomal subunit and represents the major discriminator of post-splitting ubiquitination and degradation of the aberrant polypeptide. Listerin and nuclear export mediator factor (NEMF), corresponding to Ltn1 and Rqc2 (ribosome-associated quality control complex protein 2) in yeast, recognize the blocked peptidyl-tRNA in the released 60S subunit in order to ubiquitinate the nascent polypeptide chain (Lyumkis & Oliveira dos Passos *et al.*, 2014, Shao *et al.*, 2015, Shen *et al.*, 2015). The ATPase Cdc48 can extract the ubiquitinated peptidyl-tRNA nascent chain and the adaptor Vms1 eventually cleaves the peptidyl-tRNA bond by a conserved catalytic glutamine residue that is functionally analogous to the GGQ motif of release factors (Verma *et al.*, 2018). In addition, a stall in translation causes a ribosome collision that is sensed by the ubiquitin ligase ZNF598 (Hel2 in yeast) and leads to ubiquitination of the colliding ribosome at the 40S–40S interface (Juszkiewicz & Chandrasekaran *et al.* 2018). Interestingly, Rack1 (Asc1 in yeast) of the stalled ribosome is an integral part of the di-ribosome interface and may explain its role in the detection of ribosome stalling (Sitron *et al.* 2017, Sundaramoorthy *et al.* 2017). After splitting, the mRNA and tRNA are still bound to the small ribosomal subunit. Complete ribosome recycling requires the ejection of tRNA and the release of mRNA by either canonical initiation factors (in combination eIF1, -1A, -3 and -3j (Hcr1 in yeast)), or the non-canonical initiation factor eIF2D (also known as Ligatin or Tma64 in yeast, or corresponding interacting proteins MCT-1–DENR, Tma20–22 in yeast) (Pisarev *et al.*, 2010, Skabkin & Skabkina *et al.*, 2010). Release of tRNA and mRNA allows for subsequent canonical initiation. If the mRNA is not released, re-initiation on the same mRNA is possible. An upstream open reading frame (uORF) facilitates translation of the major ORF by re-initiation (Jackson *et al.*, 2010, Skabkin *et al.*, 2013, Wethmar *et al.*, 2010). The key questions are how the ribosome discriminates between initiation and re-initiation, and how splitting and (re-)initiation are mechanistically linked to ensure energy conservation and an efficiently regulated hand-over. Notably, ABCE1 interacts with initiation factors and occupies ribosomal initiation complexes, providing a link between splitting and initiation (Andersen & Leever, 2007, Barthelme *et al.*,

2011, Chen *et al.*, 2006, Dong *et al.*, 2004, Heuer & Gerovac *et al.*, 2017, Mancera-Martínez *et al.*, 2017, Pisarev *et al.*, 2010).

In addition to ABCE1, the yeast ABC protein eEF3 splits the ribosome at the E-site and releases mRNA from the small subunit, allowing for a new round of translation and initiation (Kurata *et al.*, 2010, Kurata *et al.*, 2013). Interestingly, upon an antibiotic arrest of translating ribosomes, bacterial ABC proteins of the family F (ABCF) release the stall and cause pathogenic resistance (Arenz & Wilson, 2016). However, a broad range of conformational states remains to be elucidated for the ABC proteins of the subfamily F.

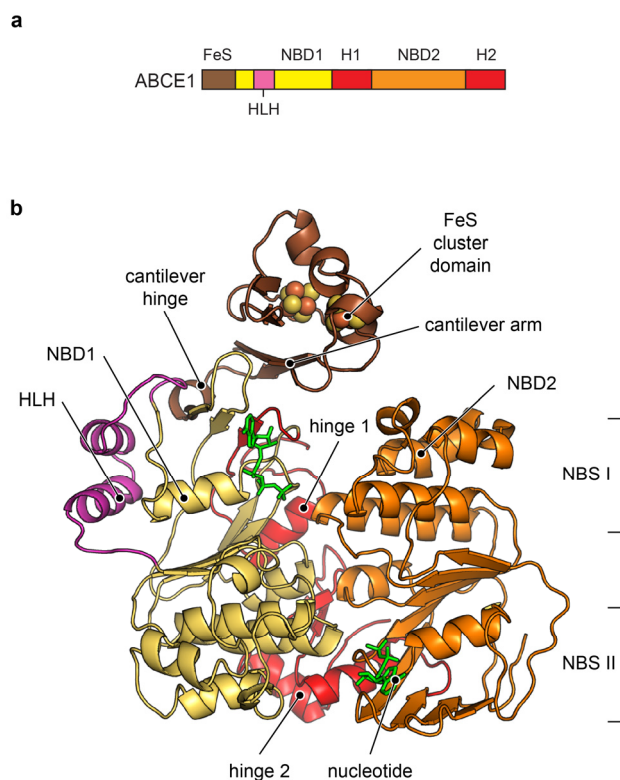


Figure 2 | Architecture of ABCE1. **a**, ABCE1 scheme. **b**, Two nucleotides are bound by two nucleotide-binding sites (NBS I & II) formed by a sandwich of two nucleotide-binding domains (NBD1 (yellow) and 2 (orange)) that are linked by hinge 1 motif (red). Hinge 2 motif (red) is C-terminal. Helix-loop-helix motif (HLH, magenta) is inserted in NBD1. N-terminally, ABCE1 harbors a FeS cluster domain (brown) that is connected by a cantilever arm and hinge (brown). PDB: 4CRM, Preis *et al.*, 2014.

1.1 From diversified, meandering functions to ribosome recycling – a brief history

While ABCE1 is one of the most conserved proteins among Eukarya and Archaea, diverse functions have been initially linked to it. The first report described ABCE1 as RNase L inhibitor (Rli1) that is upregulated upon viral infection (Bisbal *et al.*, 1995). RNase L, only encoded in

higher vertebrates, is activated by an interferon effector pathway *via* 2'-5' oligoadenylation and cleaves single-stranded RNA upon viral infection (Drappier & Michiels, 2015, Zhou *et al.*, 1993, Zhou *et al.*, 2005). ABCE1 has also been described as host protein 68 (HP68) required for HIV capsid assembly (Lingappa *et al.*, 2006, Zimmerman *et al.*, 2002). However, the mechanistic role of ABCE1 in these processes still remains opaque. The evidence for a role in translation was found in ABCE1's interaction with the small ribosomal subunit and initiation factors, thus leading to the hypothesis that ABCE1 might be involved in translation initiation (Andersen & Leever, 2007, Chen *et al.*, 2006, Dong *et al.*, 2004). ABCE1 was also discussed in the context of ribosome biogenesis as it localizes in the nucleus, stabilizes pre-rRNA, and releases pre-80S complexes (80S-like–Nob1–Pno1–Enp1–Dim1) in a translation-like cycle for maturation of pre-40S subunits (Dong *et al.*, 2004, Kispal *et al.*, 2005, Soudet *et al.*, 2010, Strunk *et al.*, 2012, Yarunin *et al.*, 2005).

The universal and fundamental function of ABCE1 in ATP-driven ribosome splitting was determined through reconstitution assays in Eukarya and Archaea (Barthelme *et al.*, 2011, Pisarev *et al.*, 2010, Shoemaker & Green, 2011). It is now well accepted that silencing of ABCE1 affects the entire translation cycle and the protein homeostasis of the cell. The effects, which are even more severe for short-lived and less abundant proteins, can involve a number of pathways that are not directly linked to ABCE1 (Mills & Green, 2017). During the last years, ABCE1 also emerged as a player in cancer development as its expression positively correlates with tumor progression (Ren *et al.*, 2012, Tian *et al.*, 2016, Zhai *et al.*, 2014). Furthermore, the FeS clusters of ABCE1 were discussed as the primary target for oxidative stress and are likely to be the essential factor for the indispensable character of mitochondria and their FeS cluster biogenesis pathways in eukaryotes (Alhebshi *et al.*, 2012, Kispal *et al.*, 2005).

1.2 The role of the recycling factor in translation termination

Canonical translation termination is defined by the hydrolysis of the peptidyl-tRNA bond by the GGQ motif of the M domain in eRF1 and subsequent peptide release (Alkalaeva & Pisarev *et al.*, 2006, Frolova *et al.*, 1999, Pisarev *et al.*, 2007, Preis *et al.*, 2014, Shoemaker *et al.*, 2010, Song *et al.*, 2000). In the *no-go* decay pathway, the eRF1 paralog Pelota (Dom34) is delivered

to the A-site by the eRF3 paralog Hbs1 (Carr-Schmid *et al.*, 2002, Franckenberg *et al.*, 2012, Jackson *et al.*, 2012, Nürenberg & Tampé, 2013, Shoemaker & Green, 2012) (**Figure 3a**). In association with ABCE1 at the ribosome, Pelota adapts the same conformation as eRF1 in post-termination complexes with a swung-out M domain (Becker & Franckenberg *et al.*, 2012, Brown & Shao *et al.*, 2015, Preis *et al.*, 2014, Shao & Murray & Brown *et al.*, 2016). However, Pelota lacks the GGQ motif and is therefore deficient in peptidyl-tRNA hydrolysis and peptide release. Thus, I designate the conformation, in which the 80S-bound eRF1 or Pelota adjusts a swung-out displacement of the M domain to the peptidyl-tRNA, as the post-termination state (**Figure 3b**). This post-termination state was not observed in complexes occupied by class I and II eRFs that were arrested in the presence of the non-hydrolysable GTP analog GMP-PNP or GMP-PCP (**Figure 3a**) (des Georges *et al.*, 2014, Preis *et al.*, 2014, Shao & Murray & Brown *et al.*, 2016, Taylor *et al.*, 2012). Consistently, ABCE1 can bind to ribosomes only after eRF3/Hbs1 are released from the A-site, because both share identical contact points for translational GTPase at the ribosome (Becker *et al.*, 2011, Becker & Franckenberg *et al.*, 2012, Brown & Shao *et al.*, 2015, Pisarev *et al.*, 2010, Preis *et al.*, 2014). In the presence of the non-hydrolysable ATP analog AMP-PNP, ABCE1 binds and arrests class I eRFs at 80S ribosomes (**Figure 3b**) (Pisarev *et al.*, 2010, Preis *et al.*, 2014). In addition, the M domain of eRF1 must be repositioned in order to allow for ABCE1 binding to the A-site in the pre-splitting state. If peptidyl-tRNA hydrolysis is prevented by mutation of the GGQ tip to AGQ or AAQ in eRF1, the 80S-eRF1(AGQ/AAQ)-ABCE1 complex is arrested prior splitting in the post-termination state (**Figure 3b**) (Alkalaeva & Pisarev *et al.*, 2006, Brown & Shao *et al.*, 2015, Pisarev *et al.*, 2010, Shao & Murray & Brown *et al.*, 2016). The superposition of pre-termination complexes (80S-eRF1-eRF3) and post-termination complexes (80S-eRF1-ABCE1) illustrates a clash of the M domain of eRF1 with the hinge 1 region of bound ABCE1 (**Figure 3b**). Therefore, the M domain of eRF1 must be repositioned in order to allow for ABCE1 binding to the A-site in the pre-splitting state. In summary, the structurally resolved termination states indicate a role of ABCE1 in termination that was also suggested in functional studies by observed accelerated peptide release by ABCE1 (Shoemaker & Green, 2011). In line with the structurally resolved termination states, peptide release by eRF1 is accelerated upon addition of ABCE1 and does not strictly require eRF3 in yeast (Shoemaker

& Green, 2011). Remarkably, no ABCE1 dependent acceleration of termination was observed in rabbit reticulocyte lysates at non-physiologically low magnesium concentration (1 mM) at which ribosomal subunits are loosely associated (Pisarev *et al.*, 2010). Hence, the strength of subunit association may also play a critical role for termination.

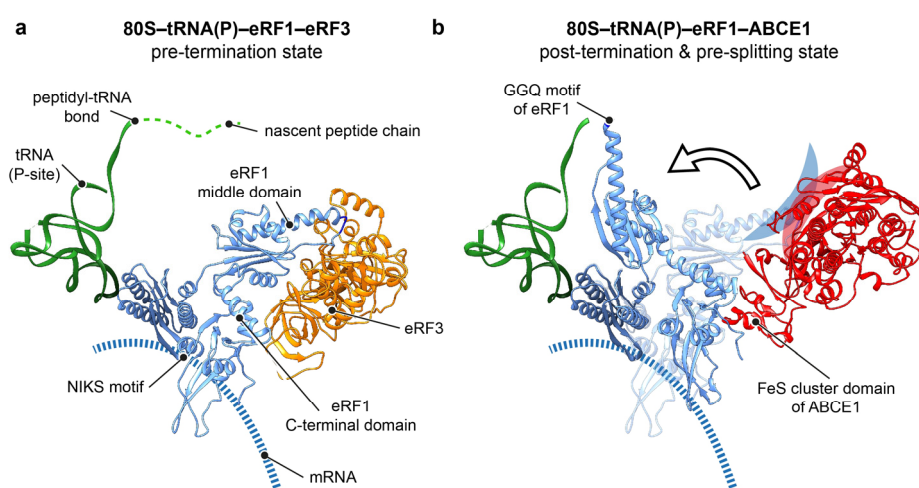


Figure 3 I Mechanism of ABCE1 in termination. **a**, In the pre-termination state, release factors of class I and II are bound to the ribosome. The middle domain of eRF1 is not swung out towards the peptidyl-tRNA bond (PDB: 5LZT, Shao & Murray & Brown *et al.*, 2016). **b**, In the post-termination and pre-splitting state, ABCE1 is bound to class I eRFs (PDB: 5LZV, Shao & Murray & Brown *et al.*, 2016). Structural re-arrangements occur in the middle and C-terminal domains of eRF1. The middle domain with the GGQ motif swings out towards the peptidyl-tRNA bond for the hydrolysis event. A superposition of these two states illustrates the clashes (red/blue line) between hinge 1 motif and NBD2 of ABCE1 and eRF1 in the pre-termination state (eRF1 in transparent blue). Reprinted with permission (Gerovac & Tampé, 2018).

In this context, it is worth mentioning that the nucleotide occupancy of ABCE1 in post-termination complexes is still unclear owing to the limited resolution of the NBDs of ABCE1 in the cryo-EM reconstructions (Becker & Franckenberg *et al.*, 2012, Brown & Shao *et al.*, 2015, Preis *et al.*, 2014, Shao & Murray & Brown *et al.*, 2016). Above all, the two NBDs are not completely closed in post-termination complexes, allowing nucleotides to be exchanged. Hence, it remains unclear how ATP hydrolysis in ABCE1 is controlled during termination.

1.3 Mechanistic basis and structural insights into ribosome splitting

In recent years, several post-termination complexes have been reported in a similar conformation with bound ABCE1 and class I eRFs eRF1 or Pelota (Becker & Franckenberg *et al.*, 2012, Brown & Shao *et al.*, 2015, Preis *et al.*, 2014, Shao & Murray & Brown *et al.*, 2016). In contrast, no splitting intermediates could be arrested up to now. Additionally, a distinct splitting and quality control mechanism may become apparent by either eRF1 or Pelota based on the presence of the peptidyl-tRNA. Notably, a lack in peptidyl-tRNA hydrolysis is the common feature between eRF1(AGQ) and Pelota, but Pelota and ABCE1 are able to split ribosomes, whereas eRF1(AGQ) and ABCE1 get arrested prior splitting. While no splitting was observed with eRF1(AGQ) and ABCE1 alone, the splitting activity was restored upon addition of eRF3(GTP) (**Figure 54**)(Shoemaker & Green, 2011). In contrast, Pelota and ABCE1 split stalled ribosomes even in the absence of Hbs1 (paralog of eRF3) without hydrolysis of the peptidyl-tRNA bond. Thus, a yet undescribed quality control mechanism in ribosome splitting distinguishes between eRF1 and Pelota at the post-termination complex. The missing link may be the essential eRF3 factor that, further to its delivery function of eRF1, has additional putative roles in termination proofreading and efficiency, as well as eRF1 recycling (Korostelev, 2011). Notably, splitting within the *no-go* decay pathway depends on class I and II eRFs, which were discussed to facilitate 3' mRNA endonucleolytic cleavage (Hilal *et al.*, 2016, Lee *et al.*, 2007, Passos *et al.*, 2009). This is consistent with the preferential splitting of post-termination complexes on mRNAs with no or only short 3' mRNA lengths after the last decoded sense codon (Pisareva & Skabkin *et al.*, 2011, Shoemaker & Green, 2011). Along the same line, the N-terminal domain of Pelota comprises a prolonged tip compared to eRF1, which fits into the free mRNA channel at the A-site being present through *no-go* decay due to cleavage of mRNA (Graille *et al.*, 2008, Hilal *et al.*, 2016, Passos *et al.*, 2009, Shao & Murray & Brown *et al.*, 2016).

1.4 How does ABCE1 power ribosome splitting?

ABC proteins are evolutionarily conserved chemo-mechanical devices that enforce conformational switches for *e.g.* chromosome segregation, DNA repair, membrane transport, and, in the case of ABCE1 and ABCF proteins, remodeling of the ribosome and control of mRNA translation (Hopfner, 2016). All ABC systems include two NBDs oriented head-to-tail, forming two composite sites for nucleotide binding and hydrolysis. Each NBD harbors a RecA-like and an α -helical subdomain. The RecA-like fold is common to a large class of ATPases, including helicases of superfamily I, II and III, AAA+-ATPases, F- and V-type ATPases, and ABC proteins (Ye & Osborne *et al.*, 2004). The nucleotide-binding motifs are the Walker A (P-loop) and B (catalytic glutamate) motifs present on each NBD. In addition, the NBDs comprise a signature motif (C-loop) that is provided *in trans* by the opposite NBD. An aromatic loop positions the nucleotide base by π - π stacking. The Q-loop and His-switch are involved in Mg(II) coordination (Hopfner, 2016, Locher, 2016, Thomas & Tampé, 2018). The two nucleotide-binding sites (NBS I and II) become asymmetric in the case of non-identical NBDs or due to auxiliary motifs, domains, or interaction partners. In the open state, nucleotides can freely exchange and bind to each NBS. In ABC proteins, ATP binding triggers the engagement of the two NBDs and nucleotide occlusion, while ATP hydrolysis causes opening of the NBDs (Chen *et al.*, 2003). Substitution of the catalytic glutamate residue close to the Walker B motif of ABCE1 with either glutamine or alanine prevents ATP hydrolysis, promotes NBS closure, and binding to the small ribosomal subunit (Barthelme *et al.*, 2011, Nürenberg-Goloub *et al.*, 2018). Remarkably, if ATP hydrolysis in NBS II of ABCE1 is blocked, hydrolysis in NBS I is enhanced 10-fold (Barthelme *et al.*, 2011, Nürenberg-Goloub *et al.*, 2018) (**Figure 54**). This effect can be explained by a regulatory mechanism in NBS II, which is likely facilitated by ABCE1 binding to the ribosome. At the first view, ribosome splitting appears to be dependent on ATP hydrolysis, because splitting was blocked by AMP-PNP.

Major part of the abstract and introduction including figures, will be published as a review (Gerovac & Tampé, 2018), and were reprinted with permission.

1.5 Scope & objectives

In my PhD thesis, I aimed at targeting key questions about the closure of the ABC system of ABCE1 and the splitting mechanism at the ribosome in a reconstituted assay. In *S. cerevisiae*, a splitting assay was established previously in the Green lab that was based on the preparation of ribosomal nascent chain complexes (RNCs). Hence, I decided to start with the yeast system and in addition to utilize genetic labeling of ribosomal subunits by fluorescent proteins for detection of RNCs. I intended to overcome barriers of the fully reconstituted RNC preparation technique by development of an *in vivo* ribosome stalling approach for generation of RNCs at native conditions for a reconstituted splitting assay. Stalled RNCs should be enriched on an overexpressed truncated mRNA that should serve as substrate for the *no-go* decay pathway. Enrichment of RNCs would require blocking of the *no-go* decay machinery. The RNC purification was aimed *via* the nascent chain that should comprise an affinity purification tag at the N-terminus of the translated nascent protein. The workflow included development of fluorescence-based splitting assays, functional quality control assays, and preparation of splitting relevant factors.

Preparation of ribosome–ABCE1 complexes was a general goal as samples for structural studies. The interaction of ABCE1 and variants with the translation machinery should be validated by *in vivo* and *in vitro* reconstituted assays. In the frame of these studies, the final goal was the structural determination of the post-splitting complex and the fully closed ABC system of ABCE1.

In order to obtain a dynamic depiction of ABCE1's actions, I aimed at tackling conformational dynamics *via* single-molecule Förster Resonance Energy Transfer (smFRET) studies. A cysteine-less variant of ABCE1 should be generated and labeled at additional cysteines *via* maleimide coupling by fluorophores.

Finally, I combined structural, functional, and physiological approaches to provide insights into the ribosome splitting mechanism of the major recycling factor ABCE1.

2 Methods and materials

2.1 General bioinformatics

2.1.1 Protein parameters

Protein parameters for molecular weight, number of amino acids, theoretical isoelectric point (pI), and extinction coefficients were calculated in the ExPASy Bioinformatics Resource Portal (Artimo & Jonnalagedda *et al.*, 2012).

2.1.2 Sequence alignment

Sequences were obtained from the Universal Protein Resource UniProt.org (The UniProt Consortium 2017) and aligned in UCSF Chimera (Pettersen *et al.*, 2004) by the *Clustal X algorithm* (Larkin *et al.*, 2007). Conservation was plotted as color code on structures using UCSF Chimera's *render by conservation* tool in the sequence viewer.

2.1.3 Model and density superposition

Structures were obtained from the Research Collaboratory for Structural Bioinformatics (RCSB) Protein Data Bank (PDB) (Berman *et al.*, 2000) and densities from the Electron Map Data Base (EMDB) (Lawson *et al.*, 2016). Structures and densities were matched through UCSF Chimera's (Pettersen *et al.*, 2004) *MatchMaker* and *Fit in Map* tools.

2.1.4 Model visualization

Structures were visualized with the PyMOL Molecular Graphics System (Version 1.7.4, Schrödinger, LLC, (Schrödinger, 2015)) or UCSF Chimera (Pettersen *et al.*, 2004).

2.2 General cloning techniques

Standard cloning procedures were used as described in literature (Green & Sambrook, 2012). All tools were strictly used as instructed in the manual if not differently stated here. I produced inserts by the polymerase chain reaction (PCR) through utilization of the thermostable Phusion® DNA polymerase. Reaction conditions were optimized by variation of the following parameters: annealing temperature between 45-55 °C; elongation time was increased up to three-times the calculated one from the instructions; addition of up to 5% (v/v) DMSO or 20% (v/v) glycerol or 2 mM magnesium ions in the reaction mixture. Primer sequences were optimized for calculated annealing temperatures by modification of the GC-content, setup of a G/C clamp at 3' and 5' positions and dimer formation prevention in CloneManager® (Sci-Ed Software). Optimized primers were ordered from MWG Eurofins. Restriction sites were introduced by primer overhangs with additional extensions of three to five G/C pairs for restriction site stability and enzyme binding possibility. Vectors and inserts were purified *via* kits by anion exchange spin chromatography (Macherey-Nagel NucleoSpin® Plasmid EasyPure and Promega Wizard® SV Gel and PCR Clean-Up System). After purification, vectors and inserts were digested by optimized restriction enzymes, *e.g.* FastDigest™ *Bam*HI, that do not show star activity and are compatible in identical buffers (Thermo Fischer Scientific™ FastDigest™ enzymes and buffers, -green buffer was used preferentially in the case of subsequent purification *via* gel). Termini of restricted vectors were directly de-phosphorylated by apyrase in order to avoid re-ligation that was quite pronounced in some cloning projects (Thermo Fischer Scientific™ FastAP). Vectors and inserts were re-purified by size separation *via* agarose gels (1-3% (w/v) agarose in TAE buffer (40 mM Tris/20 mM HOAc pH 8.0, 1 mM EDTA), staining by ethidium bromide, manual cutting of bands of interest, and extraction and purification by anion exchange chromatography kits (Promega Wizard® SV Gel and PCR Clean-Up System). Purification yields were drastically improved by optimized conditions that comprised of DNA sample application to anion exchange columns at room temperature and elution with 70 °C tempered Milli-Q® water. Ligation reactions were performed by T4 ligase in a vector-to-insert ratio of 1:3 (Thermo Fischer Scientific T4 DNA ligase). Cloning without restriction enzymes was performed by the sequence and ligation independent cloning (SLIC) method

(Li & Elledge, 2007). Inserts and vectors were amplified by PCR with about 30 base pairs complementary overhangs, 3' digestion was performed by T4 DNA polymerase and products were transformed for *in cell* ligation. In all cloning experiments, chemically competent Top10 cells were transformed with DNA, see **section 2.2.4** (Thermo Fischer Scientific™ OneShot® Top10). Cells carrying the correctly assembled plasmid were selected on agarose plates with indicated antibiotics that matched the resistance gene on the vector plasmid that was assembled, as described by (Green & Sambrook, 2012).

2.2.1 TOPO® cloning

TOPO® cloning (Thermo Fischer Scientific) was used for the integration of inserts into vectors utilizing the Vaccinia virus topoisomerase I that binds the insert sequence 5-(C/T)CCTT-3', cleaves it together with the vector strand, and re-ligates both. All reaction volumes were halved to increase possible reaction number. In addition, the recombination reaction time was halved. TOPO® cloning was only used for the initial generation of vectors for *in vivo* stalling of ribosomes.

2.2.2 Cloning of translation stalling constructs for *S. cerevisiae*

The initial reporter construct His₆-tag-phosphoglycerat kinase (PGK)-Myc-* was introduced in the pAG426 and pYes52 vectors by TOPO® cloning, see **section 2.2.1**. The modular fashion of restriction sites enabled further modification by restriction cloning (see **section 2.2**): *NcoI*-(N-terminal tag)-*Bam*HI-(Reporter)-*Sph*I-(stalling motif)-*Xho*I. An additional *NcoI* restriction site in the *URA3* marker was exchanged by site directed mutagenesis (primers: *NcoI*_del_5' CTTAACTGTGCCCTCCATCGAAAAATCAGTC and *NcoI*_del_3' GACTGATTTTTCG-ATGGAGGGCACAGTTAAG). Stalling motifs (**Table 2**) were introduced 3' of the reporter by restriction cloning *via SphI* and *XhoI* restriction sites.

Table 2 | Stalling motifs with restriction sites.

motif	sequence	references
stall loop	GCATGC-GATATCCCGTGGAGGGGCGCGTGGTGGCGG CTGCAGCCGCCACCACGCGCCCCTCCACGGCATATC- CTCGAG	(Hosoda <i>et al.</i> 2003)
ribozyme (Rz)	GCATGC-GTCGACGGATCTAGATCCGTCCTGATGAGTCC GTGAGGACGAAACGCATGATC-CTCGAG	(Haseloff & Gerlach, 1988, Taira <i>et al.</i> , 1990)
poly A	GCATGC-AAAAAAAAAAAAAAAAAAAAAAAAAAAA AAAAAA-CTCGAG	(Frischmeyer <i>et al.</i> , 2002, van Hoof <i>et al.</i> , 2002)
poly K	GCATGC-AAGAAAAAGAAAAAGAAAAAGAAAAAGAAA AAGAAA-CTCGAG	(Frischmeyer <i>et al.</i> , 2002, van Hoof <i>et al.</i> , 2002)

All stalling motifs were ordered from Integrated DNA Technologies® (IDT) as DNA oligonucleotides. Stalling motifs were designed as complementary annealing primers flanked by *SphI* and *XhoI* restriction sites, which were used for insertion. For annealing, complementary primers were heated up to 98 °C and cooled down to 25 °C. Annealed primers were phosphorylated by T4 polynucleotide kinase (New England Biolabs) and then ligated with the previously *NcoI* and *SphI* restricted reporter. Finally, ligated products were purified by agarose gel electrophoresis and ligated into the pAG426 vector (*NcoI* restriction site removed in *URA3* marker) that was previously *NcoI* and *XhoI* restricted, and that yielded the final plasmid for *in vivo* stalling.

All constructs were sequenced for verification by Eurofins Genomics and Microsynth Seqlab. In the middle of the stall loop, a *PstI* restriction site served as restriction control for the incorporated stall loop motif because the sequencing of the stall loop was not possible due to secondary structures and led to an early termination after several base pairs.

The reporter was exchanged from PGK to GFP and finally GFP-MyC₂ by restriction cloning using *BamHI* and *SphI* restriction sites. In addition, N-terminally, the affinity purification tag

was exchanged for the nano- and avi-tag, that were neglected after initial trials, and to the His₆-HA affinity purification tag *via* *Nco*I and *Sph*I restriction sites.

In summa, the reporter construct His₆-HA-GFP-Myc₂-Rz in the pAG426 vector was used for further studies; all other constructs were neglected for further studies.

2.2.3 Single site-directed mutagenesis

Mutations were introduced into vectors by site-directed mutagenesis using the same procedure as for PCR reactions with two complementary primers (10-30 nucleotides in size) that harbor the mutation. The whole vector was amplified by PCR in both directions. Longer elongation times were helpful and the number of cycles was reduced to 15 in order to avoid introduction of unwanted mutations by PCR. The methylated parental vector was digested by addition of 1 µl FastDigest *Dpn*I (Thermo Fischer Scientific) at 37 °C for 20 min. The PCR product was verified by agarose gel electrophoresis and transformed into TOP10 cells that were plated on selection plates that match the selection marker on the plasmid. Clones were selected and grown over-day to an OD of 2.0, plasmids were extracted and sent off for sequencing to Eurofins Genomics and Microsynth Seqlab.

2.2.4 Transformation into *E. coli*

Plasmid constructs were transformed into DH5α and Top10 cells (Thermo Fischer Scientific). Chemically competent cells were generated by the rubidium/calcium method as described in OpenWetWare (https://openwetware.org/wiki/RbCl_competent_cell, user Peng Ji, state as of 18.12.2017, Creative Commons license). 250 ml cells were grown in lysogeny broth (LB) media to an OD of about 0.6 and pelleted at 2,700 × g for 10 min at 4 °C. Cells were re-suspended at 4 °C in 1/3 of original volume RF1 buffer (100 mM RbCl, 50 mM MnCl₂ (tetrahydrate), 30 mM KOAc, 10 mM CaCl₂ (di-hydrate), pH 5.8 was adjusted by HOAc, filtered) and incubated for 15 min on ice. Cells were pelleted again at 500 × g for 15 min at 4 °C and resuspended in 1/25 of original volume RF2 buffer (10 mM MOPS/NaOH pH 6.8, 10 mM RbCl, 75 mM CaCl₂ (di-hydrate), 15% (w/v) glycerol, filtered) and incubated for 15 min

on ice. Cells were aliquotted in a volume of 25-50 μ l, frozen in liquid nitrogen and stored at -80 °C.

For transformation, cells were set on ice for 15 min and incubated for additional 15 min with plasmid DNA (0.01-1 μ g, as a rule of thumb 1 μ l). For transformation, cells were heat shocked for 45 s at 42 °C, set on ice for 2 min, and mixed with 100-200 μ l LB media. After an incubation at 37 °C for 0.5-1 h cells were plated onto an agarose (1%, w/v) plate with selective LB media containing antibiotics (ampicillin or carbenicillin, kanamycin, or others). Plates were incubated over-night at 37 °C and clones were picked for inoculation or colony PCR the next day. Plates were stored at 4 °C for several weeks. Liquid cultures were stored by 1:1 mixture with glycerol (86%, autoclaved) and flash freezing.

2.2.5 Transformation into *S. cerevisiae*

Single or multiple plasmids were transformed into *S. cerevisiae* strains by a standard high-efficiency yeast transformation method based on lithium acetate, sheared salmon sperm carrier DNA and polyethylenglycol (PEG3350, importantly, this PEG variant is pH stable over time) as described previously by (Gietz & Schiestl, 2007).

Yeast cells were cultured over-night in 3 ml yeast extract peptone dextrose (YPD) media. 50-100 ml media was inoculated with the complete over-night culture and incubated for 4 h at 30 °C. The cells were pelleted at 5,000 \times g, washed twice with Milli-Q® water by pelleting, and resuspended in 1-2 ml water. 100 μ l yeast cell suspensions were pelleted and 360 μ l transformation mix was added (240 μ l 50% PEG3350, 36 μ l 1 M LiOAc, 1 μ g DNA, 10 μ l sheared salmon DNA (10 mg/ml), and Milli-Q® water up to 360 μ l total volume). The cells were vortexed and incubated for 40 min at 42 °C. Milli-Q® water was added directly, mixed, and cells were pelleted and washed again with Milli-Q® water. Finally, cells were resuspended in 50 μ l Milli-Q® water. Cells were plated on agarose with minimal media that lacked single or several nutrients and/or toxic metabolites were added, *e.g.* 5-fluoroorotic acid (5-FOA), and/or antibiotics (G418 for *KanMX4* selection) as described previously by (Dunham *et al.*, 2015). Amino-acid drop-out supplements, agarose, 5-FOA and G418 were obtained from FORMEDIUM.

Agarose plates were produced by separate autoclaving of agarose, yeast nitrogen base, amino acid mix, ammonium sulfate; and carbon source solutions (e.g. glucose). All autoclaved components were mixed at 60 °C, optionally antibiotics were added, and then the media was poured into the plates for cool down and solidification.

2.2.6 Colony PCR

Colony PCR was used for verification of DNA content in cells or deficiency strains of a yeast clone based on a protocol by M.L. Summers (Department of Biology, California State University Northridge, 'Colony PCR', <http://www.csun.edu/~mls42367/Protocols/Colony%20PCR.pdf>, downloaded and state as of 01.04.2014). A colony was picked and resuspended in a PCR tube in 50 µl reaction mixture (1x Taq polymerase buffer, 1.5 mM MgCl₂, 0.2 mM dNTPs, 0.4 µM forward and reverse primers, 0.5 µl Taq polymerase (Thermo Fischer Scientific)). The PCR was performed in the thermocycler Tpersonal (Biometra) with the following program: 5 min 95 °C, (1 min 95 °C, 1.5 min 54 °C, 1 min/kb + 1 min 72 °C)_{x30}, 5 min 72 °C, ∞ 4 °C. The reaction was analyzed by agarose gel electrophoresis for corresponding bands in size.

2.3 General biochemical techniques

2.3.1 Protein, RNA and nucleotide concentration determination by absorption

Concentrations were calculated by sample absorption (A_λ) and specific extinction coefficients at indicated wavelengths. Sample absorption was measured in the NanoDrop spectrophotometer ND-1000 (Thermo Fischer Scientific). The concentration (c) was calculated by the Beer-Lambert law ($A_\lambda = \epsilon_\lambda \cdot c \cdot d$), the depth (d) was set to 0.1 cm for the measurements at the NanoDrop in the *UV-Vis mode*. All extinction coefficients (ϵ_λ) are listed in **Table 3**. The theoretical molecular weight, pI , and extinction coefficients were obtained by calculation in the ExPASy *ProtParam tool* based on the protein sequence (Artimo & Jonnalagedda *et al.*, 2012). *S. solfataricus* ABCE1 and ribosome extinction coefficients were used as previously published (Tastan, 2003, Acker *et al.*, 2007, Barthelme, 2010).

Table 3 | Extinction coefficients

compound	MW (kDa)	λ_{\max} (nm)	ϵ ($M^{-1}cm^{-1}$)	reference
ScABCE1 _{H6}	69.2	280	29.34E03	ExPASy
SsABCE1 _{H6}	71.2	280	58.72E03	(Barthelme, 2010)
1x[4Fe4S] cluster		410	16E03	(Sweeney & Rabinowitz, 1980)
ScDom34 _{H6}	44.9	280	35.55E03	ExPASy
Scelf6 _{H6}	27.3	280	9.19E03	ExPASy
<i>E.c.</i> 30S ~ <i>S.s.</i> 30S	1,000	260	1.4E07	(Tastan, 2003)
<i>E.c.</i> 50S ~ <i>S.s.</i> 50S	3,000	260	2.8E07	(Tastan, 2003)
<i>E.c.</i> 70S ~ <i>S.s.</i> 70S	4,000	260	4.2E07	(Tastan, 2003)
<i>S.c.</i> 40S	1,500	260	2.0E07	(Acker <i>et al.</i> , 2007)
<i>S.c.</i> 60S	3,500	260	4.0E07	(Acker <i>et al.</i> , 2007)
<i>S.c.</i> 80S	5,000	260	6.0E07	(Acker <i>et al.</i> , 2007)
tRNA	~26	260	7.3E05	(Chudaev <i>et al.</i> , 2013)
ATP	0.57	260	15.4E03	(Gerstein, 2002)
ADP	0.42	260	15.4E03	assumption based on ATP
AMP-PNP	0.51	259	15.4E03	Sigma-Aldrich product information
GTP	0.52	252	13.7E03	(Gerstein, 2002)
sCy3-maleimid	0.776	548	1.62E5	Lumiprobe
sCy5-maleimid	0.803	646	2.71E5	Lumiprobe

2.3.2 Nucleotide preparation

Nucleotides were obtained from Sigma-Aldrich, dissolved in ice-cold Milli-Q[®] water up to a final concentration of about 0.5 M and pH adjusted with 0.5 M NaOH to pH ~6.0 (pH was determined by indicator paper)(procedure by Gerstein, 2002). 1x MgCl₂ was added to avoid the divalent-cation chelation effect and subsequent magnesium depletion upon addition to reaction mixtures as emphasized in (Pisarev *et al.*, 2010). A final concentration of about 0.2 M was adjusted with Milli-Q[®] water. Nucleotides were aliquotted and stored at -80 °C. The concentration of nucleotides was determined by absorption *via* the extinction coefficients (Table 3).

2.3.3 SDS-PAGE

Sodium dodecyl sulfate (SDS) polyacrylamide gel electrophoresis (PAGE) was used for separation of proteins by their molecular weight in a discontinuous gel system according to the Laemmli system (Laemmli, 1970). Gels were prepared with the Mini-Protean Gel Cast System (Bio-Rad laboratories, Inc.) with a 5% (w/v) acrylamide stacking gel/buffer (1.5 M Tris/HCl pH 8.8, 0.4% (w/v) SDS) and 8-15% (w/v) acrylamide separation gel/buffer (0.5 M Tris/HCl pH 6.8, 0.4% (w/v) SDS). Polymerization was initiated upon addition of ammonium persulfate (APS) and *N,N,N',N'*-Tetramethylethylenediamine (TEMED), for a detailed recipe see **Table 4**.

Table 4 | Composition of SDS-PAGE gels

compound	4%	10%	12%	15%	5% (ml)
separation buffer	5	5	5	5	-
stacking buffer	-	-	-	-	1.25
acrylamide/bis-acrylamide (30%, w/v)	2.7	6.7	8	10	0.8
water	12.3	8.3	7	5	2.9
APS	0.16	0.16	0.16	0.16	0.04
TEMED	0.08	0.08	0.08	0.08	0.02

Samples were mixed 1:3 with 4x SDS-PAGE loading buffer (0.2 M Tris/HCl pH 6.8, 8% (w/v) SDS, 40% (v/v) glycerol, 0.08% (v/v) bromphenol blue). If not stated differently, reducing conditions were used in this thesis with 40% (v/v) 2-ME in the 4x loading buffer and samples were heated for 10 min at 95 °C. PageRuler™ Prestained Protein Ladder (5 µl, Thermo Fischer Scientific) was used as protein size marker in SDS-PAGE. If fluorescently active GFP was detected in the gel, the samples were not heated or only to 60 °C. Electrophoresis was performed in the Mini-Protean Gel Cast System (Bio-Rad laboratories, Inc.) in SDS-PAGE running buffer (25 mM Tris/HCl pH 8.3, 192 mM glycine, 0.01% (w/v) SDS) at 175-225 V for about 1 h or until the running front reached the bottom of the gel. Best resolution and sharp

band results were achieved in gels with 10 wells and 1.5 mm thick spacer plates with small loading volumes, hence concentrated samples.

2.3.4 pH-neutral SDS-PAGE

The peptidyl-tRNA bond is labile and hydrolyzed by hydroxides; hence basic conditions must be avoided. The Bis-Tris gel system (NuPAGE, Thermo Fischer Scientific, Moos *et al.*, 1988) fulfills these conditions, and was used by the Inada lab (Tsuboi *et al.*, 2012). The running buffer was 4-morpholineethanesulfonic acid (MES) based (50 mM MES/NaOH pH 7.3, 50 mM Tris Base, 0.1% SDS, 1 mM EDTA) and commercially obtained by FORMEDIUM. The loading dye was changed to the neutral loading dye (40 mM Tris/HCl pH 6.8, 10% (v/v) glycerol, 1.3% (w/v) SDS, 440 mM 2ME, 0.1% (w/v) bromphenol blue). Samples were heated up only to 60 °C because at these conditions GFP was not denatured and remained fluorescently active.

2.3.5 Urea-PAGE

RNA was separated by size for analytical purpose by urea-PAGE gel electrophoresis (Summer *et al.*, 2009). Gels were polymerized in the urea separation buffer (5-12% (w/v) acrylamide/bis-acrylamide (19:1), 8 M urea, 0.1% (w/v) APS, 0.04% TEMED, 1x TBE buffer (89 mM Tris, 89 mM boric acid, 2 mM EDTA, pH 8.0)). Samples were diluted 1:1 with 2x urea-PAGE loading dye (90% (v/v) formamide, 0.5% (w/v) EDTA, 0.1% (w/v) xylene cyanol and 0.1% (w/v) bromphenol blue) and run by electrophoresis for 1 h at 120 V, max. 0.3 A.

2.3.6 Coomassie staining

SDS-PAGE gels were incubated for 20 min in Coomassie staining solution (0.25% (w/v) Coomassie brilliant blue G250, 20% (v/v) methanol, 10% (v/v) acetic acid) and destained over-night in destaining solution (40% (v/v) ethanol, 10% (v/v) acetic acid, 50 % (v/v) water). In later studies, the colloidal Coomassie staining was preferred that was commercially obtained as InstantBlue™ Protein Stain (Expedeon). InstantBlue does not require destaining,

but was washed in water for a clearer result. Gels were archived by photographic documentation.

2.3.7 Silver staining

SDS-PAGE gels were fixed in silverstain_{fixation} solution (50% (v/v) acetone in water, 1.25% (v/v) trichloroacetic acid (TCA) and 0.015% (v/v) formaldehyde). The gel was rinsed three times with water, washed for 5 min in water, and again rinsed with water for three times. The gel was equilibrated in 50% (v/v) acetone solution for 5 min and then equilibrated for 1 min in silverstain_{pretreat} solution (0.033% (w/v) Na₂S₂O₃·5H₂O in water). The gel was rinsed three times with water and impregnated for 8 min in silverstain_{impregnation} solution (0.27% (w/v) AgNO₃, 0.37% (v/v) formaldehyde in water). The gel was rinsed two times with water and developed for 10-20 s in silverstain_{development} solution (2% (w/v) Na₂CO₃, 0.015% (v/v) formaldehyde, 0.0084% (w/v) Na₂S₂O₃·5H₂O in water). The staining reaction was quenched with 1% (v/v) glacial acid in water and the gel was rinsed and stored in water. Gels were archived by photographic documentation.

2.3.8 Immunoblotting

Proteins in SDS-PAGE gels were transferred onto nitrocellulose membranes by electro blotting. The setup was a stack of one layer of Whatman® filter paper (1.5 mm), nitrocellulose membrane (Amersham Protran® 0.45 NC, GE), SDS-PAGE gel, and a second filter paper. All components were equilibrated for 5 min in blotting buffer (25 mM Tris/HCl pH 7.5, 190 mM glycine, 0.1% (w/v) SDS, 20% (v/v) methanol). The transfer was achieved by electro-blotting (Semi-Dry Blot, Bio-Rad laboratories, Inc.) for 30-60 min at 12 V for up to four gels. The membrane was blocked in ib-blocking buffer (5% (w/v) blotto (Roth) in TBST buffer (20 mM Tris/HCl pH 7.5, 150 mM NaCl, 0.2% (v/v) Tween® 20)) for 10 min at room temperature. The first antibody was diluted directly into the blocking solution and incubated with the membrane at 4 °C over-night. NaN₃ (0.05% (w/v)) was added optionally as a preservative for long-term storage at 4 °C. The membrane was washed three times with TBST

buffer for 5 min and incubated for 1 h at room temperature with the secondary antibody that was diluted in TBST buffer. After final three washes with TBST for 5 min, the membrane was developed by incubation for 1 min in freshly prepared ECL solution (100 mM Tris/HCl pH 8.0, 2.5 mM luminol, 0.4 mM coumaric acid, 0.02% (v/v) H₂O₂) or with Clarity™ Western ECL Substrate (Bio-Rad Laboratories Inc.). The chemiluminescence was detected by the Lumi-Imager F1 (Roche) with development times between 0.25 and 5 min.

2.4 Protein production and purification

2.4.1 ABCE1_{H6} from *S. cerevisiae*

All Purification buffers were freshly prepared and pH adjusted after mixing all components. To preserve the FeS clusters of ABCE1, minimal-oxidizing conditions were ensured. All buffers were extensively degassed at vacuum conditions and stirring after pH adjustment. Detergents or reducing agents were added after degassing. All purification steps were performed at 4 °C. Production and purification procedure for ABCE1_{H6} were adapted by the Green lab and instructions of A. Schuller (JHMI, HHMI, Baltimore, USA) and heavily modified in this study.

The plasmid coding for ABCE1_{H6} from *S. cerevisiae* pYes2_ABCE1_H6 (Shoemaker & Green, 2011) was provided by R. Green (JHMI, HHMI, Baltimore, USA) and transformed (Gietz & Schiestl, 2007) into INVSc1 cells (Thermo Fischer Scientific, *MATa/MATα his3Δ1/his3Δ1 leu2/leu2 trp1-289/trp1-289 ura3-52/ura3-52*) that were plated onto selective –URA plates and incubated at 30 °C for several days. A colony was inoculated in 2x 250 ml over-night cultures of –URA media with 2% (w/v) sucrose at 30 °C. 12 l of –URA media with 2% (w/v) galactose and 2% (w/v) sucrose were inoculated at an OD of 0.2-0.4 with the over-night culture and incubated for exactly 16 h at 30 °C. The final OD was about 6. Cells were harvested at 6,000 × g for 8 min at 4 °C and the pellets were frozen at -20 °C.

A 20 ml Pellet was thawed in 100 ml lysis_{ABCE1} buffer (50 mM HEPES/KOH pH 8.0, 300 mM KCl, 10% (v/v) glycerol, 20 mM imidazole, 0.1 mM EDTA, 4 mM 2-ME, 1 Roche cOmplete Cocktail tablet/50 ml). Cells were disrupted in 2-3 rounds at 1.5 MPa by pressure force in a benchtop

CellDisrupter system (Constant Systems). The lysate was cleared at $5,000 \times g$ for 10 min and 1% (v/v) Tween[®] 20 was added. 3 ml Ni-NTA agarose beads (Qiagen) were equilibrated in lysis_{ABCE1} buffer and added. The mixture was incubated in an over-head rotor for 30 min. Beads were pelleted at $600 \times g$ for 5 min and transferred to a gravity flow column and washed with ten column volumes (cv) wash_{ABCE1} buffer (lysis_{ABCE1} buffer w/o protease inhibitor and Tween20). ABCE1_{H6} was eluted in three cv elution_{ABCE1} buffer (wash_{ABCE1} buffer with final 300 mM imidazole). Eluted fractions were diluted 1:5 in IEX-A_{ABCE1} buffer (20 mM HEPES/KOH pH 7.5, 20 mM KCl, 10% (v/v) glycerol, 4 mM 2-ME, 0.1 mM EDTA) and applied to a weak anion-exchange column (HiTrap DEAE Sepharose FF, 5 ml, GE) that was pre-equilibrates in IEX-A_{ABCE1} buffer. The flow-through (FT) was collected and applied to a strong cation-exchange column (HiTrap SP HP, 5 ml, GE) pre-equilibrated with IEX-A_{ABCE1} buffer. ABCE1_{H6} eluted at 500 mM KCl in a gradient with IEX-B_{ABCE1} buffer (IEX-A_{ABCE1} buffer with 1 M KCl). Eluted fractions were collected and concentrated by centrifugal filtration (Amicon[®], 30 K cut-off, Merck Millipore). 1 ml concentrated sample was applied on size exclusion chromatography (SEC, Superdex 75 16/600, GE) equilibrated in SEC_{ABCE1} buffer (20 mM HEPES/KOH pH 7.5, 100 mM KCl, 5% (v/v) glycerol, 4 mM 2-ME, 0.1 mM EDTA) on the Äkta Explorer system (GE). ABCE1_{H6} eluted at 58 ml and fractions were collected, concentrated, and flash frozen in liquid nitrogen.

2.4.2 Dom34_{H6} from *E. coli*

Dom34_{H6} was amplified from *S. cerevisiae* by colony PCR (primers: NcoI_Dom34: CGC-GAGCTCATGCCATGGAGATGAAGGTTATTAGTCTGAAAAAGGATTC; Dom34_H6_BamHI: CGG-GATCCTCAGTGATGGTGATGGTGATGCTCCTCACCATCGTCTTCATCAAGATCG) and cloned *via* NcoI and BamHI restriction sites into the pSA4 vector, as described in **section 2.2**. The plasmid pSA4_Dom34_H6 was transformed into BL21 cells. Cells were grown in LB media with 100 µg/ml ampicillin and 25 µg/ml chloramphenicol. At OD 0.4 protein expression was induced with 0.1 mM IPTG and the cells were grown for 16 h at 16 °C. The basic purification procedure was the same as for ABCE1, see **section 2.4.1**. Cells were cracked by sonification (Branson Sonifier 250, 3 rounds for 2 min with 50% delay and intensity level 7) and cleared

at $5,000 \times g$ for 15 min. The cation exchange chromatography (CIEX) step with potassium was changed to an anion exchange chromatography (AIEX) step with sodium because the pI of Dom34_{H6} is about 5.9. Dom34_{H6} eluted at about 250 mM NaCl. The eluted fractions were concentrated by centrifugal filtration (Amicon®, 10 kDa cut-off, Merck Millipore) and subjected to SEC (Superdex 75 16/600, GE) in SEC_{Dom34} buffer (HEPES/KOH pH 7.5, 500 mM NaCl, 5% (v/v) glycerol, 4 mM 2ME). Dom34_{H6} containing fractions were pooled and flash frozen in liquid nitrogen.

2.4.3 eIF6_{H6} from *E. coli*

eIF6 was purified based on a construct and purification strategy published by the Green lab (Shoemaker *et al.*, 2010). In summary, BL21 cells were transformed with the plasmid pET38b+_eIF6_H6 and grown at 37 °C to an OD about 0.6 in 2xYT media with 50 µg/ml kanamycine and 25 µg/ml chloramphenicol. The culture was cooled down to 15 °C and induced with 0.5 mM IPTG and incubated over-night. Cells were harvested by centrifugation at $5,000 \times g$ for 8 min and pellets were flash frozen in liquid nitrogen. For purification, cells were thawed and re-suspended in lysis_{eIF6} buffer (75 mM HEPES/KOH pH 8.0, 300 mM NaCl, 4 mM 2ME, 20 mM imidazole, 0.1 mM EDTA, 10% (v/v) glycerol), cOmplete protease inhibitor (Roche) 1 tablet/50 ml). The cells were cracked by sonification (Branson Sonifier 250, 3 round for 2 min with 50% delay and intensity level 7) and cleared at $5,000 \times g$ for 15 min. The supernatant was incubated for 30 min at 4 °C with 4 ml Ni-NTA agarose bead slurry (Qiagen) that was equilibrated previously with lysis_{eIF6} buffer. Beads were washed with 10 cv wash_{eIF6} buffer (50 mM HEPES/KOH pH 8.0, 300 mM NaCl, 4 mM 2ME, 20 mM imidazole, 0.1 mM EDTA, 10% (v/v) glycerol). eIF6_{H6} was eluted by 3 cv elution_{eIF6} buffer (50 mM HEPES/KOH pH 8.0, 300 mM NaCl, 4 mM 2ME, 300 mM imidazole, 0.1 mM EDTA, 10% (v/v) glycerol). eIF6_{H6} fractions were concentrated by centrifugal filtration (Amicon®, 5 kDa cut-off, Merck Millipore) and applied to SEC (Superdex 75 16/600, GE) in SEC_{eIF6} buffer (20 mM Tris/HCl pH 7.5, 200 mM NaCl, 0.5 mM EDTA, 1 mM DTT, 5% (v/v) glycerol). Eluted fractions were analyzed by SDS-PAGE and immunoblot. Fractions containing eIF6_{H6} were pooled and concentrated by centrifugal filtration (Amicon®, 5 kDa cut-off, Merck Millipore).

2.4.4 Crude 80S ribosomes

S. cerevisiae BY4741 cells were grown in YPD media to an OD of 1.2, harvested, and resuspended in lysis_{80S} buffer A25/500 (20 mM HEPES/KOH pH 7.5, 500 mM KCl, 25 mM MgCl₂, 4 mM 2-ME). The cells were disrupted by pressure force in 2-3 rounds at 1.5 MPa in a benchtop CellDisrupter system (Constant Systems). The lysate was cleared at 20,000 × g for 10 min. The supernatant was loaded onto a 10–50% sucrose density gradient (SDG) in lysis_{80S} buffer A25/500 and centrifuged in a SW41 rotor (Beckman Coulter) at 200,000 × g for 4 h. 80S fractions were collected and pelleted in the TLA110 rotor (Beckman Coulter) at 417,000 × g for 1 h. Ribosome pellets were resuspended in storage_{80S} buffer (50 mM Tris/OAc pH 7.0, 50 mM NH₄Cl, 5 mM Mg(OAc)₂, 2 mM spermidine, 25% (v/v) glycerol, 5 mM 2-ME) and frozen in liquid nitrogen. This section was reprinted with permission from (Heuer & Gerovac *et al.*, 2017).

2.4.5 Ribosomal subunits

Subunit preparation was based on a protocol from the Green and Lorsch labs (Acker *et al.*, 2007). *Wt* yeast cells or other strains were grown to a final OD of about 1.0 in YPD media. The cells were cracked by vortexing for 5 min at 4 °C with 1 volume 0.7 mm Zirconia Beads (11079107zx, Bio Spec Products Inc.) and 2 volumes subunit lysis_{40/60S} buffer (20 mM HEPES/KOH pH 7.4, 100 mM KOAc, 400 mM KCl, 10 mM Mg(OAc)₂, 2 mM DTT, Roche cOmplete protease inhibitor 1 pill/50ml, 1 mg/ml heparin). The lysate was cleared by centrifugation at 13,000 × g for 20 min at 4 °C in an SS-34 rotor (Thermo Fischer Scientific). Ribosomes were pelleted from the supernatant at 265,000 × g for 106 min at 4 °C in a Ti70 rotor (Beckman Coulter) through a 3 ml sucrose cushion (20 mM HEPES/KOH pH 7.4, 100 mM KOAc, 400 mM KCl, 10 mM Mg(OAc)₂, 2 mM DTT, 1 M sucrose). The pellet was resuspended by gentle shaking in subunit dissociation buffer (50 mM HEPES/KOH pH 7.4, 500 mM KCl, 2 mM MgCl₂, 2 mM DTT). The sample was transferred to 1.5 ml tubes and cleared at 15,000 × g for 3 min. The supernatant was transferred to new tubes and OD₂₆₀ was adjusted to 200. 1 mM puromycin was added from a freshly prepared 100 mM stock in water. Ribosomes were incubated for 15 min on ice and 10 min at 37 °C. Up to 500 µl

ribosomal sample was loaded onto a 5-20% SDG in separation gradient_{40/60S} buffer (50 mM HEPES/KOH pH 7.4, 500 mM KCl, 5 mM MgCl₂, 2 mM DTT, 0.1 mM EDTA) and centrifuged at 50,000 × g for 16 h at 4 °C in a SW41 rotor (Beckman Coulter). Gradients were fractionated in the Gradient Station (BioComp Instruments). Subunit fractions were pooled, concentrated and rebuffed in subunit storage_{40/60S} buffer (20 mM HEPES/KOH pH 7.4, 100 mM KOAc, 2.5 mM MgOAc₂, 2 mM DTT, 250 mM sucrose) by centrifugal filtration (Amicon®, 100 kDa cut-off, Merck Millipore) and stored at -80 °C.

2.4.5.1 Genetic labeling of the small ribosomal subunit by GFP

pYM27 was used for genomic tagging of *asc1* based on the approach published by the Knop lab (Janke *et al.*, 2004) as it was done by A. Hiekel in the Beckmann lab in an internship (Hiekel, 2007). *GFP-KanMX4* was amplified with flanking regions of *asc1-C-terminus* by PCR (Asc1-S3: GTTTGCCGGTTACACCGACAACGTCATTAGAGTTTGGCAAGTTATGACTGCTAACCG-TACGCTGCAGGTCGAC; Asc1-S4: TGACCAATAACTAGAAGATACATAAAAGAACAAATGAACT-TTATACATATTCTTAATCGATGAATTTCGAGCTCG). The PCR product was transformed into BY4743 diploid cells (Gietz & Schiestl, 2007) and selected on G418 plates for the *KanMX4* resistance cassette. Tetrad analysis was performed by P. Kötter and S. Lamberth in order to select for *MAT α* and - α strains carrying *asc1-GFP-KanMX4*, as described in literature (Dunham *et al.*, 2015). The resulting strain MG002 (*MAT α his3 Δ 1 leu2 Δ 0 ura3 Δ 0 YMR116C(asc1)::YMR116C_GFP_KanMX4*) was used for preparation of GFP-labeled ribosomes and 40S subunits.

For *in vivo* stalling of GFP-labeled ribosomes, the labeled *asc1-GFP* was introduced in the *MAT α dom34 Δ ski2 Δ* background (provided by R. Green) that was harboring a *KanMX4* resistance cassette. In MG002, the resistance cassette was exchanged from *KanMX4* to *NAT1* by transformation with *NotI* restricted pAG36 vector (provided by P. Kötter) and selection on nourseothricine plates that yielded the strain MG003 (*MAT α his3 Δ 1 leu2 Δ 0 ura3 Δ 0 YMR116C(asc1)::YMR116C_GFP_NAT1*). MG003 and *dom34 Δ ski2 Δ* strains were crossed and selected on G418 and nourseothricine plates. Tetrad analysis was performed by P. Kötter and S. Lamberth in order to select for a strain that carries *asc1-GFP-NAT1* and *dom34 Δ ski2 Δ*

(*KanMX4*) yielding MG004 (*MATa his3Δ1 leu2Δ0 ura3Δ0 YLR398C(ski2)::KanMX4 YNL001w(dom34)::KanMX4 YMR116C(asc1)::YMR116C(asc1)_GFP_NAT1*). The plasmid pAG426_H6-HA-GFP-Myc₂-Rz was transformed into MG004 for *in vivo* stalling of translation and RNC preparation.

2.4.6 assembly of *vacant* ribosomes

Vacant ribosomes were assembled by mixing subunits, and optionally mRNA and tRNA, in 200 μ l association buffer (20 mM HEPES/KOH pH 7.5, 150 mM KOAc, 5 mM MgCl₂, 2 mM DTT) and incubated for 5 min at 37 °C. Samples were applied onto a 10-30% SDG in association buffer and centrifuged for 4 h at 200,000 \times g at 4 °C in the SW41 rotor (Beckman Coulter). Gradients were fractionated by Gradient Station (BioComp Instruments). 80S fractions were collected, concentrated by centrifugal filtration (Amicon®, 100 kDa cut-off, Merck Millipore) and stored at -80 °C.

2.4.7 *In vivo* stalling of 80S ribosomes

dom34Δski2Δ (provided by R. Green) or MG004 cells were transformed with pAG426_H6-HA-GFP-Myc₂-Rz and selected on -URA plates, see **section 2.2.5**. Clones were inoculated in an over-night culture in 50 ml of -URA selective media with glucose and grown until saturation (OD₆₀₀ about 5-10) at 30 °C. 250 ml media with 2% (w/v) glucose were inoculated at an OD at 0.1 and grown over-day to an OD of about 0.4-2, and used for inoculation of 12 l of culture for over-night expression that reached the next day a final OD of 1.2. The doubling time is about 1-1.5 h. Cells were harvested at 5,000 \times g for 10 min and pellets were flash frozen in liquid nitrogen and stored at -80 °C.

One volume cells (15 ml) was resuspended in 1 additional volume lysis_{RNC} buffer (50 mM HEPES/KOH pH 7.6, 500 mM KCl, 25 mM MgCl₂, 4 mM 2ME, 1 pill/50 ml cOmplete protease inhibitor (Roche), 1 mg/ml Heparin) and disrupted in 2-3 rounds at 1.5 MPa by pressure force in a benchtop CellDisrupter system (Constant Systems). The mixture was highly dense. The sample was cleared at 30,000 \times g for 15 min and loaded onto a 10-30% SDG in lysis_{RNC}

buffer (3 ml/tube) and centrifuged in an SW41 rotor (Beckman Coulter) for 4 h at 200,000 \times g and 4 °C. 80S fractions were collected by Gradient Station (BioComp Instruments). 2 ml Ni-NTA agarose beads (Qiagen) equilibrated in lysis_{RNC} buffer with 0.1 mg/ml tRNA (10 mg/ml Yeast tRNA, cat. no.: AM7119, Thermo Fischer Scientific) were washed in lysis_{RNC} buffer and added to 80S ribosome fractions and incubated for 1 h. The sample was transferred to gravity flow columns and washed with 10 cv of lysis_{RNC} buffer. Ribosomes were eluted with 2 cv elution_{RNC} buffer (50 mM HEPES/KOH pH 7.6, 500 mM KCl, 25 mM MgCl₂, 4 mM 2ME, 100 mM imidazole) and loaded onto a 10-30% SDG in Ribo A buffer (20 mM HEPES/KOH pH 7.6, 100 mM KOAc, 2.5 mM Mg(OAc)₂, 2 mM DTT) and centrifuged in an SW41 rotor (Beckman Coulter) at 50,000 \times g for 16 h at 4 °C. 80S fractions were collected and concentrated by centrifugal filtration (Amicon®, 100 kDa cut-off, Merck Millipore). Samples were analyzed on neutral pH gels in order to preserve the peptidyl-tRNA bond, see **section 2.3.4**. Further, quality control included native PAGE, see **section 2.6.6**.

2.4.8 S100 extract and aminoacylation of tRNA^{Phe}

tRNA aminoacylation was performed as described by the Green lab (Eyler & Green, 2011). The enzyme for the chemical coupling reaction (tRNA-synthetase, 50-70 kDa) was provided in the S100 extract. *Wt* yeast cells were harvested at an OD of 1.0 and cracked by vortexing in lysis_{S100} buffer (10 mM potassium phosphate pH 7.2, 1 pill/50 ml cOmplete® protease inhibitor (Roche)) with 1/3 volume of Zirconia/Silica Beads (0.7/0.5 mm, BioSpec Products) for 5x1 min at 4 °C. Lysate was cleared at 15,000 \times g for 20 min at 4 °C in the SS-34 rotor (Thermo Fischer Scientific) and ribosomes were pelleted for 106 min at 265,000 \times g at 4 °C in the Ti70 rotor (Beckman Coulter). Post-ribosomal supernatant fractions were loaded on a DEAE weak-anion-exchange column (5 ml, GE) and washed with lysis_{S100} buffer and eluted with elution_{S100} buffer (250 mM potassium phosphate pH 6.5). The eluate was concentrated and the buffer was exchanged to storage_{S100} buffer (elution buffer + 5% (v/v) glycerol and 2 mM DTT) by centrifugal filtration (Amicon®, 5 kDa cut-off, Merck Millipore) to an OD₂₈₀ of about 300. The extract was frozen in liquid nitrogen and stored at -80 °C.

Phe-tRNA was purchased as 'ribonucleic acid, transfer, phenylalanine specific from brewer's yeast' (R4018-1MG, Sigma-Aldrich) and solubilized in diethyl pyrocarbonate (DEPC) treated water. The acylation reaction was processed in aminoacylation reaction buffer (30 mM HEPES/KOH pH 7.4, 30 mM KCl, 15 mM MgCl₂, 4 mM ATP/Mg, 100 μM phenylalanine, 5 mM DTT and 1/10 volume S100 extract) for 20 min at 37 °C. Acylated tRNA was extracted by addition of 0.3 M NaOAc pH 5.2 and 1 volume of acid-buffered phenol (Carl Roth). In a second step, the aqueous phase was extracted with one volume of phenol/chloroform/isoamylalcohol (25:24:1). In a third step, the tRNA in the aqueous phase was precipitated by addition of 2.5 volume of 100% ethanol and incubation at -20 °C over-night. After pelleting at 16,000 × g at 4 °C for 30 min, the supernatant was removed, the pellet was dried and solubilized in resuspension buffer (20 mM KOAc pH 5.2, 2 mM DTT, in DEPC treated water). The acylation reaction was verified by reversed-phase high-performance liquid chromatography (RP-HPLC) based on a protocol by the Joseph lab (Studer & Joseph, 2007) using the HPLC system 2000 with MD-2010 (Jasco) and the column PerfectSil 300 ODS C28 5 μm (C18, MZ Analysetechnik) with the buffers A (10 mM Tris/OAc pH 5.0, 400 mM NaCl, 10 mM Mg(OAc)₂) and B (A plus 60% (v/v) methanol). Acylated tRNA eluted at 40-50% buffer B, compared to non-acylated at 25%. Resuspended acylated tRNA was washed with resuspension buffer in centrifugal filter units (Amicon®, 5 kDa cut-off, Merck Millipore), in order to remove nucleotides and remaining reaction components. Finally, acylated tRNA was stored at -80 °C.

2.4.9 80S-mRNA-tRNA^{Phe}

80S ribosomes with mRNA and tRNA and an empty A-site were assembled as described by the Spahn lab (Hilal *et al.*, 2016). 10 pmol ribosomal subunits (see **section 2.4.5**), 200 pmol SDF-mRNA (GGCAAGGAGGUAAAAUUCUA, triplet coding for Phe is underlined, ordered from MWG Eurofins, Hilal *et al.*, 2016), and 20 pmol tRNA^{Phe} (see **section 2.4.8**) were mixed in 100 μl subunit association buffer (20 mM HEPES/KOH, pH 7.4, 100 mM KOAc, 5 mM Mg(OAc)₂, 2 mM DTT, 0.2 mM spermidine) and incubated for 15 min at 30 °C. Ribosomes were separated by SDG in a 10-30% gradient in Ribo A buffer (20 mM HEPES/KOH, pH 7.4,

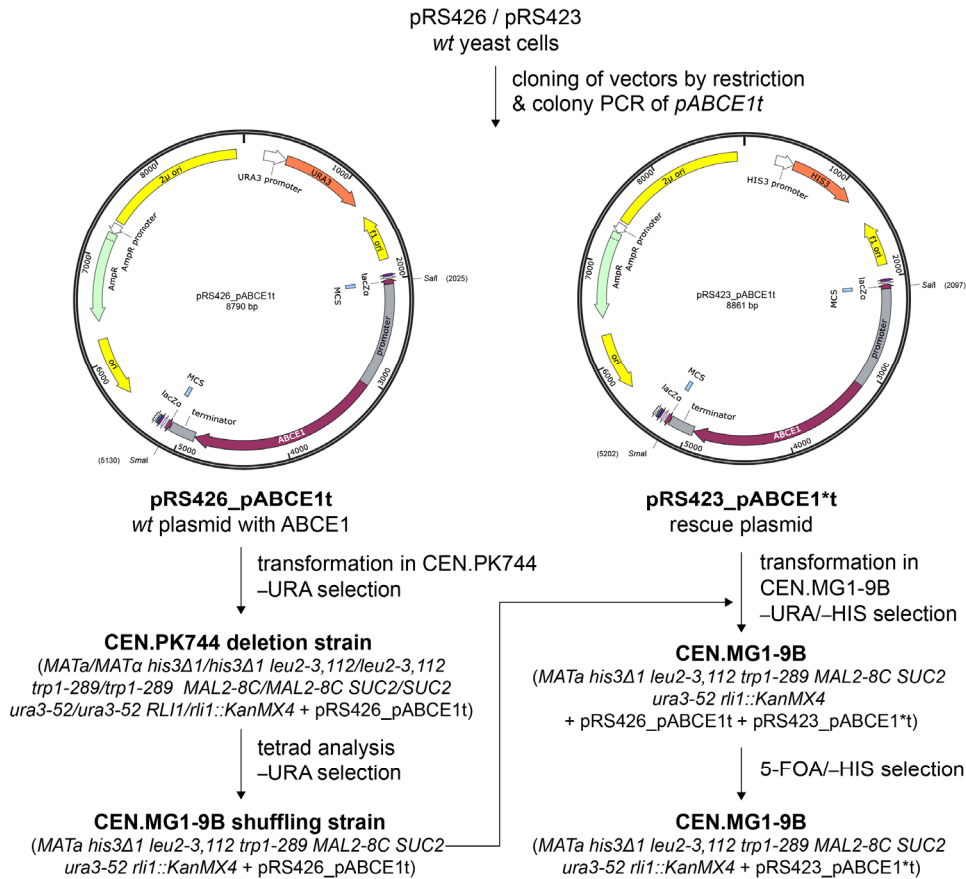
100 mM KOAc, 2.5 mM Mg(OAc)₂, 2 mM DTT, see **section 2.6.1**) for 4 h at 200,000 × g at 4 °C in the SW41 rotor (Beckman Coulter). 80S fractions were selected and analyzed by 8% urea-PAGE, see **section 2.3.5**.

2.5 *In vivo* functional assays

2.5.1 Plasmid shuffling assay in yeast

Viability of strains carrying a mutated *ABCE1** and physiological significance of key residues was checked by a plasmid shuffling assay in which wild-type *ABCE1*, that is exclusively encoded on a plasmid, was exchanged by a mutated *ABCE1** encoded on another plasmid. In a double selection process, strains were selected that carry only the plasmid encoding for the mutant *ABCE1**. Negative selection for the *wt* plasmid was achieved by 5-FOA treatment *via* the *URA3* marker, that encodes for orotidine 5'-phosphate decarboxylase, which converts 5-FOA into the toxic compound 5-fluorouracil. Positive selection for the plasmid carrying the mutated *ABCE1** was achieved by the *HIS3* marker (**Figure 4**). The diploid strain CEN.PK744 (*MATa/MATα his3Δ1/his3Δ1 leu2-3,112/leu2-3,112 trp1-289/trp1-289 MAL2-8C/MAL2-8C SUC2/SUC2 ura3-52/ura3-52 RLI1/rli1::KanMX4*) was transformed with pRS426-pABCE1t [URA3] and selected on SCD-URA. After tetrad dissection, the haploid yeast strain CEN.MG1-9B (*MATa his3Δ1 leu2-3,112 trp1-289 MAL2-8C SUC2 ura3-52 rli1::KanMX4 + pRS426_pABCE1t*) was isolated, in which the essential *ABCE1* gene (*RLI1*) was deleted by *KanMX4* and substituted by pRS426-pABCE1t expressing *wt ABCE1* under the control of the endogenous promoter. Tetrad analysis was performed by P. Kötter and S. Lamberth. Plasmids pRS423_pABCE1*t [*HIS*] and pRS426_pABCE1t [*URA*] were cloned by amplification of the *ABCE1* gene with primers in the promoter and terminator region and integrated into the vector *via* restriction sites *Sall* and *SmaI* by primer extension based PCR from genomic material (f_ *Sall*_p_ *ABCE1*: GGGCGAATTGGGTACCGGGCCCCCCTCGAGGTCGACGGTATCGA-TAAGCTTGCCCGCGGCTCCCGCAGAATCTAATCATTAAGCTTGACTAG and r_ *SmaI*_t_ *ABCE1*: GCTCCACCGCGGTGGCGGCCGCTCTAGAACTAGTGGATCCCCGGGCTGCTAAACTGGAGTAC -GGATCACCGAAGAGGAGG). Reprinted with permission from (Heuer & Gerovac *et al.*, 2017).

a



b

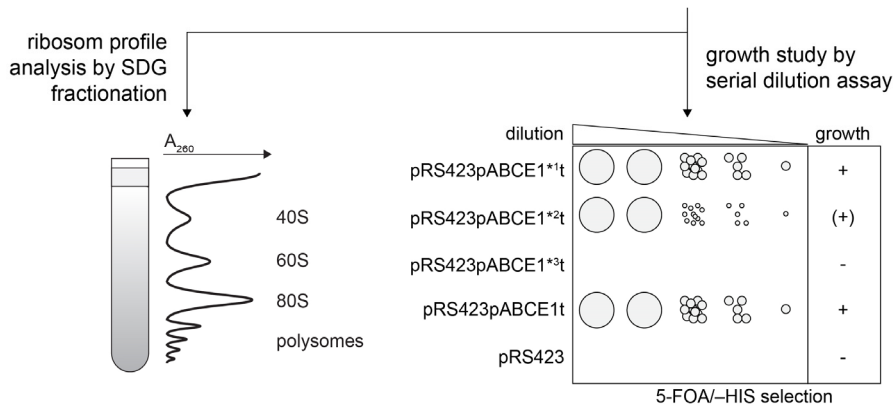


Figure 4 | Plasmid shuffling assay development. **a**, wt *ABCE1* with promoter (1000 bp) and terminator (250 bp) regions was amplified by colony PCR and cloned into pRS423/426 by restriction sites *Sall* and *SmaI*. pRS426_pABCE1t was transformed into the diploid CEN.PK744 strain, in which *ABCE1* is deleted on one allele, and selected on -URA media. Tetrad analysis revealed the haploid strain CEN.MG1-9B that is rescued by wt *ABCE1* on pRS426_pABCE1t. CEN.MG1-9B was transformed with pRS423_rABCE1*t and selected on -URA/-HIS media. wt *ABCE1* plasmid pRS426_pABCE1 was eliminated by 5-FOA treatment and selection on 5-FOA/-HIS media. The resulting strain is fully relying on the pRS423_pABCE1*_t plasmid carrying the supplementation. P. Kötter supervised me in the generation of the plasmid shuffling assay and performed with S. Lamberth the tetrad analysis for the strain CEN.MG1-9B. **b**, To probe for ribosome homeostasis or growth defects, ribosome profile analysis, and growth assays by serial dilution were performed, respectively.

2.5.2 Growth studies by serial dilution

Yeast cells were grown to an OD about 3.0, washed, and concentrated in water by pelleting at $10,000 \times g$ in a tabletop centrifuge for 1 min. The cell concentration was adjusted to OD 1.0 and diluted in serial dilution by 3-10 fold per step in a 96-well plate in water. A flame treated steel stamp was used to spot the cell dilutions on a plate. The cells were grown on the plate over-night or for several days at 30 °C and imaged. The plate selection media was chosen based on the assay and as indicated in the figures.

2.5.3 Ribosome profile analysis by SDG

Indicated strains were grown to an OD of 1.5. One volume of the cell pellet was re-suspended in two volumes Ribo A buffer (20 mM HEPES/KOH, pH 7.4, 100 mM KOAc, 2.5 mM Mg(OAc)₂, 2 mM DTT) and disrupted by addition of one volume Zirkonia beads (0.7 mm, BioSpec Products) and 5 min vortexing. The lysate was cleared at $15,000 \times g$ for 5 min and adjusted by addition of Ribo A buffer to an OD₂₆₀ of 10. 300 µl were loaded on a 10-50% SDG in Ribo A buffer and centrifuged for 14 h at $50,000 \times g$ at 4 °C in the SW41 rotor (Beckman Coulter). The ribosome A₂₆₀ profile was recorded and the gradient was collected in fractions of 600 µl in the Gradient Station (BioComp Instruments). Fractions were precipitated by addition of 7% (w/v) trichloroacetic acid and 0.02% (w/v) sodium deoxycholate and pelleted at $15,000 \times g$ for 5 min. Pellets were resuspended in SDS-PAGE loading buffer with additional 750 mM Tris/OAc pH 8.0 and analyzed by SDS-PAGE and immunoblot for the HA-tag (primary antibody: anti-HA (Abcam, [HA.C5], #ab18181); secondary antibody: anti-mouse IgG, HRP conjugate (Promega, #W4021)).

2.5.3.1 Gradient preparation, harvesting, and profile visualization

SW41Ti Open-top Polyclear™ centrifuge tubes (9/16x3-1/2 in., SETON) were filled with 5.75 ml 5/10% (w/v) sucrose solution and sub layered with 20/30/40/50% (w/v) sucrose solution in indicated gradient buffer. Rubber caps sealed the tube. The gradient was rotated on the gradient mixer Gradient Master ip (BioComp Instruments) using the appropriate

program in the system. Caps were removed and 0.1-1 ml of the gradient was discarded. 50-3,000 μl samples were loaded onto the gradient. Samples were balanced with gradient or sample buffer and the gradient was centrifuged at indicated duration and relative centrifugal field (RCF in g) in the SW41 rotor (Beckman Coulter). Gradients were fractionated using the Gradient Station (BioComp Instruments) at 0.5 ml/min speed. The ribosome profile data were recorded by WinDAQ (DATAQ Instruments) and analyzed in Origin (OriginLab).

2.6 *In vitro* functional assays

2.6.1 Ribosome profile analysis

The protocol was the same as for *in vivo* functional assays with lysates. Indicated buffers and reaction volumes were used, see **section 2.5.3**.

2.6.2 Radioactive NTPase assay

NTPase activity of ABCE1 was analyzed by formation of $^{32}\text{P}_i$ upon hydrolysis of $\gamma\text{-}^{32}\text{P}$ labeled GTP as previously described (Pisarev *et al.*, 2010, Shoemaker & Green, 2011). NTPase stimulation in ABCE1 was assayed by incubation of 0.066 μM ABCE1, 0.25 μM Dom34, 0.12 μM 40S or *vacant* 80S ribosomes, 0.1 mM ATP, 0.1 mM GTP and 0.8 μM $\gamma\text{-}^{32}\text{P}$ -GTP in 10 μl at 30 °C for 0, 5, 10, and 20 min in NTPase buffer (20 mM Tris/HCl pH 7.5, 100 mM KCl, 2.5 mM MgCl_2 , 0.25 mM spermidine, 2 mM DTT). 1 μl aliquots were spotted on polyethylene imine cellulose thin layer chromatography plates (Merck Millipore) and resolved in 0.8 M LiCl and 0.8 M acetic acid. The system was robust and allowed reactions at high temperature for over 1 h in the case of reaction components from *S. solfataricus*, there was no hypersensitivity of nucleotide hydrolysis. Release of $^{32}\text{P}_i$ was monitored by autoradiography. Intensity of spots was analyzed by the ImageJ (NIH) *gel analysis tool* based on densitometry. Evaluation was performed in Origin (OriginLabs) based on single exponential and linear regressions. This paragraph was partly reprinted with permission from (Heuer & Gerovac *et al.*, 2017).

2.6.3 Colorimetric NTPase assay

ATP hydrolysis was measured by a modified colorimetric malachite-green assay (Morbach *et al.*, 1993). The hydrolysis reaction was performed in a total volume of 25 μ l in a microplate in indicated buffers with 1 μ M ABCE1_{H6}, 10 μ M ribosomal subunits, and 2 mM ATP in triplicates. The samples were incubated at room temperature for 15-30 min in an incubator. ATP hydrolysis was quenched by addition of 175 μ l of ice-cold 20 mM H₂SO₄. The malachite-green solution was prepared by mixing of 10 ml >95% (w/v) H₂SO₄ in 40 ml Milli-Q[®] water and 73.4 mg malachite-green resulting in the concentrated malachite-green solution. Shortly before usage 2 ml of concentrated malachite-green solution were mixed with 0.5 ml 7.5% (w/v) NH₄Mo₇·4H₂O and 40 μ l 11% (v/v) Tween[®] 20 resulting in the final malachite-green solution. 50 μ l malachite-green solution were added to the quenched reaction and the colorimetric reaction was detected after 5 min incubation at room temperature by absorption at 620 nm in a fluorescence plate reader (FLUOstar Galaxy, BMG). The phosphate concentration was determined by a standard curve based on K₂PO₄.

2.6.4 Anti-association assay and preparation of the 40S–ABCE1 complex

The assay was developed based on the anti-/re-association assay to validate binding of the anti-association factor eIF6 to the large ribosomal subunit (Groft *et al.*, 2000). ABCE1_{H6} and variants (R7A, P30A, N78A, H95A, and Y301A) were expressed in INVSc1 yeast cells and purified as described, see **section 2.4.1**. High salt washed crude 80S ribosomes, see **section 2.4.4**, were mixed with ten molar excess of ABCE1_{H6} and 0.5 mM AMP-PNP in splitting facilitating buffer (20 mM HEPES/KOH pH 7.4, 515 mM KCl, 2 mM MgCl₂, 1 mM DTT), and incubated for 20 min at 25 °C. The sample was diluted 1:0.7 with re-association buffer (20 mM HEPES/KOH pH 7.4, 100 mM KCl, 25 mM MgCl₂, 1 mM DTT) and incubated for 20 min at 25 °C, cooled down to 4 °C, loaded onto a 10-30% SDG in grid buffer (20 mM HEPES/KOH pH 7.4, 100 mM KOAc, 5 mM MgCl₂, 2 mM DTT), and centrifuged at 200,000 \times g for 4 h in the SW41 rotor (Beckman Coulter). In the case of 40S–ABCE1 sample preparation for cryo-EM reconstruction, 1 mM MgCl₂ and 500 mM KCl were used in the splitting facilitating buffer, and the sample was loaded onto a 10-50% SDG and 40S fractions were

collected and re-buffered in grid buffer by PD-10 columns (GE Healthcare). The sample was diluted in grid buffer to a final ribosome concentration of 50 nM and used for cryo-EM sample preparation. This paragraph was reprinted with permission from (Heuer & Gerovac *et al.*, 2017).

2.6.5 Ribosome pelleting assay

Reactions were mixed in a total volume of 5 μ l in buffer E (20 mM Tris/HCl pH 7.5, 2.5 mM Mg(OAc)₂, 100 mM KOAc, 2 mM DTT, 0.25 mM spermidine), nucleotides (1 mM), and competitors (10 mM) were added simultaneously, ribosomes (0.2-1 μ M) and ABCE1_{H6} (1 μ M) was added as the last component as indicated for each reaction at 4 °C. The reaction mixture was set at room temperature for 20 min and stopped on ice. Samples were diluted with 50 μ l buffer E and pelleted through 0.6 ml 1.1 M sucrose cushion with buffer E for 1 h at 264,000 \times g at 4 °C in the MLA-130/TLA-120.2 rotor (Beckman Coulter). Pellets were resuspended in SDS loading buffer, heated at 95 °C for 10 min and were re-analyzed *via* SDS-PAGE and immunoblot. Sample loading differences were avoided by loading of the complete sample. Input controls served as pelleting efficiency control. ABCE1_{H6} was detected by the anti-His antibody (dilution 1:3,000 for Sigma-Aldrich, #H-1029).

2.6.6 Native PAGE and ribosome splitting assay

In the Green lab, the split ribosomal subunits were resolved in native PAGE using large sequencing gels that were 0.4 mm thick. I switched to small gels and increased the thickness to 1.5 mm. The gel composition was the same as reported by the Lorsch lab (Acker *et al.*, 2007). 3-4% acrylamide gels were required in order to preserve the sensitive subunit association. 3-4% 37.5:1 acrylamide:bis-acrylamide (Carl Roth) were mixed in THEM buffer (34 mM Tris, 57 mM HEPES, 0.1 mM EDTA, 2.5 mM MgCl₂, used as 10x stock) and polymerized upon addition of 0.1% (w/v) APS and 1 μ l/ml TEMED. The glass plates must be clamped and a 10 well comb will result in well-resolved bands, but also a comb up to 36 wells is usable at this scale, that was 3D-printed for me by P. Höllthaler.

Splitting reactions were performed in buffer E (20 mM Tris/HCl pH 7.5, 10 mM Mg(OAc)₂, 100 mM KOAc pH 7.6, 2 mM DTT, 0.25 mM spermidine; added as a 10x stock solution) in a total volume of 25 µl. The reaction mixture contained 1 mM indicated nucleotides with 1x magnesium, 100 pmol recycling factors Dom34_{H6}, and ABCE1_{H6}, and 200 pmol eIF6 (625 µM stock, but highly impure) as ribosome subunits re-association inhibitor. 4 pmol recycling competent RNCs were used for splitting (that were provided by the Green lab and generated by A. Schuller, JHMI, HHMI, Baltimore). RNCs were programmed on an mRNA coding for MF (AAUCUCUCUCUCUCUCUAUGUUCUUC, start codon is underlined, the mRNA was generated by T7 transcription). ³²P-tRNA coding for Phe paired with the mRNA in the elongation step (Shoemaker & Green, 2011). Reactions were incubated at 30 °C. At indicated time points, 2 µl samples were taken out of the reaction mix and quenched upon mixture with cold 2x native gel dye (50% (w/v) sucrose, 0.02% (w/v) bromophenol blue, 0.02% (w/v) xylene cyanol, (Acker *et al.*, 2007)). 2 µl of the quenched samples were loaded onto the running gel (3-4% THEM, no lid present, danger of high voltage!), directly after indicated time points. In order to read out radioactivity from a gel, it was dried by a gel drier (Model 583, Bio-Rad Laboratories Inc.). The gel was set onto a photostimulable phosphor plate and luminescence was detected by the Typhoon 9400 scanner (Amersham Biosciences/GE).

The native PAGE system was optimized towards small 4% polyacrylamide gels (10x8 cm) with 1.5 mm thickness. Gels were electrophoresed at 12 W for 45 min to 1 h.

Detection of RNA by fluorescence was achieved by ethidium bromide or SYBR® Gold (Life Technologies) staining in TAE buffer (40 mM Tris/20 mM HOAc pH 8.0, 1 mM EDTA, used as 50x stock) and a subsequent washing step with buffer only. *In vivo* stalled RNCs and other fluorescently labeled ribosomes were used in the assay as described above. The fluorescence in gels was detected by the Typhoon 9400 scanner (Amersham Biosciences/GE). For GFP, blue laser at 488 nm excited the fluorophore and the emission filter at 520 nm was used for detection.

2.7 Cryo-EM reconstruction

2.7.1 Electron microscopy and image processing of the 40S–ABCE1 complex

The reconstituted 40S–ABCE1 complex was obtained after *facilitated splitting* as described above, see **section 2.6.4**. Freshly prepared samples were adjusted to A_{260} of 1.5 (50 nM 40S ribosomes) and applied to 2-nm pre-coated Quantifoil R3/3 holey carbon supported grids.

Image processing of the 40S–ABCE1 complex was done by A. Heuer, T. Becker, and O. Berninghausen from the Beckmann lab (Gene Center, LMU, Munich)(Heuer & Gerovac *et al.*, 2017). Data were collected on a Titan Krios TEM (FEI Company) equipped with a Falcon II direct electron detector at 300 keV under low dose conditions of about $2.4 \text{ e}^-/\text{\AA}^2$ per frame for 10 frames in total using the software EM-TOOLS (TVIPS) and a defocus range of -0.8 to -2.4 μm . Magnification settings resulted in a pixel size of 1.084 $\text{\AA}/\text{pixel}$. Original image stacks were summed and corrected for drift and beam-induced motion at micrograph level using MotionCor2 (Zheng *et al.*, 2017). The contrast transfer function parameters and resolution range of each micrograph were estimated by Gctf (Zhang, 2016).

In the case of the reconstituted 40S–ABCE1 complex, only micrographs showing a clear signal below 4 \AA resolution were used. All 2D and 3D classifications and refinements were performed with RELION-2 (Kimanius & Forsberg *et al.*, 2016) after automated particle picking by Gautomatch (<http://www.mrc-lmb.cam.ac.uk/kzhang/>, state as of 01.06.2017). Two-dimensional reference-free classification was performed to screen for particle quality (**Figure 24**), non-ribosomal particles as well as poorly resolved 2D classes were discarded. 518,000 particles from good classes were selected for 3D refinement. Notably, the first 3D reconstructions displayed a distortion in one direction resulting from preferred orientation of 40S particles on the carbon-coated grid and misalignment. We performed two subsequent rounds of 3D classification in order to omit poorly aligned and distorted particles and to enrich 40S subunits with bound ABCE1. First, the whole dataset was classified into 4 classes: class 1 and 2 contained poorly resolved and distorted 40S ribosomes, whereas class 3 and 4 showed well-resolved 40S ribosomes with a strong ABCE1 density. Class 3 and 4 were joined (401,000 particles) for a second round of 3D classification. Here, we used a mask for the well-resolved 40S body including ABCE1 and excluded the highly flexible 40S head,

which impaired the alignment. Four out of five classes (299,000 particles in total) showed a strong distortion and were discarded. The best resolved class (102,000 particles) showed a well resolved 40S body with stoichiometric occupancy of ABCE1. This final volume was refined to 3.9 Å according to the *gold standard* criterion (FCS = 0.143), corrected for the modulation transfer function of the Falcon 2 detector and sharpened by applying a negative B-factor automatically estimated by RELION-2. Local resolution was calculated from 3.5 to 8.5 Å in steps of 0.5 Å using ResMap (Kucukelbir *et al.*, 2014).

This section was reprinted with permission from (Heuer & Gerovac *et al.*, 2017).

2.7.2 Model building of the 40S–ABCE1 complex

Model building of the 40S–ABCE1 complex was done by myself and T. Becker, A. Heuer, and C. Schmidt from the Beckmann lab (Gene Center, LMU, Munich).

For molecular interpretation, we used the crystal structure of the yeast 40S ribosomal subunit (PDB: 4V88, Ben-Shem & Garreau de Loubresse & Melnikov *et al.*, 2011) and generated homology models of ABCE1 based on the crystal structures of archaeal ABCE1 and known structures of the closed state of other ABC transporters (MalK (Oldham & Chen, 2011), BtuCD (Korkhov *et al.*, 2014), MJ0796 (Smith *et al.*, 2002)). Models were initially fitted into the electron density using UCSF Chimera (Pettersen *et al.*, 2004) and *jiggle-fitted* using Coot (Brown *et al.*, 2015, Emsley & Cowtan, 2004). Because of flexibility (**Figure 24**), the local resolution of the 40S head was significantly lower compared to the 40S body (**Figure 25**). Thus, only the model of the 40S body with ABCE1 (40S_{BODY}–ABCE1, see **Table 11**) was used for subsequent model refinement. First, the 40S_{BODY}–ABCE1 model was subjected to real-space refinement in PHENIX (Adams *et al.*, 2010). Afterwards, the model was further subjected to reciprocal space refinement using REFMAC (v5.8, Murshudov *et al.*, 1997) and restraints generated by ProSMART and LIBG as previously shown (Amunts & Brown & Bai & Llácer *et al.*, 2014, Brown *et al.*, 2015). To avoid overfitting, refinement weights were carefully estimated as described (Fernández *et al.*, 2014). FSC_{average} was monitored throughout the refinement and the final model was validated using *MolProbity* (Chen *et al.*, 2010). Cross-validation against overfitting was performed as described (Amunts & Brown & Bai & Llácer

et al., 2014, Fernández *et al.*, 2014). Figures were created with the PyMOL Molecular Graphics System (Version 1.7.4, Schrödinger, 2015) and with UCSF Chimera (Pettersen *et al.*, 2004).

This section was reprinted with permission from (Heuer & Gerovac *et al.*, 2017).

2.7.3 Preparation of the 30S–ABCE1 complex

50 nM *S. solfataricus* 30S were incubated with 100 nM *S. solfataricus* ABCE1(E238A/E485A) and 2 mM AMP-PNP in binding buffer (20 mM Tris/HCl pH 7.5, 100 mM KCl, 5 mM MgCl₂, 2 mM DTT) for 5 min at 25 °C. Samples were vitrified by the Beckmann lab (Gene Center, LMU, Munich) on carbon-supported grids by standard procedures for cryo-EM imaging. For preparation of 30S subunit and ABCE1 from *S. solfataricus*, see published methods in (Kiosze-Becker *et al.*, 2016). This section was reprinted with permission from (Kiosze-Becker *et al.*, 2016).

2.7.4 Electron microscopy and image processing of the 30S–ABCE1 complex

Reconstruction of cryo-EM data was done by A. Heuer and T. Becker from the Beckmann lab (Gene Center, LMU, Munich). A. Heuer and I optimized the sample preparation *via* imaging of negative stained grids and prepared the final sample for cryo-EM. A freshly prepared sample was applied to 2 nm pre-coated Quantifoil R3/3 holey carbon supported grids and vitrified using a Vitrobot Mark IV (FEI Company). Visualization was performed on a Spirit TEM microscope (FEI Company) with about 20 e⁻Å⁻² at a nominal magnification of 105,000x with a nominal defocus between -1 μm and -3.5 μm. Automatic particle detection was performed by the program SIGNATURE (Chen & Grigorieff, 2007). Initial *in silico* sorting of the data set consisted of 54,800 particles in total and was performed using the SPIDER software package (Chen & Grigorieff, 2007). Classes were obtained by competitive projection matching in SPIDER (Leidig *et al.*, 2014, Penczek *et al.*, 2006). The final 30S–ABCE1 data set contained 19,500 particles and the final resolution was 17 Å (Fourier shell correlation 0.5).

This paragraph was reprinted with permission from (Kiosze-Becker *et al.*, 2016).

2.7.5 Model building of the 30S–ABCE1 complex

For interpretation of the 30S–ABCE1 electron density at a molecular level, the models for the *P. furiosus* 30S subunit (PDB: 4V6U, Armache & Anger *et al.*, 2013) and ribosome-bound ABCE1 in (3J15, Becker & Franckenberg *et al.*, 2012) were fitted as rigid bodies using UCSF Chimera. The FeS cluster domain was repositioned by a rotation of $\sim 160^\circ$ around a hinge (residues 76–78) into an unaccounted electron density near ribosomal protein S12, based on the structure of 40S–ABCE1 (Heuer & Gerovac *et al.*, 2017). This section was reprinted with permission from (Kiosze-Becker *et al.*, 2016).

2.7.6 Preparation of the native 40S–ABCE1 complex

Preparation of the native 40S–ABCE1 complex was done by A. Heuer and A. Preis from the Beckmann lab (Gene Center, LMU, Munich) and was published in (Heuer & Gerovac *et al.*, 2017). For tandem affinity purification of 40S–ABCE1 complexes, the TAP-tagged ABCE1 yeast strain was used (*SC1900, MATa leu2-3 112 trp1-289 ade2 arg4 ura3-52 rli1::TAP-KIURA3*, EUROSCARF). Cells were grown in YPD media to an OD_{600} of 1.5. The cells were spun down and washed with 1% (w/v) KCl at 4 °C, then incubated for 15 min at 25 °C in 10 mM DTT with 100 mM Tris/HCl pH 8.0, and finally resuspended in lysis buffer (50 mM Tris/OAc pH 7.5, 15 mM $Mg(OAc)_2$, 50 mM KOAc, 1 mM DTT, 300 nM AMP-PNP, 300 nM GMP-PNP, 500 nM PMSF, 1 pill/50 ml Roche cOmplete EDTA-free Protease Inhibitor Cocktail). The cell suspension was processed in a cell disruptor at 1.5 MPa and the lysate was spun in a SS-34 rotor (Thermo Fischer Scientific) at $27,000 \times g$ for 15 min to remove cell debris. The lysate was clarified in a 45Ti rotor (Beckman Coulter) for 20 min at $119,000 \times g$. The cleared lysate was incubated with IgG Sepharose 6 FastFlow beads (GE) for 1 h at 4 °C. The beads were washed with TAP buffer (50 mM Tris/OAc pH 7.5, 15 mM $Mg(OAc)_2$, 50 mM KOAc, 1 mM DTT, 500 nM PMSF, 1 pill/50 ml Roche cOmplete EDTA-free Protease Inhibitor Cocktail). For elution, the beads were incubated with AcTEV protease (Thermo Fischer Scientific) in TAP buffer for 90 min at 4 °C. The eluate was loaded onto a 5–30% SDG in TAP buffer and centrifuged in a SW41 rotor (Beckman Coulter) for 15 h at $56,000 \times g$. 40S fractions were

collected and sucrose was removed using a PD-10 column (GE). The sample was then used for cryo-EM. This section was reprinted with permission from (Heuer & Gerovac *et al.*, 2017).

2.7.7 Electron microscopy, image processing, and model building of the native 40S–ABCE1 complex

Reconstruction of the native 40S–ABCE1 complex was possible by the available high-resolution structure of the post-splitting complex and done by T. Becker, A. Heuer, A. Preis and O. Berninghausen from the Beckmann lab (Gene Center, LMU, Munich) and published in (Heuer & Gerovac *et al.*, 2017).

The native 40S–ABCE1 data set was chiefly processed in the same way as the reconstituted sample using MotionCor2, Gctf, Gautomatch and RELION-2, see **section 2.7.1**. 2D classes that displayed non-ribosomal particles as well as the fatty acid synthetase (FAS) were discarded. After 3D refinement of 131,000 particles, 3D classification was performed. In the first round, three classes (63.0%, 82,000 particles) showed a clear density for ABCE1 and two of them presented additional extra density emerging from the P-site. The later ones (43.5%, 57,000 particles) were joined for a second round of classification. Here, four out of five classes only differed in the appearance of the density in the P-site. One class displayed additional density in the position where eIF1A is located. This class (17.6%, 9,500 particles) was refined to a final resolution of 14 Å according to the *gold standard* criterion (FSC = 0.143). The ABCE1 model of the post-splitting state could be fit as a rigid body into the native 40S–ABCE1 complex without further adjustments. eIF1A as well as tRNA_i could be identified by rigid body fitting of 43 and 48S-initiation complex structures (eIF1A from PDB: 4UER, Ben-Shem & Garreau de Loubresse & Melnikov *et al.*, 2011), tRNA_i from PDB: 3JAP (Llácer & Hussain *et al.*, 2015)).

This section was reprinted with permission from (Heuer & Gerovac *et al.*, 2017).

2.7.8 Data availability

EM density maps were deposited by A. Heuer in the 3D-EM database (reconstituted 40S–ABCE1 complex: EMD: 4071, native reconstituted 40S–ABCE1 complex: EMD: 3452) and the coordinates and EM-based models were deposited in the Protein Data Bank (post-splitting complex, PDB: 5LL6). This paragraph was reprinted with permission from (Heuer & Gerovac *et al.*, 2017).

The structural coordinates of ABCE1 and the electron density map of the archaeal 30S–ABCE1 complex were deposited by A. Heuer in the Protein Data Bank under (PDB: 5LW7) and the 3D-EM database (EMD: 4113). This paragraph was reprinted with permission from (Kiosze-Becker *et al.*, 2016).

2.8 smFRET studies

2.8.1 ABCE1 labeling with sCy3/sCy5

Purified ABCE1 variants that carry double-cysteine substitutions for smFRET labeling were thawed on ice and diluted to a final concentration of 15-20 μM in 75 μl labeling buffer (20 mM HEPES/KOH pH 6.5, 300 mM KCl, 0.1 mM EDTA, 10%(v/v) glycerol). Residual DTT or 2-ME in the storage buffer was removed by double buffer exchange *via* pre-equilibrated spin columns (Micro Bio-Spin® 6, Bio-Rad Laboratories, 2,000 \times g for 2 min for one round), and concurrently the buffer was completely exchanged to labeling buffer. Sulfo-Cyanin-3-maleimid and Sulfo-Cyanin-5-maleimid (sCy3 and sCy5, #11380 and #13380, respectively, Lumiprobe) were dissolved in DMSO at a concentration that yielded 5% (v/v) DMSO post dilution in the labeling reaction. The labeling reaction was started by addition of sCy3 and sCy5 in a 20x molar-excess to ABCE1, hence 500 μM . Immediately, after addition of dyes, the labeling reaction was mildly mixed by pipetting and incubated for 30 min on ice and for 5 min at room temperature. Labeling reactions were quenched, and free dye was removed by a buffer exchange step into labeling storage buffer (20 mM HEPES/KOH pH 7.5, 300 mM KCl, 0.1 mM EDTA, 4 mM 2-ME, 10% (v/v) glycerol) *via* a pre-equilibrated spin column in the same buffer. The complete sample was applied to SEC (Superdex 200 3.2/300,

GE, 0.05 ml/min flow, Ettan System, GE) equilibrated in labeling storage buffer for separation of labeled protein from free dye. Absorption was recorded for the wavelengths 280, 532, and 637 nm in order to determine the labeling efficiency based on the individual extinction coefficients (~30,000 for ABCE1, 162,000 for sCy3, and 271,000 M⁻¹cm⁻¹ for sCy5). After SEC, the monodispersly eluted labeled ABCE1 variants were pooled and flash frozen in liquid nitrogen in 20 µl aliquots. Due to a low labeling efficiency of <20% (labeled cysteine to total accessible cysteine), we did not correct for the absorption of labels at 280 nm in the calculation of the degree of labeling.

2.8.2 Surface preparation for immobilization

Glass-slides for smFRET studies were prepared by P. Höllthaler by a protocol from the Joo lab (Chandradoss *et al.*, 2014) that was heavily modified. Glass slides were plasma cleaned for 15 min in the plasma cleaner (Zepto, Diener Electronic) and sonicated in washing solution (92% (v/v) methanol, 5% (v/v) acetic acid, 3% (v/v) 3-aminopropyl trimethoxysilane (APTES)) for 1 min and incubated for 10 min at room temperature without sonication. The aminosilanized slides were washed four times with methanol and stored in methanol prior drying. The surface was passivated in a first step by biotinylated and non-biotinylated polyethyleneglycol polymers (PEG, 5,000 kDa) *via* N-Hydroxysuccinimid (NHS)-coupling. NHS-ester PEG was doped with 6.6% (w/w) biotinylated NHS-ester PEG in a tube and solubilized by gentle pipetting in PEGylation buffer (0.1 M sodium bicarbonate pH 8.5, no pH adjustment necessary, 91 mg PEG in 640 µl). The PEGylation solution was cleared for 1 min at 16,000 × g centrifugation. 70 µl supernatant of the PEGylation solution were applied onto a washed and freshly nitrogen dried cover slide. A second cover slide was attached to the first, so that the PEGylation solution was stacked in-between, air bubbles should be avoided. The half-life of the PEGylation solution is about 0.5 h. The slides were stored for up to two days in the dark at humid conditions.

A second passivation was performed with MS4PEG (Thermo Fischer Scientific) in order to quench remaining amine groups and increase the PEGylation density on the slide. 7 µl of 250 mM MS4PEG were added to 63 µl of freshly prepared 0.1 M sodium carbonate solution

and applied onto the prepared PEG slides, and again a sandwich of two slides was assembled. The PEGylation was performed for 30 min at room temperature in a humid chamber. The slide-sandwich was disassembled and the slides were washed with Milli-Q® water and dried with N₂. Finally, the PEGylated slides were set onto a microscope slide with spacers of double-sided sticky tape in-between, that resulted in a diagonal flow channel.

In a humidity chamber, 50 µl streptavidin (0.2 mg/ml) in Dulbecco's phosphate-buffered saline (DPBS) buffer (Thermo Fischer Scientific) were added per channel. In parallel, the liquid excess was removed by absorption in a cloth on the exit side of the channel. The streptavidin solution was incubated in the channel for 30 min and washed with 200 µl DPBS buffer. Lyophilized biotin-X NTA was solubilized to a final concentration of 0.1 mg/ml in 10 mM NiCl₂. 100 µl of Ni-loaded biotin-X NTA solution was applied to the channel and incubated for 20 min and washed with 200 µl storage_{FRET} buffer (20 mM HEPES/KOH pH 7.5, 300 mM KCl, 0.1 mM EDTA, 10% (v/v) glycerol, 4 mM 2-ME).

2.8.3 smFRET-ALEX setup

The smFRET-ALEX microscope setup was planned, optimized and constructed in 2016 by P. Höllthaler in the Tampé lab based on an optical setup in the Heilemann lab (Goethe University, Frankfurt/M.) that he used previously (Höllthaler, 2015). The microscope body was based on an Olympus IX73 microscope (**Figure 5**). The laser beams at 532 and 673 nm wavelength for green and red channels, respectively, were alternated by an acousto optic tunable filter (AOTF) between 20-100 ms frequency. 50 or 100 ms alternations were used for the measurements. The beam was expanded and directed onto the sample from the bottom of the microscope and resulted in an image that was split by an emission image splitter (Optosplit II, Cairn Research). The green and the red channels were separately recorded by one electron multiplying charge-coupled device (EMCCD) camera (IXON 888, Andor Technology, **Figure 6a**) that resulted in recorded movies.

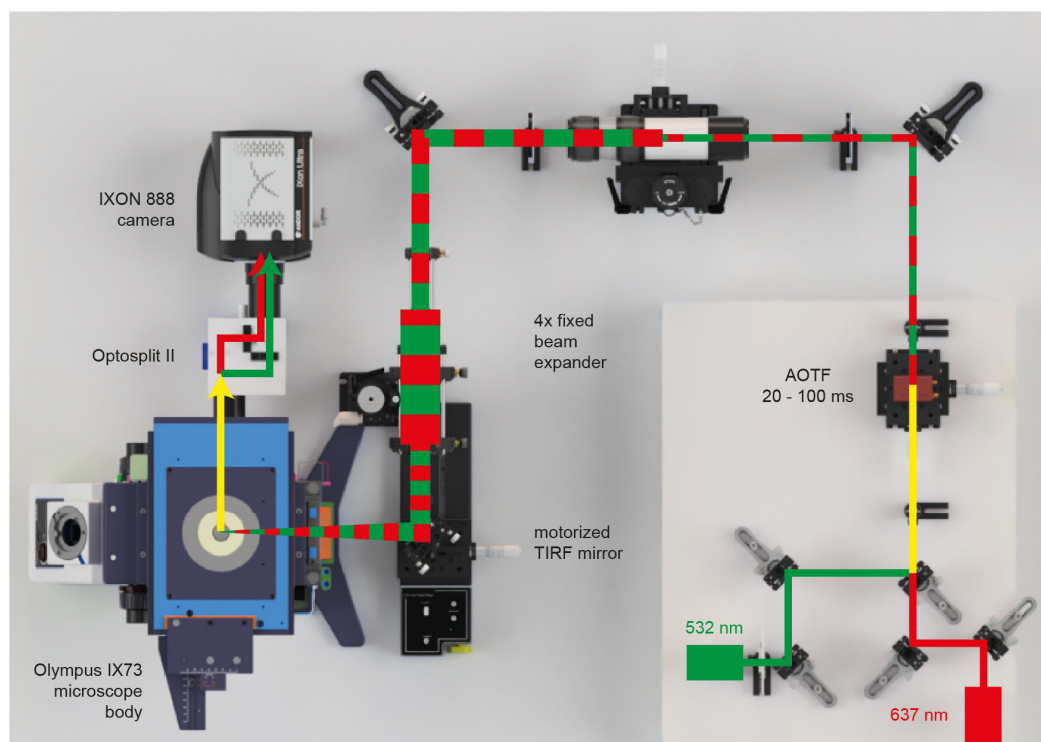


Figure 5 | smFRET-ALEX microscope setup. Alternating green and red laser excitation was used for FRET detection. P. Höllthaler generated the figure, reserved all rights, and granted permission for reprint.

2.8.4 ABCE1 immobilization and smFRET analysis

Labeled ABCE1 in storage buffer was applied on the channel at a concentration of about 2 nM and incubated for 2-5 min at room temperature. Particle density was checked by imaging in the microscope. The desired density was about 200 particles per region of interest. If the density was not sufficient, additional labeled ABCE1 was applied to the channel and incubated again. If the desired density was achieved, the reaction was started by application of 100 μ l imaging buffer. Imaging buffer contained the vitamin E analog Trolox (Sigma-Aldrich) for fluorophore lifetime extension that was dissolved at saturating conditions in storage buffer, vortexed, and incubated under UV light for 30 min and filtered two times through 0.2 μ m. The activated Trolox solution was used for the preparation of 200 μ l imaging buffer (68 μ l of storage_{FRET} buffer, 25 μ l of 40% (w/v) glucose, 5 μ l of 100 mM MgCl₂, 100 μ l of 2 mM Trolox (filtered, Roy *et al.*, 2008), and 10 μ l of Gloxy buffer (100 mg/mL glucose oxidase, 4 mg/mL catalase, 50 mM NaCl, and 10 mM Tris/HCl pH 8.0, Long *et al.*, 2016). Additionally, the imaging buffer contained optionally 0.5 mM nucleotides and

nucleotide analogs supplemented with 1x MgCl₂, and the ribosomal 40S subunit as indicated in the results part. The imaging buffer was applied to the channel and recording of the sample was started in the ALEX microscopy mode.

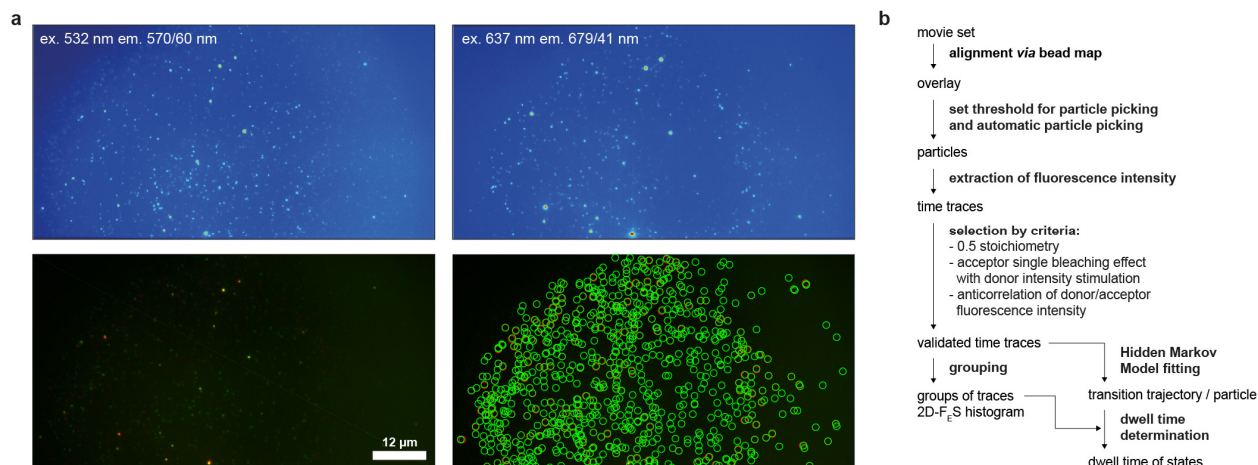


Figure 6 | Immobilized samples and data processing. **a**, Exemplary fluorescence image from a movie stack of the immobilized sample post splitting into red and green channels. The particles were super positioned and automatically picked in iSMS (green circles indicate donor peaks, red acceptor peaks and yellow-FRET pairs). P. Höllthaler produced the images. **b**, Processing scheme of movies included super-positioning, particle picking, extraction of time traces, and selection by indicated criteria in iSMS. Validated time traces were grouped and plotted in a 2D-F_ES histogram or the FRET efficiency was analyzed by Hidden Markov Model fitting for analysis of dwell times.

2.8.5 Particle picking and FRET efficiency trace extraction

Fluorescence signals of immobilized particles (**Figure 6a**) were recorded by the software Andor Solis (Andor Technology). Movies were analyzed (**Figure 6b**) by the iSMS movie processing software from V. Birkedal at the Interdisciplinary Nanoscience Center (iNANO) at Aarhus University (Preus *et al.*, 2015). The general procedure included alignment of the movie set *via* a previously recorded bead map of TetraSpeck™ microspheres (0.1 μm, Sigma-Aldrich). The particles were picked automatically based on an empirically set fluorescence threshold above background level. The fluorescence intensity was extracted for each particle automatically and time traces were represented as shown exemplary in **Figure 44**. FRET time

traces were selected by the following criteria: the stoichiometry (S , $S = [F_Y(D_{ex}D_{em}) + F(D_{ex}A_{em})]/[F_Y(D_{ex}D_{em}) + F(D_{ex}A_{em}) + F(A_{ex}A_{em})]$, Lee & Kapanidis *et al.*, 2005) equalled a value of ~ 0.5 ; upon a single bleaching event of the acceptor, the donor signal intensity increased; and donor-to-acceptor fluorescence intensity was anti-correlated. Validated time traces were grouped in a 2D- F_E S histogram in which the y-axis represented the stoichiometry (S) and the x-axis FRET efficiency (F_E , $F_E = F(D_{ex}A_{em})/[F(D_{ex}D_{em}) + F(D_{ex}A_{em})]$, Lee & Kapanidis *et al.*, 2005)). F_E populations were fitted by Gaussian distributions. In addition, for validated F_E time traces that were longer than 200 frames, the F_E traces were analyzed by the Hidden Markov Model algorithm for hidden dynamic transitions by previously published methods (Blanco & Walter, 2010, McKinney *et al.*, 2006). The final goal was the analysis of dwell times for each F_E population at different conditions, *e.g.* by HaMMY (McKinney *et al.*, 2006).

F_E population shifts from 1st to 2nd conditions were analyzed by normalization of the F_E -histogram area at both conditions to 1 and subsequent subtraction. This resulted in a difference-histogram. A threshold was set at a defined F_E in between both efficiency populations that was verified by the equal sum of areas of each population side. The area of each population shift in the difference histogram was summarized and color coded *via* the *conditional formatting* option in Excel (Microsoft) and represented in an overview.

2.9 Style points and conventions

Style and reference conventions in this thesis were based on the Council of Science Editors (CSE) manual for scientific style and format. References were managed with EndNote® x8 (Thomson Reuters) and listed in the EMBO journal style. Upper and lower case letters in titles were standardized for journal articles. Journal names were shortened using the BIOSIS journal abbreviations without dots as a term list in EndNote®. Shared first and corresponding authorships were indicated by an '&' in the reference list, except if the authors were not listed aside in the beginning or the end, respectively, or the first authors were also a corresponding author. All titles of persons were omitted in the thesis.

2.10 Materials

Table 5 | Strains and Organisms

strain name	plasmids	organism	resistance	source
cloning strain				
Top10 (F- <i>mcrA</i> Δ(<i>mrr-hsdRMS-mcrBC</i>) Φ80 <i>lacZ</i> ΔM15 Δ <i>lacX74 recA1 araD139</i> Δ(<i>araleu</i>)7697 <i>galU galK rpsL</i> (StrR) <i>endA1 nupG</i>)		bacteria		Thermo Fischer Scientific
protein production strains				
INVSc1 (<i>MAT a/α his3Δ1/ his3Δ1 leu2/leu2 trp1-289/trp1-289 ura3-52/ura3-52</i>)		yeast		Thermo Fischer Scientific
BL21(DE3)	pRARE	<i>E. coli</i>	chloramphenicol	
yeast genetics strains				
<i>wt</i> (BY4741: <i>MATa his3Δ1 leu2Δ0 met15Δ0 ura3Δ0</i>)		yeast		P. Kötter
<i>wt</i> (BY4742: <i>MATα his3Δ1 leu2Δ0 lys2Δ0 ura3Δ0</i>)		yeast		P. Kötter
<i>wt</i> (BY4743: <i>MATa/MATα his3Δ1/his3Δ1 leu2Δ0/leu2Δ0 met15Δ0/MET15; LYS2/lys2Δ 0; ura3Δ0/ura3Δ0</i>)		yeast		
<i>dom34Δ</i> (yNG102: <i>MATa leu2Δ0 met15Δ0 ura3Δ0; YNL001w::KanMX4</i>)		yeast	G418	R. Green
<i>dom34Δski2Δ</i> (yNG103: <i>MATa his3Δ1 leu2Δ0 ura3Δ0; YLR398C::KanMX4; YNL001w::KanMX4</i>)		yeast	G418	R. Green
<i>ABCE1-HAT</i> (MG001: <i>MATa his3Δ1 leu2Δ0 met15Δ0 ura3Δ0 YDR091c::YDR091c_His_TEV_protA_URA3</i>)		yeast		this work
<i>ABCE1-HAT</i> (MG002: <i>MATα his3Δ1 leu2Δ0 met15Δ0 ura3Δ0 YDR091c::YDR091c_His_TEV_protA_URA3</i>)		yeast		this work
<i>asc1-GFP</i> (MG003: <i>MATa his3Δ1 leu2Δ0 ura3Δ0; YMR116C::YMR116C_GFP_KanMX4</i>)		yeast	G418	this work
<i>asc1-GFP</i> (MG004: <i>MATa his3Δ1 leu2Δ0 ura3Δ0; YMR116C::YMR116C_GFP_NAT1</i>)		yeast	nourseo-thricine	this work
<i>dom34Δski2Δ asc1-GFP</i> (MG005: <i>MAT a his3Δ1 leu2Δ0 ura3Δ0 YLR398C::KanMX4 YNL001w::KanMX4 YMR116C::YMR116C_GFP_NAT-1</i>)		yeast	G418 nourseo-thricine	this work
<i>ABCE1/abce1Δ</i> (CEN.PK744: <i>MAT a/α his3Δ1/his3Δ1 leu2-3,112/leu2-3,112 trp1-289/trp1-289 MAL2-8C/MAL2-8C SUC2/SUC2 ura3-52/ura3-52 YDR091C/ydr091c::KanMX4</i>)		yeast	G418	P. Kötter
<i>ABCE1Δ/pRS426_ABCE1</i> (CEN.MG1-9B: <i>MATa his3Δ1 leu2-3,112 trp1-289 MAL2-8C SUC2 ura3-52 YDR091C::KanMX4 + pRS426_ABCE1</i>)	pRS426 _ABCE1	yeast	G418	this work
<i>ABCE1-TAP</i> (SC1900: <i>MATa leu2-3 112 trp1-289 ade2 arg4 ura3-52 YDR091C::TAP-KIURA3</i>)		yeast		P. Kötter

Table 6 | Plasmids

palsmid name	Purpose	cloning strategy (primer)	source
protein production			
pYes2_ABCE1_H6	<i>ABCE1_{H6}</i> expression +variants: R7A, P30A, N78A, H95A, Y301A; C38A, C236A, C276V, C292H, C506A, C561M, K128C, K181C, K403C, R439C	TOPO cloning site-directed mutagenesis	R. Green (Shoemaker & Green, 2011) mutations were introduced in this study
pYes2_Dom34_H6	<i>Dom34_{H6}</i> expression		R. Green (Shoemaker <i>et al.</i> , 2010)
ABCE1 _{H6} ^{cysless} pYes2_ABCE1(C38A, C236A, C276V, C292H, C506A, C561M)_H6	labeling studies	see pYes2_ABCE1_H6	this study
ABCE1 _{H6} ^{NBS I} pYes2_ABCE1(C38A, C236A, C276V, C292H, C506A, C561M, K128C, R439C)_H6	FRET studies	see pYes2_ABCE1_H6	this study
ABCE1 _{H6} ^{NBS II} pYes2_ABCE1(C38A, C236A, C276V, C292H, C506A, C561M, K181C, R403C)_H6	FRET studies	see pYes2_ABCE1_H6	this study
ABCE1 _{H6} ^{FeS-NBD1} pYes2_ABCE1(C236A, C276V, C292H, C506A, C561M, K128C)_H6	FRET studies	see pYes2_ABCE1_H6	this study
pSA4_Dom34_H6	<i>Dom34_{H6}</i> expression	restriction cloning by <i>NcoI/BamHI</i> : f_ <i>NcoI</i> _Dom34, r_ <i>BamHI</i> _H6_Dom34	this study
pET28(+)_eIF6_H6	<i>eIF6_{H6}</i> expression		R. Green (Shoemaker <i>et al.</i> , 2010)
pAMI_ABCE1_H6	expression	SLIC from pYes2_ABCE1_H6	S. Trowitzsch, Tampé lab, this study

cloning			
pSA4_SsABCE1_H6	cloning	restriction <i>NcoI/BamHI</i> :	Tampé lab
pAG426	cloning	restriction <i>EcoRI/BamHI</i>	R. Green
genomic tagging			
pYM27	genomic <i>GFP-HA</i> tagging	recombination, primer: f_Asc1_S3_GFP_HA_KanMX4 r_Asc1_S4_KanMX4_HA_GFP	P. Kötter
pAG36	cassette exchange	restriction & recombination <i>NotI</i>	P. Kötter
pBS1539_H6_TEV_pA	genomic <i>H6_TEV_pA</i> tagging	recombination, primer: f_ABCE1_H6_TEV_pA_URA3 r_URA3_pA_TEV_H6_ABCE1	P. Kötter
plasmid shuffling			
pRS423	cloning, plasmid shuffling	restriction <i>Sall/Smal</i> , primer: f_Sall_p_ABCE1, r_Smal_t_ABCE1	P. Kötter
pRS423_pABCE1t	plasmid shuffling +variants: R7A, P30A, N78A, H95A, Y301A; C38A, K128C, K181C, R403C, R439C; S223R, E247A, E247Q, S469R, E493A, E493Q	restriction <i>Sall/Smal</i> , primer: f_Sall_p_ABCE1, r_Smal_t_ABCE1 site-directed mutagenesis	this study
pRS426	cloning	restriction <i>Sall/Smal</i> , primer: f_Sall_p_ABCE1, r_Smal_t_ABCE1	P. Kötter
pRS426_pABCE1t	plasmid shuffling	restriction <i>Sall/Smal</i> , primer: f_Sall_p_ABCE1, r_Smal_t_ABCE1	
pRS423_TDH3- ABCE1-HA (pUJ2)	ribosome profile analysis +variants: R7A, P30A, N78A, H95A, Y301A; R7A, P30A, N78A, H95A, Y301A; S223R, E247A, E247Q, S469R, E493A, E493Q	site-directed mutagenesis	U. Jan, Tampé lab, mutations were introduced in this study
<i>in vivo</i> stalling			
pAG426_H6_HA _GFP_Rz	<i>in vivo</i> stalling	restriction cloning <i>NcoI/BamHI/SphI/XhoI</i>	this study

Table 7 | Primers

primer name	primer sequence (5'-3')
sequencing primer	
T7	TAATACGACTCACTATAGGG
T7term	GCTAGTTATTGCTCAGCGG
f_M13(-21)	TGTA AACGACGGCCAGT
f_M13(-40)	GTTTTCCCAGTCACGAC
r_M13	CAGGAAACAGCTATGAC
SK	CGGCCGCTCTAGA ACTAGTGGATC
site-directed mutagenesis	
f_ABCE1_R7A	GAGTGATAAAAACAGTGCTATCGCTATCGTTAGCGC
r_ABCE1_R7A	GCGCTAACGATAGCGATAGCACTGTTTTTATCACTC
f_ABCE1_P30A	CAAGAGTGTA AACGTTTCGTGTGCCGTTGTGAAA ACTGGTAAATTATG
r_ABCE1_P30A	CATAATTTACCAGTTTT CACAACGGCACACGAACGTTTACACTCTTG
f_ABCE1_N78A	CAAATTATCAATTTGCCAACTGCTTTAGAAGCCCATGTA ACTCACCG
r_ABCE1_N78A	CGGTGAGTTACATGGGCTTCTAAAGCAGTTGGCAAATTGATAATTTG
f_ABCE1_H95A	CAATAGTTTCAA ACTGGCCAGATTGCCAACACCAAG
r_ABCE1_H95A	CTGGTGTTGGCAATCTGGCCAGTTTGAAACTATTG
f_ABCE1_Y301A	GGTGTTCATCTGTTGCCGGTGTGTTACATTACC
r_ABCE1_Y301A	GGTAATGTAACAACACCGGCAACAGATGGAACACC
f_ABCE1_C38A	CCCGTTGTGAAA ACTGGTAAATTAGCTATTGAAGTCACTCCA ACTTC
r_ABCE1_C38A	GAAGTTGGAGTGACTTCAATAGCTAATTTACCAGTTTT CACAACGGG
f_ABCE1_C236A	GATTTGCCATTGGTATGTCAGCTGTTCAAGAGGCTGATGTTTATATGTTT
r_ABCE1_C236A	GAACATATAAACATCAGCCTCTTGAACAGCTGACATACCAATGGCAAATC
f_ABCE1_C276V	CCAACTAAATACGTTATTGTTGTTGAGCACGATTTGTCAG
r_ABCE1_C276V	CTGACAAATCGTGCTCAACAACAATAACGTATTTAGTTGG
f_ABCE1_C292H	GATTATCTTCCGATTTCGTTCATATCATATATGGTGTTCATCTG

r_ABCE1_C292H	CAGATGGAACACCATATATGATATGAACGAAATCGGAAAGATAATC
f_ABCE1_C506A	CCGAACAACGTATTATCGCTTCTAAAGTTATCAGAAG
r_ABCE1_C506A	CTTCTGATAACTTTAGAAGCGATAATACGTTGTTCCGG
f_ABCE1_C561M	GCCCCTGAATCTTTGTTGACTGGTATGAACAGATTTTTGAAGAATTTG
r_ABCE1_C561M	CAAATTCTTCAAAAATCTGTTTCATACCAGTCAACAAAGATTCAGGGGC
f_ABCE1_K128C	CCGCCTTGAAAATCTTAGCCGGTAAACAATGTCCTA- ATTTAGGTCGTTTTGATGATCCTCC
r_ABCE1_K128C	GGAGGATCATCAAAACGACCTAAATTAGGACATTGT- TTACCGGCTAAGATTTTCAAGGCGG
f_ABCE1_K181C	CCTCGTGCTATTTGTGGTCCGGTTC
r_ABCE1_K181C	GAACCGGACCACAAATAGCACGAGG
f_ABCE1_R403C	CCACTTTGATCAAATTACTAGCTGGTGCTTTGTGTC-CAGATGAAGGACAAGATATTCC
r_ABCE1_R403C	GGAATATCTTGCCTTCATCTGGACACAAAGCACCA-GCTAGTAATTTGATCAAAGTGG
f_ABCE1_R439C	GGTACTGTCAGACAATTGTTTTCAAGAAAATTTGTG- GACAATTCCTAAATCCACAGTTTCAGACTG
r_ABCE1_R439C	CAGTCTGAAACTGTGGATTTAGGAATTGTCCACAAAT- TTTCTTGAAAAACAATTGTCTGACAGTACC
f_ABCE1_S223R	GATATTGAAAAGTTACGTGGTGGTGAAGTCAAAG
r_ABCE1_S223R	CTTTGCAGTTCACCACCACGTAACTTTTCAATATC
f_ABCE1_E247A	GTTTATATGTTTCGATGCACCTTCATCTTATTTGG
r_ABCE1_E247A	CCAAATAAGATGAAGGTGCATCGAACATATAAAC
f_ABCE1_E247Q	GTTTATATGTTTCGATCAACCTTCATCTTATTTGG
r_ABCE1_E247Q	CCAAATAAGATGAAGGTGATCGAACATATAAAC
f_ABCE1_S469R	GAAGTCCAACATTTGCGTGGTGGTGAATTAC
r_ABCE1_S469R	GTAATTCACCACCACGCAAATGTTGGACTTC
f_ABCE1_E493A	CATATACTTGATTGATGCGCCATCTGCCTACTTAG
r_ABCE1_E493A	CTAAGTAGGCAGATGGCGCATCAATCAAGTATATG
f_ABCE1_E493Q	CATATACTTGATTGATCAGCCATCTGCCTACTTAG
r_ABCE1_E493Q	CTAAGTAGGCAGATGGCTGATCAATCAAGTATATG

vector modification	
f_NcoI_del	CTTAACTGTGCCCTCCATCGAAAAATCAGTC
r_NcoI_del	GACTGATTTTTCGATGGAGGGCACAGTTAAG
genomic tagging	
f_Asc1_S3_GFP_HA_KanMX4	GTTTGCCGGTTACACCGACAACGTCATTAGAGTTTGGCAAGTTATGACTGCTAACCGTACGCTGCAGGTCGAC
r_Asc1_S4_KanMX4_HA_GFP	TGACCAATAACTAGAAGATACATAAAAGAACAAATGAACTTTATACATATTCTTAATCGATGAATTCGAGCTCG
f_ABCE1_H6_TEV_pA_URA3	AAGAACA AAAAATCATCAGGAACTACTTTTTCTTGATAACACCGGTATTGAGCACCATCACCATCAC
r_URA3_pA_TEV_H6_ABCE1	GAGTTTCGTTTGGTACGAGAAGTGTGATACAGAGGTAATCTACCTATCTATACGACTCACTATAGGG
strain verification	
kanB	CTGCAGCGAGGAGCCGTAAT
kanC	TGATTTTGATGACGAGCGTAAT
dom34A	TCCCTGTGGCAGCCTCTTCTTTCTAGGAAC
dom34D	TTCATTCTTATCAGTCCAGCGCCGTTTGGG
dom34B	CCGCCGCGGTGTCTGATTATACTCG
dom34C	AGAGGTAGTTAAAGCGGCTGAGTATGGC
plasmid shuffling	
f_SalI_p_ABCE1	GGGCGAATTGGGTACCGGGCCCCCTCGAGGTCGACGGTATCGATAAGCTTGCCCCGCGGCTCCCGCAGAATCTAATCATTAAAGCTTGACTAG
r_SmaI_t_ABCE1	GCTCCACCGCGGTGGCGGCCGCTCTAGAACTAGTGGATCCCCCGGGCTGCTAAACTGGAGTACGGATCACCGAAGAGGAGG

stalling constructs

f_TOPO_His_BamHI_PGK	CACCATGGGGCACCATCACCATCACCATGGATCCACTGAAGAACAAAAT-GGAGGTGGTCAAAAAGTC
r_PGK45_SphI	CACATGCATGCTTCTACAGACTTACTTTCGTTACCGCTCTCTGTGGCTGTTG
f_NcoI-HIS-HA-BamHI-GFP	CATGCCATGGGACATCATCATCATCATCATTACCCATACG-ATGTTCCAGATTACGCTGGATCCGTGAGCAAGGGCGAGGAGCTGTTACCG
r_BamHI-eGFP-SphI	ACATGCATGCCTTGTACAGCTCGTCCATGCCGAGAG

r_Myc2_GFP_insert primer	GACGCATGCCAGGTCTTCTTCAGAGATCAGTTTCTGTTCCAGGTCTTCTTCAGAGATCA GTTTCTGTTCTTGTACAGCTCGTCCATGCCG
--------------------------	---

stalling motifs

f_SphI_SL_XhoI	C-GATATCCCGTGGAGGGGCGCGTGGTGGCGGCTGC-AGCCGCCACCACGCGCCCCTCCACGGCATATC-C
r_SphI_SL_XhoI	TCGAG-GATATGCCCGTGGAGGGGCGCGTGGTGGCGG-CTGCAGCCGCCACCACGCGCCCCTCCACGGGATATC-GCATG
f_SphI_12K_XhoI	C-AAGAAAAAGAAAAAGAAAAAGAAAAAGAAAAAGAAACT-C
r_SphI_12K_XhoI	TCGAG-TTTCTTTTTCTTTTTCTTTTTCTTTTTCTTTTTCTT-GCAT-GCATG
f_SphI_36A_XhoI	C-AAAAAAAAAAAAAAAAAAAAAAAAAAAAAAAAAAACT-C
r_SphI_36A_XhoI	TCGAG-TTTTTTTTTTTTTTTTTTTTTTTTTTTTTTTTTT-GCAT-GCATG
f_SphI_Rz_XhoI	C-GTCGACGGATCTAGATCCGTCTGATGAGTCCGTGA-GGACGAAACGCATGATC-C
r_SphI_Rz_XhoI	TCGAG-GATCATGCGTTTCGTCCTCACGGACTCATCA-GGACGGATCTAGATCCGTGAC-GCATG

insect/human cell expression

f_ABCE1	GCGCGCGGCCGCATGAGTGATAAAAACAGTCGTATCGCTATCG
r_H6_ABCE1	CGCGTCTAGATTAGTGATGGTGATGGTGATGAATACCGGTGTTA-TCCAAGAAAAGTAGTTTCC

Table 8 | Media

name	Mixture	preparation
LB	1% (w/v) tryptone/peptone from casein, 0.5% (w/v) yeast extract, 0.5% (w/v) NaCl	filled up with water, autoclaved
2xYT	1.6% (w/v) tryptone/peptone from casein, 1% (w/v) yeast extract, 0.5% (w/v) NaCl	filled up with water, autoclaved
YPD	2% (w/v) tryptone/peptone from casein, 1% (w/v) yeast extract, 2% (w/v) glucose	filled up to 80/90% (v/v) with water.
YP-Suc	2% (w/v) tryptone/peptone from casein, 1% (w/v) yeast extract, 2% (w/v) sucrose	carbon source and agar was added after autoclaving
YP-Suc/Gal	2% (w/v) tryptone/peptone from casein, 1% (w/v) yeast extract, 2% (w/v) sucrose, 2% (w/v) galactose	and separately autoclaved.
SCD-URA	770 mg/l CSM-URA, 1.9 g/l yeast nitrogen base without amino acids and ammonium sulphate, 0.5% (w/v) ammonium sulphate, 2% (w/v) glucose	5-FOA was added as solid.
SCD-HIS	770 mg/l CSM-HIS, 1.9 g/l yeast nitrogen base without amino acids and ammonium sulphate, 0.5% (w/v) ammonium sulphate, 2% (w/v) glucose	agarplates were made with the same ingredients, 2% (w/v) agar was separately auto-claved and added.
SCD-HIS (+Ura) +5-FOA	770 mg/l CSM-HIS, 1.9 g/l yeast nitrogen base without amino acids and ammonium sulphate, 0.5% (w/v) ammonium sulphate, 50 mg/l uracil, 1 g/l 5-FOA, 2% (w/v) glucose	
SCD-HIS-URA	750 mg/l CSM-HIS, 1.9 g/l yeast nitrogen base without amino acids and ammonium sulphate, 0.5% (w/v) ammonium sulphate, 2% (w/v) glucose	

Table 9 | Chemicals & resins

compound	supplier, ref. no.	aliquot, diluted with
nucleotides		
AMP-PNP (Li salt)	Sigma-Aldrich, #A2647-25MG	100 mM, H ₂ O, pH 7.0, buffered by 1 M KOH, stored at -20 °C
ATP dipotassium salt di-hydrate	Sigma-Aldrich, #A8937-1G	100 mM aliquotted in H ₂ O, pH 7.0, buffered by 1 M KOH, stored at -20 °C
ADP	Sigma-Aldrich, #A23831G	100 mM aliquotted in H ₂ O, pH 7.0, buffered by 1 M KOH, stored at -20 °C
GTP lithium salt	Sigma-Aldrich, #G5884-25MG	100 mM aliquotted in H ₂ O, pH 7.0, buffered by 1 M KOH, stored at -20 °C
[gamma] ³² P-ATP	Hartmann Analytics, #SRP-301	diluted in <i>cold</i> ATP
[gamma] ³² P-GTP	Hartmann Analytics, #SRP-302	diluted in <i>cold</i> GTP
cloning		
Phusion® High-Fidelity DNA-Polymerase	Thermo Fischer Scientific, #F530L	stored at -20 °C
FastDigest Restriction enzymes: <i>Nco</i> I, <i>Bam</i> HI, <i>Sph</i> I, <i>Xho</i> I, <i>Pst</i> I, <i>Dpn</i> I	Thermo Fischer Scientific, #FD0573, FD0055, FD0604, D0694, FD0614, FD1703	stored at -20 °C
FastAP	Thermo Fischer Scientific, #EF0652	stored at -20 °C
T4 ligase	Thermo Fischer Scientific, #15224017	stored at -20 °C
T4-Polymerase	Thermo Fischer Scientific, #EP0062	stored at -20 °C
ampicillin	Carl-Roth, #HP62.2	solid, 4 °C, dissolved in H ₂ O, stored at -20 °C
puromycin	Carl-Roth, #0240.1	solid, 4 °C, freshly dissolved in sample or water, stored at -20 °C
kanamycine	Carl-Roth, #T832.3	solid, 4 °C, dissolved in H ₂ O, stored at -20 °C

gel systems & immunoblotting		
Rotiphorese® Gel 30 (37.5:1)	Carl-Roth, #3029.1	rt
PageRuler™ Prestained Protein Ladder	Thermo Fischer Scientific, #26616	rt
Amersham™ Protran™ Supported 0.45 µm NC	GE, #10600016	rt
Clarity™ Western ECL Substrate	Bio-Rad Laboratories, #170-5061	rt
yeast genetics		
salmon sperm DNA, sheared	Thermo Fischer Scientific, #AM9680	10 mg/ml, stored at -20 °C
PEG 3350	Sigma-Aldrich, #P3640	autoclaved, stored at rt
SCD-URA	Formedium, #DCS0169	+YNB & ammonium sulfate (AS), autoclaved
SCD-HIS	Formedium, #DCS0079	+YNB & AS, autoclaved
SCD-URA-HIS	Formedium, #DCS0529	+YNB & AS, autoclaved
yeast nitrogen base without amino acids and ammonium sulfate (YNB)	Formedium, #CYN0510	+SCD & AS, autoclaved
ammonium sulfate (AS)	Carl-Roth, #3746.1	+YNB & SC-X, autoclaved
agar	Formedium, #AGA03	autoclaved separately
glucose	Sigma-Aldrich, #G8270-25KG	autoclaved separately
sucrose	Sigma-Aldrich, #S7903-5KG	autoclaved separately
galactose	Carl Roth, #4987.3	autoclaved separately
uracil	Sigma-Aldrich, #U0750-100G	autoclaved separately
G418	Carl-Roth, #0239.4	dissolved in agar for plates
5-fluoroorotic acid (5-FOA)	Thermo Fischer Scientific, R0812	dissolved in agar for plates
protein production & purification		
tryptone/peptone from casein	Carl-Roth, #8952.2	
yeast extract	Carl-Roth, #2904.3	
NaCl	Carl-Roth, #P029.2	

IPTG	Carl-Roth, #I6758	
Ni-NTA agarose	Qiagen	
Amicon® (5,10,30,100 K)	Merck Millipore	
DTT	Carl-Roth, # 6908.1	
2ME	Carl-Roth, #4227.1	
Tween® 20	Carl-Roth, #9127.1	
ribosome purification		
cOmplete Tables, Mini EDTA-free, <i>EASYpack</i>	Roche, #04 693 159 001	stored at 4 °C
puromycin, di-hydrochloride	Merck, #540222-25MG	freshly dissolved
cyclohexamide	Merck, #239764-100MG	50 mM, H ₂ O, 14 g/l
spermidine ≥99.0% (GC)	Sigma-Aldrich, #S2626-1G	1M, H ₂ O
heparin sodium salt	Carl-Roth, #7692.1	directly added
functional assays		
TLC PEI Cellulose F	Merck, #1.05579.0001	stored at 4 °C
SYBR® Gold nucleic acid gel stain	Life Technologies, #S11494	stored at 4 °C

Table 10 I Machines

name	company
incubators & tempering machines	
Thermomixer Univortemp	UniVersal Labortechnik
Tpersonal PCR machine	Biometra
Systemc autoclave	Systemc
B6 Instruments incubator	Heraeus
HT Multitron incubator	Infors
Innova 43	New Brunswick Scientific

centrifuges & rotors

Avanti J-26 XP	Beckman Coulter
JLA 8.100 fixed angle rotor (max. 15,970 g, 6x0.5 l)	Beckman Coulter
Megafuge 16R (max. 5,000 g, 16x50 ml)	Thermo Fischer Scientific
RC 5B Plus Centrifuge	Sorvall
SS-34 fixed angle rotor (max. 50,228 g, 8x50 ml))	Thermo Fischer Scientific
Optima XE-90 Ultracentrifuge	Beckman Coulter
70 Ti fixed angle rotor (max. 504,000 g, 8x39 ml)	Beckman Coulter
SW 41 Ti swing-out rotor (max. 288,000 g, 6x13.2 ml)	Beckman Coulter
Optima TLX Ultracentrifuge 120,000 rpm	Beckman Coulter
TL-110 fixed angle rotor (max. 657,000 g, 8x5.1 ml)	Beckman Coulter
Centrifuge 5417R	Eppendorf
F-45-30-11 fixed angle rotor (max. 20,800 g, 30x2 ml)	Eppendorf

cell disruption

250 Sonifier	Branson Sonifier
Basic Z model cell disrupter	Constant Systems

chromatography systems & columns

Äkta Prime Plus	GE
Äkta Explorer	GE
Äkta Purifier	GE
HiTrap Q, DEAE S, Ni-NTA HP	GE
Superdex 75 16/600	GE
Äkta Ettan mini LC	GE
Superdex 200 16/600	GE
HPLC System 2000 with MD-2010 (PU-2080 Plus, MD-2010 Plus, LCNNet II/ADC, DG2080-53, LG 2080-02S)	Jasco
PerfectSil 300 ODS C28 5 µm	MZ Analysetechnik

spectroscopy & imaging

Ultraspec 10	Amersham Biosciences
ND1000	NanoDrop
Lumi-Imager F1	Roche
Clariostar Platereader	BMG Labtech
smFRET-ALEX setup	Tampé lab, designed by Philipp Höllthaler
Plasma Cleaner Zepto	Diener Electronic
SP5 Laser Scanning Microscope	Leica Microsystems
Typhoon 9400 scanner	Amersham Biosciences/GE

protein and ribosome analysis

Piston Gradient Fractionator	BioComp Instruments
Gradient Master ip	BioComp Instruments
Econo UV Monitor	Bio-Rad Laboratories Inc.
PowerPac HC	Bio-Rad Laboratories Inc.
E143 power supply 0.3 A	Consort
MiniProtean	Bio-Rad Laboratories Inc.
TransBlot SD cell	Bio-Rad Laboratories Inc.
Gel drier Model 583	Bio-Rad Laboratories Inc.
Vortexer Reax 2000	Heidolph

3 Results

3.1 *In vivo* ribosome stalling

Stalling of translating ribosomes occurs on defective mRNAs, *e.g.* which are truncated or contain a stable secondary structure in the ORF that provokes a *no-go* situation in translation. *No-go* decay (NGD) surveillance mechanisms are initiated that resolve the situation by cleavage of the defective mRNA, splitting, degradation of the nascent protein chain, and recycling of the ribosome (Shoemaker & Green, 2012). In this section, I will give a chronological introduction into the discovery of mRNA cleavage based on ribosome stalling and continue to the generation and detection of nascent chain products in stalled ribosomes. These insights were applied for the *in vivo* stalling of ribosomal complexes.

The Parker lab reported endonucleolytic cleavage of eukaryotic mRNAs that contain a 3' stable stall loop (SL) secondary structure in the ORF (Doma & Parker, 2006). A lack of the cytoplasmic 3'→5' (directional) degradation machinery, *e.g.* the heterotrimeric SKI complex, resulted post cleavage in a 5' mRNA fragment near the stall motif. On the 5' side of the mRNA in the stalled ribosome, a lack of the 5'→3' exonuclease activity by deletion of *XRN1*, resulted in a 3' mRNA fragment. In addition, rare codons, pseudoknots, poly-prolines, and even stop codons induce also cleavage. Consequently, a delay in translation elongation was proposed as the general trigger for cleavage and degradation (Doma & Parker, 2006). To proof that stalled ribosomal translation was the trigger for these degradation events, ribosome scanning at the AUG codon was blocked by an additional 5'-SL that blocked start codon recognition by ribosomal scanning on these reporters and yielded no 5' or 3' fragments. In addition, no 3' or 5' degradation products were observed in double deletion strains of *dom34Δski7/-2Δ* and *hbs1Δxrn1Δ*, too. Hence, Dom34 and Hbs1 were proposed to recognize stalled ribosomes and trigger mRNA surveillance (Doma & Parker, 2006).

On the protein level, ribosomes translate the defective mRNAs into a nascent polypeptide chain until a stall occurs. The peptide is stuck in the large ribosomal subunit and needs to be degraded. The Inada lab investigated the degradation of the nascent polypeptide by a reporter system (Kobayashi *et al.*, 2010). A 3' *cis*-acting ribozyme was introduced in the

mRNA of a *GFP* reporter. *Cis*-cleavage of the ribozyme *in vivo* resulted in a truncated mRNA and the *no-go* decay surveillance pathway was triggered (Kobayashi *et al.*, 2010). Interestingly, in the case of the *dom34Δski2Δ* double knockout, the protein level of the reporter was heavily increased or its degradation blocked (Tsuboi *et al.*, 2012). Reporter-tRNA in the ribosome was displayable by pH neutral gels resulting in an upshift of the reporter by 15 kDa due to the covalently bound tRNA.

3.1.1 Limits of present *in vitro* ribosome stalling approaches

For generating stalled or terminated ribosome nascent chain complexes (RNCs), the Pestova and the Green labs established fully reconstituted stalling and splitting assays in rabbit (reticulocyte lysate was used as source) and in yeast, respectively (Pisarev *et al.*, 2010, Pisareva & Skabkin *et al.*, 2011, Shoemaker & Green, 2011). In both approaches, the ribosomes translate only di- or tetra-peptides. In the translation reaction, termination or surveillance factors are omitted for enrichment of termination complexes. For generation of stalled complexes, a truncated mRNA is provided as a message. Finally, in a second reconstituted reaction, release factors and ABCE1 can terminate and split the ribosomal complexes. tRNA, mRNA, or ribosomal subunits were radiolabeled for probing the splitting reaction in SDGs by t/mRNA release, and ribosomal subunit dissociation (Pisarev *et al.*, 2010). In yeast, the tRNA-peptide was radiolabeled by ³⁵S-methionine. Post splitting, the radiolabeled tRNA-peptide remained bound to the 40S subunit and the splitting was resolvable by native PAGE (Shoemaker *et al.*, 2010). The short length of the translated peptide represents an artificial situation that may be *in vivo* relevant for splitting after uORFs. Intersubunit association is weak because it is dependent on the peptidyl-tRNA bond and its interactions of the nascent peptide residues with the peptide tunnel (Merrick & Hensold, 2001). Full translation of a protein results in folding of domains outside of the 60S peptide tunnel and prohibits back-translocation (Tsuboi *et al.*, 2012). Hence, if proteins are fully translated, the protein-tRNA cannot be located on the small ribosomal subunit after splitting, as occurs in the reconstituted splitting assays for di-/tetra-peptide-tRNA (Pisarev *et al.*, 2010, Shoemaker & Green, 2011). The protein-tRNA should rather remain after

splitting or anti-association in the large ribosomal subunit, as reported *in vivo* (Shao *et al.*, 2015, Tsuboi *et al.*, 2012). Importantly, the effort for establishing a fully reconstituted system is tremendous and quality control of all components requires validation of single freshly prepared components in an already working system.

In the cryo-EM field, termination complexes were successfully assembled on truncated mRNA, or stalling by a CMV-stall motif, or utilization of an eRF1(AAQ/AGQ) variant that does not hydrolyze peptidyl-tRNA nor result in splitting of the ribosome (Becker & Franckenberg *et al.*, 2012, Brown & Shao *et al.*, 2015, Preis *et al.*, 2014, Shao & Murray & Brown *et al.*, 2016). In all cases, the RNC preparation was based on *in vitro* translation. This approach is limited in yield, requires in general ribosome pelleting to gain sufficient concentrations for cryo-EM sample preparation, and splitting after termination was inefficient or not possible. In addition, downstream processes or side processes are not fully excluded, *e.g.* ubiquitination of stalled proteins or ribosomes.

3.1.2 *In vivo* ribosome stalling – approach, constructs, and challenges

3.1.2.1 Programming construct

I started the *in vivo* stalling approach during my internship in the Green lab to generate splitting competent RNCs at native conditions and to overcome limitations of reconstituted assays and *in vitro* translation-based approaches, see **section 3.1.1**. The basic idea was to utilize a nascent chain (NC) reporter with an N-terminal affinity purification tag and a 3'-stalling motif for *in vivo* translation stalling. In theory, a *no-go* decay surveillance deficient background (*dom34Δ*) would circumvent recycling and RNC complexes could enrich for purification. The Inada lab published later a similar approach for the purification of stalled complexes that were not used for splitting (Ikeuchi & Inada, 2016).

As a first reporter, I used *PGK1* as used by the Parker lab (Doma & Parker, 2006). 3'-stalling motifs were a 66 nt long stem loop (Hosoda *et al.*, 2003), a *cis*-acting hammerhead ribozyme that generates *in vivo* a truncated mRNA by cleaving the mRNA at a defined position (Haseloff & Gerlach, 1988), and as a control a Myc-stop (Myc-*) motif (**Figure 7**).

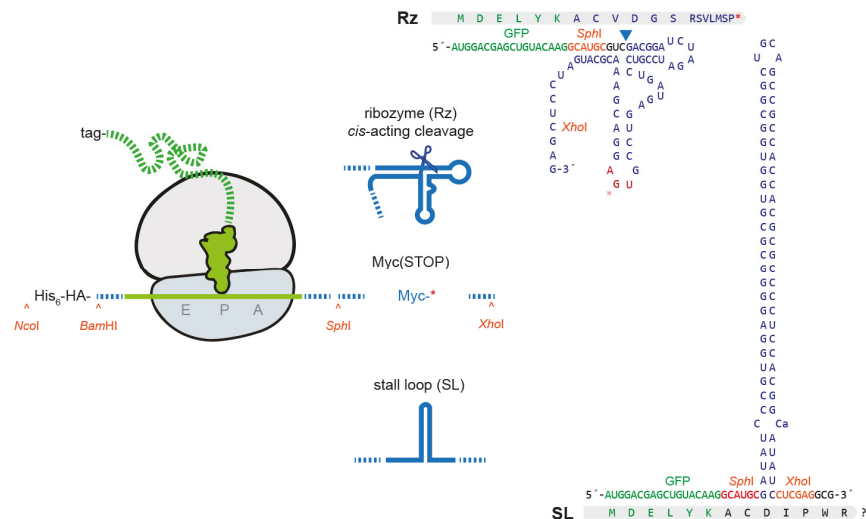


Figure 7 | *In vivo* stalling approach. Ribosomes are *in vivo* stalled by a programming construct that codes for an N-terminal affinity purification tag, GFP as a fluorescent reporter, and a 3'-stalling motif. A Myc-stop motif (Myc-*) served as control. Secondary structures of the RNAs are illustrated for the *cis*-acting cleavage ribozyme (Haseloff & Gerlach, 1988) and the stall loop (Hosoda *et al.*, 2003).

The expression plasmids were pAG426 under the control of a constitutively expressing *GPD* promoter and the pYes2 plasmid under the control of a *GAL1* promoter. The latter would be of interest, if the stalling reporters were lethal for the cells and an expression switch would become necessary. The reporter construct *PGK1-Myc** was amplified by polymerase chain reaction (PCR) and introduced by TOPO-cloning into the pAG426 and pYes2 plasmids, see **section 2.2.1**. To enable further exchange and modification by restriction enzyme cloning, restriction sites were included in a modular fashion before and after the N-terminal tag, reporter, and stalling motif (*NcoI*-tag-*BamHI*-reporter-*SphI*-stalling motif-*XhoI*, **Figure 7**). Stalling motifs were introduced by restriction and ligation as phosphorylated primer pairs with restriction site overhangs to the reporter and the backbone. N-terminally, His₆-HA-tag, a BirA biotinylation prone Avi-tag (Jan & Williams *et al.*, 2014), and the Nano-tag (Lamla & Erdmann, 2004) were inserted for purification purpose (data not shown); the His-tag was used in *in vitro* translation approaches by the Beckmann lab (Becker & Franckenberg *et al.*, 2012). Constructs were verified by sequencing; only the stem loop yielded as expected terminated reads. Finally, plasmids carrying the reporter constructs were transformed in the

surveillance deficient *dom34Δ*, and *dom34Δski2Δ* strains. In subsequent studies, the *PGK1* reporter was exchanged for the *GFP* reporter to allow for fluorescent detection.

3.1.2.2 Proof of principle - 80S–GFP-tRNA (RNC_{GFP})

In initial experiments, no growth defect was observed upon galactose induction and at constitutive expression of the stalling constructs (only partial data shown, **Figure 8a**), hence in further experiments, I switched exclusively to the pAG426 plasmid under the control of the constitutively expressing *GPD* promoter (**Figure 8a**).

In polysome profiles, 80S levels were significantly increased upon expression of the reporter with the 3' ribozyme stalling motif in the *dom34Δski2Δ* background (**Figure 8b**). In addition, GFP-tRNA co-localized with 80S fractions (**Figure 8c**). No upshift of the reporter was detectable in Tris/HCl SDS-PAGE gels based on the Laemmli system (Laemmli, 1970). Thus, the basic conditions in the resolving gel at a pH about 8.8 hydrolyze the sensitive peptidyl-tRNA bond. I switched the gel system to neutral gels based on Bis-Tris pH <7.0 (NuPage Bis-Tris gels, Thermo Fischer Scientific) that finally resulted in the published upshifted GFP-tRNA at 80S fraction as reported previously by the Inada lab (Tsuboi *et al.*, 2012).

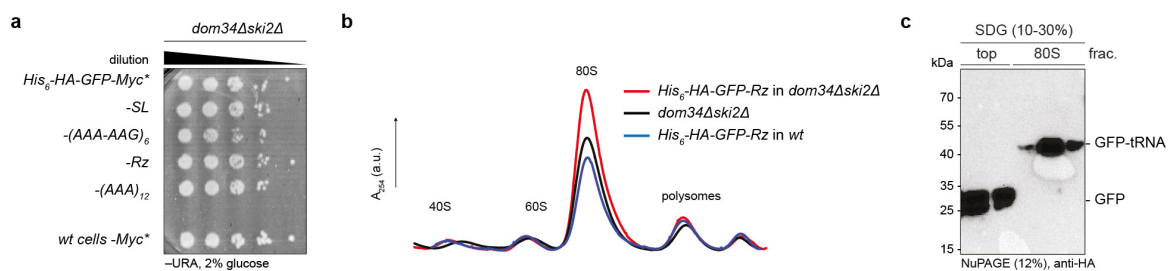


Figure 8 | Proof of principle for *in vivo* stalling. a, No growth defect was observed at constitutive expression of stalling motifs in the *dom34Δski2Δ* background (n=1). **b**, The 80S population was significantly increased upon expression of the *His₆-HA-GFP-Rz* reporter in the *dom34Δski2Δ* background (n=1). **c**, GFP localized at 80S fractions and upshifted due to covalent linked tRNA (GFP-tRNA) (n=2).

In initial experiments, the GFP reporter was stalled in the large ribosomal subunit. Hence, its C-terminal part (~10 amino acids) was not translocated completely outside the peptide tunnel, and GFP could not properly fold. The consequence was a GFP reporter that was not fluorescent at stalled ribosomes. Upon C-terminal extension of the GFP reporter by a Myc₂-tag, GFP folded and become fluorescence active. Total cell GFP production was verified by fluorescence-microscopy (**Figure 9**). Finally, an upshifted fluorescence active GFP(Myc₂)-tRNA signal at 45 kDa (referred here as GFP-tRNA) became visible at 80S fractions in polysome profiles (**Figure 9b**). Strikingly, the GFP-tRNA at 80S was only detectable in the *dom34Δski2Δ* background and not in *dom34Δ*. An additional fluorescent impurity (*) at 45 and 70 kDa could be separated in top fractions at low salt SDG conditions (150 mM KCl). The Myc^{*} control construct without a stalling motif was omitted in this thesis, because of the negative control by *dom34Δ*.

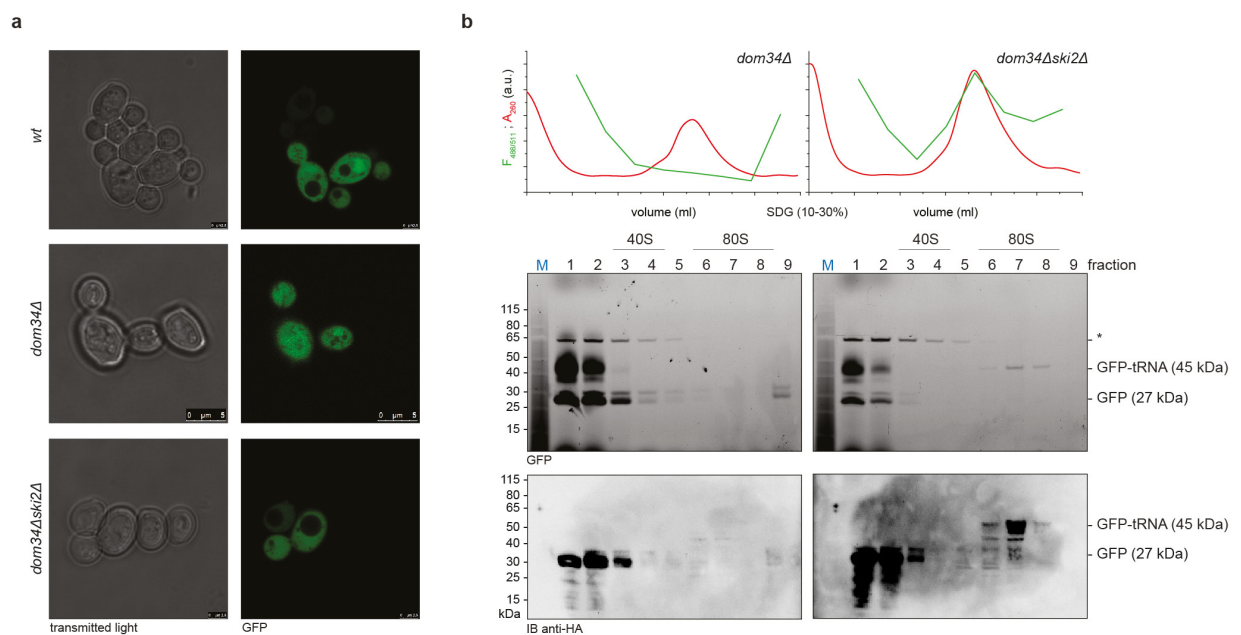


Figure 9 | GFP-Rz-tRNA co-localized in SDG with 80S ribosomes in *dom34Δski2Δ*. **a**, *No-go* surveillance deficient and *wt* yeast cells expressing stalling construct *GFP(Myc₂)-Rz* were fluorescently active. A. Klein (Institute of Biochemistry, Goethe University) contributed by taking images of yeast cells at the confocal fluorescence laser scanning microscope (n=3). **b**, The upper gel represents the GFP fluorescence, and the lower gel the anti-HA immunoblot. GFP-tRNA co-localized with 80S fractions exclusively in the *dom34Δski2Δ* background. GFP and fluorescently active impurities at 45 and 70 kDa localized at top fractions (*) (n=1).

3.1.2.3 40S-GFP (R_{GFP}) labeling for the third generation splitting assay

A fluorescently labeled nascent chain is useful in splitting experiments for tracking of the peptidyl-tRNA. Nevertheless, after splitting, only the large ribosomal subunit would be trackable by the stuck peptidyl-GFP. To visualize the small ribosomal subunit in splitting experiments by in gel detection, I decided to label a protein of the 40S subunit by GFP. Ribosomal proteins that allow a labeling by GFP are hard to identify, and fortunately, T. Becker (Beckmann lab) provided me the internship protocol of A. Hiekel, who labeled ribosomal proteins by GFP and checked the strains for cell viability (Hiekel, 2007). Asc1 (Rack1 in *H. sapiens*) was labeled by GFP at the C terminus (**Figure 10a**). S3/S4 primers were used for *GFP-HA-KanMX4* amplification from the pYM27 plasmid (encoding *GFP*, provided by P. Kötter) for generation of a PCR fragment for C-terminal recombination at *asc1*. The construct generation was performed as described by the Knop lab (Janke *et al.*, 2004, **Figure 10b**).

The genomic tagging of the small ribosomal subunit is sufficient in the case of *wt* strains but *in vivo* stalling of RNCs required the *dom34Δski2Δ* background (located on chromosomes XIV and XII, respectively). *asc1-GFP-HA-KanMX4* (strain MG002, this study) was modified by homologous recombination to *asc1-GFP-HA-NAT1* (strain MG003) by transformation of *NotI* restricted pAG36 plasmid (encoding *NAT1*, provided by P. Kötter, coding for nourseothricin resistance cassette, **Figure 10b**). *asc1-GFP-HA-NAT1* on chromosome XIII was crossed with the *dom34Δski2Δ* (*KanMX4*) background, and selected *via* tetrad analysis on G418 and nourseothricin. The final strain was *Mata ski2::KanMX4 dom34::KanMX4 asc1::asc1-GFP-HA-NAT1* (strain MG004). P. Kötter supervised the work; he and S. Lamberth performed the selection and tetrad analysis. Asc1-GFP-HA production in yeast cells was checked by confocal fluorescence laser scanning microscopy (**Figure 10c**). Asc1-GFP-HA (about 61 kDa) co-localized with 80S fractions (**Figure 10d**). In SDG, co-localization with 40S could not be visualized because the level of free 40S is low compared to 80S. Alternatively, co-localization of Asc1-GFP-HA with the 40S subunit was verified by native PAGE and in gel fluorescence after anti-association (**Figure 12a**). Free GFP (about 27-35 kDa) localized at top fractions, indicating that Asc1 was degraded. Interestingly, smaller fragments of Asc1 co-localized with

80S fractions that must be cleaved in Asc1 because the C-terminal part with GFP (35 kDa) is still fluorescently active. Of note, Asc1 has a seven bladed β -propeller structure (Coyle *et al.*, 2009). Potentially, only the C-terminal part (10-15 kDa) is required for binding to 40S or it can form multimers that bind the ribosomal subunit and compensate for the degraded blades.

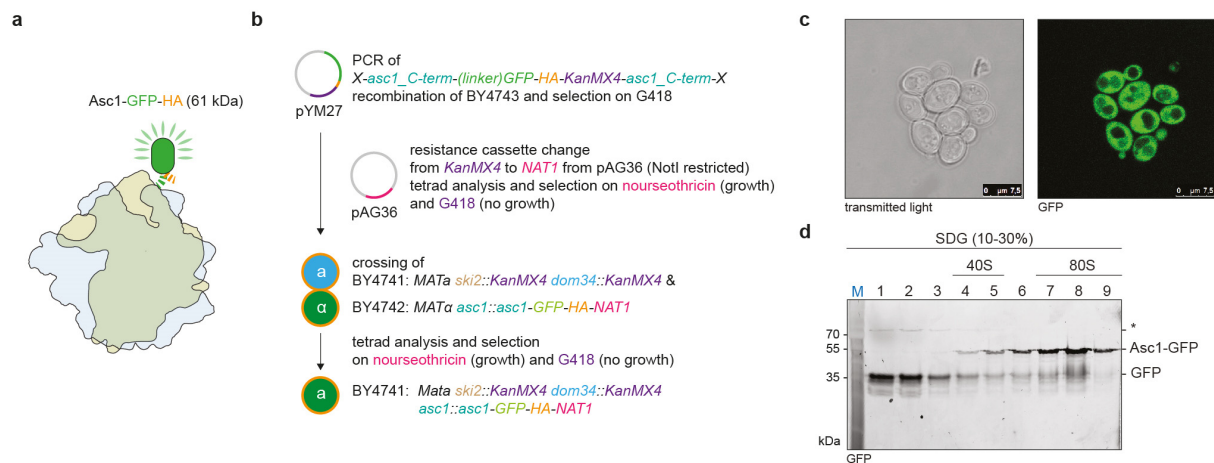


Figure 10 | 40S(Asc1-GFP-HA) production in the *dom34Δski2Δ* background. **a**, Asc1 of the small ribosomal subunit was C-terminally labeled with GFP-HA, scheme in the 80S complex. **b**, Genomic tagging was achieved by standard yeast techniques. The *GFP* insert was amplified from pYM27 with flanking regions of the C-terminal part of *asc1* by extended primer PCR. pAG36 was used for selection marker exchange from *KanMX4* to *NAT1*. The double-deletion strain *dom34Δski2Δ* was crossed with the *asc1-GFP* strain and resulted after tetrad analysis in a haploid strain that contained deletions of *dom34* and *ski2*, and the labeled *asc1-GFP-HA*. P. Kötter and S. Lamberth performed the tetrad analysis for the generation of the strain MG004. **c**, Yeast cells were fluorescent due to production of Asc1-GFP-HA. A. Klein contributed by taking images of yeast cells at the confocal fluorescence laser scanning microscope (n=3). **d**, Asc1-GFP co-localized in 80S fractions in SDG. A fluorescent degradation product at 36 kDa was present in top fractions (n=2). * indicates a fluorescent protein in yeast that was also present in **Figure 9**.

3.1.2.4 Purification and validation of R_{GFP}NC_{GFP} constructs

Affinity purification by streptavidin *via* the Avi- and Nano-tag constructs did not yield any ribosome pattern in elution samples (data not shown). In the literature, I realized that the Nano-tag is only usable in prokaryotes because the N-terminal methionine must be formylated (fMet) in order to bind into the streptavidin pocket (Perbandt *et al.*, 2007). The

Avi-tag purification suffered most likely from high biotin levels in the lysate or the inability of nascent peptide chain biotinylation by BirA (data not shown). For the sake of progress, I decided to use the metal-affinity purification *via* His-tag that could be later exchanged.

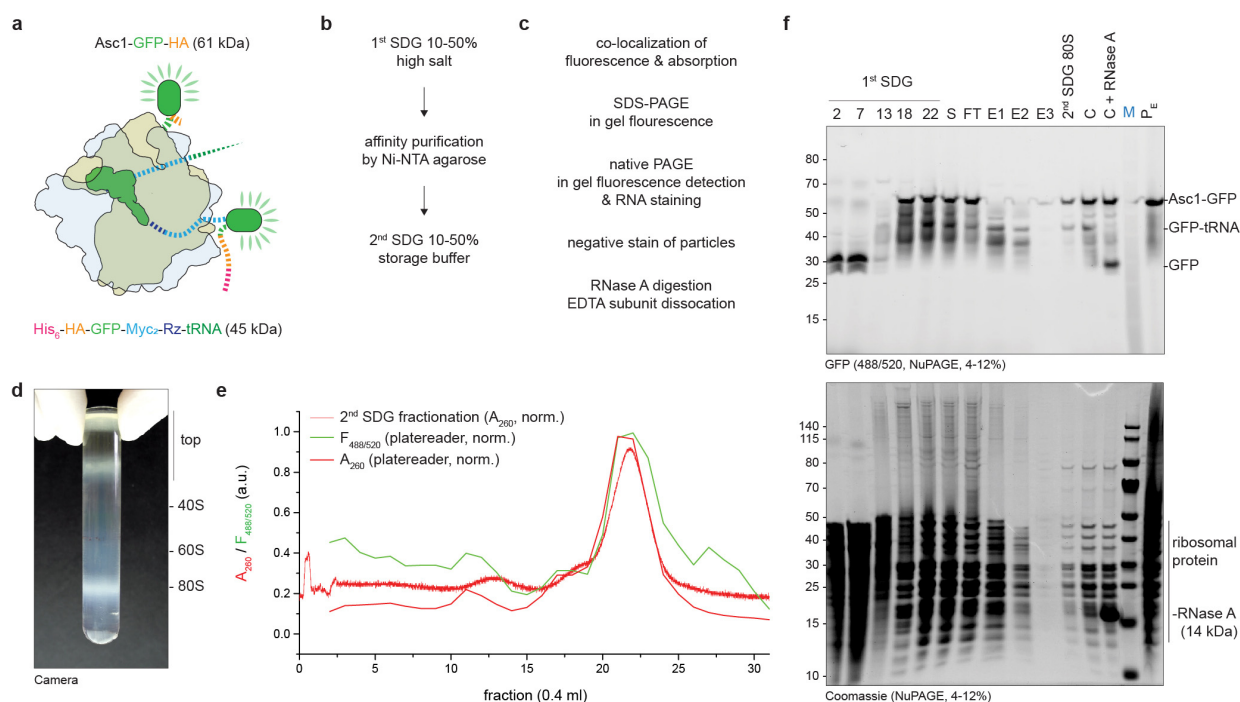


Figure 11 | Purification of 80S-GFP-Rz. **a**, Illustration of an RNC that is stalled on truncated mRNA with a GFP reporter nascent chain and GFP labeled Asc1. **b**, Purification plan including SDG and affinity purification. **c**, Quality control steps. **d**, First SDG step. **e**, The GFP fluorescence correlated in the second SDG profile with 80S fractions displayed by absorption at 260 nm. **f**, Purification steps were analyzed by SDS-PAGE (NuPAGE). The final concentrated sample showed a fluorescence signal for Asc1-GFP and for the nascent chain GFP reporter that was downshifted upon RNase A treatment to the size of GFP. Fluorescence intensity for Asc1 and the GFP from the nascent chain were equal after RNase A treatment. The total ratio of stalled RNCs to unlabeled ribosomes was low and could not be determined. (n=3)

Cobalt-based IMAC was used as resin for affinity purification of RNCs that carry a His-tagged nascent chain, as reported by the Beckman lab (Becker & Frankenberg *et al.* 2012). The purification buffer conditions were set to a pH of 7.0, 250 mM KOAc salt, and 25 mM MgCl₂. In the optimization of the purification procedure, I figured out that increased salt concentrations are necessary for efficient binding of RNCs to the resin, most likely because

of reduced charge repulsion. In agreement, a high salt concentration in purification buffers was also used in the Christodoulous lab for 70S RNC preparation by metal chelate affinity purification (Cabrita *et al.*, 2009, Cassaignau & Launay *et al.*, 2016). The affinity purification resins Ni- or Co-NTA did not make a difference in purification efficiency or quality (data not shown).

In the here used purification procedure, I utilized an initial high salt SDG run at 500 mM KCl and 25 mM MgCl₂ for 80S ribosome selection. In a second step, Ni-NTA affinity purification selected for the programmed ribosomes that produced the His-tagged nascent chain. Eluted fractions were collected and loaded on a second gradient in storage buffer at 150 mM KCl and 2.5 mM MgCl₂ (for a detailed procedure see methods **section 2.4.7**). In SDS-PAGE, RNCs yielded fluorescent bands at 45 kDa for the GFP-tRNA nascent chain (**Figure 11**). In addition, no free GFP co-sedimented with 80S. Notably, the fluorescent GFP-tRNA and the Asc1-GFP band are hardly distinguishable from other proteins in the Coomassie stained SDS-PAGE gel, hence the yield of R_{GFP}NC_{GFP} to 80S ribosomes was low. Nevertheless, the fluorescence readout enables a tracking of splitting by native PAGE and in gel fluorescence.

Importantly, Asc1-GFP was preserved at the R_{GFP}NC_{GFP} ribosome after the second gradient. An RNase A treatment degraded the tRNA part of the GFP-tRNA and shifted the band to GFP size. Strikingly, the fluorescence intensities of the Asc1-GFP and GFP-tRNA bands were equal after RNase A treatment (**Figure 11f**, lane C). In agreement, the Inada lab has shown that if *dom34* is knocked-out, *asc1* is required for 3' mRNA cleavage at stalled complexes (Ikeuchi & Inada, 2016, Matsuda & Ikeuchi & Nomura *et al.*, 2014). Peptidyl-tRNA levels were elevated in *dom34Δski2Δ* strains if Asc1 was present. In addition, Asc1 repressed the E3 ubiquitin ligase (Ltn1 and Not4) and the Cdc48 dependent proteasomal degradation of nascent chains, and acted as a fail-safe in the *no-go* decay pathway (Ikeuchi & Inada, 2016, Matsuda & Ikeuchi & Nomura *et al.*, 2014). Apparently, the purified RNCs that carry a fluorescent nascent chain are occupied stoichiometrically by Asc1 that based on literature preserves the complex from proteasomal degradation. Importantly, no fluorescent signal was detected in the pocket of the gel lane that would occur upon poly-ubiquitination of the nascent chain or ribosome. In agreement with published work, splitting is a strict

requirement prior ubiquitination that was prevented here because Dom34 was deleted in the here used strains (Lyumkis & Oliveira dos Passos *et al.*, 2014, Shao *et al.*, 2015).

Sample verification by native PAGE resulted in fluorescently active $R_{GFP}NC_{GFP}$ ribosomes, and upon 1 mM EDTA treatment the subunits disassociated and released the peptidyl-tRNA (**Figure 12a**). Parallel purification of R_{GFP} and $R_{GFP}NC_{GFP}$ enabled the identification of the peptidyl-tRNA and 40S–Asc1 bands. In addition, RNA staining enabled the identification of 40S/60S bands. Interestingly, the Inada lab showed that EDTA treated extracts resulted in GFP-tRNA localization at the 60S fractions in polysome profiles (Tsuboi *et al.*, 2012). In the R_{GFP} sample, at 60S a slight shadow is still preserved that may represent 60S–tRNA-GFP (**Figure 12a**). Most likely, the EDTA concentration was set too high and the tRNA-nascent chain in the 60S subunit was released or hydrolyzed by a pH shift. The nascent chain GFP-fluorescence intensity was equal to the intensity of the 40S–Asc1-GFP signal, as discussed above (see **Figure 11f**). In addition, the particle homogeneity and concentration was ideal for cryo-EM reconstruction probed by negative staining (**Figure 12b**) with kind support of A. Heuer (Beckmann lab).

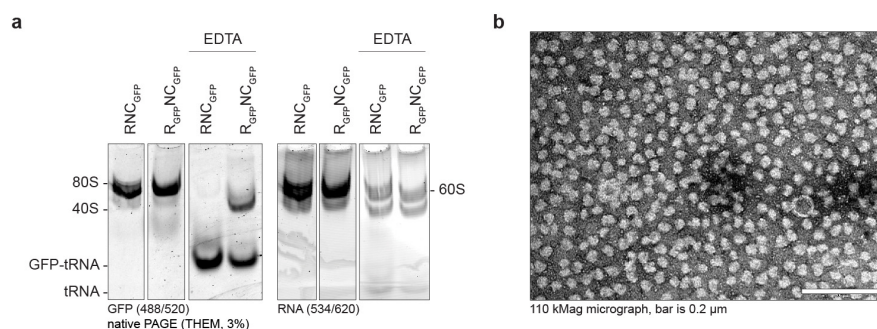


Figure 12 | Quality control of 80S–GFP–Rz. **a**, R_{GFP} and $R_{GFP}NC_{GFP}$ were compared in native PAGE (THEM, 3%). Both run as a single 80S band and upon 1 mM EDTA treatment the GFP-tRNA (NC) is released and 40S(Asc1-GFP) became apparent as a distinct band. Ribosomal subunits and tRNA were stained by SYBR® Gold (n=2). **b**, Negative stained and EM imaged $R_{GFP}NC_{GFP}$ samples were homogeneous in distribution and particle size. A. Heuer contributed by negative staining and EM imaging (n=1).

The purification yield of *in vivo* stalled RNCs from a 4 l liter culture (OD of ~1.5) was about 200 nM in 200 μ l (40 pmol). Finally, the ratio of splitting competent ribosomes in the fluorescently active fraction can be determined in a splitting assay, see **section 3.4**. Prospectively, the affinity purification tag should be exchanged to the FLAG- or protein-A-tag with a TEV cleavage site to improve purification and to rule out impurities by non-stalled 80S complexes.

Notably, the purity of programmed RNCs is not determinable by fluorescence because upon a stall, the mRNA is processed at the ribosomal 5' site or the following translating ribosome collides and stacks with the leading stalled ribosome resulting in a truncated mRNA or reduced translated message, respectively, that codes for a shorter reporter construct. The truncated reporter is not anymore fluorescently active upon translation and stalling because the truncated variant is not able to fold outside of the ribosome. It is worth mentioning that C-terminal Myc₂ tag insertion was necessary to yield a fluorescently active GFP reporter (see **section 3.1**). Formally, the non-fluorescent RNCs represent also a substrate for the *no-go* decay pathway. In reference to ribosome profiling studies, collided ribosomes (disomes) were significantly enriched and represented the majority of stalled ribosomes (Guydosh & Green, 2014). The equal fluorescence signal of Asc1-GFP and the full-length GFP nascent chain reporter in *in vivo* stalled and purified ribosomes (**Figure 12a**) could be explained by selective Asc1 binding to the leading stalled ribosome. Recently, collided ribosomes were reconstructed in which only the stalled 80S–eRF1(AAQ)–ABCE1 ribosome was occupied by Rack1 (Asc1 in yeast) that was in close proximity to ubiquitination sites at uS3 and uS10 of the colliding ribosome (Juzskiewicz & Chandrasekaran *et al.* 2018). Hence, the here proposed occupation of the leading stalled ribosome by Asc1 is valid. Subsequent fluorescence-based splitting assays with the here produced *in vivo* stalled RNCs probe exclusively for splitting of the leading stalled RNCs with bound Asc1.

3.2 *In vitro* programming of ribosomes

Empty 80S ribosomes that lack mRNA and tRNA are called *vacant* because the subunits are only loosely associated due to the missing tRNA–mRNA pairing and stabilization of peptidyl-

tRNA in the peptide channel (Merrick & Hensold, 2001). The Pestova lab showed that *vacant* ribosomes are split by Pelota and ABCE1 (Pisareva & Skabkin *et al.*, 2011). In addition, a mRNA free A-site was strictly required for Pelota and ABCE1 dependent splitting. Consequently, Pelota and ABCE1 were only able to split pre-termination complexes with a stop-codon in the A-site after treatment with RelE that cleaves the mRNA in the A-site. This is in agreement with the structural observation that the prolonged N-domain in Pelota occupies the mRNA-free A-site and senses a *no-go* situation (Hilal *et al.*, 2016).

Ribosomes for splitting studies with a free A-site were prepared from subunits, mRNA, and aminoacylated tRNA. High salt and low magnesium conditions in SDG disassociated puromycin treated 80S ribosomes into subunits, see **sections 2.4.5** and **3.2.2**. Re-association resulted in *vacant* 80S ribosomes that showed a clear and exclusive ribosomal protein pattern in SDS-PAGE (**Figure 34a**). In addition, the Spahn lab showed that occupation of 80S by Dom34/Hbs1 required tRNA and mRNA (Hilal *et al.*, 2016). The preparation of 80S–mRNA–Phe-tRNA^{Phe} was followed up in the **next sections**.

3.2.1 Aminoacylation of Phe-tRNA^{Phe}

To prepare RNCs with a free A-site, the mRNA in the ribosome must be fixed at a defined position by pairing with a corresponding aminoacylated-tRNA. The Spahn lab used phenylalanine-tRNA (Phe-tRNA^{Phe}) that must be bound in the ribosome to stabilize the subunit interaction and downstream purification by SDG fractionation. Aminoacylation was executed enzymatically by the S100 extract, ATP, phenylalanine, and Phe-tRNA from *brewer's yeast* (commercially available name from Sigma-Aldrich), as established by the Green lab (Eyler & Green, 2011). Aminoacylated tRNA was purified by reversed-phase high-performance liquid chromatography (RP-HPLC) as previously described for the bacterial system (Studer & Joseph, 2007). The efficiency of aminoacylation was determined by a shift in the RP-HPLC elution profile and an upshift of aminoacylated tRNA in urea-PAGE as described previously (Walker & Fredrick, 2008, Studer & Joseph, 2007).

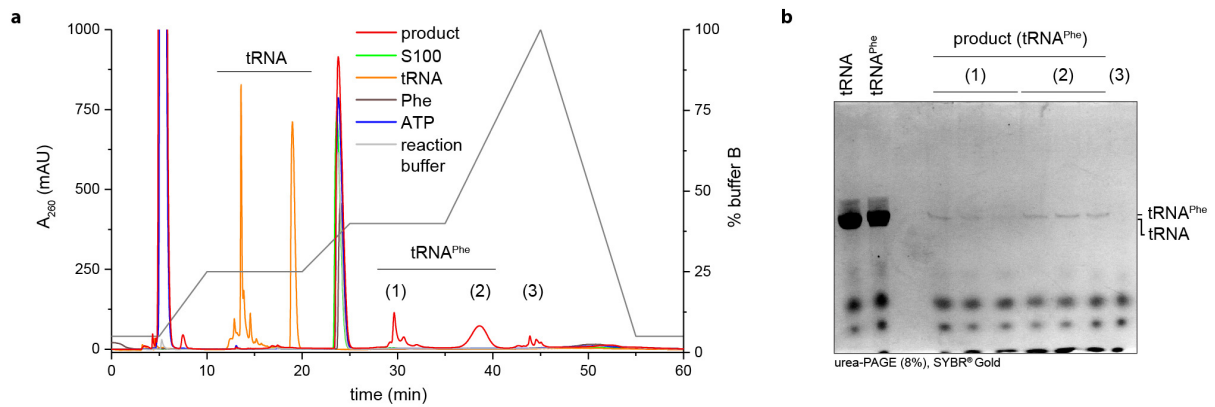


Figure 13 | Aminoacylation of tRNA^{Phe}. **a**, tRNA elution was shifted upon phenylalanine-aminoacylation from 25% to 45-60% (v/v) buffer B in RP-HPLC (C18 column, n=1). Buffer A (20 mM Tris/OAc pH 5.0, 400 mM NaCl, 10 mM MgOAc₂), buffer B was the same as buffer A with 60% (v/v) methanol. **b**, Aminoacylated tRNA was up-shifted in 8% (w/v) urea-PAGE and collected in fractions 1 and 2 (n=1).

tRNA^{Phe} eluted in RP-HPLC at 25% (v/v) buffer B in a number of defined peaks (yellow). Hence the population was not pure and may correlate with the two possible tRNAs that code for phenylalanine, plus secondary modifications and isoforms (e.g. 10 for Phe-tRNA^{Phe}-GAA, Chan & Lowe, 2016, **Figure 13a**). ATP eluted at 7% buffer B. At 40% a defined peak eluted that was present in all samples and corresponded to the reaction buffer. Most likely, the peak represents the reducing agent DTT in the reaction buffer (5 mM). In the oxidized form, DTT absorbs in the ultraviolet region (Cleland, 1964). Phe-aminoacylated tRNA (Phe-tRNA^{Phe}, product, red) eluted as of 45% buffer B in two distinct peak regions that contained upshifted tRNA as indicated in urea-PAGE (**Figure 13b**). No tRNA eluted in the product sample at 25%, hence, all tRNA was aminoacylated. tRNA was concentrated and stored at acidic conditions. The tRNA concentration was determined by an extinction coefficient of 733,000 M⁻¹cm⁻¹ as reported previously for *E. coli* tRNA (Chudaev *et al.*, 2013).

3.2.2 Preparation of ribosomal subunits

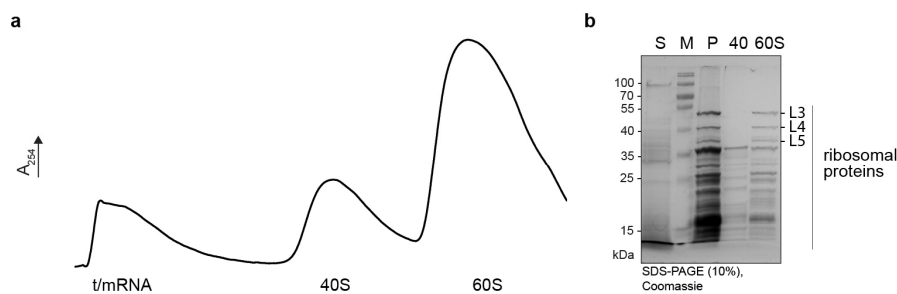


Figure 14 | Preparation of ribosomal subunits. a, Ribosomal subunits were anti-associated at high salt and low magnesium conditions in a 5-20% SDG after puromycin treatment. **b,** In SDS-PAGE, pelleted crude ribosomes (P) showed a 80S protein size pattern, and ribosomal subunits an 40/60S subunit pattern (n=3).

Ribosomal subunits were prepared by a protocol of the Green lab that was based on a Lorsch lab protocol (Acker *et al.*, 2007). Ribosomes were pelleted through a high salt cushion and puromycin treated for peptide release (see **section 2.4.5**). Subunits were anti-associated in a high salt and low magnesium gradient (**Figure 14a**). This strategy yielded finally pure subunits (**Figure 14b**). The purity of the small subunit was highly dependent on high salt conditions and sample amount because the separation efficiency between top and subunit fractions is limited in SDG fractionation. The purity of the small subunit is crucial because factors from top fractions can co-localize in the final high salt SDG and associate in subsequent steps. Only if the subunits showed a pure ribosomal pattern in SDS-PAGE, re-association at low potassium conditions was efficiently possible. Importantly, if the cell disrupter (French press) was used for cell lysis, the ribosomal subunits did not yield a pure ribosomal pattern in SDS-PAGE (data not shown), most likely because the nucleus was also disrupted yielding ribosomal biogenesis complexes. Finally, cell lysis by Zirconia beads and vortexing was satisfactory for subunit preparation, see methods **section 2.4.5**.

3.2.3 Assembly of 80S–mRNA–tRNA complexes

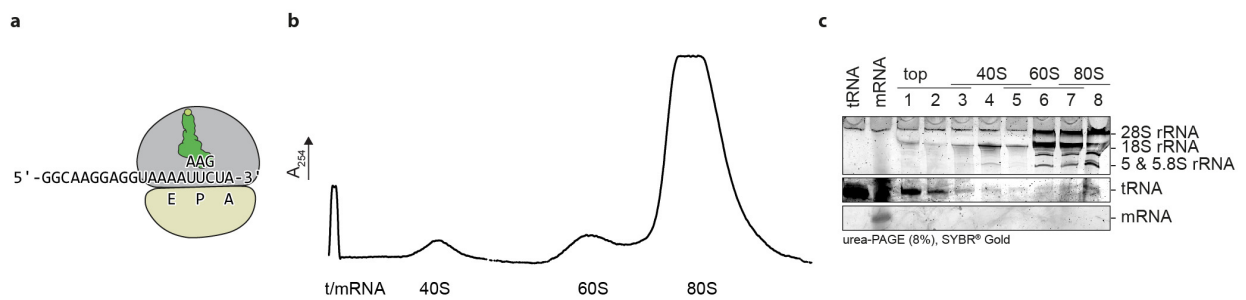


Figure 15 | Joining of ribosomal subunits, tRNA, and mRNA. **a**, Illustration of the 80S–mRNA–tRNA complex with two nucleotides in the A-site. **b**, Subunits joined nearly completely to 80S complexes in a 10-30% SDG. **c**, In 80S fractions, the tRNA intensity increased; indicating that the 80S complex assembled with bound mRNA (not detectable at this amount) and tRNA ($n=1$).

As published by the Spahn lab (Hilal *et al.*, 2016), *vacant* 80S ribosomes or ribosomal subunits bind and position mRNA in the intersubunit space by pairing with the supplied Phe-tRNA^{Phe} (**Figure 15a**). If only a single position on the mRNA codes for phenylalanine the phenylalanine-tRNA will pair with the mRNA and lock the mRNA in this position with the tRNA in the P-site. Re-associated 80S complexes were resolved by SDG fractionation and resulted in nearly full subunit joining (**Figure 15b**). mRNA and tRNA binding to 80S were verified by urea-PAGE. Based on the number of nucleotides of the 18S and 28S rRNA (~1900 and 4700 nt, respectively), the tRNA (~70-90 nt) is much smaller and its intensity in the gel is ~30-70 times lower compared to the rRNA in the 80S fractions. Notably, in 80S samples, the tRNA was present and visualizable (**Figure 15c**). The here used mRNA was even shorter (GGCAAGGAGGUAAAAUUCUA, 20 nt) and not detectable at all. In general, the 80S-loading with mRNA and tRNA was hardly determinable by RNA staining in urea-PAGE. Alternatively, mRNA loading could be checked by primer extension assays, if the mRNA is longer, or by radiolabeled mRNA and tRNA (Skabkin & Skabkina *et al.*, 2010). Cryo-EM reconstruction at low resolution is also a practicable and fast option for validation of complex assembly.

3.3 Production and purification of yeast translation factors

3.3.1 ABCE1_{H6}

In my internship in the Green lab (JHMI, HHMI, Baltimore, USA), I acquired, with kind support of A. Schuller, the knowledge about the production and purification of ABCE1 based on previously published protocols (Shoemaker & Green, 2011). R. Green provided the expression plasmid. In the Tampé lab, I modified the expression procedure for the sake of cost reduction (**Figure 16a-c**). Expression of ABCE1_{H6} was induced by galactose *via* the *GAL1* promoter on the pYes2_ABCE1_{H6} yeast expression vector (Thermo Fischer Scientific). Carbon catabolite repression blocks galactose induction in the presence of glucose. Hence, other carbon sources were necessary, *e.g.* raffinose, as used by the Green lab, but raffinose is extremely expensive. I was forced to find an alternative carbon source. Fortunately, raffinose can be exchanged to sucrose that is an inexpensive carbon source. Sucrose is hydrolyzed in yeast to glucose and fructose by Sucp, Malx2p, and Imap that are expressed in constitutive fashion (as reviewed in Marques *et al.*, 2016). Interestingly, the glucose resulting from sucrose hydrolysis did not repress the galactose induction. This was evident by the comparable yield of ABCE1 to purifications in the Green lab with raffinose. Notably, after induction, the production time should not exceed 16 h because ABCE1 C-terminal degradation was observed that is only detectable in immunoblots because the protein size changed marginally. Nevertheless, the purification strategy by IMAC and SEC did not yield pure protein. Hence, the purification strategy was modified by addition of a cation exchange chromatography (CIEX) step (**Figure 16c**). The Pestova lab used this CIEX step for the purification of native human ABCE1 (Pisarev *et al.*, 2010). The elution fractions of the CIEX were already pure and ABCE1 eluted monodispersely as a monomer in SEC (**Figure 16d,e**), for the purification strategy see methods **section 2.4.1**. Strikingly, I provided proof that the long-standing requirement of magnesium in the purification buffers is negligible. Moreover, addition of 0.1 mM EDTA did not harm the ABC system nor the FeS clusters. As favored in general, protein degradation by metalloproteases can be reduced by removal of divalent ions. The final polishing SEC step can be omitted, and the purification speeded up that preserves the sensitive FeS clusters from oxidation.

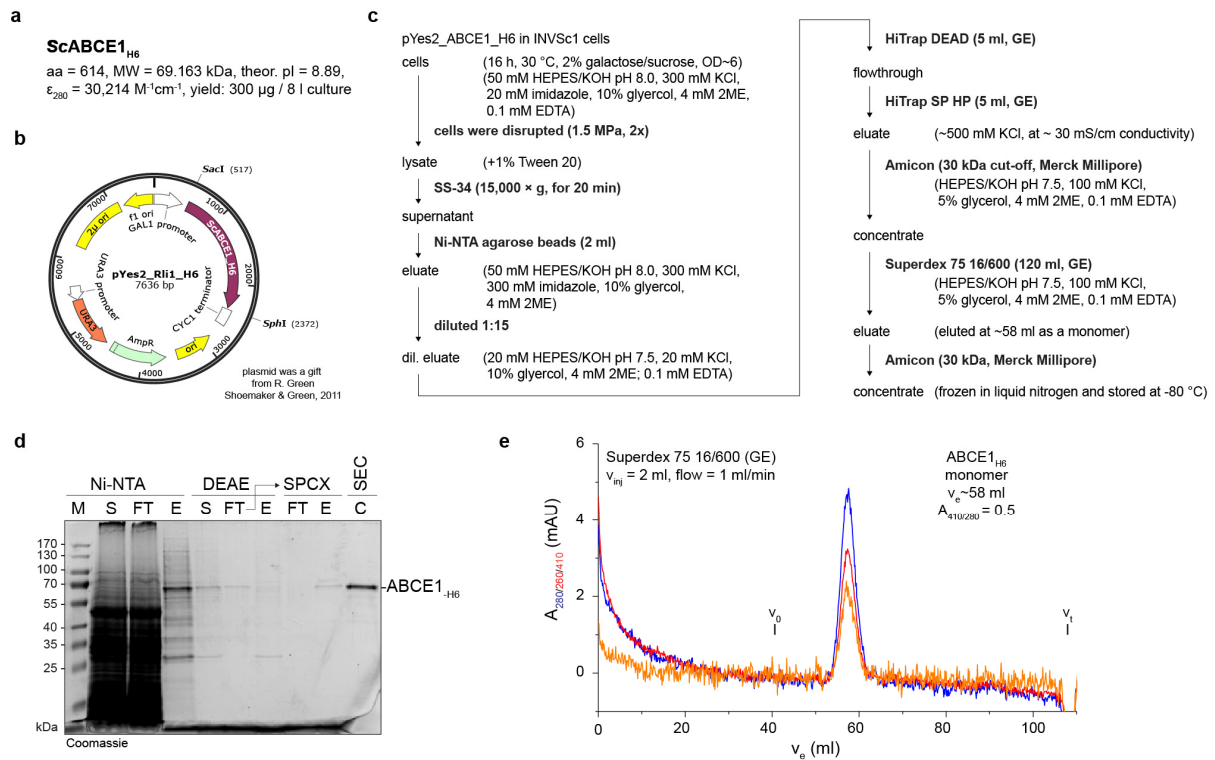


Figure 16 | Purification of ABCE1_{H6}. **a**, ABCE1_{H6} *wt* construct with C-terminal hexahistidine tag and protein parameters. **b**, pYes2_Rli1_H6 plasmid visualized by SnapGene®. **c**, The purification strategy included IMAC, AIEX(FT), CIEX, and SEC. **d**, ABCE1_{H6} was resolved as a pure band at 70 kDa in SDS-PAGE. **e**, In SEC, ABCE1_{H6} eluted monodispersely as a monomer at 58 ml corresponding to 70 kDa in size. v_0 and v_t indicate void and total volume, respectively ($n=5$).

In general, the quality of the isolated ABCE1_{H6} was evaluated by the 410/280 nm absorption ratio that is directly related to the ratio of assembled FeS clusters. The extinction coefficient at 410 nm is about $4,000 \text{ M}^{-1}\text{cm}^{-1}$ per iron, *i.e.* for two 4Fe-4S systems $32,000 \text{ M}^{-1}\text{cm}^{-1}$ (Sweeney & Rabinowitz, 1980). In agreement with the literature (Shoemaker & Green, 2011), the maximum observed ratio of 410/280 nm was 0.5. Taken the absorption coefficients into account (**Table 3**), the purification yielded only 50% of assembled FeS clusters. A reason could be oxidation of the FeS clusters because the purification was not conducted at anaerobic conditions. In conclusion, the highest ratio of assembled FeS clusters was obtained after extensive degassing of purification buffers and supplementation of all buffers with 4 mM 2-ME or 2 mM DTT reducing agents. In summary, this optimized production and

purification strategy for ABCE1_{H6} yielded pure protein in sufficient amount for functional assays. The ratio of 410/280 nm absorption indicated 50% assembled FeS clusters, which is consistent with previous publications (Shoemaker & Green, 2011).

Heterologous production of ABCE1 in *E. coli* would allow for substitution of catalytic residues that is lethal in the case of homologous expression in yeast. I cloned yeast ABCE1_{H6} in the pSA4 vector. However, yeast ABCE1 could not be produced in *E. coli* (data not shown).

In collaboration with S. Trowitzsch (Institute of Biochemistry, Goethe University), I tried to express ABCE1_{H6} from *S. cerevisiae* under the control of the *P10* promoter in Sf21 insect cells via the baculovirus expression system (Trowitzsch *et al.*, 2010). I cloned ABCE1_{H6} into the transfer plasmid pAMI by SLIC (see **section 2.2**) and S. Trowitzsch conducted all selection and expression steps. The transfer plasmid was transformed in DH10Bac™ cells carrying the bacmid (bMON14272: *mini-F replicon, kan, LacZ, attTn7, YFP*, 136 kB) and helper plasmid (pMON7142: *transABCD region*, 13.2 kB). Cells that carry the bacmid with ABCE1_{H6} were selected by blue/white screening. The bacmid DNA carrying ABCE1_{H6} was isolated and used for transfection of insect cells. The baculovirus was produced by the cells and isolated from the supernatant for infection of cells and subsequent protein production. Protein production was examined in a small purification screen. In summary, this approach yielded a high level of ABCE1 but all was in the pellet fraction (data not shown).

I supervised T. Reichhart, a student in the Tampé lab, who cloned ABCE1 from the thermophilic yeast *Thermomyces lanuginosus* into the pSA4, pYes2, and pAG426 vectors for expression in BL21 and INVSc1 cells, respectively. Extraordinarily, the FeS cluster domain comprised of introns and exons on the genomic level. Hence, the ABCE1_{H6} gene was assembled *in silico* without introns and ordered on a plasmid. In the end, no ABCE1 with present FeS clusters could be purified (Reichhart, 2015).

3.3.2 Dom34_{H6}

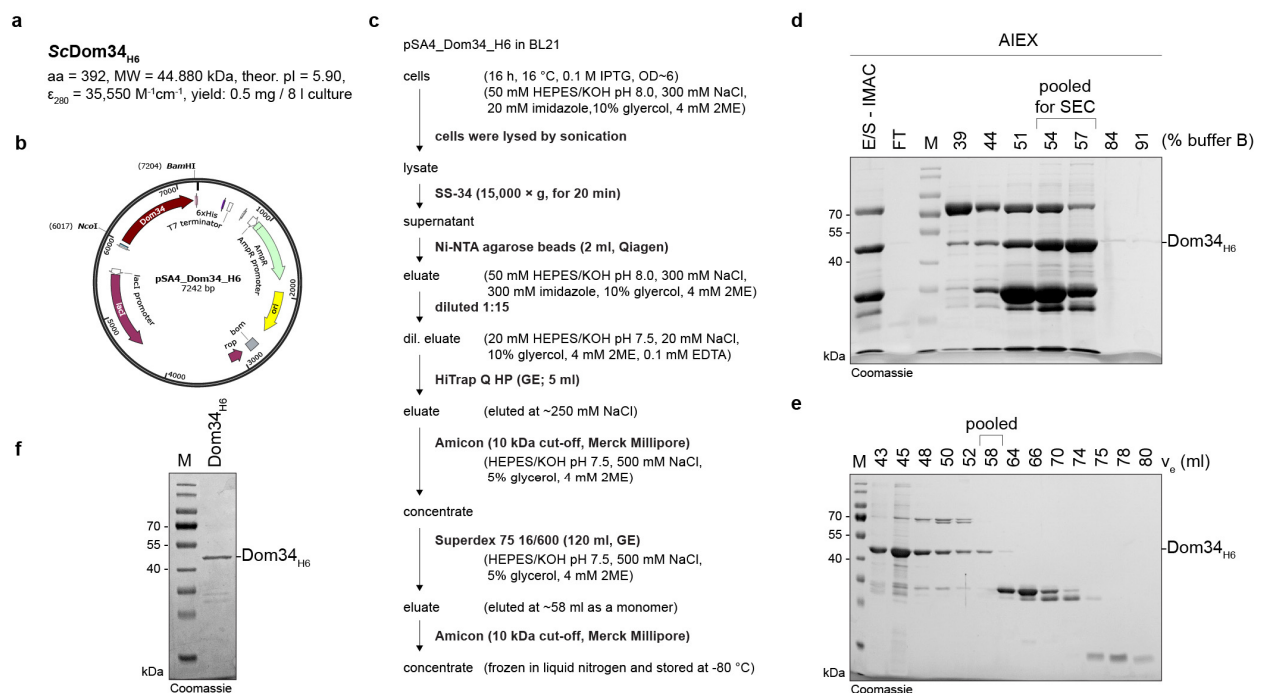


Figure 17 | Purification of Dom34_{H6}. **a**, Dom34_{H6} construct harboring a C-terminal hexahistidine tag and protein parameters. **b**, pSA4_Dom34_H6 plasmid visualized by SnapGene®. **c**, Purification strategy included **d**, IMAC, AIEX, and **e**, SEC. **f**, Purified Dom34_{H6} resolved by SDS-PAGE (12.5%) (n=3).

Release factor Dom34_{H6} was produced in *E. coli* by the Parker and Pestova labs (Passos *et al.*, 2009, Pisareva & Skabkin *et al.*, 2011), and in addition in yeast by the Green lab (Shoemaker *et al.*, 2010). In literature, all recombinantly produced Dom34/Pelota variants were successfully used in splitting assays with ABCE1 (Pisareva & Skabkin *et al.*, 2011, Shoemaker & Green, 2011). In a first attempt, I expressed Dom34_{H6} in *S. cerevisiae* (INVSc1) from the pYes2_Dom34_H6 plasmid and purified it as previously published (Shoemaker *et al.*, 2010). In the Tampé lab, I used the modified expression conditions as established for ABCE1_{H6}, see **section 3.3.1**, for Dom34_{H6} production. Unfortunately, I was unable to purify Dom34_{H6}. In a second attempt, I cloned *Dom34* from genomic *S. cerevisiae* DNA into the pSA4 vector with a C-terminal hexahistidine-tag for production in the BL21 *E. coli* strain (**Figure 17a,b**). The purification strategy (**Figure 17c**), see methods **section 2.4.2**, utilized IMAC, AIEX, and SEC, and yielded a pure protein that eluted monodispersely as a monomer in SEC (**Figure 17d-f**). Interestingly, all release factors (also from *S. solfataricus* and *T. kodakaraensis*, data not

shown) resulted a turbidity effect upon cooling down to 4 °C. This effect was reverted at the temperature shift to room temperature. Finally, Dom34_{H6} functionality was analyzed in a splitting assay, see **section 3.4**.

3.3.3 eIF6_{H6}

After splitting, ribosomal subunit re-association is blocked by the anti-association factor eIF6 that occupies the 60S subunit (Groft *et al.*, 2000). eIF6 was purified based on a procedure and expression plasmid (pET28b+_eIF6_H6) from the Green lab (JHMI, HHMI, Baltimore, USA) (Shoemaker *et al.*, 2010), see methods **section 2.4.3** and **Figure 18**. In general, the purified protein is impure and needed to be concentrated in order to obtain a sufficiently concentrated sample as an input in assays. In the immunoblot, the detected band at 35 kDa in the SEC elution (at $v_e \sim 70$ ml, **Figure 18d**) is located at slightly higher molecular weight than the pronounced band in the Coomassie stain. Interestingly, C-terminal truncation of eIF6 from *S. cerevisiae* was described previously. For cryo-EM studies, a truncated eIF6 construct was used that resulted in higher production yields (Groft *et al.*, 2000). Nevertheless, a slightly higher band at 37 kDa and $v_e \sim 55$ ml in SEC (**Figure 18d**) was immunoblot active indicating N-terminal degradation of the final product. Interestingly, no oligomerization of eIF6 was reported in literature, but detected in this study. Hence, the immunoblot active band at 37 kDa was neglected. The anti-association effect of purified eIF6 was analyzed by an anti-/re-association assay (**Figure 19a**) as previously reported (Groft *et al.*, 2000). In addition, eIF6 was bound to 60S subunits in polysome profile analysis as described in (Gartmann *et al.*, 2010, Groft *et al.*, 2000)(**Figure 19b**). In splitting experiments, eIF6 was added in excess in order to ensure saturating conditions despite high impurity. This is in agreement with the procedure in the Green lab (Shoemaker & Green, 2011).

Based on experience with the anti-/re-association assay for eIF6 activity validation, I decided to use this assay with ABCE1 in order to probe for its interaction with the 40S subunit and for purification of the post-splitting complex, see **section 3.5.2**.

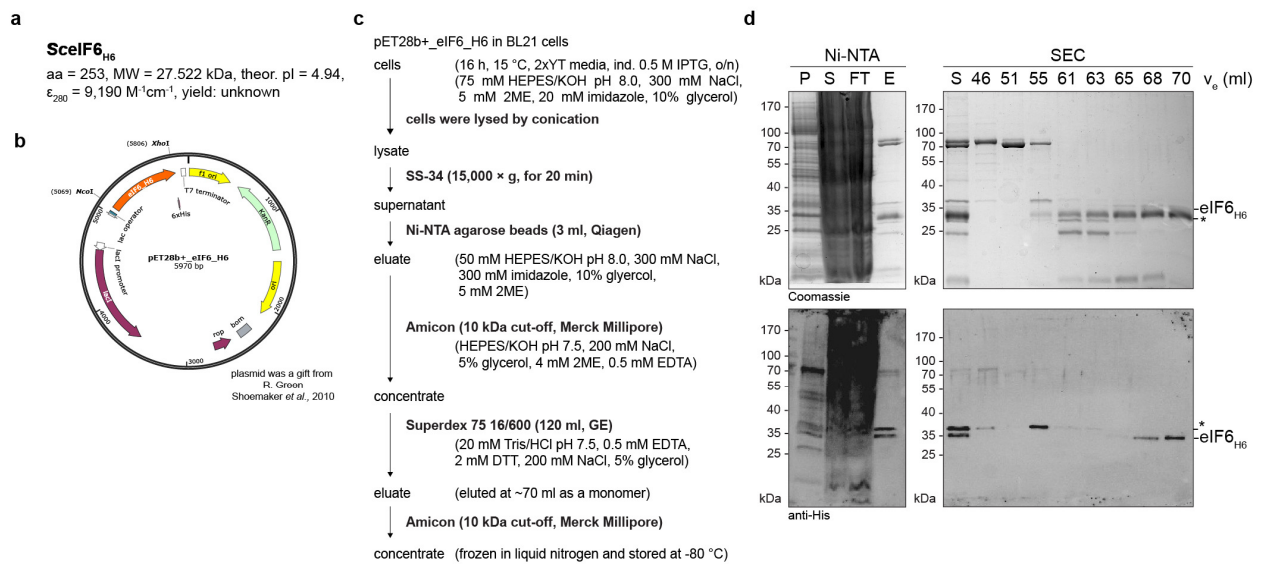


Figure 18 | Purification of eIF6. **a**, eIF6_{H6} construct harboring a C-terminal hexahistidine tag and protein parameters. **b**, pET28b+_eIF6_H6 plasmid visualized by SnapGene®. **c**, Purification strategy by IMAC and SEC. **d**, Purification steps and final product resolved by SDS-PAGE (12.5%), Coomassie stain and immunoblot against the His-tag (n=4). * indicates impurities.

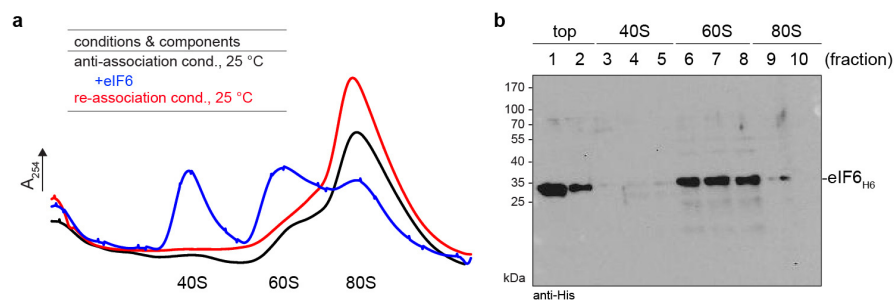


Figure 19 | Anti-association activity of eIF6. **a**, eIF6 anti-associated ribosomal subunits at anti-associating conditions. **b**, eIF6 occupied the 60S subunit in 10-30% SDG fractionation (n=1).

3.4 In gel splitting assay

In an internship in the Green lab (JHMI, HHMI, Baltimore, USA), I acquired, with kind support of A. Schuller, the knowledge about the in gel splitting assay. The splitting assay was used in previous studies and developed by D. Eyler and C. Shoemaker in the Green lab (Shoemaker *et al.*, 2010, Shoemaker & Green, 2011). Originally, the gel-based electrophoretic mobility shift assay was used for analysis of initiation complex formation in the Lorsch lab (Acker *et al.*, 2007). Splitting detection requires a radioactively labeled ^{35}S -Met-nascent chain-tRNA in a stalled 80S ribosome that after splitting remains mostly bound to the small ribosomal subunit because of peptide back-translocation in the 60S peptide tunnel (**Figure 20a**). Importantly, in theory, if the peptidyl-tRNA is not cleaved as in the case of Dom34, the protein-tRNA remains bound to the large subunit and serves as a quality control marker, see **introduction**. In the case of a short nascent peptide, after splitting the peptidyl-tRNA remains bound to 40S. In this study, the gel-based system was used for splitting assays, but the RNCs were detected by fluorescence-based RNA staining that may be applicable to other RNCs, too. The staining of ribosomes by ethidium bromide or SYBR[®]Gold resulted in clear bands. However, upon addition of splitting factors the bands got smeary (**Figure 20b**). In the Tampé lab, the in gel-based splitting assay was advanced by utilizing GFP fluorescence as a readout for the small ribosomal subunit and the nascent chain by $R_{\text{GFP}}\text{NC}_{\text{GFP}}$ complexes that were described in **section 3.1.2.4 (Figure 20c)**. The gel thickness was increased from 0.1 to 1.5 mm and the gel size was reduced to the common SDS-PAGE format of the MiniProtean II system (Bio-Rad Laboratories Inc.), therefore the sample loading become easier and the signal-to-noise ratio increased. Ribosomes were separated by a 3 or 4% polyacrylamide gel and at the bottom part of the gel a 15% step was added that focused all released components and tRNA. In 3% gels, ribosome splitting was resolvable by a separation of 80S and 40S, but 60S was hardly distinguishable from 40S (**Figure 20c**). Hence, the gel percentage was increased in following studies to 4%, as used in the original protocol by the Lorsch lab. The setup resulted in clearly distinguishable bands of 80S ribosomes and subunits (**Figure 21**).

Finally, ATP-dependent splitting of R_{GFP}NC_{GFP} complexes was observable with the produced splitting factors ABCE1, Dom34, and eIF6 (**Figure 21**). No splitting was detected with AMP-PNP as previously reported (Pisarev *et al.*, 2010, Shoemaker & Green, 2011). Interestingly, in the AMP-PNP sample with all splitting factors a distinct band appeared slightly above the GFP-tRNA band indicating free GFP that is migrating slower due to less negative charge upon hydrolysis from tRNA. This explanation is in line with the identical observation upon puromycin treatment. The free GFP may indicate a peptidyl-tRNA hydrolysis event, that is caused by ABCE1(AMP-PNP) and Dom34 and may be facilitated by the ribosome. This was not observed previously, but the published reconstituted splitting assays lack fully translated proteins with folded domains and additional interactions with the ribosome.

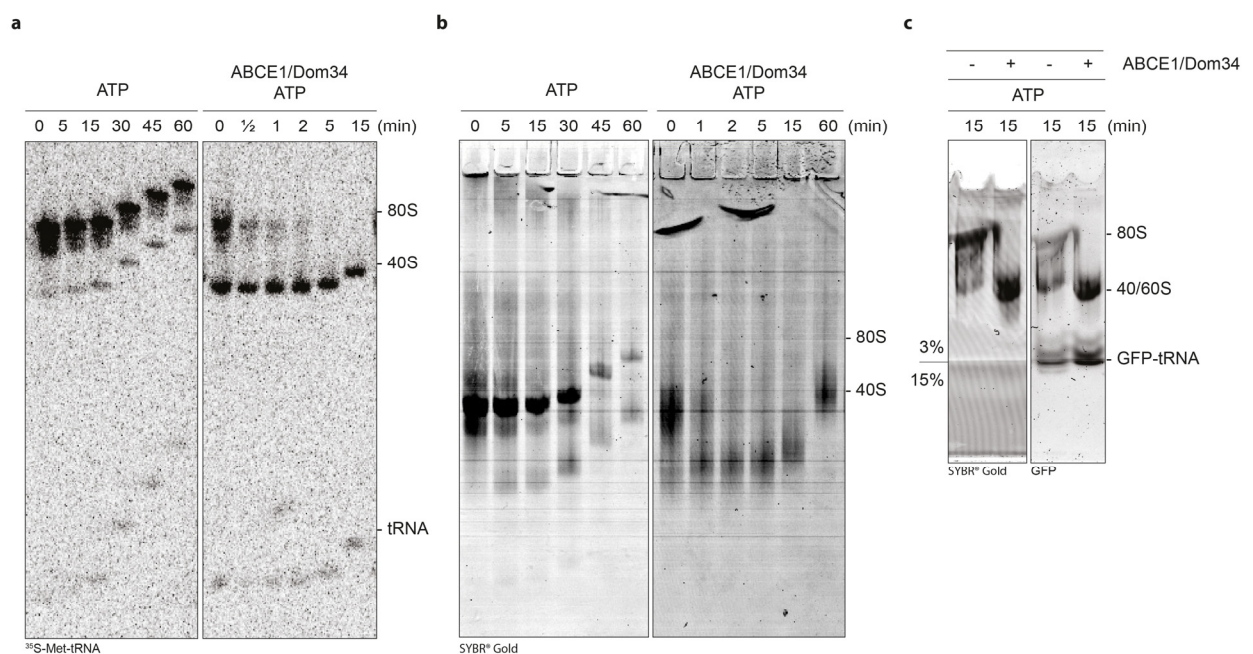


Figure 20 | Splitting assay development. eIF6 was present in all experiments. **a**, ³⁵S-Met-tRNA based detection of splitting by radioactivity. Samples were applied on a electrophoresing gel at discrete time-points. A. Schuller supervised me in the in gel splitting assay practice in the Green lab (JHMI, HHMI, Baltimore, USA)(n=2). **b**, Fluorescence-based detection of splitting by staining of ribosomes with SYBR[®]Gold. Bands become diffusive upon addition of protein factors. This experiment was conducted in the Green lab (n=2). **c**, On the left side, RNA was stained as in (b). On the right side the small ribosomal subunit was detected by the fluorescent Asc1-GFP signal and the nascent chain by GFP-tRNA. In all cases ribosomes are split upon addition of ABCE1, Dom34, eIF6, and ATP (n=1).

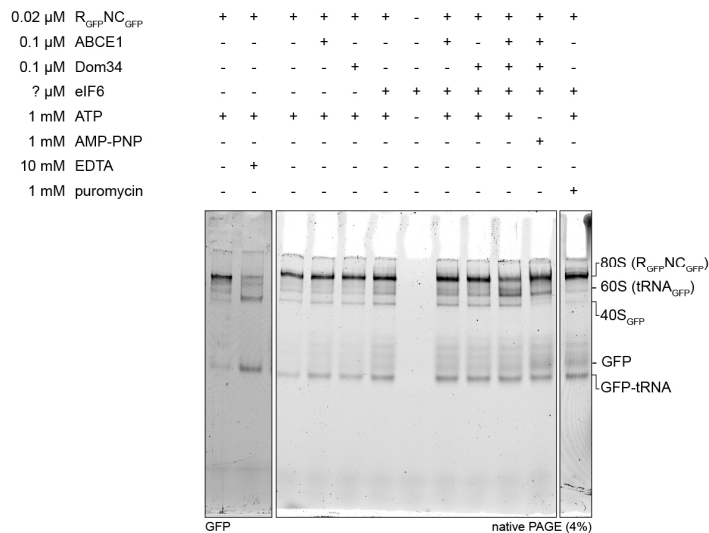


Figure 21 | Splitting of $R_{GFP}NC_{GFP}$ with ABCE1/Dom34/eIF6. Splitting was only observed in the case of present ABCE1, Dom34, eIF6, and ATP, and not with AMP-PNP. Interestingly, the AMP-PNP sample showed a similar band as in the puromycin treated sample that was assigned to free GFP from the nascent chain. Splitting was executed with indicated components in the splitting buffer (20 mM Tris/HCl pH 7.4, 100 mM KOAc, 2.5 mM $Mg(OAc)_2$, 0.25 mM spermidine, 2 mM DTT) for 40 min at 26 °C. RNCs and splitted ribosomal subunits were resolved by native PAGE (4%) in THEM buffer (34 mM Tris, 57 mM HEPES, 0.1 mM EDTA, 2.5 mM $MgCl_2$) for 60 min at 12 W (n=3).

Remarkably, after splitting, the intensity of the $40S_{GFP}$ band remained constant, whereas the 60S (nascent chain GFP-tRNA) band did increase in intensity in two distinct bands (**Figure 21**). This observation could be explained by a release of Asc1-GFP post-splitting that previously protected the stalled ribosome, as discussed in **section 3.1.2.4**. The role of Asc1 in ribosome recycling and post-splitting events remains to be investigated.

3.5 Structure of the eukaryotic 40S–ABCE1 post-splitting complex

The Tampé lab achieved the AMP-PNP dependent binding of ABCE1 to the small ribosomal subunit from *S. solfataricus* (Barthelme *et al.*, 2011). Catalytically inhibited variants of ABCE1 were generated that bind to the small ribosomal subunit and arrest the post-splitting state at room temperature. The mild conditions allowed to skip the heating step and to generate samples for purification of ribosomal complexes for structural studies (Barthelme *et al.*, 2011, Nürnberg-Goloub *et al.*, 2018). Armed with this optimized reconstitution approaches, we initiated in 2013 at the Zing ribosome conference in Napa Valley a collaboration with the Beckmann lab for reconstruction of the post-splitting complex by cryo-EM. Initially, we examined reconstituted complexes from *S. solfataricus*, but no density classes could be identified with bound ABCE1. The anti-/re-association-based preparation of the post-splitting complex from *S. cerevisiae* was developed in this thesis and yielded a pure sample that was resolvable in cryo-EM reconstruction to a resolution of 3.9 Å. With the structure of the post-splitting complex, we were able to interpret important mass spectrometrically (MS) determined crosslink products of the proteolytically digested post-splitting complex from *S. solfataricus* from structural studies by K. Kiosze-Becker (in collaboration with the Beck lab, EMBL, Heidelberg). In addition, based on the high-resolution structure we reconstructed a low-resolution density map of the post-splitting state in the *S. solfataricus* samples that was jointly published with the crosslink-MS data in (Kiosze-Becker *et al.*, 2016). In the revision period of the post-splitting complex from *S. cerevisiae*, the high-resolution structure from this study was improved by the Beckmann lab, and in the Tampé lab, we performed plasmid shuffling, *in vivo* and *in vitro* functional studies, and ATPase assays that safeguarded the structural interpretations. Guided by the high-resolution structure, the Beckmann lab analyzed *in vivo* pulled ABCE1 datasets and reconstructed a post-splitting complex with initiation factors and tRNA_i. The joint work was published in (Heuer & Gerovac *et al.*, 2017).

The results of the **sections 3.5**, **discussion 4.1**, and **method 2.7 sections** were generated and written by myself, R. Tampé, S. Trowitzsch, in collaboration with T. Becker, A. Heuer, and R. Beckmann from the Beckmann lab (Gene Center, LMU, Munich). This work was published

in 2017, hence I copied verbatim or partly passages and marked this at the end of the section (Heuer & Gerovac *et al.*, 2017, Kiosze-Becker *et al.*, 2016).

3.5.1 AMP-PNP dependent binding of ABCE1 to 40S

AMP-PNP stimulated binding of ABCE1 to the small ribosomal subunit was reported for *S. solfataricus* (Barthelme *et al.*, 2011), *D. melanogaster* (Andersen & Leever, 2007), and in reticulocyte lysates (Pisarev *et al.*, 2010). For *S. cerevisiae*, I performed ribosome-pelleting experiments in the Green lab to confirm ABCE1 binding to the small ribosomal subunit (JHMI, HHMI, Baltimore, USA) (**Figure 22**), see methods **section 2.6.5**. Only full-length ABCE1 co-sedimented with 40S subunits in an AMP-PNP stimulated fashion. No binding was observed for the N-terminally truncated band slightly below 70 kDa in input fractions. No nucleotide, ATP, and ADP samples also resulted in binding at lower level. This was previously reported for no nucleotide samples by the Pestova lab, too (Pisarev *et al.*, 2010).

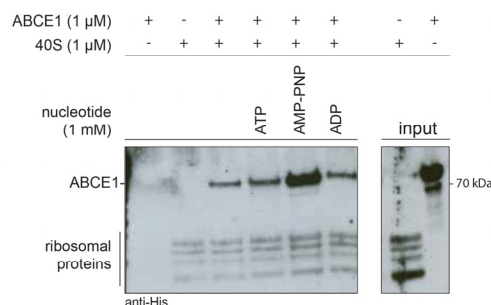


Figure 22 | AMP-PNP stimulated binding of ABCE1 to 40S. ABCE1 bound AMP-PNP stimulated to 40S. No nucleotide, ATP, and ADP yielded less binding to 40S. This experiment was conducted in the Green lab (JHMI, HHMI, Baltimore, USA), 40S ribosomes were provided by A. Schuller (n=2).

3.5.2 Anti-association activity of ABCE1

In a previous experiment, I verified eIF6 anti-association activity by the anti-/re-association assay (see **section 3.3.3**). The here presented approach was focused on ABCE1, hence the anti-association factor eIF6 was exchanged for ABCE1 and nucleotides were added. I set the

principal assumption that if ABCE1 can split ribosomes in a nucleotide-dependent fashion, then it should also act as an anti-association factor. I neglected the possibilities that other factors, *e.g.* release factors, would be necessary for anti-association or the ribosomes must be in a defined splitting competent state. 500 mM KCl high salt washed, SDG fractionated, and subsequently pelleted crude 80S ribosomes were anti-associated at 500 mM KCl high salt and low 1-2 mM magnesium condition. Side experiments showed that the high salt wash was an integral part in the preparation of stable 80S ribosomes for this assay. The major part of ribosomes is disintegrated at high salt conditions and pelleted in SDG, this is in agreement with (Merrick & Hensold, 2001), see methods **section 2.4.4**. This observation clearly sets the requirement of high salt washed ribosomes for this assay because a quantification at different conditions is not possible using labile 80S ribosomes (data not shown). In addition, the 60S population was still present in large-scale 80S preparations because the selective separation was not possible in the SW41 rotor, but the 60S/80S mix was still usable for the experiments because the 60S level remained constant and ensured full re-association of and with free 40S subunits. In summary, the assay enabled probing for anti-association activity using even highly impure ABCE1 samples (**Figure 34a**). The logical value read-out was the appearance of a 40S peak at simultaneous decrease of the 80S peak. The 40S peak corresponded to the formation of the 40S–ABCE1 complex in the ribosome profile analysis.

3.5.3 Preparation of the 40S–ABCE1 post-splitting complex

The transient state after splitting was efficiently captured by a *facilitated splitting* approach under conditions that allow anti-association of 80S ribosomes by ABCE1 at low magnesium and high potassium levels and trapping of the post-splitting state in the presence of the non-hydrolysable ATP analog AMP-PNP. This approach bypasses the AMP-PNP-dependent arrest of the pre-splitting state (Becker & Franckenberg *et al.*, 2012, Pisarev *et al.*, 2010, Preis *et al.*, 2014, Shoemaker & Green, 2011) and thereby enables population of 40S subunits with ABCE1, which are specifically stabilized in the post-splitting state. The 40S–ABCE1 post-splitting complex was harvested in SDG fractionation under conditions that promote re-association of ribosomal subunits to 80S complexes (**Figure 23**), see methods

section 2.6.4. Upon addition of AMP-PNP, ABCE1 was stably bound to the 40S subunit and displayed anti-association activity, which in turn allowed the preparation of a highly enriched 40S–ABCE1 fraction that was used in cryo-EM sample preparation, see methods **section 2.7.1.**

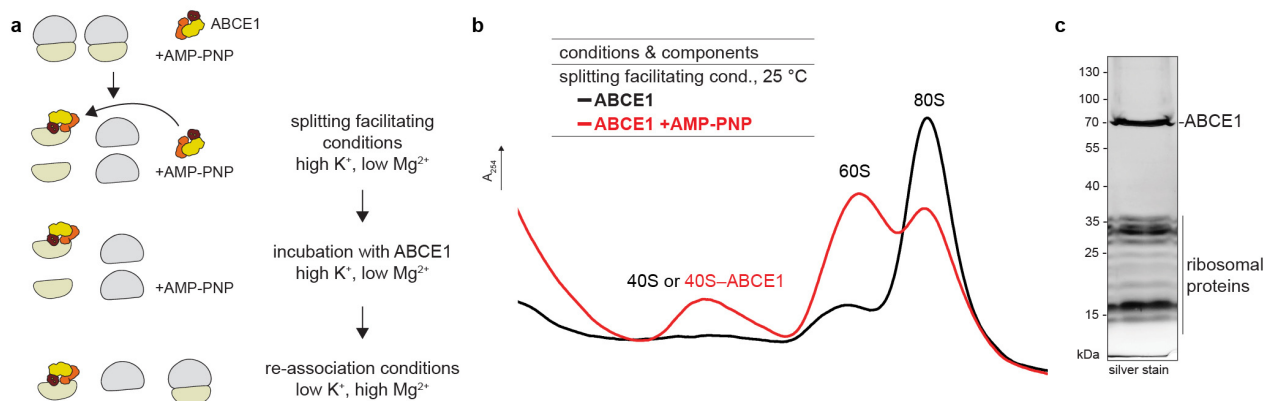


Figure 23 | Preparation of the 40S–ABCE1 post-splitting complex. **a**, Outline of the *facilitated splitting* approach: 80S ribosomes were dissociated under high potassium (500 mM) and low magnesium (1 mM) conditions, followed by AMP-PNP-dependent ABCE1 binding to the 40S subunits. Under re-association conditions (100 mM low potassium and 20 mM high magnesium concentration, free 40S subunits were allowed to rejoin with free 60S subunits. A representative profile of four individual preparations is shown. **b**, In ribosome profiles, the 40S–ABCE1 complex only appears in the 40S fraction if AMP-PNP is present and ABCE1 is added at splitting-facilitating conditions. **c**, Pooled 40S ribosomal fractions showed stoichiometric binding of ABCE1 to 40S subunits as analyzed by SDS-PAGE (n=2). Sample preparation for cryo-EM (only panel c) was conducted in collaboration with A. Heuer. Reprinted with permission (Heuer & Gerovac *et al.*, 2017).

3.5.4 3D classification of particles

The reconstituted and purified post-splitting complex was subjected to single-particle cryo-EM analysis in collaboration with the Beckmann lab (Gene Center, LMU, Munich). After 2D and 3D classification (**Figure 24**) and masking of the flexible head region of the 40S subunit, we obtained a structure of the 40S–ABCE1 post-splitting complex at an average resolution of 3.9 Å according to the *gold-standard* criterion (**Figure 25**, EMD: 4071). Local resolution was between 3.5 and 4.5 Å for the 40S body, the ABCE1 FeS cluster domain, and NBS I, but was lower for NBS II and flexible regions such as the 40S head. We built, refined,

and validated a molecular model based on known structures of ABCE1 and the 40S ribosomal subunit (**Figure 25** and **Figure 26**).

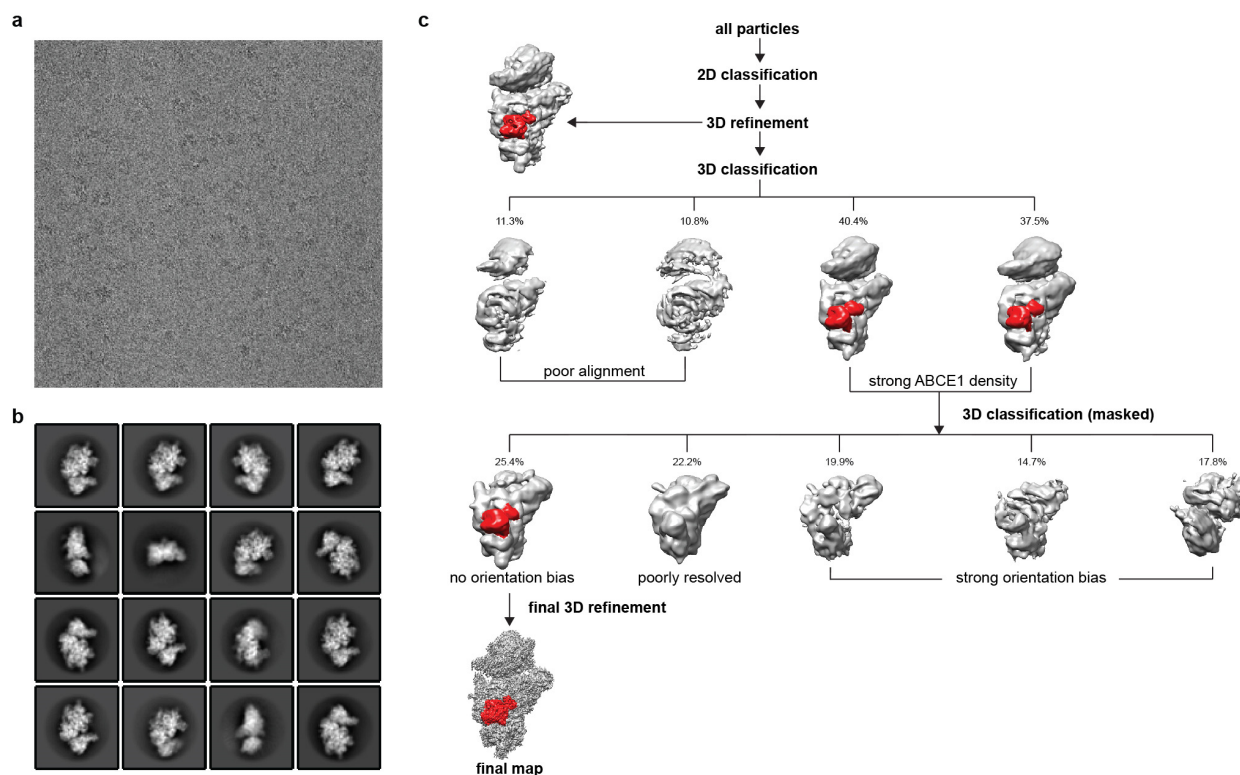


Figure 24 | Raw cryo-EM data and classification of the reconstituted 40S-ABCE1 complex. **a**, Representative micrograph showing 40S-ABCE1 particles. **b**, Representative 2D classes predominantly showing various side views of the 40S subunits. **c**, 3D classification scheme. After 2D classification and removal of non-ribosomal particles, the dataset was refined and subjected to 3D classification in RELION-2. The dataset was initially classified into four classes: class 1 and 2 contained poorly resolved and distorted 40S ribosomes whereas class 3 and 4 showed well-resolved 40S ribosomes with a strong ABCE1 density. These classes were joined for a second round of 3D classification (five classes) using a mask excluding the highly flexible 40S head. Four out of five classes showed either a strong distortion which is likely a result of orientation bias or poor alignment and were discarded. The best resolved class 1 showed a strong ABCE1 density and a well resolved 40S body and was used for the refinement yielding a map at 3.9 Å resolution. A. Heuer, T. Becker, O. Berninghausen recorded, classified the data, and reconstructed the density map of the particle. Reprinted with permission (Heuer & Gerovac *et al.*, 2017).

Figure 25 | Cryo-EM structure of the reconstituted 40S–ABCE1 complex and assessment of resolution.

a, Cryo-EM density of the 40S–ABCE1 complex and isolated ABCE1 low-pass filtered at 3.9 Å showing the 40S subunit (grey), and ABCE1 (red), as well as local resolution as calculated by ResMap. The ResMap plots showed a range from maximum 3.5 to 8.5 Å in the periphery. Notably, in ABCE1, the FeS cluster domain and NBD1 are well resolved whereas resolution in NBD2 and peripheral regions of ABCE1 is slightly decreased. Maps are contoured at 3.5 σ . **b**, FSC plot shows the 3.9 Å average resolution of the map according to the *gold standard* criterion (FSC = 0.143, top) and FSC curves calculated between the cryo-EM map and the final models (bottom) as calculated by REFMAC. Values were plotted for the model versus the final map (FSC_{average}, black), for the model that was refined into the first half-map and FSC calculated either for the same map (model vs first half-map, orange) or for the second half-map (model vs second half map, blue). **c**, Density snapshots of isolated ABCE1 (contoured as indicated in the panels) with the fitted model shown in three orientations. Below, selected areas are shown illustrating the quality of the map (side chain densities in the α -helices forming the HLH motif; a separated β -sheet in NBD1 and a β -sheet with resolved bulky side chains in hinge 2). Domains are colored as indicated in the schematic panel. A. Heuer and T. Becker produced all data. Reprinted with permission (Heuer & Gerovac *et al.*, 2017).

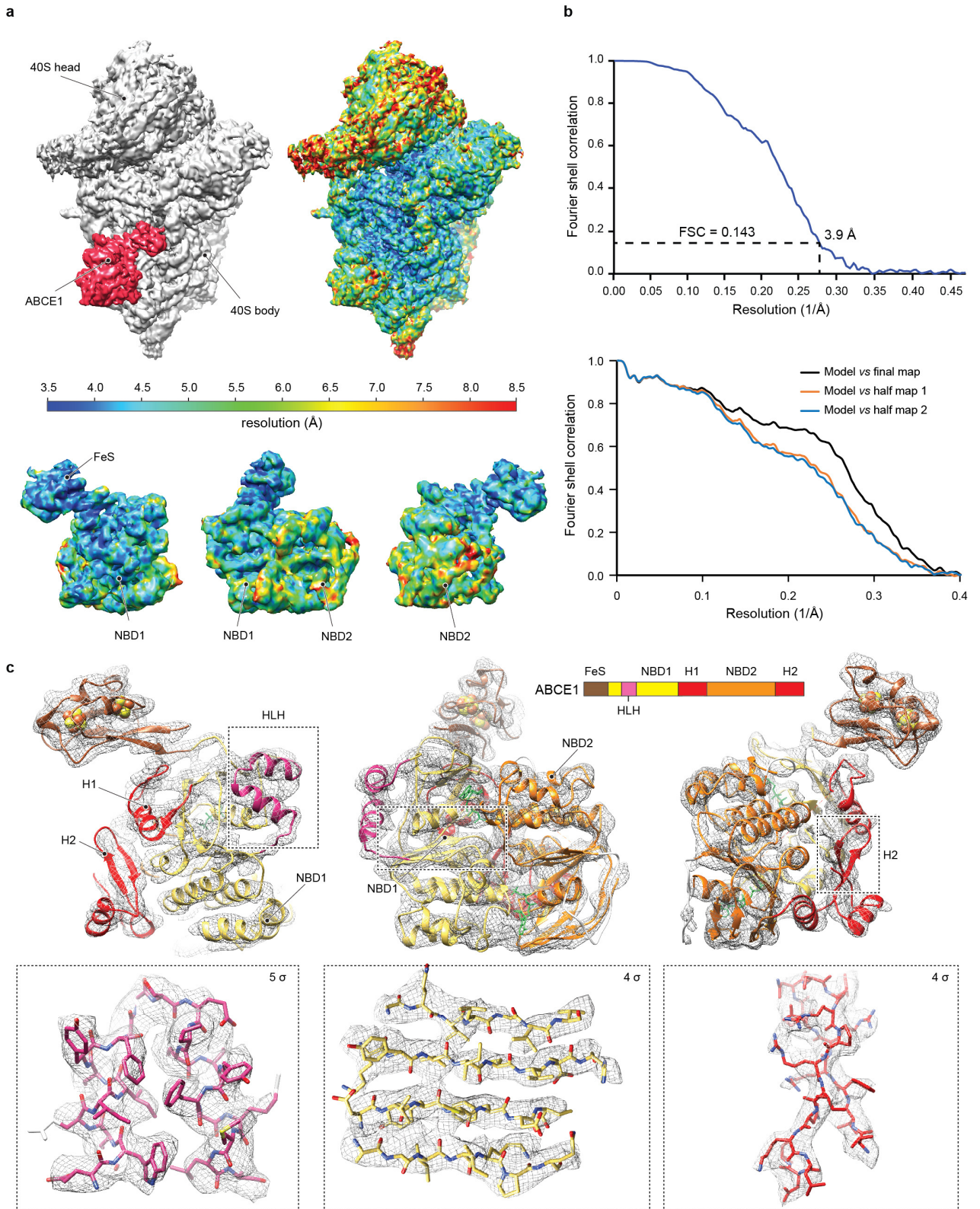


Table 11 | EM data collection and refinement statistics

data collection		
particles	101,000	
pixel size (Å)	1.084	
defocus range (µm)	800-2500	
voltage (kV)	300	
electron dose (e ⁻ Å ⁻²)	28	
model refinement	40S_{BODY}-ABCE1	ABCE1
	(EMD: 4071, PDB: 5LL6)	
model composition		
non-hydrogen atoms	55,263	4,645
protein residues	3,431	578
RNA bases	1,325	–
refinement		
resolution for refinement (Å)	4.0	4.0
map sharpening B-factor (Å ²)	-96.9	-96.9
average B-factor (Å ²)	131.6	130.6
FSC(average)	0.82	0.71
r.m.s. deviations		
bond lengths (Å)	0.0114	0.0283
bond angles (°)	1.41	2.49
validation & statistics	40S_{BODY}-ABCE1	ABCE1
validation		
<i>MolProbity</i> score	2.16	2.98
clash score, all atoms	4.87	15.41
good rotamers (%)	97.78	94.15
Ramachandran plot		
favoured (%)	85.74	82.23
outliers (%)	3.66	3.48
validation (RNA)		
correct sugar puckers (%)	95.1	–
good backbone conformations (%)	62.0	–

A. Heuer and T. Becker produced all data.

Reprinted with permission (Heuer & Gerovac *et al.*, 2017).

3.5.5 Structure of the 40S–ABCE1 post-splitting complex

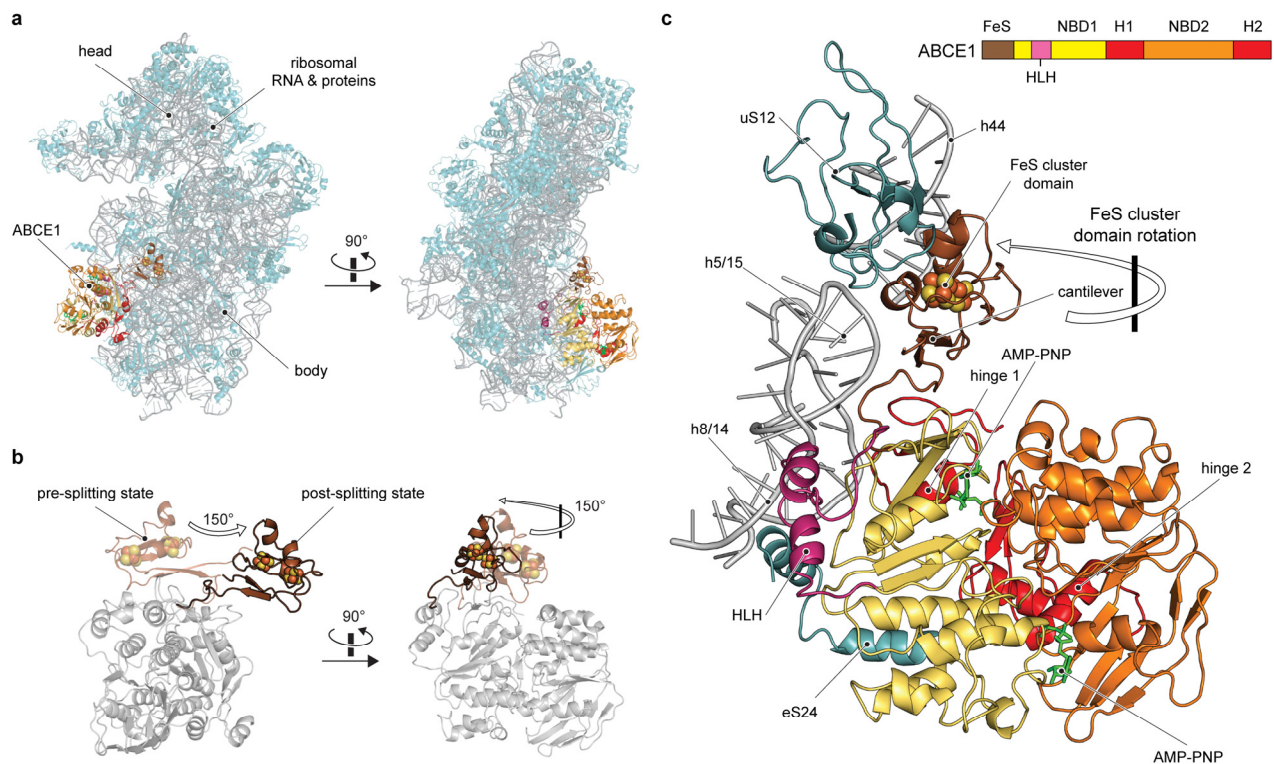


Figure 26 | Overall structure of the 40S–ABCE1 post-splitting complex. **a**, Structure of the 40S–ABCE1 post-splitting complex in front and side views with ribosomal proteins in teal, rRNA in grey, and ABCE1. Domains of ABCE1 are colored as indicated in the schematic panel in **c**. AMP-PNP is shown in green. **b**, Movement of the FeS cluster domain by 150-degree rotation from the pre-splitting state (PDB: 4CRM, Preis *et al.*, 2014, in transparent) to the post-splitting state (brown). The body of ABCE1 (lacking the FeS cluster domain) in the pre-splitting state is shown in grey. **c**, Interactions of ABCE1 with the small 40S ribosomal subunit. The FeS cluster domain interacts with h5, h44, and uS12, the HLH and hinge domains form contacts to rRNA (h5-h15 and h8-h14) and to eS24. The two NBDs are closed with two AMP-PNP molecules occluded. A. Heuer, C. Schmidt, T. Becker, and I modelled the structure of the post-splitting complex. Reprinted with permission (Heuer & Gerovac *et al.*, 2017).

The structure revealed that ABCE1 binds the 40S subunit at a site used by other translation factors, *i.e.* eRF3 or Hbs1, eEF1A, eEF2, or eIF5B (**Figure 26**, PDB: 5LL6)(Becker *et al.*, 2011, Behrmann & Loerke *et al.*, 2015, Fernández & Bai *et al.*, 2013, Preis *et al.*, 2014, Spahn *et al.*, 2004, Taylor *et al.*, 2007). We found the NBDs of ABCE1 re-positioned with NBD1, the HLH, and the hinge regions (H1 and H2), contacting the 18S rRNA and the ribosomal protein eS24. Compared to the pre-splitting state, the FeS cluster domain is dramatically re-arranged and

binds to a pocket formed by uS12 and rRNA helices h5 and h44. The interaction site of the FeS cluster domain has been mapped by chemical cross-linking and mass spectrometry in the archaeal post-recycling complex (Kiosze-Becker *et al.*, 2016), see **section 3.5.10**. Notably, the NBDs are in a closed conformation and both NBSs clearly occlude a bound nucleotide.

3.5.6 Structure of an asymmetric ABC system in a fully closed conformation

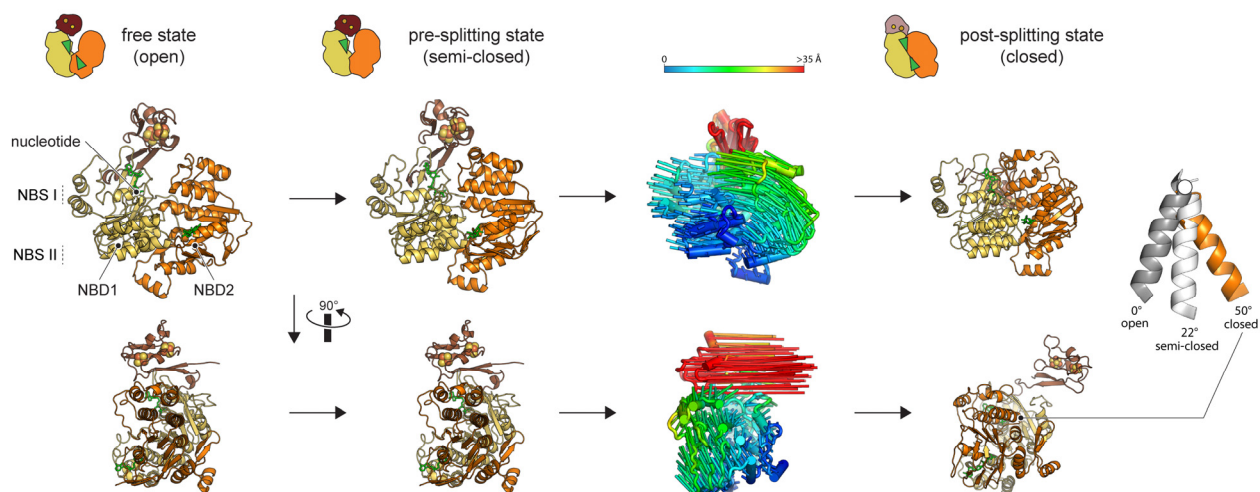


Figure 27 | Conformational transition of NBSs of ABCE1 from pre- to post-splitting state. Free state of ABCE1 (PDB: 3BK7, Karcher *et al.*, 2008), intermediate, semi-closed pre-splitting state bound to 80S ribosomes (PDB: 4CRM, Preis *et al.*, 2014), and 40S-bound fully closed post-splitting state with nucleotides shown in green. Conformational transitions from 80S ribosome-bound pre- to 40S subunit-bound post-state are represented by vectors (superimposed on the 40S subunit). NBD closing is exemplified by a helix in NBD2 (residue 500-516 in yeast ABCE1), with rotation angles of 0, 22, and 50 degrees for open, semi-closed, and closed, respectively. Models were superimposed onto NBD1 and the pivot point is indicated by a white circle. A. Heuer generated the motion bar diagram based on a structure assembly that I provided. Reprinted with permission (Heuer & Gerovac *et al.*, 2017).

So far, ABCE1 has only been observed in the free, ADP-bound open conformation (Barthelme *et al.*, 2011, Karcher *et al.*, 2008) or in an intermediate, semi-closed 80S-associated pre-splitting state. In the structures of the pre-splitting state, the nucleotide occupancy in either NBS is unclear (Becker & Franckenberg *et al.*, 2012, Brown & Shao *et al.*, 2015, Preis *et al.*, 2014). Compared to the pre-splitting state, the post-splitting state shows a rotation of

NBD2 towards NBD1 (**Figure 27a**). This rotation results in a full closure of the two NBSs and occlusion of two nucleotides (**Figure 27a**). In the post-splitting state, the phosphates and the ribose of the bound nucleotides are coordinated by the Walker A and B motifs as well as the C-loops of the opposing NBDs (**Figure 28a-c**).

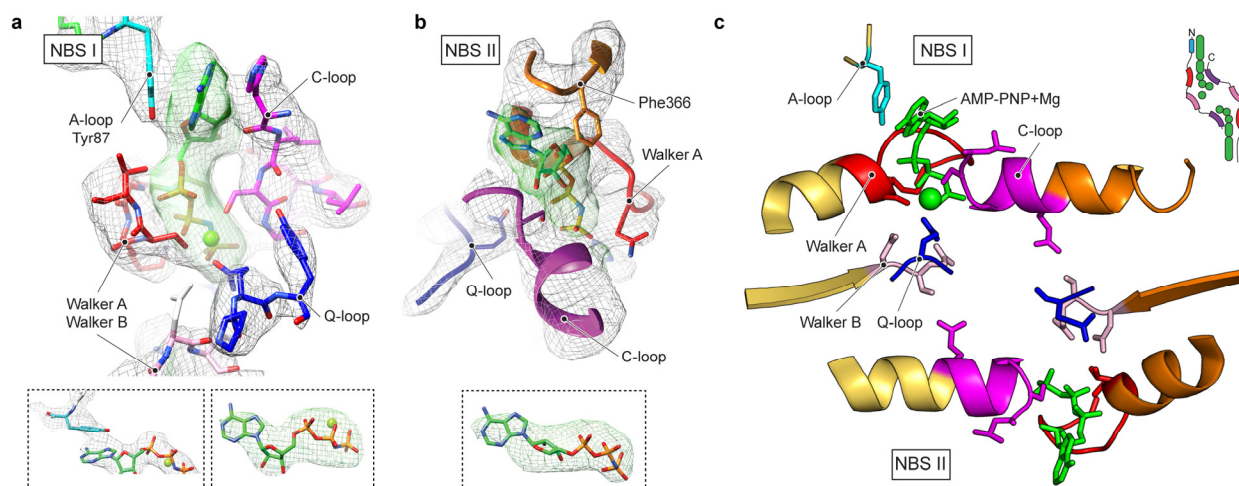


Figure 28 | NBS are occluded with ATP. **a**, Isolated densities with models of NBS I **b**, and II with AMP-PNP occluded by Walker A, and Walker B motifs, C-, and Q-loops. Side chains not visible in the map are colored white for NBS I or omitted for NBS II. Isolated densities of the AMP-PNP and the π - π stacking of Tyr87 (A-loop of NBS I) with the adenosine base are shown in the boxes below. For NBS I, densities are low-pass filtered to 3.9 Å and displayed at 6 σ . For NBS II maps were low-pass filtered at 4.5 Å and displayed at 4.5 σ . **c**, Model and schematic representation (inlet) of both NBSs occluding two AMP-PNP (green) in the post-splitting state. In all panels the conserved motifs of ABC-ATPases are colored as follows: Walker A in red, Walker B in light pink, C-loop in magenta, and Q-loop in blue. Tyr87 in the A-loop of NBS I (cyan) forms a π - π stacking with the base of the nucleotide. Notably, no A-loop motif is present in NBS II. Density map images were generated by T. Becker. Reprinted with permission (Heuer & Gerovac *et al.*, 2017).

In NBS I, density is clearly present for an AMP-PNP–Mg moiety and we observe a π - π stacking of the adenosine base with a tyrosine residue (Tyr87) in the A-loop (**Figure 28a**). Moreover, critical residues in the C-loop of NBD2, the Walker A motif of NBD1, and the Q-loop of NBD1 are well defined by the density and adopt similar conformations as observed in structures of other ABC proteins in the NBD-closed state (Korkhov *et al.*, 2014, Oldham & Chen, 2011). Clear density for a bound nucleotide was also present in NBS II

(**Figure 28b**), but the local resolution was lower (**Figure 25c**). Yet, based on the structure of AMP-PNP-bound BtuCD (Korkhov *et al.*, 2014) we were able to build a model for NBS II showing a similar arrangement of the Walker A motif and the C-loop as in NBS I (**Figure 28c**). In addition to the canonical motifs forming the NBSs in ABC proteins, we identified the conserved Phe366 of NBD2 to contribute to the coordination of the nucleotide ribose moiety. Taken together, in the post-splitting state, we observe the NBDs of ABCE1 fully closed with two occluded nucleotides. The hallmark residues involved in ATP binding are in a similar conformation as in canonical ABC-type ATPases (**Figure 28c**).

3.5.7 Repositioning of the FeS cluster domain

The most striking reorganization from the pre- to the post-splitting state is the repositioning of the FeS cluster domain on the ribosome by rotation of 150-degrees around a flexible linker (cantilever hinge) into a binding cleft formed by rRNA helices h5-h15, h44 and the ribosomal protein uS12 (**Figure 26b**). This interaction is established by salt bridges between basic residues of the FeS cluster domain and the rRNA (**Figure 29a,b**) and by a hydrophobic contacts between Pro30 of ABCE1 and Ile52 of uS12 (**Figure 29c**). In addition, the HLH motif as well as the hinge 1 and 2 motifs of ABCE1 form contacts with the h8-h14 rRNA helices *via* Asp587 and Ser588 (**Figure 26c** and **Figure 29d-f**). For the sake of completeness, Ser588 substitution to glutamic acid was lethal in plasmid shuffling experiments (Märtens, 2007).

Notably, these ABCE1–rRNA interactions largely differ from the pre-splitting state: While hinge 2 still contacts the junction between h8 and h14 by Arg573, which plays a role in the activation of translational GTPases (Villa & Sengupta *et al.*, 2009), hinge 1 moves closer to the 40S subunit towards the base pair A51:U440 forming the h5/15 junction (**Figure 29f**). This A:U base pair is also contacted in the pre-splitting state by the HLH motif, which rearranges to establish a new contact with h15 (U440) by Ser150 (**Figure 29d,f**). The contact between the C-terminal helix of eS24 and NBD1 (Gln262) is maintained in pre- and post-splitting states in yeast, but differs significantly between yeast and human where it is found in 90-degree rotated conformation (**Figure 29g**).

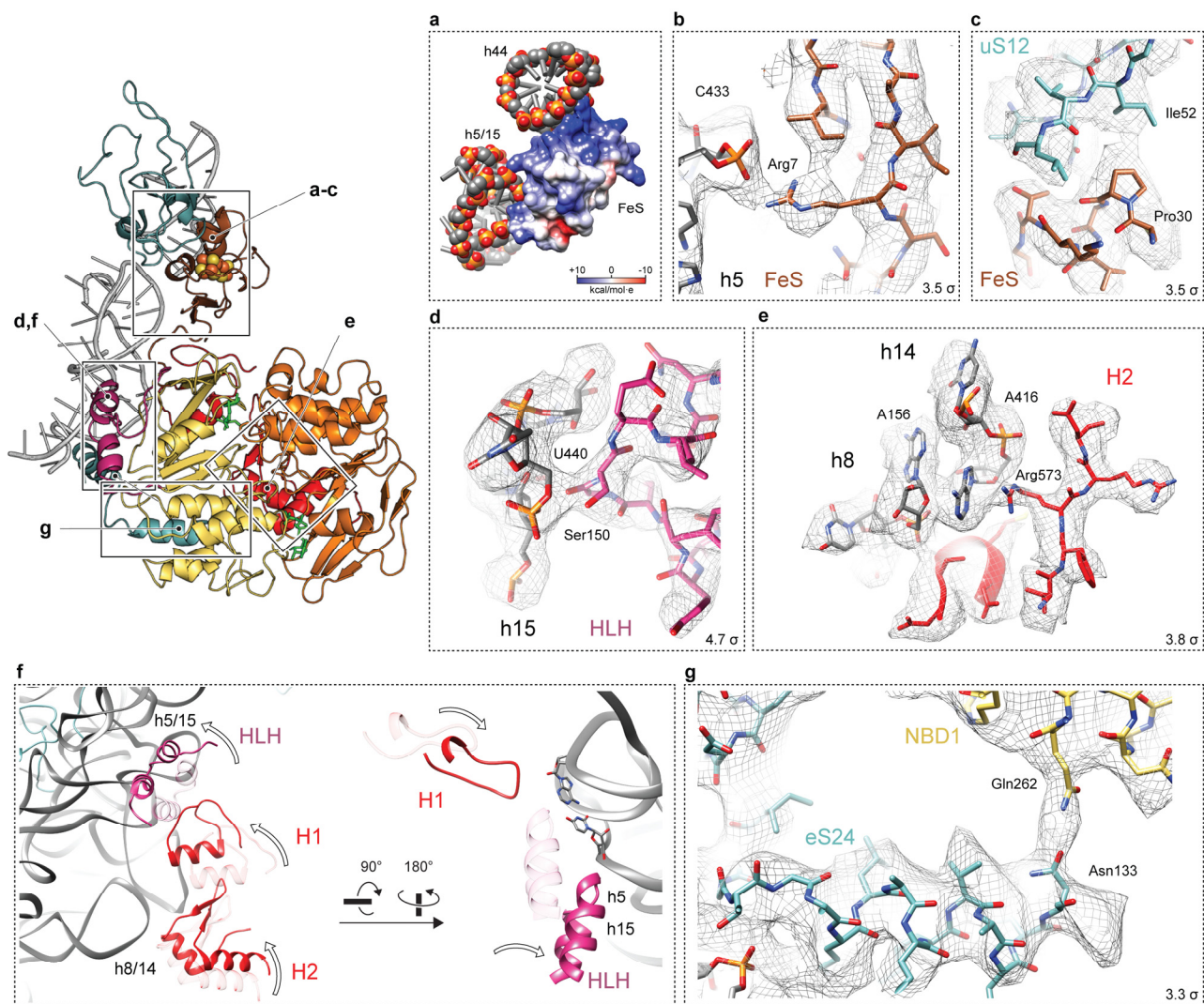


Figure 29 I Interactions between the 40S subunit and ABCE1 in the post-splitting state. **a**, Electrostatic surface potential of the FeS cluster domain (blue: positive, red: negative) bound to the 40S subunit, positive charges face towards the phosphate backbone of the rRNA (h44 and h5-h15). **b**, Zoom on the cantilever β -sheet displaying the contact of Arg7 (brown) to the phosphate backbone of h5. The density map is shown as grey mesh at the 3.5σ level. **c**, Zoom on the interaction between the Pro30 (FeS cluster domain) and Ile52 of uS12 (density shown as mesh at 3.5σ). **d**, Close-up view on the HLH motif, contacting the backbone of U440 in h15 (mesh; 4.7σ). **e**, Zoom on hinge 2 interactions with the h8-h14 junction (formed by A156 and A416) (density shown as mesh at 3.8σ). Arg573 likely stacks to A416 *via* a cation- π interaction. A second interaction is observed between the loop (Asp587 and Ser588) preceding the terminal helix of hinge 2 (shown in ribbon) and the backbone of A156. **f**, Rearrangements in the HLH, hinge 1 and 2 motifs and their interactions with h5-h15 and h8-h14. ABCE1 in the pre-splitting state is superimposed in transparent on the post-splitting model. All other parts of ABCE1 are omitted for clarity. **g**, Model for the C-terminal helix of eS24 in the post-splitting state (cyan) contacting NBD1 (density shown as mesh at 3.3σ). The density was low-pass filtered at 3.9 \AA for all snapshots. T. Becker generated images of density maps with structures, I assembled the figure. Reprinted with permission (Heuer & Gerovac *et al.*, 2017).

Interestingly, the cantilever hinge, which forms an α -helix in the pre-splitting complex, is unwound in the post-splitting state. (**Figure 30a,b** and **Figure 31**). This unwinding establishes a new intramolecular contact between the cantilever hinge and NBD1 by a side chain-backbone interaction between the conserved residues Tyr301 and Asn78. The new position of the FeS cluster domain is stabilized by a number of contacts to the rRNA (h5 and h44) and uS12 (Pro30), and in particular by the contact between the conserved Arg7 of the cantilever arm and helix h5 of the rRNA (**Figure 30b**).

3.5.8 The post-splitting state is essential for cellular homeostasis

To address the physiological significance of the 40S–ABCE1 structure, I tested if substitution of key interaction residues of the FeS cluster domain and NBD1 in the post-splitting state could impair the function of ABCE1 *in vitro* or *in vivo*. Importantly, the *in vitro facilitated splitting* assay allowed assessing the anti-association activity (inhibition of 40S–60S re-joining) of *wt* and mutant ABCE1. To this end, I analyzed the ribosomal subunit (40S and 60S) to monosome (80S) ratio in ribosome profiles. In the presence of AMP-PNP, *wt* ABCE1 showed anti-association activity as in the case of anti-association factor eIF6 (**Figure 30c** and **Figure 23**, Groft *et al.*, 2000). Strikingly, substitution of either Arg7, Pro30, or Tyr301 to alanine impaired the anti-association activity of ABCE1, as indicated by high levels of 80S ribosomes and a low subunit-to-monomer ratio as compared to 80S ribosomes alone or with *wt* ABCE1 without addition of AMP-PNP. In contrast, substitution of His95, which is not involved in stabilizing FeS cluster domain contacts, and Asn78, which is only interacting with Tyr301 *via* its backbone, still exerted full anti-association activity (**Figure 30c**).

The ABCE1 mutants that showed anti-association activity were analyzed for growth defects *in vivo* by a plasmid shuffling assay, in which the endogenous *ABCE1* gene (*RLI1*) was chromosomally deleted and substituted by plasmid-encoded *wt* or mutant *ABCE1*. P. Kötter supervised me in the generation of the plasmid shuffling assay and performed with S. Lamberth the tetrad analysis for the generation of the CEN.MG1-9B strain, see **section 2.5.1**.

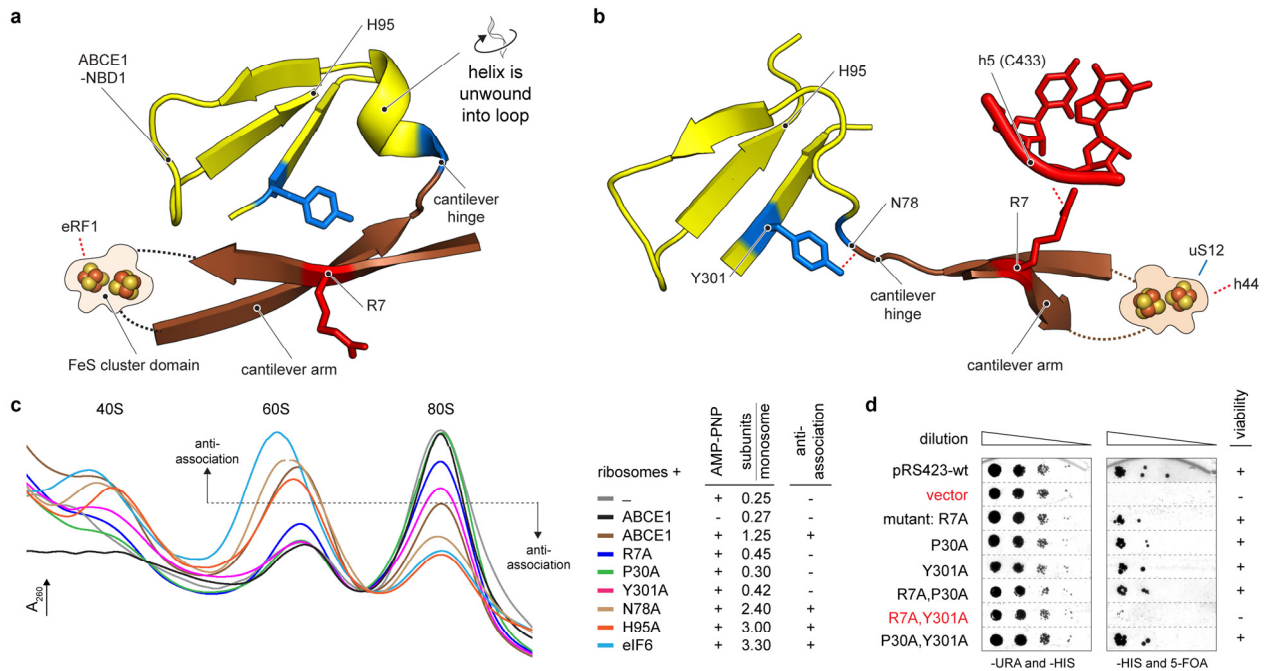


Figure 30 | NBD1 stabilizes the FeS cluster domain in post-splitting state by an essential cantilever arm interaction. **a**, In the pre-splitting state, the cantilever (CL) hinge forms an α -helix, which is unwound in the post-splitting state (**b**). **b**, Upon splitting, the FeS cluster domain rotates by 150 degrees. In the post-splitting state, the FeS cluster domain is mainly stabilized by two interactions of the cantilever arm (brown): the backbone of Asn78 interacts with Tyr301 (blue) of NBD1 (yellow) and Arg7 with the rRNA backbone of C433 at h5 (red). **c**, Ribosome profiles recorded after the *facilitated splitting* reaction. ABCE1 mutants of Arg7, Pro30, and Tyr301 are defective in anti-association of 80S ribosomes in the *facilitated splitting* assay. Wild-type ABCE1, alanine substitutions of His95 and Asn78, and eIF6 show a strong anti-association effect. An increase of 40S and 60S subunit populations indicated an anti-association effect. Representative profiles of two independent experiments are shown. **d**, Combined alanine substitutions of Arg7 and Tyr301 are lethal after plasmid shuffling in yeast strains, which survival relies only on mutated ABCE1. The data shown represent growth studies of two independent experiments. P. Kötter supervised me in the generation of the plasmid shuffling assay and performed with S. Lamberth the tetrad analysis for the strain CEN.MG1-9B. Reprinted with permission (Heuer & Gerovac *et al.*, 2017).

Surprisingly, cells expressing ABCE1 carrying single alanine substitutions for Arg7, Pro30, and Tyr301 were still viable, whereas a double substitution of Arg7 and Tyr301 was lethal (**Figure 30d**). In order to examine, if these alanine substitutions impact ribosome splitting, I over-expressed epitope-tagged (HA) wild-type and mutant ABCE1 and recorded ribosome

profiles (**Figure 32a**). A significant increase of the 80S ribosome population was observed in cells expressing alanine substitutions of Arg7, Pro30 and Tyr301 as compared to wild-type *ABCE1*. In addition, I observed a strongly increased enrichment of mutant *ABCE1* protein in 80S ribosome fractions (**Figure 32b**).

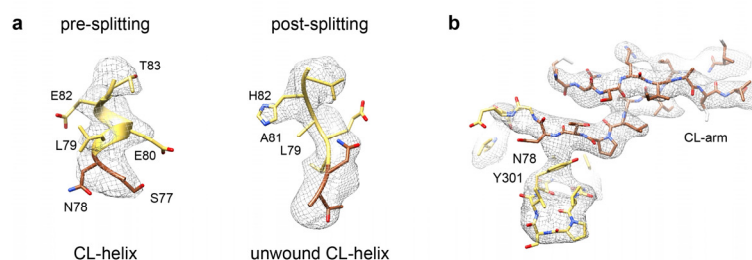


Figure 31 | Dynamic conformation of the cantilever. a, In the pre-splitting state (left, 3JAH, Brown & Shao *et al.*, 2015), the cantilever (CL) forms an α -helix, which is unwound in the *ABCE1* post-splitting state (right). Isolated densities are low-pass filtered at 3.9 Å (contoured at 5 σ) and shown with the respective models. **b**, In the post-splitting state, the FeS cluster domain is mainly stabilized by two interactions of the cantilever arm: the backbone of Asn78 interacts with Tyr301 of NBD1. Density of the *ABCE1* post-splitting complex was low-pass filtered at 3.9 Å (contoured at 5 σ). T. Becker generated images of density maps with structures. Reprinted with permission (Heuer & Gerovac *et al.*, 2017).

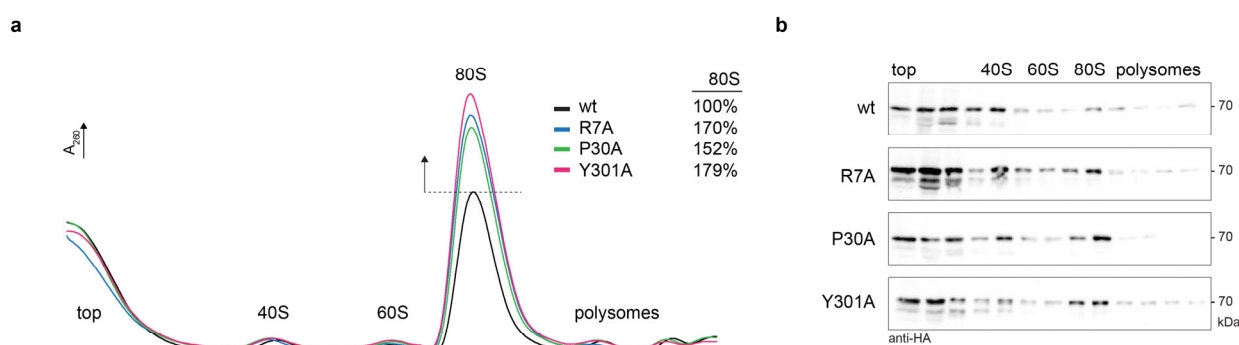


Figure 32 | Ribosome profiles from cells expressing wild-type and mutant *ABCE1*. **a**, Lysates from cells expressing wild-type and mutant *ABCE1* were subjected to 10-50% SDG fractionation. Compared to *wild-type* (wt, black), the relative amount of 80S ribosome was strongly increased in the alanine substitutions R7A, P30A and Y301A. **b**, SDS-PAGE and immunoblotting of the gradient fractions using an anti-HA antibody to probe for tagged *ABCE1*. Wild-type *ABCE1* was mainly found in the top fractions or bound to 40S subunits, while the mutants R7A, P30A, and Y301A were enriched in 80S ribosomes (n=1). Reprinted with permission (Heuer & Gerovac *et al.*, 2017).

The physiological relevance is underlined by the partial or complete loss of anti-association activity of ABCE1 *in vitro* that confirms a stabilizing role of the three proposed interaction residues. In addition, a lethal phenotype is observed for the double substitution of Arg7 and Tyr301 to alanine. Moreover, enrichment of interaction variants (Arg7, Pro30, Tyr301) of ABCE1 on 80S ribosomes points towards an impaired splitting activity that may be explained by a lack of stabilization in the post-splitting state or by a compromised conformational freedom of the FeS cluster domain. Similarly, enriched 80S ribosomal fractions were observed upon impairment of ABCE1 activity or translational stalling *in vivo* (Andersen & Leever, 2007, Dong *et al.*, 2004, Tsuboi *et al.*, 2012, Young & Guydosh *et al.*, 2015), strongly indicating that these ABCE1 interaction variants are defective in ribosome splitting and accumulate as 80S–ABCE1 pre-splitting complexes.

3.5.9 NTPase activity of ABCE1 in the post-splitting complex

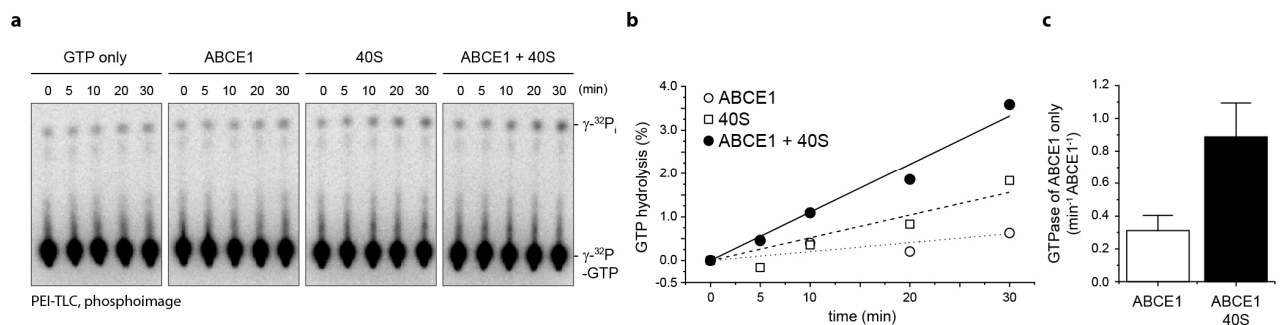


Figure 33 | NTPase stimulation of ABCE1 by the 40S subunit. **a**, Hydrolyzed γ - ^{32}P -GTP resulted in released $^{32}\text{P}_i$ that was separated by polyethylenimine (PEI) thin layer chromatography (TLC) and quantified by autoradiography. **b**, Time traces of $^{32}\text{P}_i$ formation were normalized to GTP only and time point 0 min and analyzed by a linear fit. NTP hydrolysis by ABCE1 was stimulated by addition of 40S subunit. **c**, Corrected GTPase of ABCE1 only shows stimulation by 3-fold upon addition of 40S subunit. Data derived from the slopes in panel b are given as mean \pm s.e.m. ($n = 5$). S. Trowitzsch executed the NTPase experiment in the radioactive lab. My own contribution was the design of the assay and experiment, preparation of all components for the assay, supervision of S. Trowitzsch, data analysis, and figure design. S. Trowitzsch, R. Tampé and I verified the data analysis. The justifications for this division of work were legal guidelines in radioactive working. The Beckmann lab provided 40S. Reprinted with permission (Heuer & Gerovac *et al.*, 2017).

Apparently, ABCE1 remains bound to the 40S subunit with both NBSs in the closed state only in the presence of non-hydrolysable ATP analogs but not in the presence of ATP as demonstrated previously (Andersen & Leever, 2007, Barthelme *et al.*, 2011, Dong *et al.*, 2004, Pisarev *et al.*, 2010). This indicates that ATP hydrolysis still has to occur and may be required for release of ABCE1 from the 40S subunit. In agreement with this idea, GTPase assays with ABCE1 in the presence of 40S ribosomes revealed a weak stimulation (2-3 fold) of nucleotide hydrolysis (**Figure 33**).

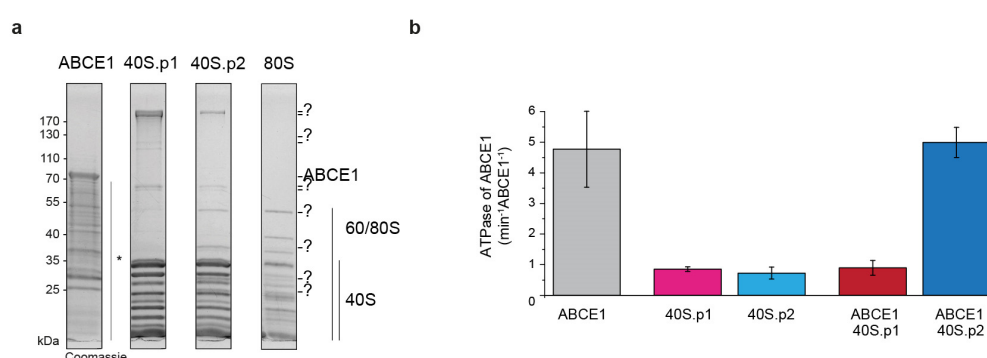


Figure 34 | ABCE1's ATPase can be shut-down by the 40S subunit. **a**, SDS-PAGE of used ABCE1 and 40S (preparation 1 (p1) and -2 (p2)). Additional bands are indicated by '?' that are not present in the 80S *vacant* preparation. **b**, ATPase of ABCE1 is shut-down by 40S.p1, but not by 40S.p2. Error bars indicate s.d. of 3 replicates (n=3).

Notably, colorimetric Malachite green ATPase experiments with 40S samples, that were not well resolved in the gradient due to overloading, revealed that ABCE1's ATPase activity could be inhibited or stay constant upon addition of 40S (**Figure 34**). This observation indicated a regulation by downstream processes and associated factors. Most likely, this effect is caused by initiation factors that remained bound to the small ribosomal subunit during preparation (**Figure 34a**). Importantly, the here used preparation of ABCE1 was purified by the old strategy (Shoemaker & Green, 2011), with minor modifications, and was impure. But an inhibited ATPase must still rely on an exclusive link to ABCE1 because the 40S samples showed no ATPase activity. In addition, in Archaea, E. Nürenberg-Goloub demonstrated also an inhibition of ABCE1's NTPase upon addition of 30S from *S. solfataricus* (Nürenberg-

Goloub *et al.*, 2018). Ribosomes from *S. solfataricus* are hardly associated as 70S in an SDG. Consequently, the small subunit cannot be prepared by puromycin and anti-association of 70S, as done in *S. cerevisiae* (**Figure 33**). The small ribosomal subunit is harvested directly after gradient fractionation. 30S sediments in close proximity to the top fractions; hence the contamination with additional factors is pre-existing. In addition, ribosome biogenesis complexes will co-sediment in 30S fractions, too. It remains open what exactly causes the NTPase shutdown in ABCE1. To my best knowledge, a substrate facilitated NTPase shutdown was not determined in any other ABC system up to now, and represents a new regulation mechanism. Major parts of **section 3.5** were published in (Heuer & Gerovac *et al.*, 2017) and are reprinted with permission.

3.5.10 Post-splitting complex in Archaea

In parallel in Archaea, in collaboration with the Beck lab (EMBL, Heidelberg), K. Kiosze-Becker used crosslinking, digestion, and mass-spectrometrical analysis of crosslinked peptides (XL-MS) to gain insights in the structure of the 30S–ABCE1 complex (Kiosze-Becker *et al.*, 2016). A single peptide cross-link between K40 of S12 and K60 of the FeS cluster domain of ABCE1 showed a long-distance link compared to the pre-splitting state (**Figure 35**). This striking observation became explainable by knowledge about the rotation of the FeS cluster domain from the post-splitting complex structure. In addition, a number of crosslinks were reported to S24, which were in agreement with the post-splitting complex structure.

In collaboration with T. Becker and A. Heuer from the Beckmann lab (Gene Center, LMU, Munich), we reconstructed a low-resolution density map of the 30S–ABCE1 post-splitting complex of *S. solfataricus* from the initial cryo-EM studies (EMD: 4113, PDB: 5LW7). For the reconstitution of this complex we used the ABCE1(E238A/E485A) variant, in which the catalytic glutamate residues close to the Walker B motifs were substituted to alanine. E. Nürnberg-Goloub engineered, characterized, and provided the ABCE1 variant (Nürnberg-Goloub *et al.*, 2018), see **section 3.5.11**. The low-resolution reconstruction showed a comparable rotation of the FeS cluster domain in the post-splitting state to the previously described high-resolution structure in yeast.

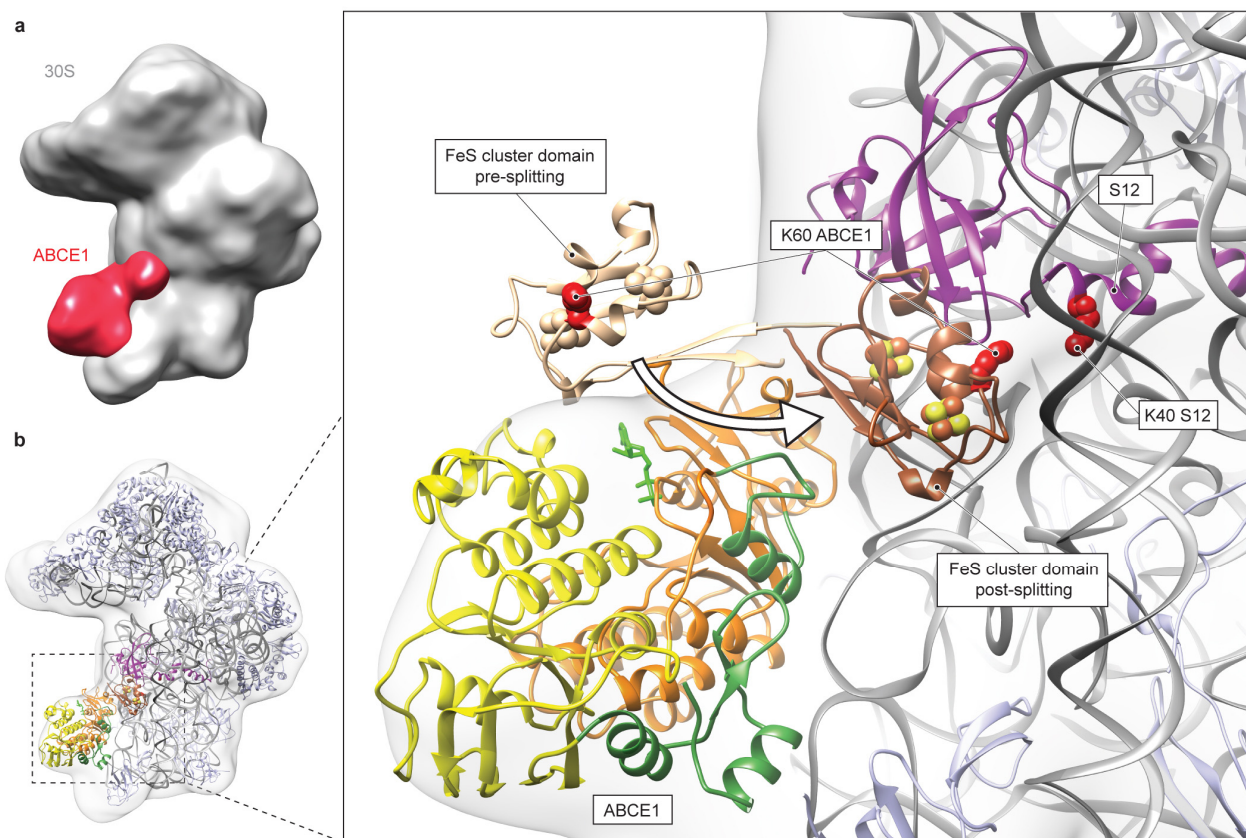


Figure 35 | Low-resolution cryo-EM reconstruction of the 30S–ABCE1 post-splitting complex. **a**, Overview of the 30S–ABCE1 post-splitting complex electron density map, low-pass filtered at ~ 25 Å. The final 30S–ABCE1 data set contained 19,500 particles and the final resolution was 17 Å (Fourier shell correlation 0.5). The ABCE1 extra density is shown in red. **b**, Model of the 30S–ABCE1 complex in post-splitting state showing the models of the *P. furiosus* small 30S subunit (grey; PDB: 4V6U, Armache & Anger *et al.*, 2013) and ribosome-bound ABCE1 (FeS cluster domain, brown; NBD1 orange and NBD2 yellow; hinges 1 and 2 green, ADP-bound green; PDB: 3J15, Becker & Franckenberg *et al.*, 2012). The FeS cluster domain was fitted into the extra density located near the ribosomal protein S12 (purple). **c**, Zoom on the FeS cluster domain shows the pre-splitting (wheat) and post-splitting (brown) state. The post-splitting state was modelled based on a specific inter-crosslink in XL-MS between Lys60 of ABCE1 (lysine 64 in *P. furiosus*) and Lys40 of S12 (shown in red). Because of this conformational change, the C_{α} – C_{α} distance between these highly conserved lysines in Archaea, yeast and human is reduced from 59.5 Å in the pre-splitting state to 17.5 Å in the post-splitting state. K. Kiosze-Becker provided the 30S subunit. E. Nürnberg-Goloub provided the ABCE1 variant. A. Heuer and I conducted sample preparation at the Gene Center and LMU Munich. A. Heuer and I performed screening of conditions for cryo-EM. A. Heuer and O. Berninghausen recorded the micrographs. A. Heuer and T. Becker reconstructed the low-resolution density map of the post-splitting 30S–ABCE1 complex. My own contribution was the analysis, visualization, and evaluation of the low-resolution density map for publication. T. Becker prepared the image of the density map. I prepared the figure and included data by K. Kiosze-Becker. Figure and caption are reprinted with permission (Kiosze-Becker *et al.*, 2016).

3.5.11 Catalytic mutants of ABCE1

Substitution of key residues in the NBSs impairs the catalytic NTPase mechanism and can yield insights about function and connected nucleotide binding and hydrolysis event order (Andersen & Leever, 2007, Barthelme *et al.*, 2011). E. Nürenberg-Goloub generated ABCE1 variants in Archaea, in which the ATPase activity was reduced by catalytic base substitutions of the glutamate residue to alanine or glutamine next to Walker B motifs. In addition, substitution of residues in the C-loop to bulky arginine residues were used to block the closure of the ABC system (**Figure 36a**) (Barthelme *et al.*, 2011, Nürenberg-Goloub *et al.*, 2018). ATP hydrolysis and nucleotide binding of ABCE1 variants were determined for the free state, and the 30S and 70S bound states (Nürenberg-Goloub *et al.*, 2018). The splitting activity was determined in a splitting assay that was dependent on release factors and AMP-PNP (Nürenberg-Goloub *et al.*, 2018). In summary, the insights are consistent with a previously observed ATPase hyper-activation of site I if site II is closed by a catalytic base substitution to glutamine close to the Walker B motif (Barthelme *et al.*, 2011). In addition, 30S binding is enforced by catalytic base substitution to glutamine in any NBS or both. Importantly, these substitutions resulted in ABCE1 variants that did not require AMP-PNP in order to bind to 30S (Barthelme *et al.*, 2011). In addition, if the same residues were substituted to alanine even AMP-PNP and elevate working temperatures were not required for binding of ABCE1 to the 30S subunit (Nürenberg-Goloub *et al.*, 2018). ABCE1(E238A/E485A) represented the most stable configuration and could freely bind the small ribosomal subunit or split the ribosome dependent on release factors (Nürenberg-Goloub *et al.*, 2018); hence it was used for cryo-EM reconstruction of the 30S–ABCE1 complex at mild conditions, see **section 2.7.3** (Kiosze-Becker *et al.*, 2016).

Importantly, ABCE1 binding to 70S required a closed site II. 70S splitting required in addition an active site I (Nürenberg-Goloub *et al.*, 2018). The explanation for this intriguing observation is a *control site II* that operates the *power-stroke site I*. The *power-stroke* is indeed most likely facilitated by site I that is in agreement with the determined Tyr301–Asn78 interaction from NBD1 to the cantilever arm of the FeS cluster domain (**Figure 31**).

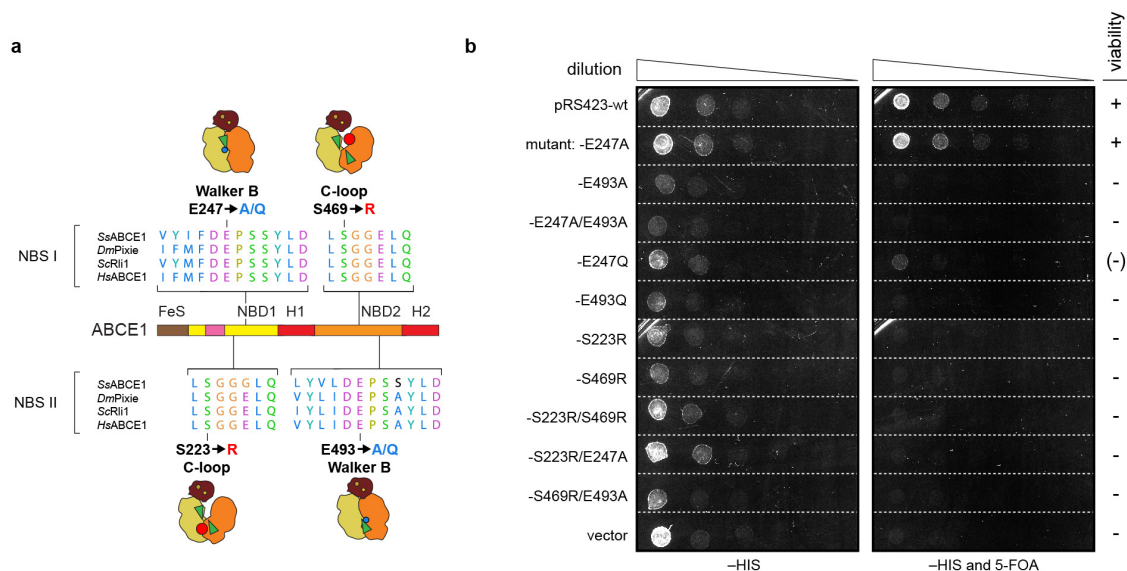


Figure 36 | Catalytic mutants show a strong growth defect. **a**, Overview of catalytic Glu-to-Ala/Gln mutants in the Walker B motif that prevent ATP hydrolysis, and Ser-to-Arg mutants in the C-loop that prevent closure. **b**, A representative yeast plasmid shuffling experiment illustrates the significance of an intact *control site II*. Only *wt* (+) and ABCE1(Glu247Ala, site I, '+') remained viable, ABCE1(Glu247Gln, site I) showed a growth defect (-), while all other mutations were lethal. I provided the plasmids and E. Nürenberg-Goloub introduced mutations. I conducted the experiment (n=2). Reprinted with permission (Nürenberg-Goloub *et al.*, 2018).

To determine the physiological effect of these ABCE1 variants *in vivo*, I performed plasmid shuffling experiments in yeast (**Figure 36b**, see method **section 2.5.1**, plasmids were mutated by E. Nürenberg-Goloub and I conducted the assay). Interestingly, catalytic substitutions of the glutamate next to Walker B or disengagement substitutions of site II were lethal, whereas site I substitutions were tolerated. This is in full agreement with the importance of site II for ribosome binding and viability. In addition, while the Glu247Gln mutant was hardly growing as reported in this study or lethal as previously reported (Märtens, 2007), at the same time, the Glu247Ala mutant was viable. Strikingly, all site II engagement substitutions (Glu493Gln/Ala) and optionally additional substitutions in site I (Glu247Gln/Ala or Ser223Arg), reflected a dominant negative effect on the growth of the cells upon co-expression with *wt* ABCE1 (Nürenberg-Goloub *et al.*, 2018). This clearly indicated an arrested translation machinery by the catalytically inhibited ABCE1 variants. Consistently with literature, this observation was shown for the site II ATPase inactive

mutants in *D. melanogaster* and *S. cerevisiae* (Andersen & Leever, 2007, Dong *et al.*, 2004). As in literature discussed, this effect is most likely linked to an arrested ABCE1 at the small ribosomal subunit, or it could be stalling of initiation complexes. In addition, 80S splitting could be impaired. Prospectively, initiation complexes intermediates could be arrested by catalytically impaired ABCE1 variants that showed a dominant negative growth effect in this study.

3.6 ABCE1 in initiation complexes

To complement our observations, the Beckmann lab (work by André Heuer and Anne Preis, (Heuer & Gerovac *et al.*, 2017)) decided to express affinity-tagged ABCE1 and to purify native 40S–ABCE1 complexes from yeast cells cultivated in logarithmic growth phase. The cryo-EM reconstruction of these complexes became possible by the resolved 40S–ABCE1 complex.

In the presence of AMP-PNP, isolated complexes contained in addition to ABCE1 also initiation factors eIF1A, eIF2 and subunits of eIF3 as identified by mass spectrometry (**Figure 37a,b**). Cryo-EM analysis showed that 63% of the particles contained ABCE1 in a conformation indistinguishable from that observed in the *in vitro* reconstituted sample (**Figure 37c,d**). Moreover, several 3D sub-classes were identified with characteristic density for the initiator tRNA (tRNA_i) in the P-site and one class with additional density for eIF1A in the A-site (**Figure 37d,e** and **Figure 38**, EMD: 3452). No clear density was observed for eIF2 or eIF3, which apparently dissociate under the chosen freezing conditions. Difference maps between the *in vitro* reconstituted and the native 40S–ABCE1 complexes not only confirmed the presence of eIF1A and tRNA_i, but also demonstrated an identical conformation of ABCE1 in the native and the *in vitro* reconstituted complexes. Thus, the EM reconstructions of the native 40S–ABCE1 complexes corroborate the reconstructions of the reconstituted complex. Moreover, the presence of initiation factors in native 40S–ABCE1 complexes supported the idea of a principle role of ABCE1 in formation of initiation complexes, for a detailed discussion see **section 4.2**.

This section was reprinted with permission from (Heuer & Gerovac *et al.*, 2017).

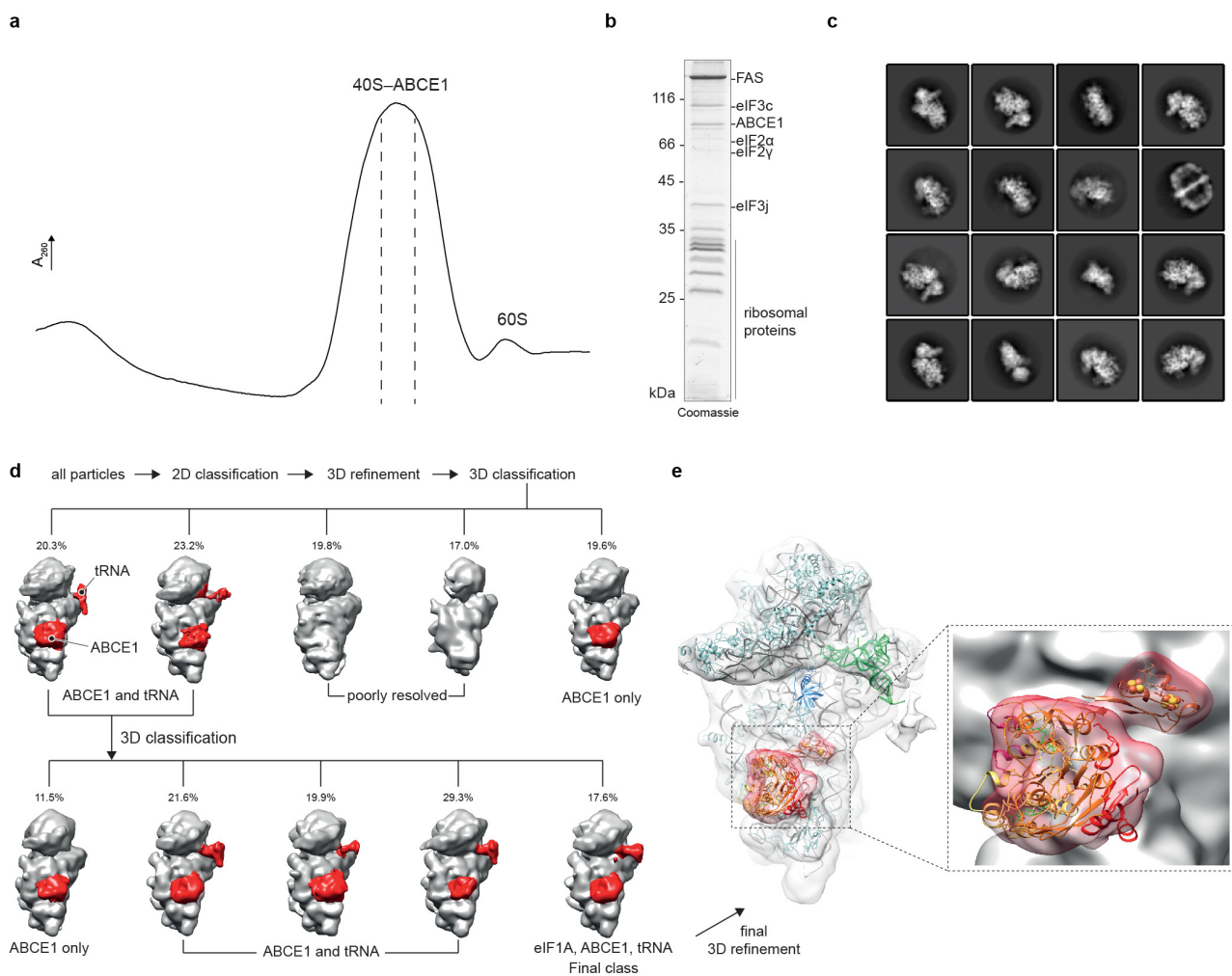


Figure 37 | Preparation and cryo-EM of the native 40S-ABCE1 complex. **a**, The TEV-eluate of affinity purified tandem-affinity tagged ribosome-ABCE1 complexes was applied to a 5-30% sucrose density gradient and the A260 profile was recorded. **b**, Fractions containing 40S subunits and ABCE1 were pooled and analyzed by SDS-PAGE. Proteins were identified by mass spectrometry. Notably, in addition to ABCE1 and 40S proteins, the complex also contains components of the 43S pre-initiation complex (eIF2 α and eIF2 γ , eIF3c and eIF3j) together with the fatty acid synthase as a common contaminant of 40S preparations. **c**, Samples were subjected to cryo-EM and single-particle analysis. The fatty acid synthase could be easily sorted out during 2D classification. **d**, After refinement, 3D classification was performed in RELION-2. In the first round, three classes (63%) show a clear density for ABCE1, and two of them showed additional extra density emerging from the P-site. These classes (43.5%) were joined for a second round of classification. Here, four of five classes only differ in the appearance of the density in the P-site, which most likely represents initiator tRNA (tRNA_i) in various positions. One class, however showed additional density in the position where eIF1A is located. This class (17.6%; 9,500 particles) was refined to a final resolution of 14 Å (**e**) according to the *gold standard* criterion (FSC = 0.143). The model of ABCE1 in the post-splitting state was fitted as a rigid body without further

adjustments into the ABCE1 density. eIF1A (blue) as well as tRNA_i (green) could be identified by rigid body fitting of 43- and 48S-initiation complex structures (eIF1A from PDB: 4UER, Aylett *et al.*, 2015), tRNA_i from PDB: 3JAP, Ll acer & Hussain *et al.*, 2015). A. Heuer, A. Preis, O. Berninghausen, T. Becker, and R. Beckmann produced all data. Reprinted with permission (Heuer & Gerovac *et al.*, 2017).

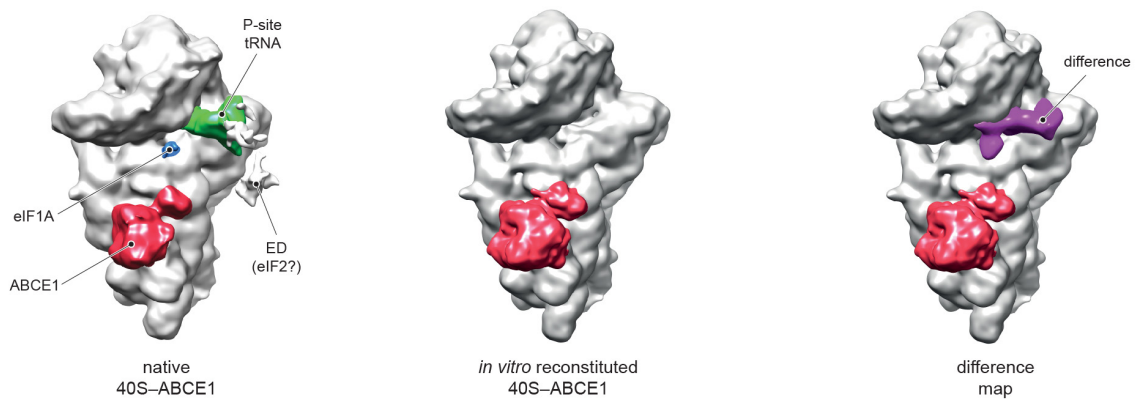


Figure 38 | Native 40S-ABCE1 initiation complex. A difference map was calculated between the native (left) and the *in vitro* reconstituted 40S-ABCE1 maps (middle). The difference map was superimposed to the *in vitro* reconstituted 40S-ABCE1 map (contoured at 3.5 σ). Notably, significant difference between the two maps (left and middle) occurred in the region of initiator tRNA (tRNA_i) and eIF1A. No conformational differences were observed for ABCE1. A. Heuer, A. Preis, O. Berninghausen, T. Becker, and R. Beckmann produced all data. Reprinted with permission (Heuer & Gerovac *et al.*, 2017).

3.7 Conformational dynamics of ABCE1 probed by smFRET

The current mechanical understanding of ABC systems is based on a tweezer-like closure and opening of two NBSs that stack two nucleoside triphosphates (Chen *et al.*, 2003). In **sections 3.4** and **3.5**, the closure of two NBSs of ABCE1 was analyzed functionally and structurally in the presence or absence of nucleotides or ribosomes. Nevertheless, the conformational dynamics of the ABC system remained elusive. To probe for conformational dynamics of ABCE1, we developed here a real-time readout of conformational transitions. Single-molecule Förster Resonance Energy Transfer (smFRET, Förster, 1948, Lerner & Cordes *et al.*, 2018) is a viable technique that utilizes *radiationless* energy transfer between a donor and acceptor fluorophore for relative distance measurements of immobilized single molecules. Alternating-laser excitation (ALEX) takes advantage of the individual excitation of the donor and acceptor fluorophore over time and enables resolution of FRET efficiency (F_E), and acceptor bleaching and blinking events (Hohlbein *et al.*, 2014, Kapanidis & Lee *et al.*, 2004, Lee & Kapanidis *et al.*, 2005). In addition, the setup allows for donor and acceptor molecule counting at single-molecule level. Finally, a classified view results for the single-particle population that is labeled by one donor and acceptor fluorophore at a stoichiometry (S) of 0.5.

K. Kiosze-Becker (Tampé lab, Goethe University, Frankfurt/M.) established smFRET studies with ABCE1 from *S. solfataricus* in collaboration with the Cordes lab (University of Groningen, NL)(Kiosze-Becker *et al.*, 2018). A confocal microscope setup was used that records freely diffusing particles through a confocal element and summarizes FRET events. No immobilization is required and F_E states of single molecules can be efficiently determined in high-throughput fashion. The disadvantage of the confocal setup is a lack in conformational tracking because of the lack of single-particle observation over time. Only bulk measurements of populations can be determined, hence no real-time dynamics are resolved. In addition, the archaeal system requires elevated working temperatures that are not suitable for the smFRET setup because operating temperatures above 37 °C denature the imaging buffer components (glucose oxidase and catalase) and harm the precision integrity of the

system. Consequently, all samples must be measured after heating up and cooling down in an energetically favored artificial conformational state (Kiosze-Becker *et al.*, 2018).

I decided to use ABCE1 from *S. cerevisiae* as a target for tracking of conformational dynamics in ABC systems in real-time at room temperature. The setup of a FRET assay requires specific labeling of ABCE1 with donor and acceptor fluorophores. I used cysteines for the maleimide-based fluorophore labeling approach that requires an engineered cysteine-less (cl) variant of ABCE1. Additional cysteines for labeling by fluorophores were inserted at equal positions that K. Kiosze-Becker reported for *S. solfataricus* ABCE1 (Kiosze-Becker *et al.*, 2018). Tracking of conformational dynamics requires immobilization of the protein of interest and a microscope setup in total internal reflection fluorescence (TIRF) mode. The immobilization was achieved *via* the His-tag and metal-affinity chelation that was previously used for purification. Luckily, the smFRET experiments could be conducted at a smFRET ALEX setup in TIRF mode that P. Höllthaler (Tampé lab, Goethe University, Frankfurt/M.) built.

The smFRET assay and labeled ABCE1 as a model protein were validated by the known conformational transitions of NBD dimerization and FeS cluster domain rotation at the small ribosomal subunit. We were interested in the dynamic conformational switching interdependency of *closure of site II* → *closure of site I* and *site I closure* → *FeS cluster domain rotation*. We aimed to deduce information about the order of these switches by analysis of the dwell times of defined conformational states.

3.7.1 Engineering of a cysteine-less ABCE1 variant

The major requirement for FRET studies is the site-specific protein labeling by fluorophores. ABCE1 from *S. cerevisiae* has six endogenous cysteines (Cys38/236/278/292/506/561), in addition to the eight cysteines from the FeS clusters. I aligned protein sequences of ABCE1 from the organisms *S. solfataricus*, *D. melanogaster*, *S. cerevisiae* and *H. sapiens*, and many more (data not shown), and checked for the conservation of the additional cysteines (**Figure 39**). As *S. solfataricus* ABCE1 has no additional cysteines, and is predestined for labeling studies, there were a number of alternative residues that could be used for substitution of the additional cysteines to achieve a cysteine-less variant for ScABCE1, too.

E.g. Cys38 was previously reported being exchangeable to alanine and serving as a swapping or rescue residue (Barthelme *et al.*, 2007). Cys236 and Cys506 showed no conserved alternative residue, so both were substituted by alanine. Cys276 was supplemented by valine, and Cys561 clearly showed methionine as alternative residue in sequence alignments, the same strategy was applicable for Cys292 that was supplemented by histidine. Cysteines for fluorescent labeling were inserted by site-directed mutagenesis. Based on the data by K. Kiosze-Becker in *S. solfataricus*, I selected the complementary residues for NBS I (Lys128Cys, Arg439Cys) and NBS II (Lys181Cys, Lys403Cys) (Kiosze-Becker *et al.*, 2018). Additionally, the endogenous Cys38 of *S. cerevisiae* was used to probe for the FeS cluster domain rotation, see methods **section 2.2.3**.

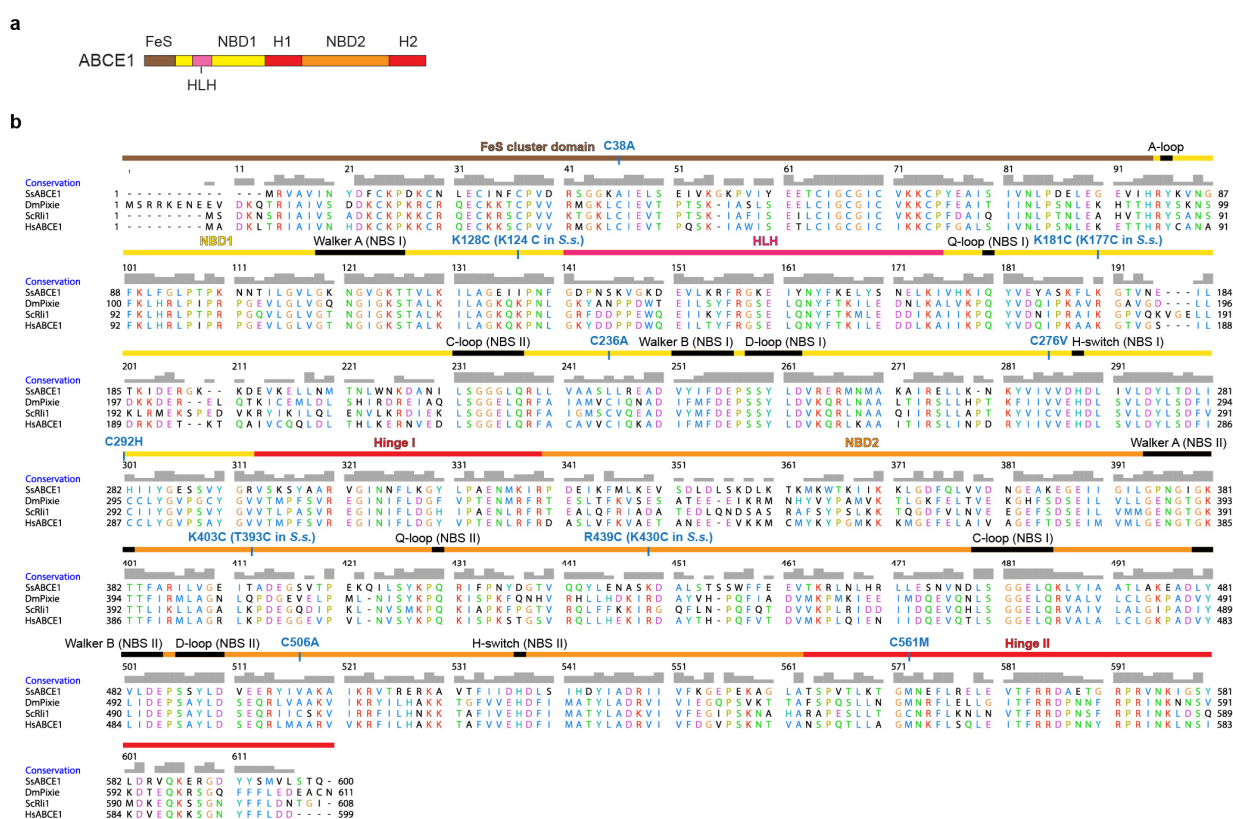


Figure 39 | Sequence alignment of ABCE1 with cysteine-mutations. **a**, Scheme of ABCE1. **b**, ABCE1 from *S. solfataricus*, *D. melanogaster*, *S. cerevisiae* and *H. sapiens* were aligned with Clustal W in Chimera. Domains and ABC motifs are indicated as colored bars as in a. Endogenous cysteines that were substituted to other residues are indicated in blue. Additionally introduced cysteines for fluorophore labeling are indicated in blue with corresponding substitutions in *S. solfataricus* (Kiosze-Becker *et al.*, 2018).

Importantly, the FeS clusters must be completely preserved and not oxidized in order to disallow labeling of the FeS cluster-forming cysteines. However, the labeling reaction by maleimide-thiol coupling must be accomplished at non-reducing conditions that favor oxidation of the FeS clusters and disintegrity of the whole domain. In general, for labeling, the protein must be pure, that could be ensured for ABCE1 by the improved purification strategy, see **section 2.4.1**.

3.7.2 Double-cysteine variants of ABCE1 for smFRET

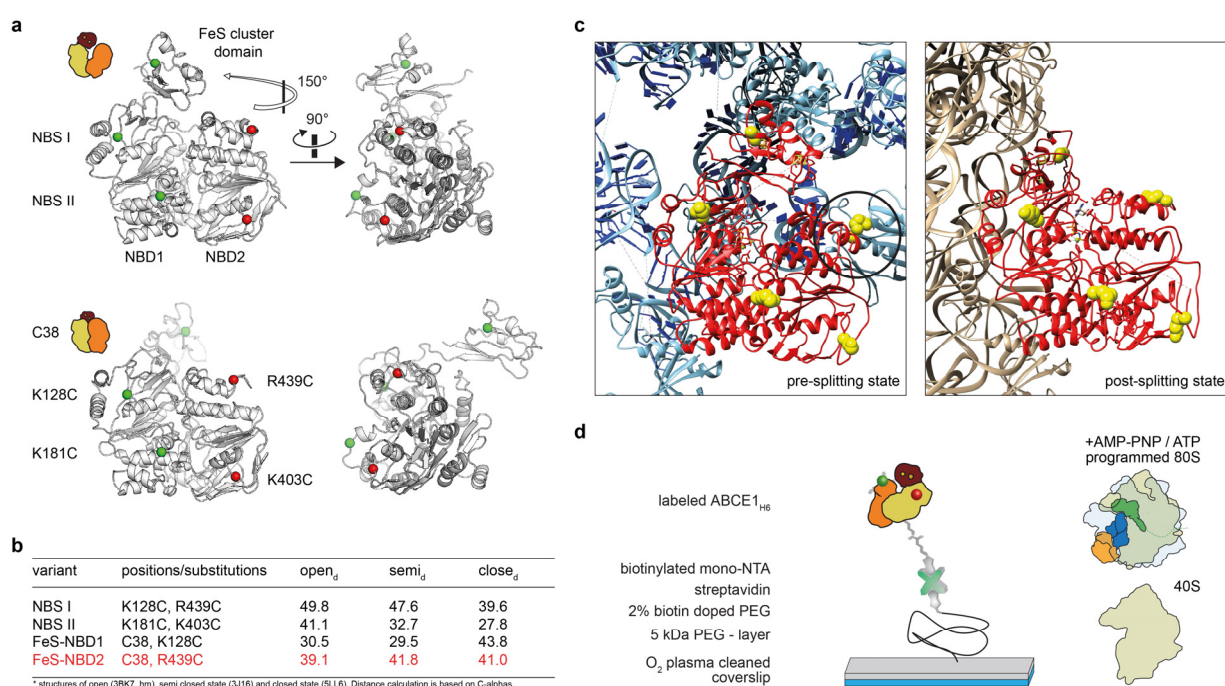


Figure 40 | Fluorophore probe positions and immobilization setup. a, Indicated positions for fluorophore probes in the pre-splitting state (top, PDB: 3J16, Becker & Franckenberg *et al.* 2012) and post-splitting state (bottom, PDB: 5LL6). **b**, Distance changes of C_α labeling positions from open to semi-closed, and closed conformation in (Å). **c**, General fitting of the substituted residues (yellow) of ABCE1 (red) at the pre- (blue, PDB: 3J16) and post-splitting ribosome (teal). Labeling at Cys439 may provoke a clash with the large ribosomal subunit, as indicated by a black circle. **d**, Immobilization strategy based on the C-terminal His₆-tag and biotin-NTA on a glass cover slip. Panel d contains graphical elements for immobilization that were designed by P. Höllthaler, reprinted with permission.

To evaluate the chosen labeling positions, the theoretical distances were calculated based on the C α positions of the residues for the available open, semi-closed, and closed structures, as discussed in **section 3.5.6**. The positions of the labels for site I (Lys128, Arg439) and site II (Lys181, Lys403) resulted in a distance difference from the open to the closed state of about 10 and 13 Å, respectively, hence should be usable for FRET studies and showed in previous work FRET efficiencies between 0.2 and 0.8 (Kiosze-Becker *et al.*, 2018). The position in the FeS cluster domain (Cys38) and NBD1 (Lys128) resulted in a distance difference of about 13 Å that is usable for FRET studies. The FeS cluster domain label at Cys38 and NBD2 (Arg439) resulted in only 2 Å distance difference between the open and closed conformations (**Figure 40a,b**), hence were not usable for FRET studies. In site I, labeling at the position Arg439 may provoke a clash with the large ribosomal subunit in the pre-splitting state and may cause incompatibility in 80S binding and splitting studies (**Figure 40c**). For immobilization, we used the C-terminal His₆-tag of ABCE1_{H6} for affinity immobilization at biotinylated mono-nitrilotriacetic acid (NTA) that was bound to a glass cover slide *via* streptavidin on a biotin doped polyethylenglycol (PEG) surface. P. Höllthaler established the immobilization of ABCE1 (**Figure 40d**), based on a strongly modified strategy by the Joo lab (Chandradoss *et al.*, 2014), see method **section 2.8.2**.

3.7.3 Viability and purification of cysteine-less and double-cysteine ABCE1 variants

I cloned the cysteine-less ABCE1 (ABCE1_d) and double-cysteine variants by site-directed mutagenesis in the plasmid shuffling vector pRS423_pRli1t and the production vector pYes2_Rli1. Plasmid shuffling of the mutated *ABCE1*^{*} in the CEN.MG1-9B strain resulted in viable strains upon 5-FOA treatment (**Figure 41a-c**). The purification strategy was the same as for *wt* ABCE1_{H6} and resulted in a pure and monodispersly eluting protein in SEC with efficiently assembled FeS clusters as determined by a 410/280 nm absorption ratio of 0.45 (**Figure 41d-e**). An equal purification quality was achieved for ABCE1 double-cysteine variants (**Figure 42c**).

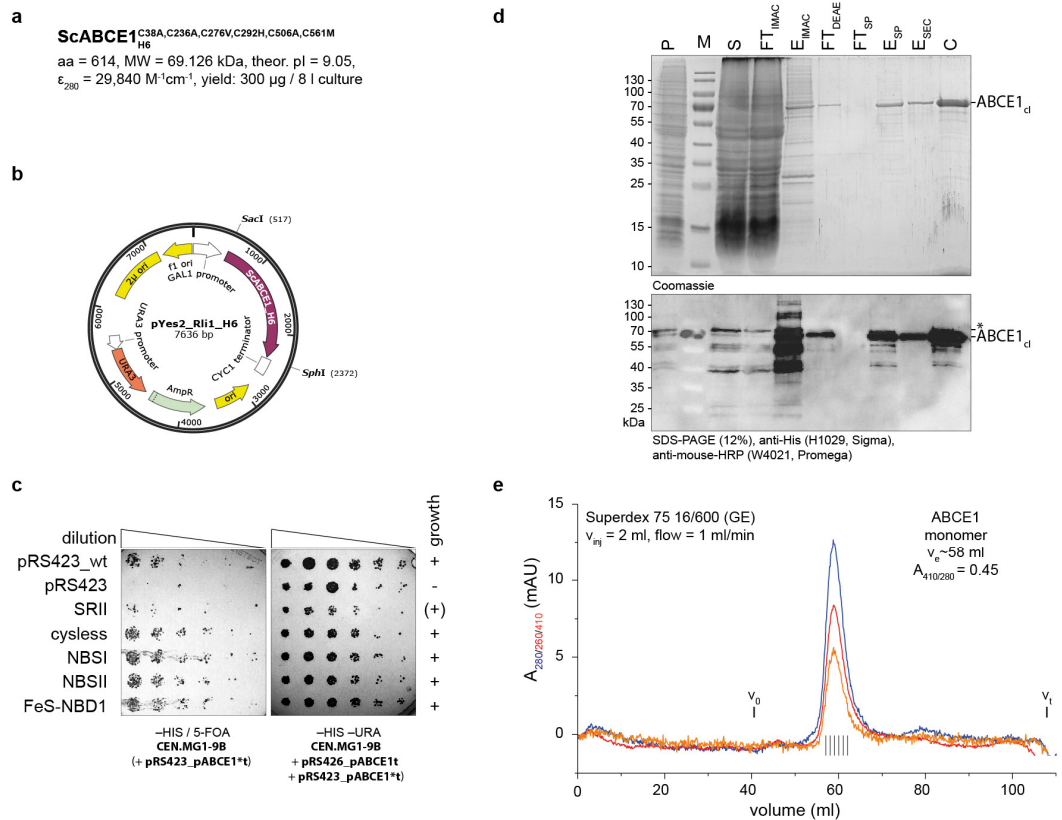


Figure 41 | Viability and production of cysteine-less and double-cysteine variants. **a**, Protein parameters for the cysteine-less variant ABCE1_{c1}. **b**, Production vector **c**, All constructs were viable in the plasmid shuffling assay. **d**, ABCE1_{c1} was purified as described for ABCE1_{H6}. **e**, In SEC, ABCE1 eluted monodispersely as a monomer with assembled FeS clusters and an $A_{410/280 \text{ nm}}$ ratio of 0.45. * indicates an immunoblot active impurity.

3.7.4 Labeling of ABCE1 and immobilization

In collaboration with P. Höllthaler, we labeled double-cysteine variants of ABCE1, see method **section 2.8.1**. The labeling-reaction was executed in storage buffer at pH 6.5 without reducing agents by addition of sCy3/-5-maleimid in 20x molar excess. The buffer was exchanged and the reaction quenched by spin columns and the labeled protein purified by SEC (**Figure 42a**). The labeling efficiency was calculated by the specific absorption coefficients of the dyes (**Figure 42b,c** and **Table 3**). Absorption of fluorophores at 280 nm was omitted in calculations due to the low labeling efficiency (<20%). Importantly, the indicated labeling efficiency is related to two free cysteines for each dye omitting the FeS cluster cysteines. In essence, 50% labeling efficiency by each dye corresponds to 100% labeling. Of note for future experiments, 16x sCy3 and 20x sCy5 should be used in order to

correct for sCy3 over-labeling that is consistent with data from the Blanchard lab (Dyla & Terry *et al.*, 2017).

Binding of labeled ABCE1 variants to 40S was evaluated in pelleting assays (**Figure 43**). All labeled ABCE1 variants resulted in AMP-PNP stimulated binding to 40S. However, no nucleotide addition yielded also binding to 40S that was consistent with the experiments of *wt* ABCE1, see **Figure 22**. The fluorescence intensity ratio in the sCy3 and sCy5 channels of pelleted ABCE1 to input was equal; hence, the attached dyes did not affect the binding to 40S. The small subunit was added in 2x excess to ABCE1, but labeled ABCE1 was pelleted only to about 20-30% compared to input samples and unlabeled *wt* ABCE1 (**Figure 22**). The incomplete pelleting of labeled ABCE1 may be related to the labeling procedure. Hence, the level of functional ABCE1 in FRET studies was about one third. Consistently with previous experiments, only the full-length ABCE1, and no impurities or degradation products, co-sedimented with the 40S subunit.

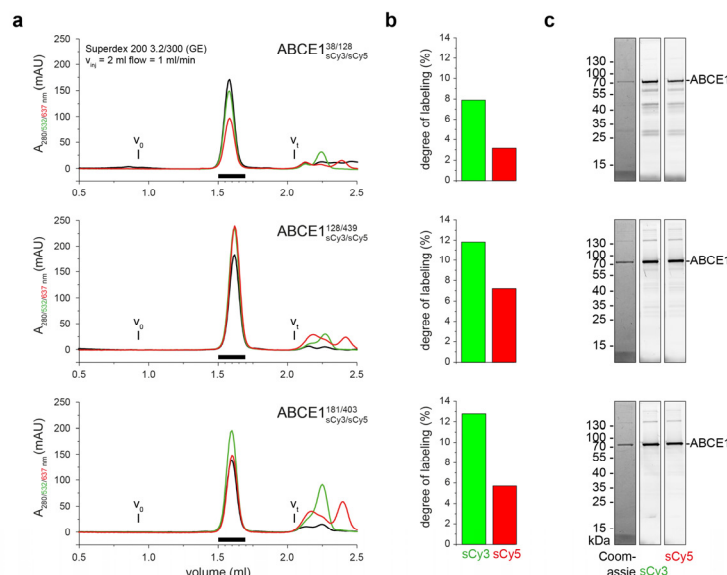


Figure 42 | Labeling of ABCE1 by sCy3/-5. a, SEC purification of sCy3/-5 labeled ABCE1 variants. **b**, Calculated labeling efficiency is based on two available free cysteines for labeling. **c**, SDS-PAGE of labeled ABCE1 variants, imaged on a Typhoon 9400 (GE). ABCE1 was labeled in collaboration with P. Höllthaler. P. Höllthaler recorded the SEC profiles. I provided the isolated proteins, designed and supervised these experiments.

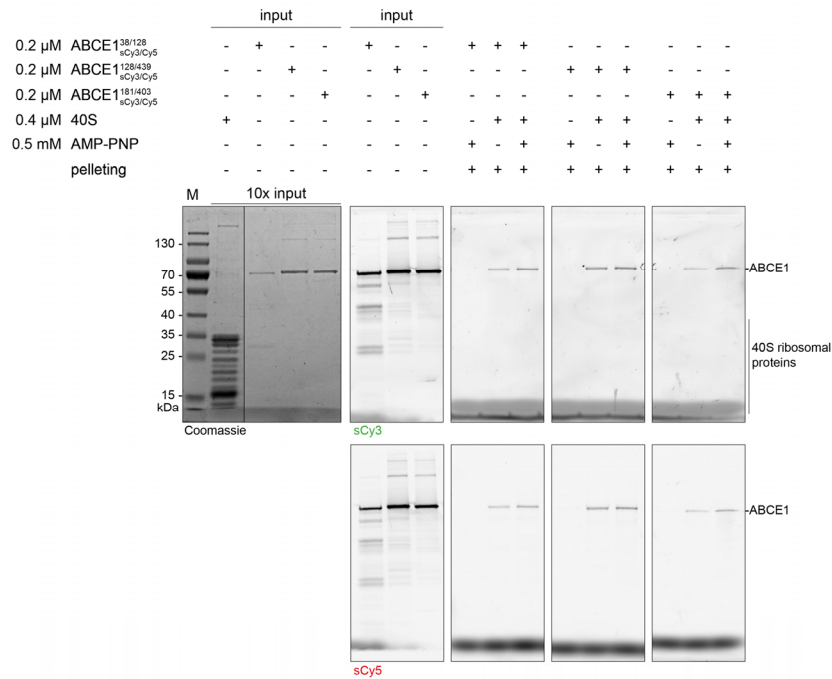


Figure 43 | Binding of sCy3/sCy5 labeled ABCE1 variants to 40S. All labeled ABCE1 variants resulted in AMP-PNP stimulated binding to 40S. No nucleotide results also in binding to 40S that is consistent to low salt conditions in pelleting experiments with *wt* ABCE1, see **Figure 22**.

3.7.5 Conformational dynamics

I produced and analyzed all data in collaboration with P. Höllthaler. R. Kleebach, internship student in the Tampé lab, supported this work.

Labeled ABCE1 was successfully immobilized on the surface and movie traces revealed a dynamic behavior of single-molecule FRET efficiency (F_E) traces in about 20-30% of the recorded particles (see exemplary trace in **Figure 44**).

The conformational state of the FeS cluster domain was probed with the labeled FeS-NBD1 variant. The F_E and S (F_{ES})-heat-diagrams revealed high- (F_E at 0.6) and low- F_E (at 0.2) populations that were linked to a non-rotated and rotated FeS cluster domain position, respectively, relative to lobe 1 of NBD1 (**Figure 45**). Upon addition of 40S and present AMP-PNP, the F_E population shifted completely to 0.2 (low- F_E) and fitted to the predicted low-FRET state in the post-splitting state as expected from structural studies, in which the FeS cluster domain is rotated away from NBD1 towards helix 44, see **section 3.5**.

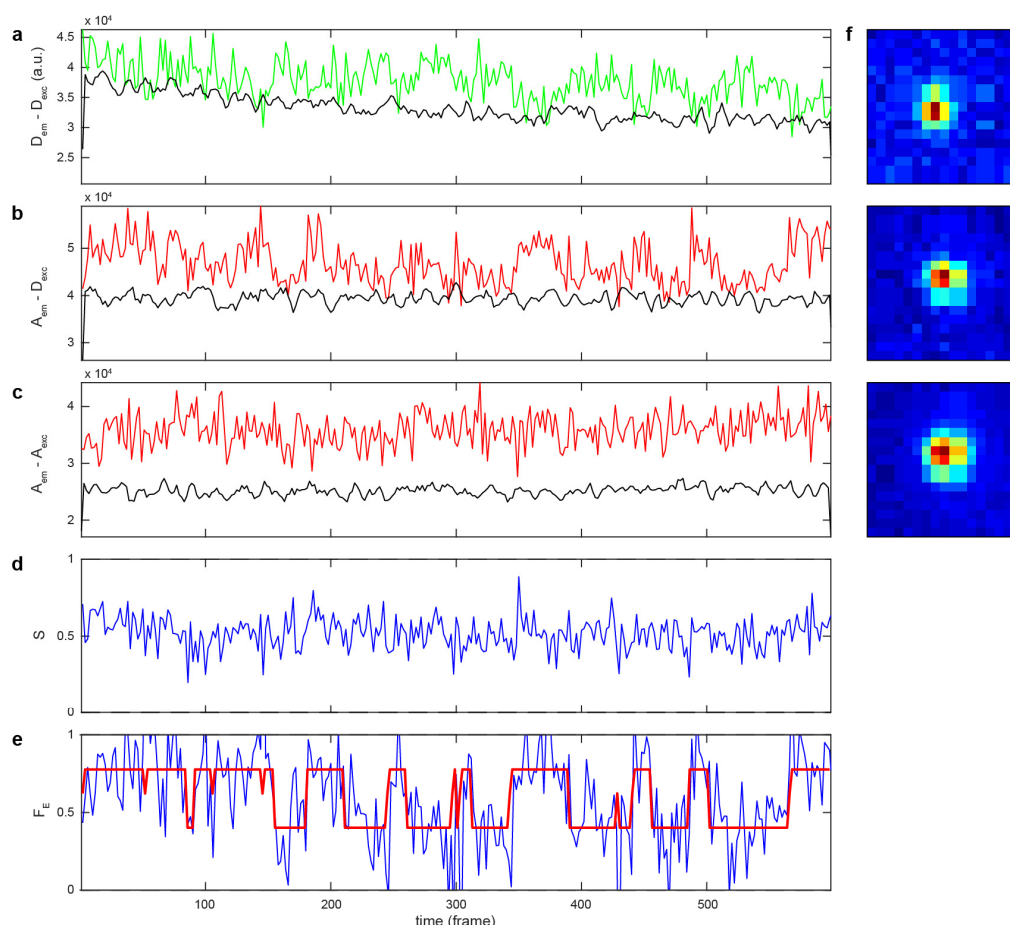


Figure 44 | Dynamic FRET efficiency trace of the sCy3/sCy5 labeled NBS II variant with 40S and AMP-PNP. **a**, Donor only fluorescence channel, $I_D = D_{em} - D_{exc}$. **b**, Acceptor excitation and donor emission channel, $I_{DA} = A_{em} - D_{exc}$. **c**, Acceptor only fluorescence channel, $I_A = A_{em} - A_{exc}$. **d**, Fluorophore stoichiometry (S) calculated by $D_{exc}/(D_{exc} + A_{exc})$; 0.5 corresponds to a 1:1 labeling ratio. **e**, FRET efficiency (F_E) calculated by $I_A/(I_A + I_D)$. In red line, conformational dynamics are depicted by Hidden Markov Model in an idealized two state system **f**, Particle position and environment in the movie. P. Höllthaler analyzed and exported the data. I supervised these experiments and assembled the figure.

Consistently, the ATP sample showed a minor F_E population about 0.6 (high- F_E), but it was less populated than in the no nucleotide (apo) and ADP samples. Of note, the FeS-NBD1 variant behaved nearly identical for the 40S and AMP-PNP condition, the ATP, and the apo condition. The low- F_E state in the apo and ATP conditions may be due to conformational freedom of the FeS cluster domain because it is linked by a flexible cantilever arm to NBD1. Interestingly, in the AMP-PNP sample without 40S, the F_E was widely distributed between 0.2-0.8 indicating a number of different conformational states of the FeS cluster domain.

This unexpected observation can be linked to the direct interaction of NBS I to the cantilever arm, which may be present even without 40S and stabilize the FeS cluster domain position near NBD1 in a rotated orientation. Notably, the fluorescent probe is located in lobe 1 of NBD1 closely to the nucleotide-binding pocket in NBS I.

In summary, the FeS-NBD1 variant showed a 40S and AMP-PNP dependent rotation of the FeS cluster domain. In addition, without present 40S, the FeS cluster domain showed most likely conformational freedom. Without present 40S, we observed an AMP-PNP dependent conformational distribution in which the FeS cluster domain and NBD1 were also closer positioned that can be explained by a crosstalk of NBD1 with the FeS cluster domain in a ribosome unbound state.

In addition, in the case of 40S and AMP-PNP, we observed a dynamic conformational behavior of the FeS cluster domain in the Hidden Markov Model (HMM) analysis of the F_E trace (Blanco & Walter, 2010, McKinney *et al.*, 2006). The HMM fit revealed a high frequency switching in an idealized two F_E state system between 0.25 and 0.0 (**Figure 51a**). This observation may indicate that the FeS cluster domain attempts for relaxation but is firmly rotated back away again, because the *control site I* remains closed. In the case of ATP and ADP, we did not observe any dynamic switching towards 0.0 F_E . In line with this observation, a number of F_E traces may have been missed in the particle selection process based on donor and acceptor presence, because there was no acceptor fluorescence detected in the rotated post-splitting state. In addition, the iSMS analysis platform corrects F_E -heat diagram construction by selection for F_E values >0.1 . In manually calculated histograms, F_E values <0.1 were also present (data not shown). In future studies, the conformational switches of the FeS-NBD1 variant at low- F_E values should not be excluded by filtering and examined in detail by manual calculation of histograms.

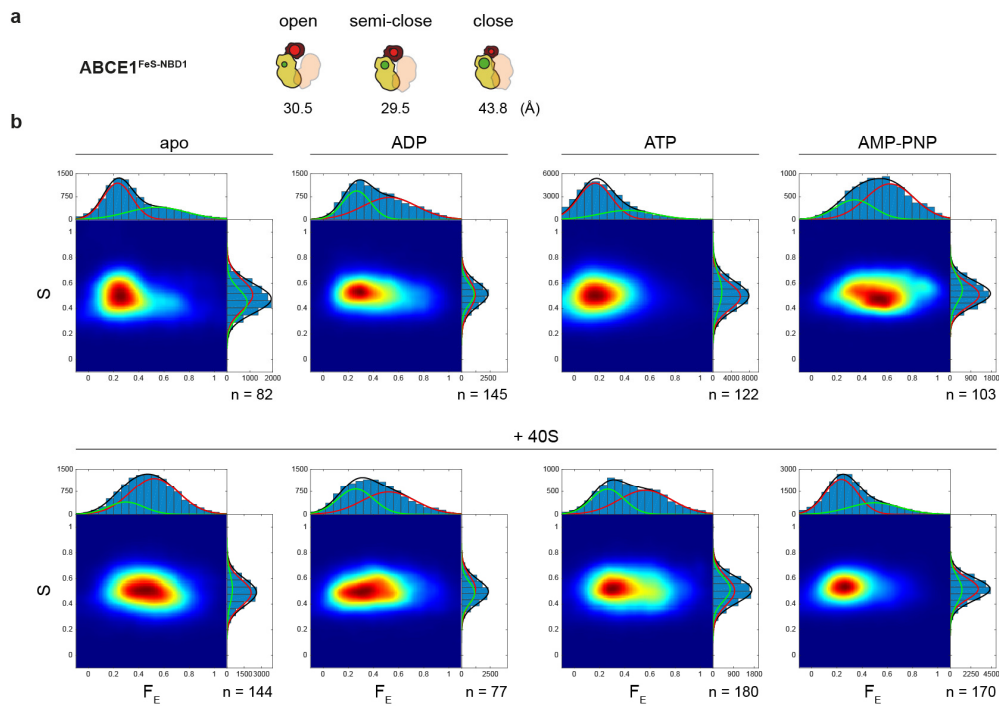


Figure 45 I Conformational populations of the FeS-NBD1 variant. **a**, Pictogram of ABCE1^{FeS-NBD1} with indicated fluorophores, putative states and theoretical FRET pair distances. **b**, F_E-heat-diagrams of F_E populations dependent on nucleotide and 40S addition. P. Höllthaler and I analyzed the data. I designed and supervised these experiments and assembled the figure.

The site I variant (NBS I), a low-F_E about 0.2 was observed in all samples. In the presence of 40S and AMP-PNP the, site I closed and yielded a high-F_E about 0.6 (**Figure 46**). This clearly indicated closure of the ABC system upon binding to 40S and formation of the post-splitting complex as determined in the cryo-EM reconstruction. Remarkably, with 40S, only AMP-PNP yielded a F_E population at 0.6, but not ATP, as observed for the FeS-NBD1 variant. Hence, the nucleotide-dependent conformational switches are independent or occur at different time scales for NBSI closure and FeS cluster domain rotation.

Only 20-30% of labeled ABCE1 were stably bound to the small ribosomal subunit in binding studies (**Figure 43**, see **section 3.7.4**). This was consistent with the large population of ABCE1 that did not yield any conformational switch upon addition of 40S and nucleotides.

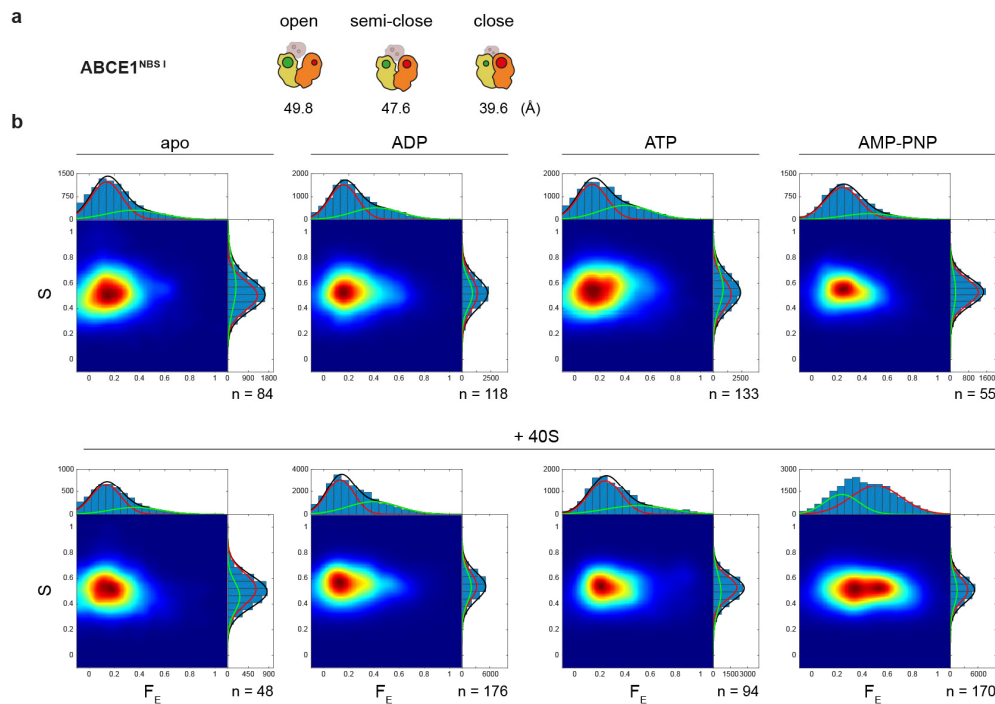


Figure 46 | Conformational populations of the NBS I variant. **a**, Pictogram of ABCE1^{NBS I} with indicated fluorophores, putative states and theoretical FRET pair distances. **b**, F_ES-heat-diagrams of F_E populations dependent on nucleotide and/or 40S addition. P. Höllthaler and I analyzed the data. I designed and supervised these experiments and assembled the figure.

To probe for low-level shifts in F_E populations, the initial observations for the FeS-NBD1 and NBS I variants in the F_ES-heat-diagrams were evaluated by difference histograms (**Figure 47a**). A relative representation of F_E shifts focuses on the population that performs a conformational switch. The FeS-NBD1 and the NBS I variants behaved oppositional with 40S, as evident in each F_E population shift diagram in the lower-right quadrant (**Figure 47b**). The NBS I closed and the FeS cluster domain rotated away and yielded increased or decreased F_E population shifts, respectively. Strikingly by addition of 40S, a correlation became apparent between nucleotides in the logical line apo→ADP→ATP→AMP-PNP with the F_E population shifts in the lower right quadrant (indicated by color coding, **Figure 47b,c**). In the case of the NBS I variant, the same was true for the upper-left quadrant, that may indicate also a closure of the ABC system without 40S, but at lower rate (**Figure 47c**). For the FeS-NBD1 variant without 40S, no clear logical line of conformational changes was deducible because the AMP-PNP only sample yielded a wide conformational distribution (**Figure 45**).

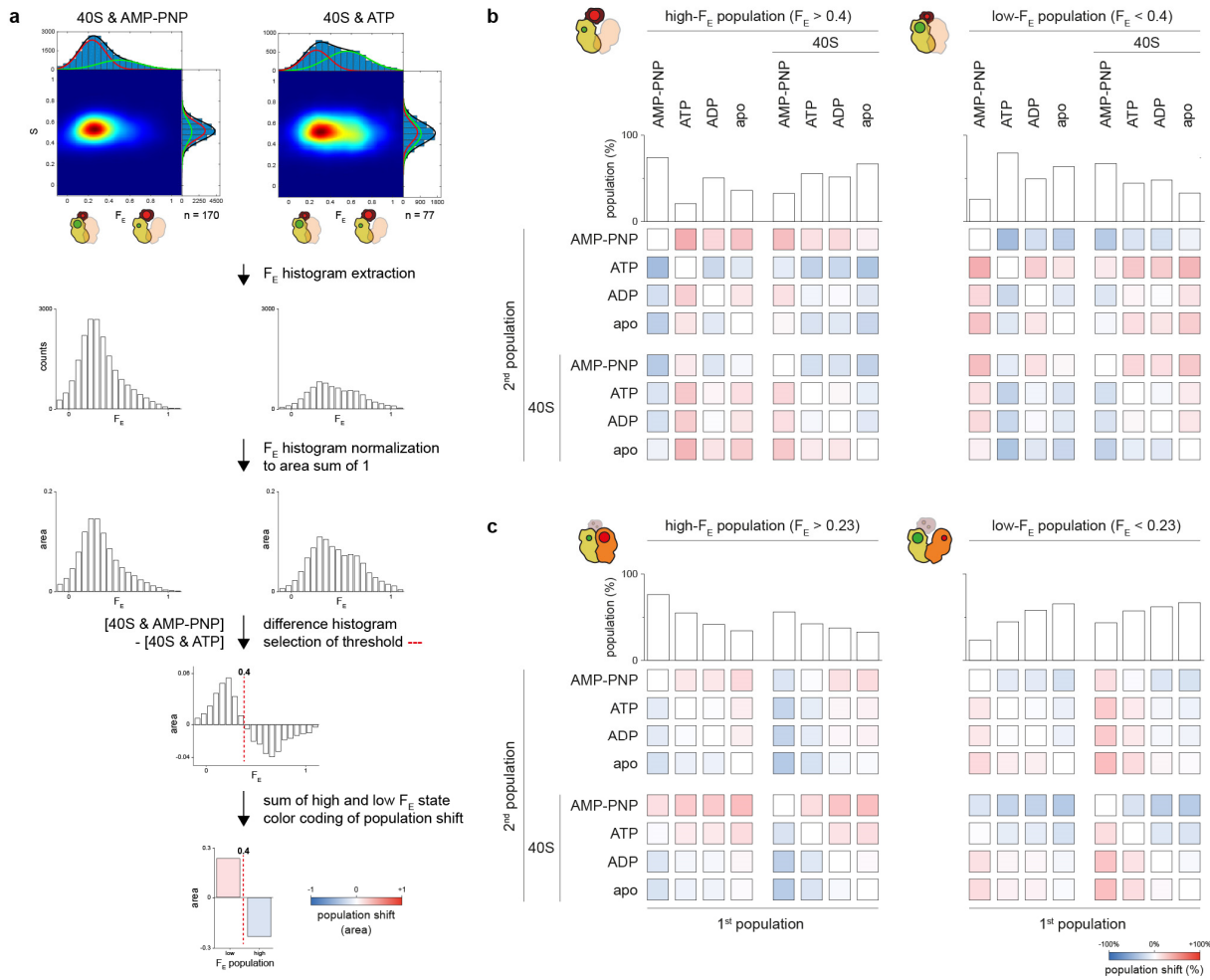


Figure 47 | FRET efficiency population shifts of the FeS-NBD1 and NBS I variants. **a**, The analysis included normalization of each FRET histogram to the total area of 1 and subtraction for generation of a difference-histogram. A threshold was set at the maximum rise that divides the high and the low- F_E population. Each side of the divided difference histogram was summarized and yielded a shift value that was color coded and represented in a diagram that considered a 1st→2nd population value. **b**, In the FeS-NBD1 variant with present 40S, the FeS cluster domain rotated away from NBD1 upon addition of AMP-PNP because the high- F_E population decreased (blue), see (a). The population shift was most pronounced from apo→AMP-PNP. **c**, In the NBS I variant, the site I closed in the logical line apo→ADP→ATP→AMP-PNP. The high- F_E population increased from apo→AMP-PNP. P. Höllthaler and I analyzed the data. I designed and supervised these experiments and assembled the figure.

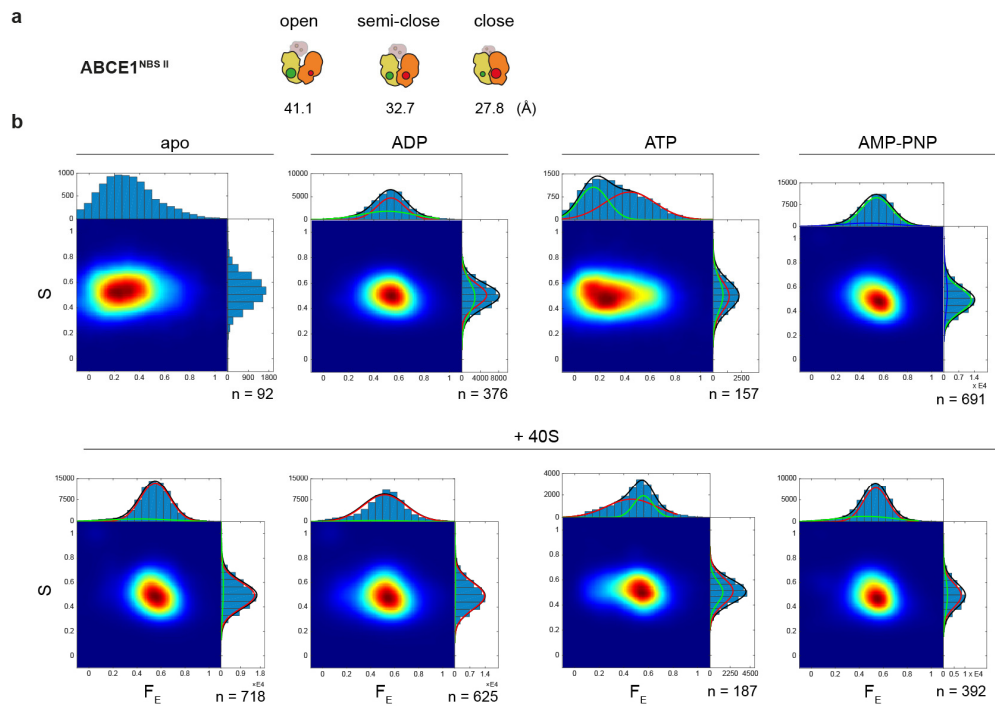


Figure 48 | Conformational populations of the NBS II variant. **a**, Pictogram of ABCE1^{NBS I} with indicated fluorophores, putative states and theoretical FRET pair distances. **b**, F_E S-heat-diagrams of F_E populations dependent on nucleotide and/or 40S addition. P. Höllthaler and I analyzed the data. I designed and supervised these experiments and assembled the figure.

For the site II variant (NBS II), we observed a significant F_E population at 0.6 (**Figure 48**). F_E population shifts were hardly visible in the heat maps. Interestingly, in the nucleotide-only measurements, ADP and AMP-PNP samples behaved similarly yielding a defined FRET efficiency of about 0.6. Apo and ATP samples shifted towards lower F_E populations as if opening of the ABC system would become allowed. Importantly, upon addition of 40S, the ATP sample showed conformational freedom, but apo and AMP-PNP samples behaved highly defined at an F_E about 0.6. The detailed analysis of F_E population shifts by difference histograms yielded the same results (**Figure 49**). This observation is in agreement with published data from the Pestova lab (Pisarev *et al.*, 2010), that showed binding of ABCE1 to 40S with AMP-PNP and to a significant extent at apo conditions, too. The same was true for binding of ABCE1 to 80S. Unspecific interactions were excluded because these should be present with all nucleotides. The closure at apo and 40S conditions may be physiologically relevant and is only present in the F_E population analysis for the

NBS II variant. It is worth stating that site II is relevant for the stable interaction with the small ribosomal subunit, see **section 3.5.11** (Nürenberg-Goloub *et al.*, 2018). Importantly, aside this claim, in the pelleting assays in yeast, ABCE1 showed binding to 40S at all conditions, but AMP-PNP significantly stimulated its co-sedimentation (**Figure 22**).

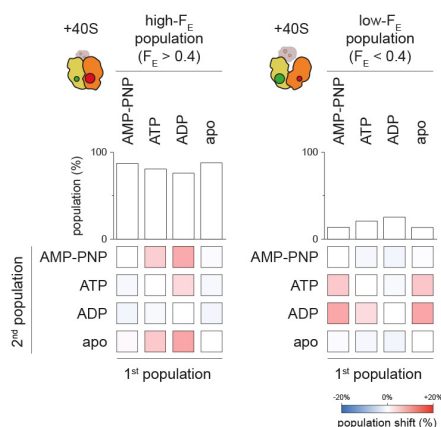


Figure 49 | FRET efficiency population shifts of the NBS II variant with 40S. a, The high- F_E population increased from ADP/ATP→AMP-PNP. AMP-PNP and apo behaved similarly and did not result in population shifts. P. Höllthaler and I analyzed the data. I designed and supervised these experiments and assembled the figure.

In the HMM analysis, we observed frequent spikes for the site II variant, which suggested a highly dynamic behavior that we could not resolve by the here used resolution at 100 ms integration time. We decreased the integration time of the camera to 50 ms to obtain an increased time-resolution. In line with our assumption, in a pilot experiment, the spikes were resolved and the traces yielded F_E populations from 0.2 to 0.7 (**Figure 50**). Strikingly, at 50 ms time-resolution, a closure of site II became apparent at an F_E population about 0.7 with 40S and AMP-PNP. In contrast, in the 40S and ATP sample, the high- F_E population was not densely present in the F_E S-heat diagram.

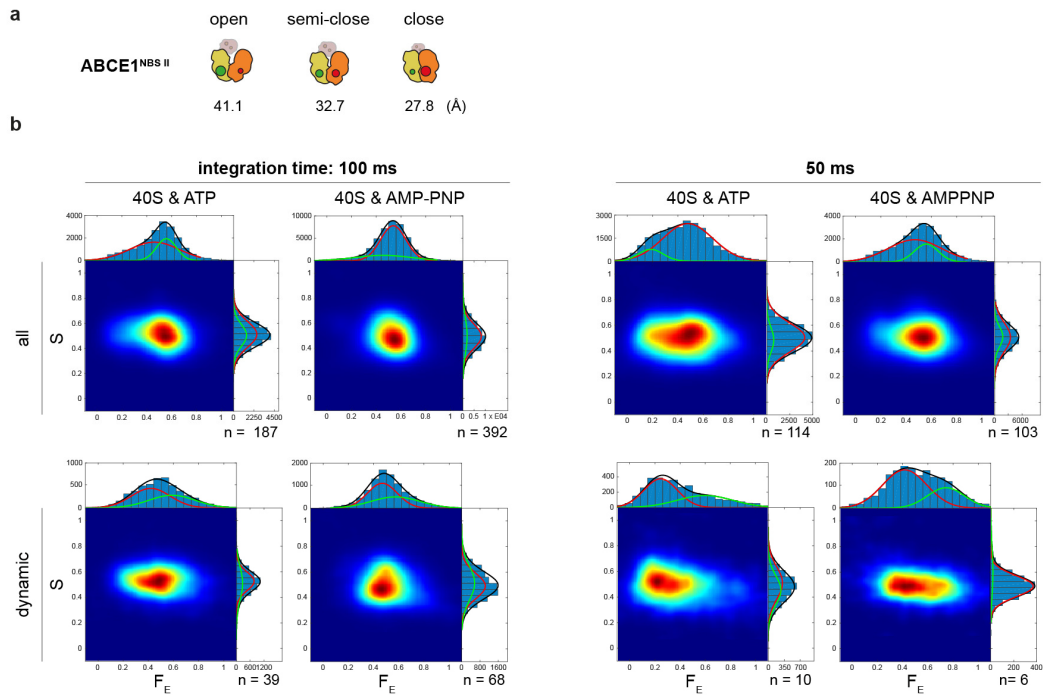


Figure 50 I Integration time dependency of populations in the case of the NBS II variant. a, Pictogram of ABCE1^{NBS II} with indicated fluorophores, putative states and distances. **b**, F_E S-heat-Diagrams at 100 ms (left) and 50 ms (right) integration time. In addition only dynamic traces were selected. The lower integration time resulted in a higher time-resolution of the FRET efficiency, and this yielded a F_E population distribution between 0.2 and 0.7. In the case of 40 and AMP-PNP, the 0.7 F_E was populated, hence with 40S the NBS II variant closed upon addition of AMP-PNP compared to ATP. P. Höllthaler and I analyzed the data. I designed and supervised these experiments and assembled the figure.

In conclusion, the site II conformational switching frequency is higher than we could resolve at 100 ms integration time. To probe for its conformational dynamics we need to decrease the integration time and this will decrease the signal-to-noise ratio. In summary, based on preliminary observations, site I is slower than site II, but closure of the ABC system is by far more frequent than the measured ATP hydrolysis rate in **section 3.5.9 (Figure 33)**. It is tempting to record that closure and ATPase are uncoupled. In line, the *control site II* is a high frequency site that is most likely sensing a signal by the ribosome *via* rapid conformational dynamics or an *elastic conformational behavior*. In addition, the slower opening and closing *power-stroke site I* utilizes the ATP binding for the rotation of the FeS cluster domain. This is in line with power-transferring mechanics, as a slower rate can utilize more force. In addition, we observed rapid F_E switches of the FeS cluster domain but a full relaxation to the high-

FRET state was prohibited in the case of 40S and AMP-PNP (**Figure 51**). In general, the noisy traces could be linked to the dynamic conformational behavior of proteins from mesophilic organisms.

Notably, in all three variants, we observed conformational dynamics with 40S and AMP-PNP, hence the conformation of the post-splitting state is not stably formed, rather favored at these conditions, and most likely frozen upon cool down post reaction and analysis by density gradient fractionation. Future studies should reveal in longer recorded time-traces if these observations are due to prolonged stationary phases that are interrupted by highly dynamic phases, or if the conformational dynamics are persistently present and could not be resolved by the here utilized time-resolution. In general, we should aim at higher time-resolution also for the FeS-NBD1 and NBS I variants in order to probe for additional short-lived F_E states that may uncover deeper mechanics.

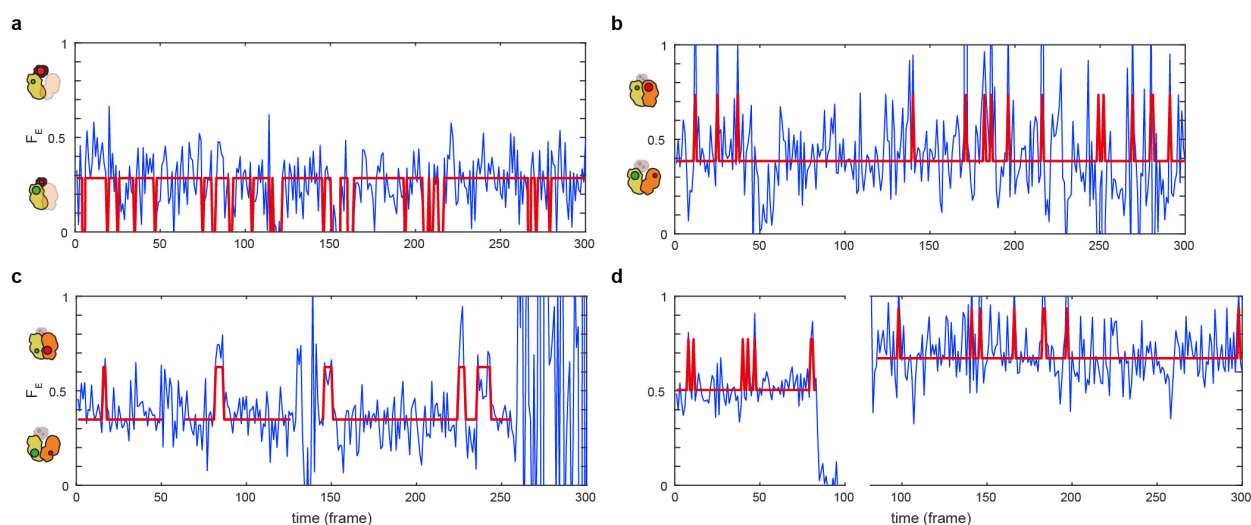


Figure 51 | Dynamic F_E -traces of ABCE1 variants with 40S & AMP-PNP. **a**, FeS-NBD1 variant opened up to F_E values of 0.0 in a reversible manner. **b**, F_E of the NBS I variant spiked to higher values in a dynamic population. **c** and **d**, NBS II variant spiked between two F_E states. P. Höllthaler and I analyzed the data. I designed and supervised these experiments and assembled the figure.

4 Discussion

4.1 How does ABCE1 split the ribosome?

The FeS cluster domain is an ancient prosthetic group involved in various cellular processes (Lill, 2009). In this work, the FeS cluster domain of ABCE1 is described as a mechanical module on an ABC system for dissociation of ribosomal subunits. Despite an extreme displacement from the pre- to the post-splitting state, the structure of the FeS cluster domain of ABCE1 remains essentially unchanged. Hence, the FeS cluster domain serves as a compact and rigid entity. To examine how the transition from the pre- to the post-splitting state may result in subunit dissociation, the potential transition trajectory of the FeS cluster domain was examined from the pre- to the post-splitting state. Based on these findings, ribosome splitting can be divided into two phases (corresponding to the two red arrows in **Figure 52**). In the first phase, the FeS cluster domain is in contact with the C-terminal domain of eRF1 or Pelota located in the A-site (Becker & Franckenberg *et al.*, 2012, Brown & Shao *et al.*, 2015, Preis *et al.*, 2014, Shao & Murray & Brown *et al.*, 2016) and pushes these factors into the intersubunit space upon closure of the two NBDs. The A-site factors, eRF1 or Pelota, likely act as a *molecular wedge* and destabilize intersubunit bridges. In agreement with this idea, the presence of an A-site factor was shown to be essential for splitting activity of ABCE1 (Barthelme *et al.*, 2011, Pisarev *et al.*, 2010, Pisareva & Skabkin *et al.*, 2011, Shoemaker & Green, 2011, van den Elzen *et al.*, 2014). In the second phase, once the A-site factor and the 60S are unlocked, the FeS cluster domain can complete its transition by fully rotating into its new interaction site on the 40S subunit (Kiosze-Becker *et al.*, 2016). In this position, ABCE1 is stabilized by new contacts to the 40S subunit, preventing 60S re-association through steric hindrance. The intersubunit bridge B5, which is formed in 80S ribosomes between the 60S protein uL14 and the 40S rRNA helix h44, would clash with the FeS cluster domain, thus explaining the observed anti-association property of ABCE1 (**Figure 52** and **Figure 23**).

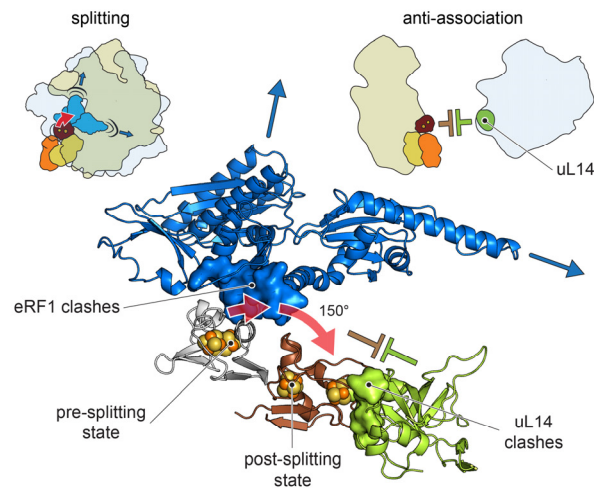


Figure 52 | FeS cluster domain rotation and implications on ribosome splitting. The trajectory of the FeS cluster domain rotation leads to a clash into the C-terminal domain of the A-site factor eRF1 (blue; PDB: 3JAH, Brown & Shao *et al.*, 2015) or Pelota, which is pushed into the intersubunit space. In the post-splitting state, the FeS cluster domain occupies a position that prevents rejoining of the 60S subunit by steric hindrance with uL14 (green; PDB: 3JAH). Clashing residues are shown as surface. I identified the FeS cluster domain clash with uL14. The Beckmann lab verified this observation. I generated the figure. Reprinted with permission (Heuer & Gerovac *et al.*, 2017).

In conclusion, we propose a model for ribosome recycling based on our near-atomistic structure of the post-splitting complex (**Figure 53**). The recycling process is initiated by recognition of ribosomal pre-termination complexes or stalled ribosomes by eRF1–eRF3 or Pelota–Hbs1, respectively, followed by dissociation of the GTPase factor, eRF3 or Hbs1, and binding of ABCE1. ATP binding to the pre-splitting complex and closure of the NBDs pushes the FeS cluster domain towards the A-site factors eRF1 or Pelota, which are in turn forced into the intersubunit space. After splitting, re-association of the 60S and 40S subunits is prevented by the translocated FeS cluster domain now clashing with uL14 of the 60S subunit. ABCE1 remains transiently bound to the 40S subunit, a state that can be trapped *in vitro* and *in vivo* using AMP-PNP.

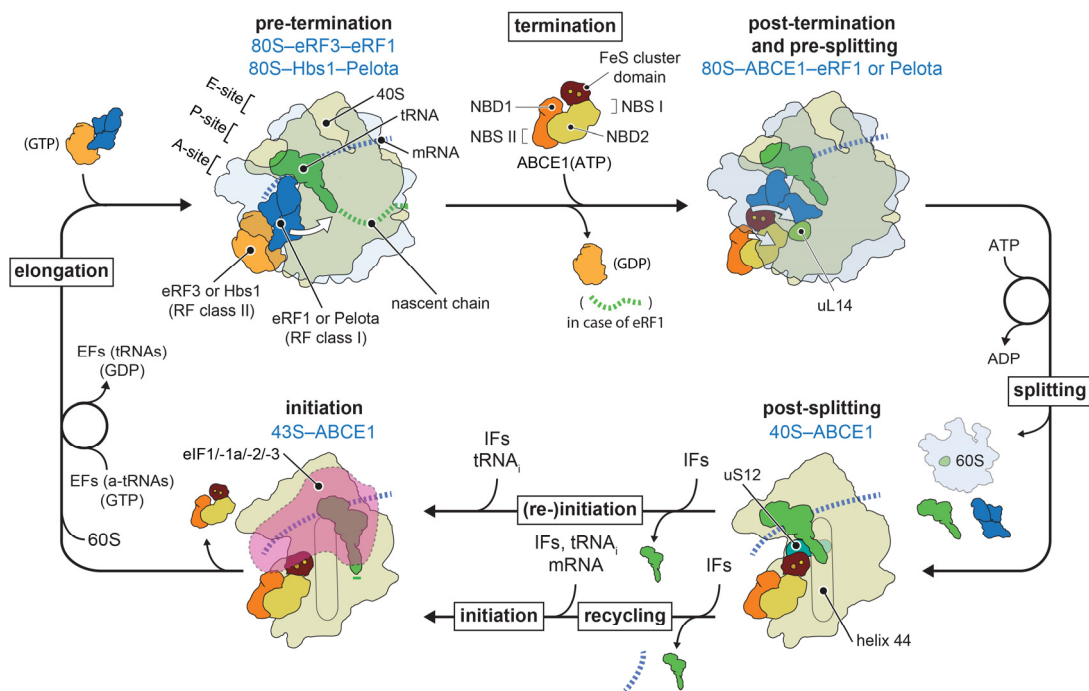


Figure 53 | Model of ribosome recycling. Translating ribosomes in the elongation phase are terminated at a stop-codon when the release factor eRF1 is delivered to the A-site by eRF3. In the *no-go* decay pathway, stalled ribosomes are recognized by Pelota and Hbs1. ABCE1 occupies the 80S termination complex, where it may trigger peptide release. The peptide is illustrated as dashed green line. ABCE1 splits the ribosome in collaboration with eRF1 or Pelota by multiple ATP binding and hydrolysis rounds. In the post splitting state, the FeS cluster domain of ABCE1 is located at helix 44 and may form a platform for (re-)initiation upon interaction with initiation factors in a 43S complex. Alternatively, mRNA (dashed blue line) and tRNA are released by initiation factors, which are responsible for loading of tRNA_i. Objects of this figure were published in (Heuer & Gerovac *et al.*, 2017). Reprinted with permission (Gerovac & Tampé, 2018).

This mechanistic model is in agreement with our *in vitro* and *in vivo* analysis of ABCE1 mutants (**Figure 30** and **Figure 32**), in which substitutions of key interacting residues of the FeS cluster domain impair the formation of a post-splitting complex. Strikingly, in *Drosophila*, mutation of a conserved proline, corresponding to Pro30 in our study, is lethal at larval stage. Our structure suggests that this substitution weakens the interaction of the FeS cluster domain to uS12. In addition, substitutions in hinge 1 and the HLH motif of *Drosophila* ABCE1 result in reduced wing size (Coelho *et al.*, 2005), an effect presumably resulting from impaired 40S subunit interaction. This underlines the importance of the post-splitting state in cellular homeostasis, embryogenesis, and morphogenesis.

The structure of the 40S–ABCE1 post-splitting complex provides an example of an asymmetric twin ABC-type ATPase system in a fully closed, nucleotide-occluded state. Nevertheless, the question remains how termination, recycling, and initiation are connected *via* the ATPase cycle of the two asymmetric NBSs of ABCE1 (Barthelme *et al.*, 2011, Nürnberg-Goloub *et al.*, 2018). Based on existing biochemical data and three structures of ABCE1 in free, pre-splitting, and post-splitting state, we can derive the following working model on the nucleotide hydrolysis cycle. Free ABCE1 has a low intrinsic ATPase and GTPase activity (Barthelme *et al.*, 2011, Pisarev *et al.*, 2010, Shoemaker & Green, 2011), which is strongly stimulated by ATP occlusion in NBS II (Barthelme *et al.*, 2011, Nürnberg-Goloub *et al.*, 2018), and binding to pre-termination complexes containing eRF1 or Dom34/Pelota (Pisarev *et al.*, 2010, Shoemaker & Green, 2011). It is in agreement with other ABC systems (Hopfner, 2016, Rees *et al.*, 2009, Schmitt & Tampé, 2002) that closure of NBDs by ATP occlusion leads to a *power-stroke*, which in the case of ABCE1 is required for ribosome splitting. We speculate that NTP hydrolysis in NBS I might drive ribosome splitting because it is in direct contact with the FeS cluster domain and its ATPase is hyper-stimulated upon ATP occlusion in NBS II. In fact, our structures show that this closed state must exist during the process of ribosome splitting. Nucleoside triphosphate (NTP) hydrolysis of ABCE1 is stimulated in the splitting reactions of class I eRF terminated ribosomes (Pisarev *et al.*, 2010, Shoemaker & Green, 2011). Notably, splitting was blocked by AMP-PNP (**Figure 53**). Hence, at the first view, ribosome splitting appears to be dependent on ATP hydrolysis (Pisarev *et al.*, 2010, Shoemaker & Green, 2011). However, the twin-ATPase occludes two AMP-PNP molecules in the post-splitting state, indicating that ATP binding drives splitting (Heuer & Gerovac *et al.*, 2017). The gap between these observations can be filled with a refined model, which implies several rounds of ATP binding and hydrolysis in NBS I until the final post-splitting state is reached (**Figure 54**). Accordingly, the splitting efficiency may depend on the strength of subunit association being increased by the presence of a peptidyl-tRNA bond (Merrick & Hensold, 2001). The required number of ATP hydrolysis cycles for a splitting round may correlate with the subunit association strength. This hypothesis is based not only on the abolished splitting if peptidyl-tRNA-hydrolysis is circumvented by eRF1(AGQ) (Shoemaker & Green, 2011), but also on the increased NTP hydrolysis rate of ABCE1

whenever post-termination complexes cannot be split by inactive eRF1(AGQ), most likely due to repeated rounds of NTPase in ABCE1 (Pisarev *et al.*, 2010). These effects were observed for the translation of short di- or tetra-peptides (Pisarev *et al.*, 2010, Shoemaker & Green, 2011) and may even be stronger for a fully translated protein. Prospectively, the splitting efficiency is dependent on the stability of subunit association. If splitting is not possible, ABCE1 can occupy stalled ribosomes and may help to mediate binding of yet unidentified interaction partners of defective nascent protein and mRNA decay pathways. For example, stalled translation at the outer mitochondrial membrane recruits Pelota, ABCE1, and NOT4 that ubiquitinates ABCE1 and triggers mitophagy (Wu & Wang *et al.*, 2018). Thus, RNA and protein quality control are linked to organelle quality control.

Major parts of this section were published in (Heuer & Gerovac *et al.*, 2017) and (Gerovac & Tampé, 2018) and are reprinted with permission.

4.2 What is the role of the recycling factor in translation (re-)initiation?

Translation initiation on the small ribosomal subunit requires the recognition of mRNA's start codon (AUG) by initiator tRNA_i and initiation factors (eIFs) (reviewed in Hinnebusch & Lorsch, 2012, Jackson *et al.*, 2010). The 43S pre-initiation complex (40S–eIF1/-1A/-3/-5) is loaded with methionylated tRNA_i by the ternary eIF2(GTP)–tRNA_i complex. The eIF4F multi-protein factor and the poly(A)-binding protein (PABP), both assemble a messenger ribonucleoprotein particle (mRNP) that activates mRNA by a closed loop between the 3'-poly(A) tail and the 5'-7-methylguanosine cap. The 43S pre-initiation complex binds near the 5'-cap of the mRNP and scans the mRNA in 5'-to-3' direction for an AUG start codon. After positioning of the start codon at the P-site by base-pairing with the tRNA_i, the 48S initiation complex is formed. Further, eIF5 triggers GTP hydrolysis in eIF2, which is subsequently released. Initiation factors dissociate and eIF5B(GTP) mediates 60S joining and formation of the 80S initiation complex. The complex is ready to start elongation at the tRNA_i in the P-site.

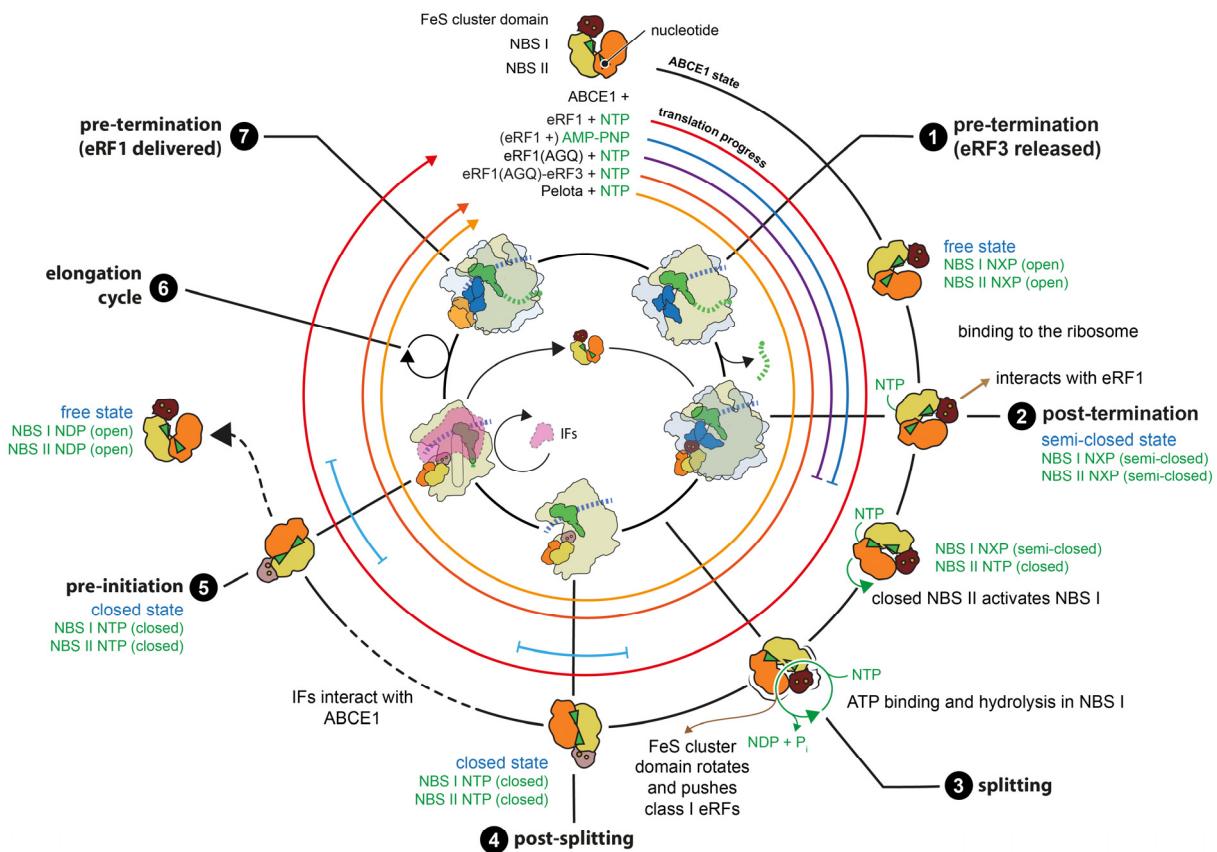


Figure 54 | Mechanochemistry of ABCE1 in ribosome recycling and translational control. The translation progress is indicated by the colored circles for indicated release factors and nucleotides. The conformational and nucleotide-binding states of ABCE1 are indicated in the outer circle (black line). eRF3 is released from the termination complex (1) and ABCE1 is free to bind at the A-site in an ATP-binding dependent fashion, consequently the post-termination state (2) is arrested by AMP-PNP. In addition, peptide release is stimulated by ATP binding in ABCE1. eRF1(AGQ) is impaired in peptidyl-tRNA hydrolysis and post-termination complexes (2) accumulate with bound ABCE1. NBS II in ABCE1 occludes ATP and activates NBS I to bind and hydrolyze ATP until the FeS cluster domain is rotated for 60S release during the splitting step (3). In the post-splitting state (4), the NBDs are closed and occlude two ATPs. Initiation factors bind to the post-splitting complex and form the pre-initiation complex (5), in which ABCE1 is in the closed state with rotated FeS cluster domain. The exact role of ABCE1 in the recruitment of initiation factors and its regulation are unknown and indicated by a dashed line. After a stop-codon in the elongation cycle (6), eRF1 is delivered by eRF3 in the pre-termination state (7). Reprinted with permission (Gerovac & Tampé, 2018).

Each round of mRNA translation is efficiently linked to the next one to ensure rapid regulation of the cycle and energy conservation. On this premise, it is not surprising that

translation factors share recycling and initiation functions, such as eIFs 1/1A/3/3j and Ligatin or MCT-1–DENR, which mediate the release of mRNA and tRNA, and facilitate the formation of the 43S pre-initiation complex (Pisarev *et al.*, 2010, Skabkin & Skabkina *et al.*, 2010). Importantly, at physiological magnesium concentrations, the recycling of mRNA and tRNA by initiation factors requires preceding ribosome splitting by ABCE1, because subunits cannot freely anti-associate (Nierhaus, 2014, Pisarev *et al.*, 2010, Zinoviev *et al.*, 2015). Hence, it is inviting to assume that ABCE1 is closely linked to initiation, because it directly interacts with initiation factors, and catalyzes the high-level formation of pre-initiation complexes (Andersen & Leever, 2007, Chen *et al.*, 2006, Dong *et al.*, 2004). In addition, depletion of ABCE1 affects initiation and consequently the formation of translating 80S ribosomes (Andersen & Leever, 2007). Cryo-EM reconstruction of native pull-outs of ABCE1 with AMP-PNP revealed an 43S pre-initiation complex with bound ABCE1 in the post-splitting state (**Figure 38**, Heuer & Gerovac *et al.*, 2017). The high-resolution cryo-EM structure of the post-splitting complex (Heuer & Gerovac *et al.*, 2017) initiated a re-interpretation of a misassigned low-resolution reconstruction of a 40S–ABCE1–eIF2–tRNA_i density (**Figure 55**, Mancera-Martínez *et al.*, 2017, Simonetti *et al.*, 2016). After start-codon recognition, ABCE1 was found to be part of the late 48S initiation complex along with eIF2 and the eIF3 octamer, but the additional b-g-i module of eIF3 was missing (Mancera-Martínez *et al.*, 2017), which is present in the 48S initiation complex (Llácer & Hussain *et al.*, 2015). Intriguingly, the FeS cluster domain of ABCE1 in the post-splitting state may fit well between the ribosome and the eIF3 b-g-i module in initiation complexes (**Figure 56a**).

In addition, start-codon recognition by eIF2 could be mediated through the FeS cluster domain interaction with helix 44. Notably, the position is exactly at the opposing site of an unusual kink in helix 44 (nucleotide 1650-1660 in yeast). The eIF2 γ domain III transiently binds to this kink in helix 44, which appears distorted in structural studies (Coureux *et al.*, 2016, Shin *et al.*, 2011) (**Figure 56b**). In contrast, a reconstruction of the pre-initiation complex with ABCE1 showed eIF2 γ released from helix 44 and the tRNA_i locked in the P-site (Mancera-Martínez *et al.*, 2017). Hence, the interaction of the FeS cluster domain and eIF2 γ with helix 44, appears mutually exclusive or requires a processive mechanism possibly mediated by a base-switch at the kink in helix 44. Nevertheless, direct interactions of ABCE1

with initiation factors have not been observed in structural studies up to now. Alternatively, ABCE1 could serve as an anti-association timer to ensure a sufficient initiation factor recruitment (Hashem & Frank, 2018, Heuer & Gerovac *et al.*, 2017). The precise interaction of ABCE1 with eIF3 remains unknown but could be key to elucidate the role of ABCE1 in both initiation and recycling, since eIF3 remains loosely bound to the small subunit after initiation, and associates to early terminating ribosomes with ABCE1 (Beznosková & Cuchalová *et al.*, 2013, Mohammad *et al.*, 2017).

In higher eukaryotes, initiation may also take place after a 5'-uORF, which regulates the translation efficiency of the major ORF upon re-initiation. The re-initiation events can occur after short or long uORFs, or within coding regions that are all independently regulated through enhancers or repressors of permissive and non-permissive uORFs (reviewed in Gunišová *et al.*, 2018). After splitting by ABCE1, the mRNA remains bound to 40S and re-initiation can occur at nearby 5'-AUG start codons (Skabkin *et al.*, 2013). The eIF2 ternary complex must deliver the tRNA_i to the P-site and match with an AUG as in canonical initiation. Recently, the re-initiation complex 40S–eIF2D (Ligatin) has been structurally described (Weisser *et al.*, 2017). The complex complements the structure and function of 40S–MCT-1–DENR for mRNA and tRNA recycling, and tRNA_i delivery (Ahmed & Schleich *et al.*, 2018, Lomakin *et al.*, 2017, Schleich *et al.*, 2017, Skabkin & Skabkina *et al.*, 2010). In contrast to MCT-1–DENR, eIF2D comprises an additional WH domain that interacts with helix 44 (Ahmed & Schleich *et al.*, 2018, Lomakin *et al.*, 2017, Schleich *et al.*, 2017, Skabkin & Skabkina *et al.*, 2010). The WH domain would clash with the FeS cluster domain of ABCE1 in the post-splitting state. Hence, these two factors mutually exclude each other in the resolved conformations suggesting two distinct pathways of re-initiation or a systematic mechanism (**Figure 56c**).

mRNA footprints of ORF 3'-ends revealed 40S recycling intermediates that have a *more open* entry channel and were hypothesized to be linked to post-splitting bound ABCE1 *in vivo* (Archer & Shirokikh *et al.*, 2016). The same readouts illuminated after splitting 5'-extended protection relative to the stop codon at 40S subunits. Protection at the 5'-site could be linked to additional occupation by initiation factors and thus indicate the presence of 40S–ABCE1–

eIF complexes that possibly link recycling and re-initiation at the termination and splitting event, as already reported for eIF3 (Mohammad *et al.*, 2017).

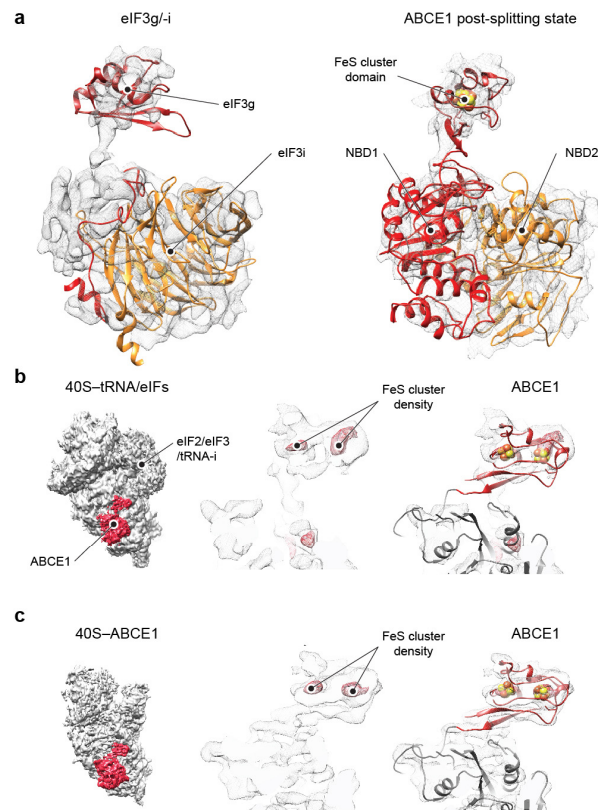


Figure 55 | Cryo-EM structures of the 40S–ABCE1 post-splitting complex and the 48S initiation complex.

a, The isolated density (EMD: 8190, Simonetti *et al.*, 2016) of the 48S initiation complex was attributed to eIF3g (red) and eIF3i (yellow) with fitted models for eIF3g/-i (left; red and yellow; PDB: 5K0Y, Simonetti *et al.*, 2016) and post-splitting ABCE1 (right; NBD1 red, NBD2 orange, FeS cluster domain dark red; PDB: 5LL6, Heuer & Gerovac *et al.*, 2017). **b**, Cryo-EM map of the 48S initiation complex (left; EMD: 8190) and zoom on the isolated density attributed to eIF3g/-i. A model for ABCE1 was fitted into this density (right; FeS cluster domain red, ABC system grey). Notably, strong density for the FeS clusters was visible in this map, which had the strongest electron density at high contour level. **c**, Cryo-EM map of the 40S–ABCE1 post-splitting complex (right; EMD: 4071) and ABCE1 model as above fitted into the isolated ABCE1 density. We concluded that the eIF3g/-i density was misinterpreted and needed to be attributed to ABCE1. T. Becker created the images with density maps. I created the figure in collaboration with T. Becker for pre-submission inquiry in Cell Press, 30th March 2017.

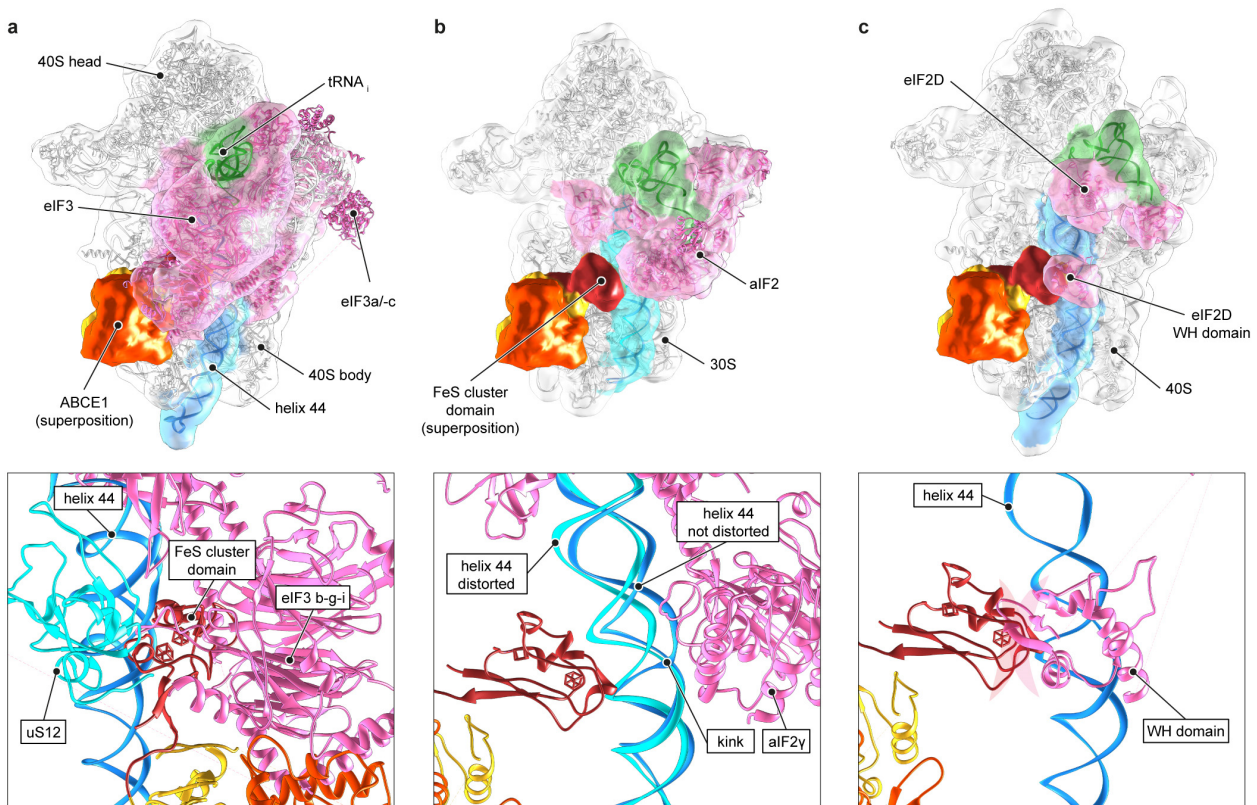


Figure 56 | ABCE1 superposition in initiation and re-initiation complexes. **a**, In superposition, FeS cluster domain of ABCE1 in post-splitting state fits in-between 40S and eIF3 b-g-i subunits (pink, see zoom-in) of the 48S initiation complex (40S–eIF1/-1a/-2/-3, PDB: 3JAP, Llácer & Hussain *et al.*, 2015). tRNA_i is shown in green. Density is Gaussian filtered and shown in transparent. **b**, In initiation, aIF1/-1a/-2 (pink) bind to 30S and the aIF2 γ subunit contacts a distorted helix 44 (cyan) at the opposite site as the FeS cluster domain of ABCE1 interacts with it (PDB: 5JBH, Coureux *et al.*, 2016). For reference, a non-distorted helix 44 from (a) is superpositioned in blue. **c**, In re-initiation, eIF2D (Ligatin, pink) binds to 40S and its WH domain interacts with helix 44 and would clash with the FeS cluster domain of ABCE1 in the post-splitting state indicated by transparent lines (red/pink) (PDB: 5OA3, Weisser *et al.*, 2017). Reprinted with permission (Gerovac & Tampé, 2018).

ABCE1 depletion resulted in re-initiation of post-terminated 80S ribosomes at sense-codons in the 3' untranslated region (Young & Guydosh *et al.*, 2015). Importantly, re-initiation at AUG codons requires preceding ABCE1-driven splitting (Pisarev *et al.*, 2010, Skabkin & Skabkina *et al.*, 2010, Skabkin *et al.*, 2013). Hence, ABCE1 may have an additional role after splitting. Re-initiation may also occur independently of ABCE1 at termination upstream ribosomal binding sites (TURBS), because in this case splitting is mediated by initiation factors (Zinoviev *et al.*, 2015). In addition, post-terminated 80S ribosomes can directly

re-initiate without preceding splitting (Young & Guydosh *et al.*, 2015, Zinoviev *et al.*, 2015). Further studies are needed to reveal the effect of ABCE1 on recycling and re-initiation within specific mRNA populations.

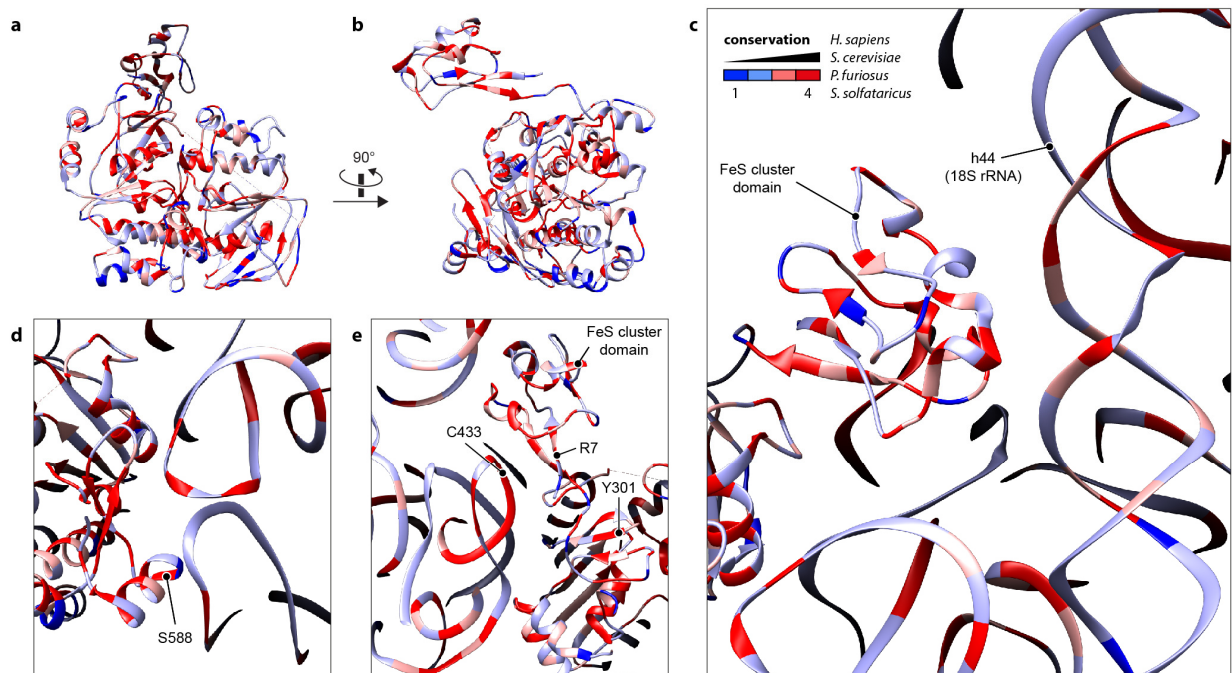


Figure 57 | Conservation of ABCE1 and 18S rRNA in the post-splitting complex. **a** and **b**, show ABCE1 residue conservation and conformation in the post-splitting state. **c-e**, indicate nucleotide conservation of 18S rRNA from yeast. Highest residue conservation according to the here used species is shown in red. The following organisms were used for conservation analysis: *H. sapiens*, *S. cerevisiae*, *P. furiosus*, *S. solfataricus*. Plots were generated with UCSF Chimera.

In summary, all initiation events are orchestrated at helix 44 that is present throughout all living organisms and crucial for translation. In a structural residue conservation analysis, interacting residues become apparent by high conservation that are hardly determinable in a density map at 3.9 Å resolution (**Figure 57**), but agree with observed weak density bridges (**Figure 29**). Importantly, the FeS cluster domain and helix 44 harbor conserved residues and nucleotides (represented in red), respectively, that point towards each other (**Figure 57c**). How the interaction takes place and how it is regulated, remains elusive. Base-pair flip-outs and -ins are known mechanisms that could transmit information from one side of helix 44

to the other, and towards initiation factors, or lead to a bending, elongation, or compression of helix 44. To solve these questions, a higher resolution of these complexes will be necessary.

Major parts of this section were published in (Heuer & Gerovac *et al.*, 2017) and (Gerovac & Tampé, 2018) and are reprinted with permission.

4.3 Conformational dynamics and elastic NBD dimerization

The structural work on ABCE1 sets the scope for conformational re-arrangements of the ABC machinery between the pre- and the post-splitting state. However, the dynamic fashion of conformational switches remains to be elucidated that certainly will reveal a vivid picture of the working mode of ABC systems in general. To enable real-time tracking of conformational switches in ABCE1, we established a smFRET system and validated it by characterization of labeled ABCE1 variants. Relative distance changes of fluorophore probes in the FeS cluster domain to NBD1, and NBS I and II were determined at defined conditions that were supposed to yield shifts towards reported conformational states. The FeS-NBD1 variant showed a 40S and AMP-PNP dependent distance increase that corresponded to a rotation of the FeS cluster domain as previously determined by cryo-EM reconstruction. The other two variants probed for the 40S and AMP-PNP dependent closure of the NBSs and showed an increase in high FRET efficiency populations. As in agreement with previous work, both NBSs closed. We resolved the conformational switches in the variants FeS-NBD1 and NBS I at a time-resolution of 100 ms integration time. For the NBS II variant, we observed faster switches that could be resolved by 50 ms. The faster dynamics of the NBS II compared to site I are possibly necessary for its sensing of the ribosome and control of the ATPase in site I (Barthelme *et al.*, 2011, Nürnberg-Goloub *et al.*, 2018). Optimally, an integration time of <25 ms would be required. Interestingly, a trend in relative conformational population shifts was detectable in line of apo→ADP→ATP→AMP-PNP and present 40S for the NBS closure or the FeS cluster domain rotation. Strikingly, in a major part of traces, we observed FRET efficiency switches with nucleotides only. Accordingly, the ABC-system is opening and closing. Even more astonishing was the observation of conformational switching for the

condition with 40S and AMP-PNP that should be in theory in a locked state. In conclusion, the ABC system is not as static as expected. The observed conformational switching in FRET studies was faster than the reported ATPase indicating a disconnection between ATPase and NBD dimerization. Hence, we propose an *elastic dimerization model* of the NBDs in which the NBDs open and close at high frequency, and defined populations are enriched dependent on available nucleotides and substrate.

Of note, in binding experiments, in general, the samples are prior analysis cooled down and accommodate an energetically favored conformation. smFRET studies allow for real-time detection in a homogeneous assay that includes re-binding and balance of equilibrium at room temperature. Future experiments at higher time-resolution will yield detailed insights in conformational switches, and if there are highly dynamic phases that are interrupted by static periods. To solve these questions the recording times of traces must be increased by stable fluorophores.

In future studies, the here developed *in vivo* stalled RNC based splitting assay (see **section 3.4**) could be used for probing of ABCE1 dynamics in splitting. The open questions are whether the *power-stroke site I* indeed opens and closes in one splitting round several times and how the nucleotides are processed. The setup enables modification of the nascent chain for labeling by other fluorophores. Ribosomal subunits may be in addition labeled and allow for setting of the time point of contact between ABCE1 and the splitting competent ribosome. The extension of information layers in a real-time assay will allow for classification of conformational dynamics and a cleared up view on the complexity of action.

4.4 Impact on ribosome homeostasis and ribosomopathies

Ribosome splitting by ABCE1 regulates the availability of ribosomal subunits, which is crucial for cell homeostasis. In the *ribosome concentration hypothesis*, limiting levels of translating ribosomes cause preferential translation of efficiently initiating mRNAs and lead to disorders in cell homeostasis (Lodish, 1974, Mills & Green, 2017). In the case of inefficient recycling at stop codons, translation continues into the 3' untranslated region, which may evoke the

generation of immunogenic peptides (Guydosh & Green, 2014, Mills *et al.*, 2016, Starck *et al.*, 2012, Young & Guydosh *et al.*, 2015). Surveillance mechanisms, such as nonsense-mediated decay at pre-mature stop codons, discharge into the *no-go* decay pathway due to mRNA cleavage and finally recycling by ABCE1 (Arribere & Fire, 2018, Shoemaker & Green, 2012). The mRNA levels of ABCE1 and Hbs1 are significantly downregulated in brain tissues of Parkinson's disease patients (Wu & Wang *et al.*, 2018). Interestingly, a loss of ABCE1 is complemented by increasing levels of Pelota, as described in primary reticulocytes for hemoglobin production during hematopoiesis (Mills *et al.*, 2016). This indicates alternative recycling pathways by Pelota, which become apparent as physiological disorders upon *Pelota* knockout (Liakath-Ali *et al.*, 2018). Global translation is upregulated and short ribosome footprints accumulate, resulting in abnormal differentiation and hyperproliferation of epidermal stem cells. Undoubtedly, ABCE1 in interplay with release factors plays a crucial role in ribosomopathies, which are associated with translation efficiency and ribosome availability (Mills & Green, 2017).

4.5 Ribosome remodeling by the fungal

ABC-type elongation factor eEF3

In addition to the two canonical elongation factors eEF1A and eEF2, the fungal specific ABC-type elongation factor eEF3 is essential and involved in tRNA release at the E-site (Dasmahapatra & Chakraborty, 1981, Triana-Alonso *et al.*, 1995, Kurata *et al.*, 2013). Interestingly, eEF3 drives ribosome splitting at the E-site (Kurata *et al.*, 2010, Kurata *et al.*, 2013) and antagonizes translational repression by the starvation factor Stm1 (Hayashi *et al.*, 2018). eEF3 and eEF1A can occupy the ribosome at the same time and may coordinate the expulsion of tRNA at the E-site and loading of aminoacylated tRNA at the A-site (Anand *et al.* 2003, Andersen & Becker *et al.* 2006). The N-terminal HEAT and 4-helix bundle domains correspond to the FeS cluster domain in ABCE1 and are similarly linked by long unstructured linker regions that contain in one state a short helix, which can unwind and allow for rotation analogous as in ABCE1. In the presence of AMP-PNP, eEF3 binds to the E-site of an 80S ribosome with a tRNA in the P-site (Andersen & Becker *et al.*, 2006). The NBDs of eEF3 are

dimerized and most likely occlude two ATP as in the post-splitting state of ABCE1 (**Figure 58a,b**).

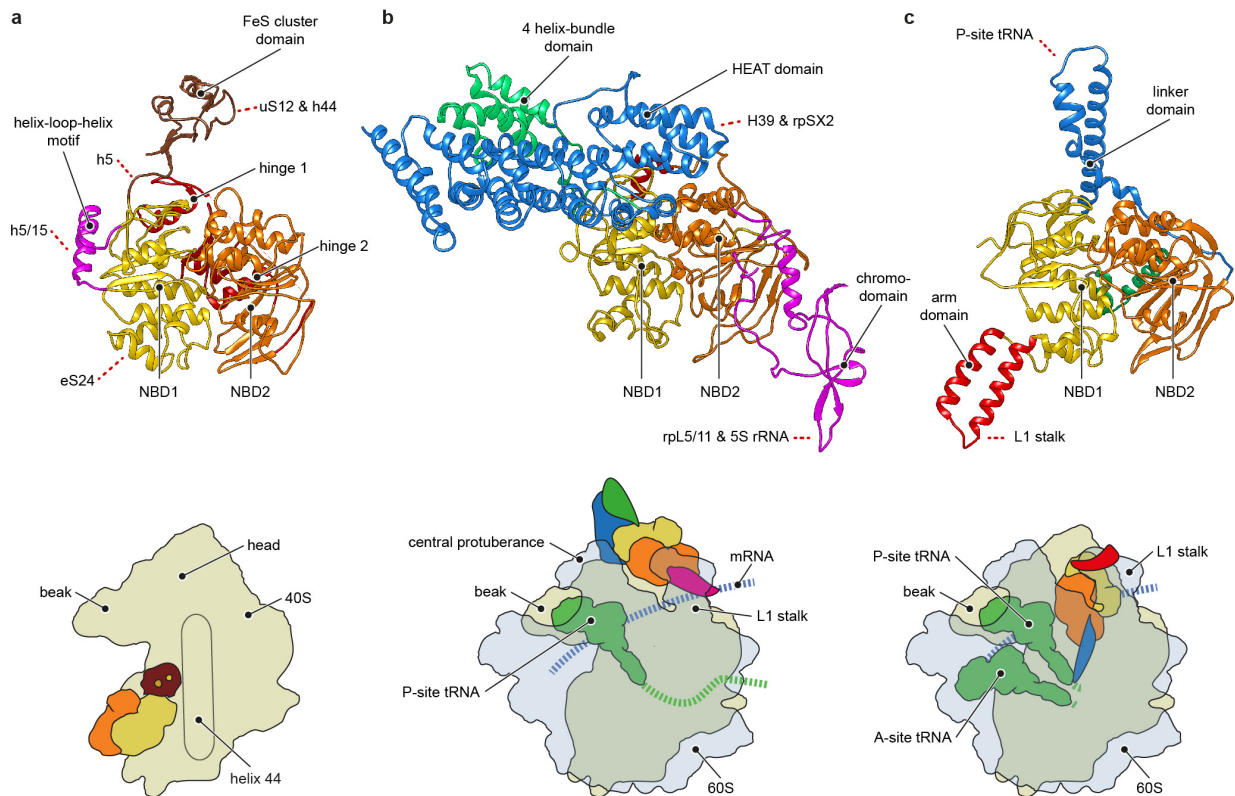


Figure 58 | Closed ABC systems bound to the ribosome. a, ABCE1 (PDB: 5LL6, Heuer & Gerovac *et al.*, 2017) bound to the 40S subunit in a closed conformation with swung-out FeS cluster domain that interacts with helix 44 and uS12. **b**, eEF3 bound to the 80S ribosome (PDB: 2IX8, Andersen & Becker *et al.*, 2006). Chromo domain interacts with rpL5/-11 and 5S rRNA. The HEAT domain interacts with the 40S head rpSX2 and helix 39 of 60S. **c**, Etta (YjJK, ABCF family) bound to the 70S ribosome (PDB: 3J5S, Chen *et al.*, 2014). The linker domain interacts with the P-site tRNA and stabilizes it and the arm domain with the L1 stalk. The ABC systems are shown in similar orientation and in the ATP-occluded state. Reprinted with permission (Gerovac & Tampé, 2018).

The conformational switch of the associated HEAT and chromo domains in the ABC system remains elusive. Compared to X-ray structures (Andersen & Becker *et al.*, 2006), the NBDs must perform a tweezer-like motion that opens up the ABC system and the ribosomal E-site upon ATP hydrolysis, followed by ribosome splitting (Kurata *et al.*, 2013). In line with the role

of ABCE1 in splitting of hibernating 80S–Stm1 ribosomes, eEF3 antagonizes translation repression by Stm1 (Hayashi *et al.*, 2018). Remarkably, the ABC system is in the closed state when bound to 80S and splits the subunits after ATP hydrolysis and release (Yang *et al.*, 1996). This indicates a *modus operandi* different from ABCE1, which is in a closed state after splitting. Apart from splitting, eEF3 triggers the release of deacylated-tRNA and mRNA (Kurata *et al.*, 2010, Kurata *et al.*, 2013). After mRNA release, no re-initiation on the same mRNA is possible, whereas, after splitting by ABCE1, mRNA remains bound to 40S, allowing for re-initiation. This section was reprinted with permission from (Gerovac & Tampé, 2018).

4.6 Antibiotic resistance and translational control

Multidrug-resistance mediated by ABC proteins is of key medical relevance for anti-cancer therapies and for treatments against pathogens. The largest group comprises ABC transporters that expel drugs and toxins out of the cell by the associated transmembrane domains (Rees *et al.*, 2009, Thomas & Tampé, 2018). The ribosome is the major target for clinically relevant drugs (Arenz & Wilson, 2016). Strikingly, ABC proteins of the F subfamily displace drugs from bacterial ribosomes (Sharkey *et al.*, 2016). In the working model, ABCF proteins bind to the ribosomal E-site, as structurally elucidated for the *E. coli* ortholog Etta (Yjjk). Etta is built up by two NBD protomers with additional arm and linker domains, which interact with L1 and the P-site tRNA, respectively. Etta binds in an ATP-dependent manner to the ribosome as a NBD dimer in a closed conformation (**Figure 58c**, Chen *et al.*, 2014). Substitution of the catalytic glutamate arrests translation *in vivo* after initiation complex formation and translation of the first peptide bond (Boël *et al.*, 2014). Etta blocks translation progression into the elongation cycle by occupying the E-site, which was validated by a lack of tripeptide formation and polysome loss after induction of a catalytically inactive variant. The arrest was related to sensing of the low-energetic state at starvation by Etta. When energy levels in the cell return, Etta facilitated the re-start of cell growth (Boël *et al.*, 2014). Importantly, the linker domain is essential for 70S binding and, together with the arm domain, stabilizes the outward position of the L1 stalk allowing ejection of the E-site tRNA (Frank *et al.*, 2007). However, the link between the ATPase cycle of Etta and the

conformational switches of the associated domains leading to tRNA interaction is still unclear. These aspects are directly connected to the antibiotic resistance mechanism of ABCF proteins. A number of antibiotics target the peptidyl-transferase center and inactivate its transpeptidase reaction. Recently, the ABCF protein VgaA was reported to reset peptidyl-transferase activity after antibiotic treatment that was followed by restored puromycin reactivity, which mimics an aminoacyl-tRNA and prematurely terminates translation by puromylation of the nascent chain (Murina *et al.*, 2018). Importantly, an ATPase silenced variant did not restore the peptidyl-transferase activity but rather inhibited it independently of antibiotic presence. This observation indicates that ATP hydrolysis is the trigger for VgaA release. The ABCF protein and macrolide resistance factor MsrE utilizes the same mechanism for the streptotagmin B drug class displacement (Su & Kumar & Ding *et al.*, 2018). In its ATP-bound form, MsrE positions an extended loop that corresponds to the linker domain of Etta in the peptidyl-transferase center. The loop shifts the P-site tRNA position and bends its acceptor stem towards the A-site. Subsequently, the drug is released. VmlR is a resistance factor for the streptotagmin A antibiotics class and binds in a similar conformation to the 70S ribosome for drug displacement (Crowe-McAuliffe *et al.*, 2018). It differs to MsrE and Etta by an additional C-terminal extension that interacts with the small ribosomal subunit at its Shine-Dalgarno cavity. It is still pending whether the length of nascent peptide influences drug displacement by ABCF proteins and if the translation continues after resetting.

This section was reprinted with permission from (Gerovac & Tampé, 2018).

4.7 Outlook

Translation is tightly controlled at all stages and crucial for quality control of nascent polypeptide chain and mRNA. ABCE1 bridges translation initiation, termination, and splitting by representing a structural and functional linker (Heuer & Gerovac *et al.*, 2017, Schuller & Green, 2017, Mancera-Martínez *et al.*, 2017, Hashem & Frank, 2018). Remarkably, the nature of ABCE1's interaction is transient and must apply for various situations, which are solved by introduction of auxiliary factors, such as eRF1 and Pelota in the case of termination and mRNA surveillance, respectively. Moreover, an intra-molecular communication between the

two asymmetric NBSs may trigger diverse events in the recycling process that are mediated by ABCE1 (Barthelme *et al.*, 2011, Nürnberg-Goloub *et al.*, 2018). In addition, ABCF proteins, including eEF3, show distinct modes of chemo-mechanical action at the ribosome. The interaction between ABCE1 and various partners in translation initiation, *e.g.* eIF1/-1a/-2γ/-3, eIF2D/Listerin or MCT-1-DENR, is enigmatic and may depend on specific mRNAs and initiation pathways. In accordance with the *specialized ribosome hypothesis*, physiological disorders based on ribosomopathies may only be visualized in a subset of translating ribosomes or in physiological disorders in specific tissue (Mills & Green, 2017, Wu & Wang *et al.*, 2018, Xue & Barna, 2012). Furthermore, specific states and interactions may be populated only shortly, or will only be discernable by an acceleration in kinetic studies upon addition of ABCE1; but could cause disorders in sensitive processes such as embryogenesis and morphogenesis, as shown for ABCE1 mutants in *D. melanogaster*, and *C. elegans* (Coelho *et al.*, 2005, Zhao *et al.*, 2004, and others as reviewed in Navarro-Quiles *et al.*, 2018), or selective autophagy of organelles (Wu & Wang *et al.*, 2018).

ABCF proteins modulate ribosome-associated kinases (GCN20, Vazquez de Aldana *et al.*, 1995), influence ribosome biogenesis (Arb1, Dong *et al.*, 2005), or promote translation initiation (ABC50, Tyzack *et al.*, 2000), for review see (Murina & Kasari *et al.*, 2017). The diversity of functions driven by ABC-type systems is built on the nucleotide-based control of associated domains. Without doubt, we are just beginning to understand how these sophisticated molecular machines are constructed, how they allosterically couple modular domains to the dimerization of the NBDs, and how they control the recruitment and release of interaction partners in many fundamental processes. In future studies, trapping of transition states will be the key challenge for understanding of the inner mechanics of ABC systems.

This section was reprinted with permission from (Gerovac & Tampé, 2018).

5 Acknowledgements

I thank my supervisor Robert Tampé for the opportunity to accomplish my PhD thesis in his lab. He constantly challenged and promoted me in respect to scientific and soft skills by guiding me in my studies, encouraging me to visit conferences, present my work, apply for fellowships, and to write publications. I had great freedom and support in the selection of my research topics, execution of experiments, and collaboration with others. Mostly, I enjoyed the open and detailed discussions that were very welcome in our seminars and fundamental for my development as a critical scientist.

I thank my colleagues in the ABCE1/RNA group Elina Nürenberg-Goloub, Kristin Kiosze-Becker, Simon Trowitzsch, Umar Jan, Bianca Hetzert, and Holger Heinemann, who supported my work by collaboration in the lab, and knowledge exchange in the seminars. I thank Thomas Reichhart for taking the challenge as a bachelor student at my supervision. A special thank earns Philipp Höllthaler, together we set up smFRET studies on ABCE1 and a completely new project in an internal collaboration, and his student Robin Kleebach for analysis of the data. I thank Peter Kötter and his assistant Stefanie Lamberth for helping me with yeast genetics, tetrad analysis, experience, interesting discussions, strains, and plasmids. I greatly acknowledge Roland Beckmann, Thomas Becker, André Heuer, Anne Preis, Christian Schmidt, and Otto Berninghausen, who were my major collaborators in our cryo-EM studies at the Gene Center and the Ludwig-Maximilians University in Munich for the reconstruction of the ABCE1–ribosome complexes. The work in Munich was in addition financially supported by FOR1805 – *Ribosome dynamics in regulation of speed and accuracy of translation* (to R.B.). I thank Rachel Green (JHMI, HHMI, Baltimore) for the warm welcome in her lab as a visiting student, constant support in my thesis, and at conferences. At front, Anthony Schuller who supervised me, and Nick Guydosh, Allen Buskirk, Kristin Smith-Koutmou, Chris Woolstenhulme, Colin Wu, Jae Yeon Hwang, and Julie Brunelle and Elizabeth Rogers for technical assistance.

I thank my thesis committee in person of Robert Tampé, Peter Kötter, and Martin Hengesbach. I thank our staff and my lab colleagues who stood by for questions, material and support: Rupert Abele, Stefan Brüchert, Alina Klein, Markus Braner, Volker and Karl

Gatterdam, Andreas Hinz, Franz Tumulka, Christoph Bock, Christoph Thomas, Michael Urban, Andrés Arriagada, Andreas Brees, Sunesh Sethumandavan, Tim Diederichs, Susanne Hank, Valentina Herbring, Eike Jöst, Phillipp Grab, Nicole Koller, Maryna Diskowski, Dorith Wunnicke, Heike Krüger, Ines Katharina Müller, Ralph Wienecke, Roger Draheim, Robert Ernst, Peter Mayerhofer, Gerda Fleischmann, Irina Jan, Noemi Laboria, Alexander Kleefen, Anne Nöll, Tina Zollmann. I thank Kerstin Zehl, Renate Guntrum, and Gerhard Spatz-Kümbel for the lab management. Christine Le-Gal, Andrea Pott, and Inga Nold for smooth and efficient handling of my applications in the office, and proofreading of our manuscripts.

I thank Harald Schwalbe, Michaela Müller-McNicoll, Ulrich Göringer, and Beatrix Süß, and for administration Marco Betz and Anna Wacker, from the CRC902 – *Molecular Principles of RNA-based Regulation* (to R.T.) for financial support of my work, the organization of winter schools, seminars, and a lot more. I acknowledge the Goethe University, the Ludwig-Maximilians University, the Gene Center Munich, and the Johns Hopkins Medical Institutions for the excellent scientific environment. I also thank the CRC807 – *Molecular Understanding of Transmembrane Processes* (to R.T.) and the Cluster of Excellence Frankfurt – *Macromolecular Complexes* (to R.T.) for financial support of the microscope setup for the smFRET studies. Obviously, I thank the Deutsche Forschungsgemeinschaft (DFG) for funding.

I thank the Boehringer Ingelheim Fonds for financial support of my work by a PhD fellowship. I thank the Studienstiftung des deutschen Volkes for a fellowship, and the Cluster for Membrane Proteomics for a fellowship in the beginning of my studies.

Finally and most important, I thank my family for financial and mental support, and encouraging words outside of the lab.



6 References

- Acker MG, Kolitz SE, Mitchell SF, Nanda JS, Lorsch JR (2007) Reconstitution of yeast translation initiation. *Methods Enzymol* 430: 111-45
- Adams PD, Afonine PV, Bunkoczi G, Chen VB, Davis IW, Echols N, Headd JJ, Hung LW, Kapral GJ, Grosse-Kunstleve RW, McCoy AJ, Moriarty NW, Oeffner R, Read RJ, Richardson DC, Richardson JS, Terwilliger TC, Zwart PH (2010) PHENIX: a comprehensive Python-based system for macromolecular structure solution. *Acta Crystallogr D Biol Crystallogr* 66: 213-21
- Ahmed YL & Schleich S, Bohlen J, Mandel N, Simon B, Sinning I & Teleman AA (2018) DENR–MCTS1 heterodimerization and tRNA recruitment are required for translation reinitiation. *PLoS Biol* 16: e2005160
- Alhebshi A, Sideri TC, Holland SL, Avery SV (2012) The essential iron-sulfur protein Rli1 is an important target accounting for inhibition of cell growth by reactive oxygen species. *Mol Biol Cell* 23: 3582-90
- Alkalaeva EZ & Pisarev AV, Frolova LY, Kisselev LL & Pestova TV (2006) *In vitro* reconstitution of eukaryotic translation reveals cooperativity between release factors eRF1 and eRF3. *Cell* 125: 1125-36
- Amunts A & Brown A & Bai XC & Ll acer JL, Hussain T, Emsley P, Long F, Murshudov G, Scheres SH & Ramakrishnan V (2014) Structure of the yeast mitochondrial large ribosomal subunit. *Science* 343: 1485-9
- Anand M, Chakraborty K, Marton MJ, Hinnebusch AG, Kinzy TG (2003) Functional interactions between yeast translation eukaryotic elongation factor (eEF) 1A and eEF3. *J Biol Chem* 278: 6985-91
- Andersen CB & Becker T, Blau M, Anand M, Halic M, Balar B, Mielke T, Boesen T, Pedersen JS, Spahn CM, Kinzy TG, Andersen GR & Beckmann R (2006) Structure of eEF3 and the mechanism of transfer RNA release from the E-site. *Nature* 443: 663-8
- Andersen DS, Leever SJ (2007) The essential *Drosophila* ATP-binding cassette domain protein, Pixie, binds the 40 S Ribosome in an ATP-dependent manner and is required for translation initiation. *J Biol Chem* 282: 14752-60
- Archer SK & Shirokikh NE, Beilharz TH, Preiss T (2016) Dynamics of ribosome scanning and recycling revealed by translation complex profiling. *Nature* 535: 570-4
- Arenz S, Wilson DN (2016) Bacterial protein synthesis as a target for antibiotic inhibition. *Cold Spring Harb Perspect Med* 6: a025361
- Armache JP & Anger AM, M arquez V, Franckenberg S, Fr ohlich T, Villa E, Berninghausen O, Thomm M, Arnold GJ, Beckmann R & Wilson DN (2013) Promiscuous behaviour of archaeal ribosomal proteins: Implications for eukaryotic ribosome evolution. *Nucleic Acids Res* 41: 1284-93
- Arribere JA, Fire AZ (2018) Nonsense mRNA suppression via nonstop decay. *eLife* 7:e33292

Artimo P & Jonnalagedda M, Arnold K, Baratin D, Csardi G, de Castro E, Duvaud S, Flegel V, Fortier A, Gasteiger E, Grosdidier A, Hernandez C, Ioannidis V, Kuznetsov D, Liechti R, Moretti S, Mostaguir K, Redaschi N, Rossier G, Xenarios I *et al.* (2012) ExpASY: SIB bioinformatics resource portal. *Nucleic Acids Res* 40: W597-603

Aylett CHS, Boehringer D, Erzberger JP, Schaefer T, Ban N (2015) Structure of a Yeast 40S–eIF1–eIF1A–eIF3–eIF3j initiation complex. *Nat Struct Mol Biol* 22: 269-71

Barthelme D (2010) The power to dissociate – Molecular function of the twin-ATPase ABCE1 in archaeal ribosome recycling. PhD thesis, Johann Wolfgang Goethe-University Frankfurt am Main

Barthelme D, Dinkelaker S, Albers SV, Londei P, Ermler U, Tampé R (2011) Ribosome recycling depends on a mechanistic link between the FeS cluster domain and a conformational switch of the twin-ATPase ABCE1. *Proc Natl Acad Sci U S A* 108: 3228-33

Barthelme D, Scheele U, Dinkelaker S, Janoschka A, Macmillan F, Albers SV, Driessen AJ, Stagni MS, Bill E, Meyer-Klaucke W, Schunemann V, Tampé R (2007) Structural organization of essential iron-sulfur clusters in the evolutionarily highly conserved ATP-binding cassette protein ABCE1. *J Biol Chem* 282: 14598-607

Becker T, Armache JP, Jarasch A, Anger AM, Villa E, Sieber H, Motaal BA, Mielke T, Berninghausen O, Beckmann R (2011) Structure of the no-go mRNA decay complex Dom34-Hbs1 bound to a stalled 80S ribosome. *Nat Struct Mol Biol* 18: 715-20

Becker T & Franckenberg S, Wickles S, Shoemaker CJ, Anger AM, Armache JP, Sieber H, Ungewickell C, Berninghausen O, Daberkow I, Karcher A, Thomm M, Hopfner KP, Green R, Beckmann R (2012) Structural basis of highly conserved ribosome recycling in eukaryotes and archaea. *Nature* 482: 501-6

Behrmann E & Loerke J, Budkevich TV, Yamamoto K, Schmidt A, Penczek PA, Vos MR, Burger J, Mielke T, Scheerer P, Spahn CM (2015) Structural snapshots of actively translating human ribosomes. *Cell* 161: 845-57

Ben-Shem A & Garreau de Loubresse N & Melnikov S, Jenner L, Yusupova G, Yusupov M (2011) The structure of the eukaryotic ribosome at 3.0 Å resolution. *Science* 334: 1524-9

Berman HM, Westbrook J, Feng Z, Gilliland G, Bhat TN, Weissig H, Shindyalov IN, Bourne PE (2000) The protein data bank. *Nucleic Acids Res* 28: 235-42

Bertram G, Bell HA, Ritchie DW, Fullerton G, Stansfield I (2000) Terminating eukaryote translation: domain 1 of release factor eRF1 functions in stop codon recognition. *RNA* 6: 1236-47

Beznosková P & Cuchalová L, Wagner S, Shoemaker CJ, Gunišová S, von der Haar T, Valášek LS (2013) Translation initiation factors eIF3 and HCR1 control translation termination and stop codon read-through in yeast cells. *PLoS Genet* 9: e1003962

Bisbal C, Martinand C, Silhol M, Lebleu B, Salehzada T (1995) Cloning and characterization of a RNase L inhibitor. A new component of the interferon-regulated 2-5A pathway. *J Biol Chem* 270: 13308-17

Blanco M, Walter NG (2010) Analysis of complex single molecule FRET time trajectories. *Methods Enzymol* 472: 153-78

Boël G, Smith PC, Ning W, Englander MT, Chen B, Hashem Y, Testa AJ, Fischer JJ, Wieden HJ, Frank J, Gonzalez RL Jr. & Hunt JF (2014) The ABC-F protein EttA gates ribosome entry into the translation elongation cycle. *Nat Struct Mol Biol* 21: 143-51

Brown A, Long F, Nicholls RA, Toots J, Emsley P, Murshudov G (2015) Tools for macromolecular model building and refinement into electron cryo-microscopy reconstructions. *Acta Crystallogr D Biol Crystallogr* 71: 136-53

Brown A & Shao S, Murray J, Hegde RS & Ramakrishnan V (2015) Structural basis for stop codon recognition in eukaryotes. *Nature* 524: 493-6

Cabrita LD, Hsu ST, Launay H, Dobson CM & Christodoulou J (2009) Probing ribosome-nascent chain complexes produced in vivo by NMR spectroscopy. *Proc Natl Acad Sci U S A* 106: 22239-44

Carr-Schmid A, Pfund C, Craig EA, Kinzy TG (2002) Novel G-protein complex whose requirement is linked to the translational status of the cell. *Mol Cell Biol* 22: 2564-74

Cassaignau AM & Launay HM, Karyadi ME, Wang X, Waudby CA, Deckert A, Robertson AL, Christodoulou J & Cabrita LD (2016) A strategy for co-translational folding studies of ribosome-bound nascent chain complexes using NMR spectroscopy. *Nat Protoc* 11: 1492-507

Chan PP, Lowe TM (2016) GtRNADB 2.0: an expanded database of transfer RNA genes identified in complete and draft genomes. *Nucleic Acids Res* 44: D184-9

Chandradoss SD, Haagsma AC, Lee YK, Hwang JH, Nam JM, Joo C (2014) Surface passivation for single-molecule protein studies. *J Vis Exp* 86: e50549

Chen B, Boël G & Hashem Y, Ning W, Fei J, Wang C, Gonzalez RL Jr. & Hunt JF & Frank J (2014) EttA regulates translation by binding the ribosomal E site and restricting ribosome-tRNA dynamics. *Nat Struct Mol Biol* 21: 152-9

Chen J, Lu G, Lin J, Davidson AL, Quijcho FA (2003) A tweezers-like motion of the ATP-binding cassette dimer in an ABC transport cycle. *Mol Cell* 12: 651-61

Chen JZ, Grigorieff N (2007) SIGNATURE: A single-particle selection system for molecular electron microscopy. *J Struct Biol* 157: 168-73

Chen VB, Arendall WB, 3rd, Headd JJ, Keedy DA, Immormino RM, Kapral GJ, Murray LW, Richardson JS, Richardson DC (2010) *MolProbity*: all-atom structure validation for macromolecular crystallography. *Acta Crystallogr D Biol Crystallogr* 66: 12-21

Chen ZQ, Dong J, Ishimura A, Daar I, Hinnebusch AG, Dean M (2006) The essential vertebrate ABCE1 protein interacts with eukaryotic initiation factors. *J Biol Chem* 281: 7452-7

Chudaev M, Poruri K, Goldman E, Jakubowski H, Jain MR, Chen W, Li H, Tyagi S, Mandeck W (2013) Design and properties of efficient tRNA:EF-Tu FRET system for studies of ribosomal translation. *Protein Eng Des Sel* 26: 347-57

Cleland WW (1964) Dithiothreitol, a new protective reagent for SH groups. *Biochemistry* 3: 480-2

Coelho CM, Kolevski B, Bunn C, Walker C, Dahanukar A, Leever SJ (2005) Growth and cell survival are unevenly impaired in pixie mutant wing discs. *Development* 132: 5411-24

Coureur PD, Lazennec-Schurdevin C, Monestier A, Larquet E, Cladiere L, Klaholz BP, Schmitt E & Mechulam Y (2016) Cryo-EM study of start codon selection during archaeal translation initiation. *Nat Commun* 7: 13366

Coyle SM, Gilbert WV, Doudna JA (2009) Direct link between RACK1 function and localization at the ribosome *in vivo*. *Mol Cell Biol* 29: 1626-34

Crowe-McAuliffe C., Graf M., Huter P., Takada H., Abdelshahid M., Nováček J., Murina V., Atkinson G.C., Haurlyuk V., Wilson D.N. (2018). Structural basis for antibiotic resistance mediated by the *Bacillus subtilis* ABCF ATPase VmlR. *Proc Natl Acad Sci U S A* 115: 8978-83

Dasmahapatra B, Chakraburty K (1981) Protein synthesis in yeast. I. Purification and properties of elongation factor 3 from *Saccharomyces cerevisiae*. *J Biol Chem* 256: 9999-10004

des Georges A, Hashem Y, Unbehaun A, Grassucci RA, Taylor D, Hellen CUT, Pestova TV & Frank J (2014) Structure of the mammalian ribosomal pre-termination complex associated with eRF1·eRF3·GDPNP. *Nucleic Acids Res* 42: 3409-18

Doma MK, Parker R (2006) Endonucleolytic cleavage of eukaryotic mRNAs with stalls in translation elongation. *Nature* 440: 561-4

Dong J, Lai R, Jennings JL, Link AJ, Hinnebusch AG (2005) The novel ATP-binding cassette protein ARB1 is a shuttling factor that stimulates 40S and 60S ribosome biogenesis. *Mol Cell Biol* 25: 9859-73

Dong J, Lai R, Nielsen K, Fekete CA, Qiu H, Hinnebusch AG (2004) The essential ATP-binding cassette protein RLI1 functions in translation by promoting preinitiation complex assembly. *J Biol Chem* 279: 42157-68

Drappier M, Michiels T (2015) Inhibition of the OAS/RNase L pathway by viruses. *Curr Opin Virol* 15: 19-26

Dunham M, Gartenberg M, Brown GW (2015) *Methods in Yeast Genetics and Genomics, 2015 Edition: A CSHL Course Manual*. Cold Spring Harbor Laboratory Press, New York, USA

Dyla M & Terry DS, Kjaergaard M, Sørensen TL, Lauwring Andersen J, Andersen JP, Rohde Knudsen C, Altman RB, Nissen P & Blanchard SC (2017). Dynamics of P-type ATPase transport revealed by single-molecule FRET. *Nature* 551: 346-51

Emsley P, Cowtan K (2004) Coot: model-building tools for molecular graphics. *Acta Crystallogr D Biol Crystallogr* 60: 2126-32

Eyler DE, Green R (2011) Distinct response of yeast ribosomes to a miscoding event during translation. *RNA* 17: 925-32

- Fernández IS & Bai XC, Hussain T, Kelley AC, Lorsch JR & Ramakrishnan V & Scheres SH (2013) Molecular architecture of a eukaryotic translational initiation complex. *Science* 342: 1240585
- Fernández IS, Bai XC, Murshudov G, Scheres SH, Ramakrishnan V (2014) Initiation of translation by cricket paralysis virus IRES requires its translocation in the Ribosome. *Cell* 157: 823-31
- Förster Th (1948) Zwischenmolekulare Energiewanderung und Fluoreszenz. *Ann Phys* 437: 55-75
- Franckenberg S, Becker T & Beckmann R (2012) Structural view on recycling of archaeal and eukaryotic ribosomes after canonical termination and ribosome rescue. *Curr Opin Struct Biol* 22: 786-96
- Frank J, Gao H, Sengupta J, Gao N, Taylor DJ (2007) The process of mRNA-tRNA translocation. *Proc Natl Acad Sci U S A* 104: 19671-8
- Frischmeyer PA, van Hoof A, O'Donnell K, Guerrerio AL, Parker R, Dietz HC (2002) An mRNA surveillance mechanism that eliminates transcripts lacking termination codons. *Science* 295: 2258-61
- Frolova L, Le Goff X, Zhouravleva G, Davydova E, Philippe M, Kisselev L (1996) Eukaryotic polypeptide chain release factor eRF3 is an eRF1- and ribosome-dependent guanosine triphosphatase. *RNA* 2: 334-41
- Frolova L & Seit-Nebi A, Kisselev L (2002) Highly conserved NIKS tetrapeptide is functionally essential in eukaryotic translation termination factor eRF1. *RNA* 8: 129-36
- Frolova LY, Tsivkovskii RY, Sivolobova GF, Oparina NY, Serpinsky OI, Blinov VM, Tatkov SI, Kisselev LL (1999) Mutations in the highly conserved GGQ motif of class 1 polypeptide release factors abolish ability of human eRF1 to trigger peptidyl-tRNA hydrolysis. *RNA* 5: 1014-20
- Gartmann M, Blau M, Armache JP, Mielke T, Topf M, Beckmann R (2010) Mechanism of eIF6-mediated inhibition of ribosomal subunit joining. *J Biol Chem* 285: 14848-51
- Gerovac M, Tampé R (2018) Control of mRNA translation by versatile ATP-driven machines. *Trends Biochem Sci, in press*
- Gerstein AS (2002) *Nucleotides, Oligonucleotides, and Polynucleotides*. In *Molecular Biology Problem Solver*, Gerstein AS (ed), p. 267-89, John Wiley-Liss Inc., New Jersey, USA
- Gietz RD, Schiestl RH (2007) High-efficiency yeast transformation using the LiAc/SS carrier DNA/PEG method. *Nat Protoc* 2: 31-4
- Graille M, Chaillet M, van Tilbeurgh H (2008) Structure of yeast Dom34: a protein related to translation termination factor eRF1 and involved in no-go decay. *J Biol Chem* 283: 7145-54
- Green MR, Sambrook J (2012) *Molecular Cloning - A Laboratory Manual - 4th ed.* Inglis J (ed), Cold Spring Harbor Laboratory Press, New York, USA

- Groft CM, Beckmann R, Sali A, Burley SK (2000) Crystal structures of ribosome anti-association factor IF6. *Nat Struct Biol* 7: 1156-64
- Gunišová S, Hronová V, Mohammad MP, Hinnebusch AG, Valášek LS (2018) Please do not recycle! Translation reinitiation in microbes and higher eukaryotes. *FEMS Microbiol Rev* 42: 165-92
- Guydosh NR, Green R (2014) Dom34 rescues ribosomes in 3' untranslated regions. *Cell* 156: 950-62
- Haseloff J, Gerlach WL (1988) Simple RNA enzymes with new and highly specific endoribonuclease activities. *Nature* 334: 585-91
- Hashem Y & Frank J (2018) The jigsaw puzzle of mRNA translation initiation in eukaryotes: a decade of structures unraveling the mechanics of the process. *Annu Rev Biophys* 47: 125-51
- Hayashi H, Nagai R, Abe T, Wada M, Ito K, Takeuchi-Tomita N (2018) Tight interaction of eEF2 in the presence of Stm1 on ribosome. *J Biochem* 163: 177-85
- Heuer A & Gerovac M, Schmidt C, Trowitzsch S, Preis A, Kötter P, Berninghausen O, Becker T, Beckmann R & Tampé R (2017) Structure of the 40S-ABCE1 post-splitting complex in ribosome recycling and translation initiation. *Nat Struct Mol Biol* 24: 453-60
- Hiekel A (2007) Investigation of the Sec61 complex's oligomere binding state on the 80S ribosome complex. Master thesis, Ludwig-Maximilians-University Munich
- Hilal T, Yamamoto H, Loerke J, Burger J, Mielke T, Spahn CM (2016) Structural insights into ribosomal rescue by Dom34 and Hbs1 at near-atomic resolution. *Nat Commun* 7: 13521
- Hinnebusch AG & Lorsch JR (2012) The mechanism of eukaryotic translation initiation: new insights and challenges. *Cold Spring Harb Perspect Biol* 4: a011544
- Hohlbein J, Craggs TD, Cordes T (2014) Alternating-laser excitation: single-molecule FRET and beyond. *Chem Soc Rev* 43: 1156-71
- Höllthaler P (2015) Establishing Single-Molecule Förster Resonance Energy Transfer Studies of MsbA. Master thesis, Johann Wolfgang Goethe-University Frankfurt am Main
- Hopfner KP (2016) Architectures and mechanisms of ATP binding cassette proteins. *Biopolymers* 105: 492-504
- Hosoda N, Kobayashi T, Uchida N, Funakoshi Y, Kikuchi Y, Hoshino S, Katada T (2003) Translation termination factor eRF3 mediates mRNA decay through the regulation of deadenylation. *J Biol Chem* 278: 38287-91
- Ikeuchi K, Inada T (2016) Ribosome-associated Asc1/RACK1 is required for endonucleolytic cleavage induced by stalled ribosome at the 3' end of nonstop mRNA. *Sci Rep* 6: 28234
- Jackson RJ, Hellen CUT, Pestova TV (2010) The mechanism of eukaryotic translation initiation and principles of its regulation. *Nat Rev Mol Cell Biol* 11: 113-27
- Jackson RJ, Hellen CUT, Pestova TV (2012) Termination and post-termination events in eukaryotic translation. *Adv Protein Chem Struct Biol* 86: 45-93

- Jan CH & Williams CC, Weissman JS (2014) Principles of ER cotranslational translocation revealed by proximity-specific ribosome profiling. *Science* 346: 1257521
- Janke C, Magiera MM, Rathfelder N, Taxis C, Reber S, Maekawa H, Moreno-Borchart A, Doenges G, Schwob E, Schiebel E, Knop M (2004) A versatile toolbox for PCR-based tagging of yeast genes: new fluorescent proteins, more markers and promoter substitution cassettes. *Yeast* 21: 947-62
- Juszkiewicz S & Chandrasekaran V, Lin Z, Kraatz S, Ramakrishnan V & Hegde RS (2018) ZNF598 is a quality control sensor of collided ribosomes. *Molecular Cell* 72: 1-13
- Kapanidis AN & Lee NK, Laurence TA, Doose S, Margeat E, Weiss S (2004) Fluorescence-aided molecule sorting: analysis of structure and interactions by alternating-laser excitation of single molecules. *Proc Natl Acad Sci U S A* 101: 8936-41
- Karcher A, Schele A, Hopfner KP (2008) X-ray structure of the complete ABC enzyme ABCE1 from *Pyrococcus abyssi*. *J Biol Chem* 283: 7962-71
- Kimanius D & Forsberg BO, Scheres SH & Lindahl E (2016) Accelerated cryo-EM structure determination with parallelisation using GPUs in RELION-2. *eLife* 5:e18722
- Kiosze-Becker K, Gouridis G, de Boer M, Hetzert B, Cordes T, Tampé R (2018) An asymmetric dynamic conformational equilibrium controls the ribosome recycling factor ABCE1. *submitted*
- Kiosze-Becker K, Ori A, Gerovac M, Heuer A, Nürenberg-Goloub E, Rashid UJ, Becker T, Beckmann R, Beck M, Tampé R (2016) Structure of the ribosome post-recycling complex probed by chemical cross-linking and mass spectrometry. *Nat Commun* 7: 13248
- Kispal G, Sipos K, Lange H, Fekete Z, Bedekovics T, Janáky T, Bassler J, Aguilar Netz DJ, Balk J, Rotte C, Lill R (2005) Biogenesis of cytosolic ribosomes requires the essential iron-sulphur protein Rli1p and mitochondria. *EMBO J* 24: 589-98
- Kobayashi K, Ishitani R, Nureki O (2013) Recent structural studies on Dom34/aPelota and Hbs1/aEF1 α : important factors for solving general problems of ribosomal stall in translation. *Biophysics* 9: 131-40
- Kobayashi K, Kikuno I, Kuroha K, Saito K, Ito K, Ishitani R, Inada T, Nureki O (2010) Structural basis for mRNA surveillance by archaeal Pelota and GTP-bound EF1 α complex. *Proc Natl Acad Sci U S A* 107: 17575-9
- Korkhov VM, Mireku SA, Veprintsev DB, Locher KP (2014) Structure of AMP-PNP-bound BtuCD and mechanism of ATP-powered vitamin B12 transport by BtuCD-F. *Nat Struct Mol Biol* 21: 1097-9
- Korostelev AA (2011) Structural aspects of translation termination on the ribosome. *RNA* 17: 1409-21
- Korostelev AA & Asahara H & Lancaster L, Laurberg M, Hirschi A, Zhu J, Trakhanov S, Scott WG, Noller HF (2008) Crystal structure of a translation termination complex formed with release factor RF2. *Proc Natl Acad Sci U S A* 105: 19684-9

- Kucukelbir A, Sigworth FJ, Tagare HD (2014) Quantifying the local resolution of cryo-EM density maps. *Nat Methods* 11: 63-5
- Kurata S, Nielsen KH, Mitchell SF, Lorsch JR, Kaji A, Kaji H (2010) Ribosome recycling step in yeast cytoplasmic protein synthesis is catalyzed by eEF3 and ATP. *Proc Natl Acad Sci U S A* 107: 10854-9
- Kurata S, Shen B, Liu JO, Takeuchi N, Kaji A, Kaji H (2013) Possible steps of complete disassembly of post-termination complex by yeast eEF3 deduced from inhibition by translocation inhibitors. *Nucleic Acids Res* 41: 264-76
- Laemmli UK (1970) Cleavage of structural proteins during the assembly of the head of bacteriophage T4. *Nature* 227: 680-5
- Lamla T, Erdmann VA (2004) The Nano-tag, a streptavidin-binding peptide for the purification and detection of recombinant proteins. *Protein Expr Purif* 33: 39-47
- Larkin MA, Blackshields G, Brown NP, Chenna R, McGettigan PA, McWilliam H, Valentin F, Wallace IM, Wilm A, Lopez R, Thompson JD, Gibson TJ, Higgins DG (2007) Clustal W and Clustal X version 2.0. *Bioinformatics* 23: 2947-8
- Laurberg M & Asahara H & Korostelev A, Zhu J, Trakhanov S, Noller HF (2008) Structural basis for translation termination on the 70S ribosome. *Nature* 454: 852-7
- Lawson CL, Patwardhan A, Baker ML, Hryc C, Garcia ES, Hudson BP, Lagerstedt I, Ludtke SJ, Pintilie G, Sala R, Westbrook JD, Berman HM, Kleywegt GJ, Chiu W (2016) EMDDataBank unified data resource for 3DEM. *Nucleic Acids Res* 44: D396-403
- Lee HH, Kim YS, Kim KH, Heo I, Kim SK, Kim O, Kim HK, Yoon JY, Kim HS, Kim DJ, Lee SJ, Yoon HJ, Kim SJ, Lee BG, Song HK, Kim VN, Park CM, Suh SW (2007) Structural and functional insights into Dom34, a key component of no-go mRNA decay. *Mol Cell* 27: 938-50
- Lee NK & Kapanidis AN, Wang Y, Michalet X, Mukhopadhyay J, Ebricht RH, Weiss S (2005) Accurate FRET measurements within single diffusing biomolecules using alternating-laser excitation. *Biophys J* 88: 2939-53
- Leidig C, Thoms M, Holdermann I, Bradatsch B, Berninghausen O, Bange G, Sinning I, Hurt E, Beckmann R (2014) 60S ribosome biogenesis requires rotation of the 5S ribonucleoprotein particle. *Nat Commun* 5: 3491
- Lerner E & Cordes T, Ingargiola A, Alhadid Y, Chung S, Michalet X, Weiss S (2018) Toward dynamic structural biology: two decades of single-molecule Förster resonance energy transfer. *Science* 359: eaan1133
- Li MZ, Elledge SJ (2007) Harnessing homologous recombination *in vitro* to generate recombinant DNA via SLIC. *Nat Methods* 4: 251-6
- Liakath-Ali K, Mills EW, Sequeira I, Lichtenberger BM, Pisco AO, Sipilä KH, Mishra A, Yoshikawa H, Wu CC-C, Ly T, Lamond AI, Adham IM, Green R, Watt FM (2018) An evolutionarily conserved ribosome-rescue pathway maintains epidermal homeostasis. *Nature* 556: 376-80

- Lill R (2009) Function and biogenesis of iron-sulphur proteins. *Nature* 460: 831-8
- Lingappa JR, Dooher JE, Newman MA, Kiser PK, Klein KC (2006) Basic residues in the nucleocapsid domain of Gag are required for interaction of HIV-1 Gag with ABCE1 (HP68), a cellular protein important for HIV-1 capsid assembly. *J Biol Chem* 281: 3773-84
- Llácer JL & Hussain T, Marler L, Aitken CE, Thakur A, Lorsch JR & Hinnebusch AG, Ramakrishnan V (2015) Conformational differences between open and closed states of the eukaryotic translation initiation complex. *Mol Cell* 59: 399-412
- Locher KP (2016) Mechanistic diversity in ATP-binding cassette (ABC) transporters. *Nat Struct Mol Biol* 23: 487-93
- Lodish HF (1974) Model for the regulation of mRNA translation applied to haemoglobin synthesis. *Nature* 251: 385-8
- Lomakin IB, Stolboushkina EA & Vaidya AT, Zhao C, Garber MB, Dmitriev SE, Steitz TA (2017) Crystal structure of the human ribosome in complex with DENR-MCT-1. *Cell Rep* 20: 521-28
- Long X, Parks JW, Stone MD (2016) Integrated magnetic tweezers and single-molecule FRET for investigating the mechanical properties of nucleic acid. *Methods* 105: 16-25
- Lyumkis D & Oliveira dos Passos D, Tahara EB, Webb K, Bennett EJ, Vinterbo S, Potter CS, Carragher B & Joazeiro CA (2014) Structural basis for translational surveillance by the large ribosomal subunit-associated protein quality control complex. *Proc Natl Acad Sci U S A* 111: 15981-6
- Mancera-Martínez E, Brito Querido J, Valasek LS, Simonetti A & Hashem Y (2017) ABCE1: a special factor that orchestrates translation at the crossroad between recycling and initiation. *RNA Biol* 0: 1-7
- Marques WL, Raghavendran V, Stambuk BU, Gombert AK (2016) Sucrose and *Saccharomyces cerevisiae*: a relationship most sweet. *FEMS Yeast Res* 16: fov107
- Märtens B (2007) Die Funktion der ABC-ATPase Rli1p in der Translation. PhD thesis. Ludwig-Maximilians-University Munich
- Matsuda R & Ikeuchi K & Nomura S, Inada T (2014) Protein quality control systems associated with no-go and nonstop mRNA surveillance in yeast. *Genes Cells* 19: 1-12
- McKinney SA, Joo C, Ha T (2006) Analysis of single-molecule FRET trajectories using hidden Markov modeling. *Biophys J* 91: 1941-51
- Merrick WC, Hensold JO (2001) Analysis of eukaryotic translation in purified and semipurified systems. *Curr Protoc Cell Biol* 8: 11.9.1-.26
- Mills EW, Green R (2017) Ribosomopathies: there's strength in numbers. *Science* 358: eaan2755
- Mills EW, Wangen J, Green R & Ingolia NT (2016) Dynamic regulation of a ribosome rescue pathway in erythroid cells and platelets. *Cell Rep* 17: 1-10

Mohammad MP, Munzarova Pondělíčková V, Zeman J, Gunišová S, Valášek LS (2017) *In vivo* evidence that eIF3 stays bound to ribosomes elongating and terminating on short upstream ORFs to promote reinitiation. *Nucleic Acids Res* 45: 2658-74

Moos M, Jr., Nguyen NY, Liu TY (1988) Reproducible high yield sequencing of proteins electrophoretically separated and transferred to an inert support. *J Biol Chem* 263: 6005-8

Morbach S, Tebbe S, Schneider E (1993) The ATP-binding cassette (ABC) transporter for maltose/maltodextrins of *Salmonella typhimurium*. Characterization of the ATPase activity associated with the purified MalK subunit. *J Biol Chem* 268: 18617-21

Murina V, Kasari M, Haurlyuk V & Atkinson GC (2018) Antibiotic resistance ABCF proteins reset the peptidyl transferase centre of the ribosome to counter translational arrest. *Nucleic Acids Res* 46: 3753-63

Murina V & Kasari M, Reith M, Haurlyuk V, Atkinson G (2017) ABCF ATPases involved in protein synthesis, ribosome assembly and antibiotic resistance: structural and functional diversification across the tree of life. *bioRxiv* doi:10.1101/220046

Murshudov GN, Vagin AA, Dodson EJ (1997) Refinement of macromolecular structures by the maximum-likelihood method. *Acta Crystallogr D Biol Crystallogr* 53: 240-55

Navarro-Quiles C, Mateo-Bonmatí E, Micol JL (2018) ABCE proteins: from molecules to development. *Front Plant Sci* 9: 1125

Nierhaus KH (2014) Mg²⁺, K⁺, and the ribosome. *J Bacteriol* 196: 3817-19

Nissen P & Hansen J & Ban N, Moore PB, Steitz TA (2000) The structural basis of ribosome activity in peptide bond synthesis. *Science* 289: 920-30

Nürenberg-Goloub E, Heinemann H, Gerovac M, Tampé R (2018) Ribosome recycling is coordinated by processive events in two asymmetric ATP sites of ABCE1. *Life Sci Alliance* 1: 3 e201800095

Nürenberg E, Tampé R (2013) Tying up loose ends: ribosome recycling in eukaryotes and archaea. *Trends Biochem Sci* 38: 64-74

Oldham ML, Chen J (2011) Snapshots of the maltose transporter during ATP hydrolysis. *Proc Natl Acad Sci U S A* 108: 15152-6

Passos DO, Doma MK, Shoemaker CJ, Muhlrud D, Green R, Weissman J, Hollien J, Parker R (2009) Analysis of Dom34 and its function in no-go decay. *Mol Biol Cell* 20: 3025-32

Penczek PA, Frank J, Spahn CM (2006) A method of focused classification, based on the bootstrap 3D variance analysis, and its application to EF-G-dependent translocation. *J Struct Biol* 154: 184-94

Perbandt M, Bruns O, Vallazza M, Lamla T, Betzel C, Erdmann VA (2007) High resolution structure of streptavidin in complex with a novel high affinity peptide tag mimicking the biotin binding motif. *Proteins* 67: 1147-53

Pettersen EF, Goddard TD, Huang CC, Couch GS, Greenblatt DM, Meng EC, Ferrin TE (2004) UCSF Chimera—a visualization system for exploratory research and analysis. *J Comput Chem* 25: 1605-12

- Pisarev AV, Hellen CUT, Pestova TV (2007) Recycling of eukaryotic posttermination ribosomal complexes. *Cell* 131: 286-99
- Pisarev AV, Skabkin MA, Pisareva VP, Skabkina OV, Rakotondrafara AM, Hentze MW, Hellen CUT, Pestova TV (2010) The role of ABCE1 in eukaryotic posttermination ribosomal recycling. *Mol Cell* 37: 196-210
- Pisareva VP & Skabkin MA, Hellen CUT, Pestova TV & Pisarev AV (2011) Dissociation by Pelota, Hbs1 and ABCE1 of mammalian vacant 80S ribosomes and stalled elongation complexes. *EMBO J* 30: 1804-17
- Polikanov YS, Steitz TA, Innis CA (2014). A proton wire to couple aminoacyl-tRNA accommodation and peptide-bond formation on the ribosome. *Nat Struct Mol Biol* 21: 787-93
- Preis A, Heuer A, Barrio-Garcia C, Hauser A, Eyler DE, Berninghausen O, Green R, Becker T & Beckmann R (2014) Cryoelectron microscopic structures of eukaryotic translation termination complexes containing eRF1-eRF3 or eRF1-ABCE1. *Cell Rep* 8: 59-65
- Preus S, Noer SL, Hildebrandt LL, Gudnason D, Birkedal V (2015) iSMS: single-molecule FRET microscopy software. *Nat Methods* 12: 593-4
- Rees DC, Johnson E, Lewinson O (2009) ABC transporters: the power to change. *Nat Rev Mol Cell Biol* 10: 218-27
- Reichhart T (2015) Expression and Purification of ABCE1 from *Thermomyces lanuginosus*. Bachelor thesis, Johann Wolfgang Goethe-University Frankfurt am Main
- Ren YI, Li Y, Tian D (2012) Role of the *ABCE1* gene in human lung adenocarcinoma. *Oncolog Rep* 27: 965-70
- Roy R, Hohng S, Ha T (2008) A practical guide to single-molecule FRET. *Nat Methods* 5: 507-16
- Saito S & Hosoda N, Hoshino S (2013) The Hbs1-Dom34 protein complex functions in non-stop mRNA decay in mammalian cells. *J Biol Chem* 288: 17832-43
- Sleich S, Acevedo JM, Clemm von Hohenberg K, Teleman AA (2017) Identification of transcripts with short stuORFs as targets for DENR·MCTS1-dependent translation in human cells. *Sci Rep* 7: 3722
- Schmitt L, Tampé R (2002) Structure and mechanism of ABC transporters. *Curr Opin Struct Biol* 12: 754-60
- Schrödinger, LLC (2015) The PyMOL Molecular Graphics System
- Schuller AP, Green R (2017) The ABC(E1)s of ribosome recycling and reinitiation. *Mol Cell* 66: 578-80
- Shao S, Brown A, Santhanam B, Hegde RS (2015) Structure and assembly pathway of the ribosome quality control complex. *Mol Cell* 57: 433-44
- Shao S & Murray J & Brown A, Taunton J, Ramakrishnan V & Hegde RS (2016) Decoding mammalian ribosome-mRNA states by translational GTPase complexes. *Cell* 167: 1229-40

Sharkey LK, Edwards TA, O'Neill AJ (2016) ABC-F proteins mediate antibiotic resistance through ribosomal protection. *MBio* 7: e01975

Shaw JJ, Green R (2007) Two distinct components of release factor function uncovered by nucleophile partitioning analysis. *Mol Cell* 28: 458-67

Shen PS, Park J, Qin Y, Li X, Parsawar K, Larson MH, Cox J, Cheng Y, Lambowitz AM, Weissman JS & Brandman O & Frost A (2015) Rqc2p and 60S ribosomal subunits mediate mRNA-independent elongation of nascent chains. *Science* 347: 75-8

Shin BS, Kim JR, Walker SE, Dong J, Lorsch JR, Dever TE (2011) Initiation factor eIF2 γ promotes eIF2-GTP-Met-tRNA^{iMet} ternary complex binding to the 40S ribosome. *Nat Struct Mol Biol* 18: 1227-34

Shoemaker CJ, Eyler DE, Green R (2010) Dom34:Hbs1 promotes subunit dissociation and peptidyl-tRNA drop-off to initiate no-go decay. *Science* 330: 369-72

Shoemaker CJ, Green R (2011) Kinetic analysis reveals the ordered coupling of translation termination and ribosome recycling in yeast. *Proc Natl Acad Sci U S A* 108: E1392-8

Shoemaker CJ, Green R (2012) Translation drives mRNA quality control. *Nat Struct Mol Biol* 19: 594-601

Simonetti A, Brito Querido J, Myasnikov AG, Mancera-Martinez E, Renaud A, Kuhn L, Hashem Y (2016) eIF3 peripheral subunits rearrangement after mRNA binding and start-codon recognition. *Mol Cell* 63: 206-17

Sitron CS, Park JH, Brandman O (2017) Asc1, Hel2, and Slh1 couple translation arrest to nascent chain degradation. *RNA* 23, 798-810

Skabkin MA & Skabkina OV, Dhote V, Komar AA, Hellen CUT & Pestova TV (2010) Activities of Ligatin and MCT-1/DENR in eukaryotic translation initiation and ribosomal recycling. *Genes Dev* 24: 1787-801

Skabkin MA, Skabkina OV, Hellen CUT, Pestova TV (2013) Reinitiation and other unconventional posttermination events during eukaryotic translation. *Mol Cell* 51: 249-64

Smith PC, Karpowich N, Millen L, Moody JE, Rosen J, Thomas PJ, Hunt JF (2002) ATP binding to the motor domain from an ABC transporter drives formation of a nucleotide sandwich dimer. *Mol Cell* 10: 139-49

Song H, Mugnier P, Das AK, Webb HM, Evans DR, Tuite MF, Hemmings BA, Barford D (2000) The crystal structure of human eukaryotic release factor eRF1—mechanism of stop codon recognition and peptidyl-tRNA hydrolysis. *Cell* 100: 311-21

Soudet J, Gelugne JP, Belhabich-Baumas K, Caizergues-Ferrer M, Mougou A (2010) Immature small ribosomal subunits can engage in translation initiation in *Saccharomyces cerevisiae*. *EMBO J* 29: 80-92

Spahn CM, Gomez-Lorenzo MG, Grassucci RA, Jørgensen R, Andersen GR, Beckmann R, Penczek PA, Ballesta JP, Frank J (2004) Domain movements of elongation factor eEF2 and the eukaryotic 80S ribosome facilitate tRNA translocation. *EMBO J* 23: 1008-19

- Stansfield I, Jones KM, Kushnirov VV, Dagkesamanskaya AR, Poznyakovski AI, Paushkin SV, Nierras CR, Cox BS, Ter-Avanesyan MD, Tuite MF (1995) The products of the *SUP45* (eRF1) and *SUP35* genes interact to mediate translation termination in *Saccharomyces cerevisiae*. *EMBO J* 14: 4365-73
- Starck SR, Jiang V, Pavon-Eternod M, Prasad S, McCarthy B, Pan T, Shastri N (2012) Leucine-tRNA initiates at CUG start codons for protein synthesis and presentation by MHC class I. *Science* 336: 1719-23
- Strunk BS, Novak MN, Young CL, Karbstein K (2012) A translation-like cycle is a quality control checkpoint for maturing 40S ribosome subunits. *Cell* 150: 111-21
- Studer SM, Joseph S (2007) Binding of mRNA to the bacterial translation initiation complex. *Methods Enzymol* 430: 31-44
- Su W & Kumar V & Ding Y, Ero R, Serra A, Lee BST, Wong ASW, Shi J, Sze SK, Yang L & Gao YG (2018) Ribosome protection by antibiotic resistance ATP-binding cassette protein. *Proc Natl Acad Sci U S A* 115: 5157-62
- Sundaramoorthy E, Leonard M, Mak R, Liao J, Fulzele A, Bennett EJ (2017) ZNF598 and RACK1 regulate mammalian ribosome-associated quality control function by mediating regulatory 40S ribosomal ubiquitylation. *Mol Cell* 65, 751-60
- Summer H, Grämer R, Dröge P (2009) Denaturing urea polyacrylamide gel electrophoresis (urea PAGE). *J Vis Exp* 32: 1485
- Svidritskiy E, Korostelev AA (2018) Conformational control of translation termination on the 70S ribosome. *Structure* 26: 821-8
- Sweeney WV, Rabinowitz JC (1980) Proteins containing 4Fe-4S clusters: an overview. *Annu Rev Biochem* 49: 139-61
- Taira K, Oda M, Shinshi H, Maeda H, Furukawa K (1990) Construction of a novel artificial-ribozyme-releasing plasmid. *Protein Eng* 3: 733-7
- Tastan AÖ (2003) How Lazy are the tRNAs on the Ribosome? - New Insights for the α - ϵ Model. PhD thesis, Free University of Berlin
- Taylor D, Unbehauen A, Li W, Das S, Lei J, Liao HY, Grassucci RA, Pestova TV, Frank J (2012) Cryo-EM structure of the mammalian eukaryotic release factor eRF1-eRF3-associated termination complex. *Proc Natl Acad Sci U S A* 109: 18413-8
- Taylor DJ, Nilsson J, Merrill AR, Andersen GR, Nissen P, Frank J (2007) Structures of modified eEF2-80S ribosome complexes reveal the role of GTP hydrolysis in translocation. *EMBO J* 26: 2421-31
- The UniProt Consortium (2017) UniProt: the universal protein knowledgebase. *Nucleic Acids Res* 45: D158-69
- Thomas C & Tampé R (2018) Multifaceted structures and mechanisms of ABC transport systems in health and disease. *Curr Opin Struct Biol* 51: 116-28
- Tian Y, Tian X, Han X, Chen Y, Song CY, Jiang WJ, Tian DL (2016) ABCE1 plays an essential role in lung cancer progression and metastasis. *Tumour Biol* 37: 8375-82

- Triana-Alonso FJ, Chakraburttty K, Nierhaus KH (1995) The elongation factor 3 unique in higher fungi and essential for protein biosynthesis is an E Site factor. *J Biol Chem* 270: 20473-8
- Trowitzsch S, Bieniossek C, Nie Y, Garzoni F, Berger I (2010) New baculovirus expression tools for recombinant protein complex production. *J Struct Biol* 172: 45-54
- Tsuboi T, Kuroha K, Kudo K, Makino S, Inoue E, Kashima I, Inada T (2012) Dom34:Hbs1 plays a general role in quality-control systems by dissociation of a stalled ribosome at the 3' end of aberrant mRNA. *Mol Cell* 46: 518-29
- Tyzack JK, Wang X, Belsham GJ, Proud CG (2000) ABC50 interacts with eukaryotic initiation factor 2 and associates with the ribosome in an ATP-dependent manner. *J Biol Chem* 275: 34131-9
- van den Elzen AM, Schuller A, Green R, Séraphin B (2014) Dom34-Hbs1 mediated dissociation of inactive 80S ribosomes promotes restart of translation after stress. *EMBO J* 33: 265-76
- van Hoof A, Frischmeyer PA, Dietz HC, Parker R (2002) Exosome-mediated recognition and degradation of mRNAs lacking a termination codon. *Science* 295: 2262-4
- Vazquez de Aldana CR, Marton MJ, Hinnebusch AG (1995) GCN20, a novel ATP binding cassette protein, and GCN1 reside in a complex that mediates activation of the eIF-2 α kinase GCN2 in amino acid-starved cells. *EMBO J* 14: 3184-99
- Verma R, Reichermeier KM, Burroughs AM, Oania RS, Reitsma JM, Aravind L & Deshaies RJ (2018) Vms1 and ANKZF1 peptidyl-tRNA hydrolases release nascent chains from stalled ribosomes. *Nature* 557: 446-51
- Villa E & Sengupta J, Trabuco LG, LeBarron J, Baxter WT, Shaikh TR, Grassucci RA, Nissen P, Ehrenberg M, Schulten K, Frank J (2009) Ribosome-induced changes in elongation factor Tu conformation control GTP hydrolysis. *Proc Natl Acad Sci U S A* 106: 1063-8
- Voorhees RM, Schmeing TM, Kelley AC, Ramakrishnan V (2010) The mechanism for activation of GTP hydrolysis on the ribosome. *Science* 330: 835-8
- Walker SE, Fredrick K (2008) Preparation and evaluation of acylated tRNAs. *Methods* 44: 81-6
- Weisser M, Schäfer T, Leibundgut M, Böhringer D, Aylett CHS, Ban N (2017) Structural and functional insights into human re-initiation complexes. *Mol Cell* 67: 447-56
- Weixlbaumer A & Jin H, Neubauer C, Voorhees RM, Petry S, Kelley AC, Ramakrishnan V (2008) Insights into translational termination from the structure of RF2 bound to the ribosome. *Science* 322: 953-6
- Wethmar K, Smink JJ, Leutz A (2010) Upstream open reading frames: molecular switches in (patho)physiology. *Bioessays* 32: 885-93
- Wu Z & Wang Y, Lim J, Liu B, Li Y, Vartak R, Stankiewicz T, Montgomery S, Lu B (2018) Ubiquitination of ABCE1 by NOT4 in response to mitochondrial damage links co-translational quality control to PINK1-directed mitophagy. *Cell Metabol* 28: 130-44

- Xue S, Barna M (2012) Specialized ribosomes: a new frontier in gene regulation and organismal biology. *Nat Rev Mol Cell Biol* 13: 355-69
- Yang H, Hamada K, Terashima H, Izuta M, Yamaguchi-Sihta E, Kondoh O, Satoh H, Miyazaki M, Arisawa M, Miyamoto C, Kitada K (1996) A point mutation within each of two ATP-binding motifs inactivates the functions of elongation factor 3. *Biochim Biophys Acta* 1310: 303-8
- Yarunin A, Panse VG, Petfalski E, Dez C, Tollervey D, Hurt EC (2005) Functional link between ribosome formation and biogenesis of iron-sulfur proteins. *EMBO J* 24: 580-8
- Ye J & Osborne AR, Groll M, Rapoport TA (2004) RecA-like motor ATPases—lessons from structures. *Biochim Biophys Acta* 1659: 1-18
- Young DJ & Guydosh NR, Zhang F, Hinnebusch AG & Green R (2015) Rli1/ABCE1 recycles terminating ribosomes and controls translation reinitiation in 3'UTRs *in vivo*. *Cell* 162: 872-84
- Zhai C, Li Y, Mascarenhas C, Lin Q, Li K, Vyrides I, Grant CM, Panaretou B (2014) The function of ORAOV1/LTO1, a gene that is overexpressed frequently in cancer: essential roles in the function and biogenesis of the ribosome. *Oncogene* 33: 484-94
- Zhang K (2016) Gctf: Real-time CTF determination and correction. *J Struct Biol* 193: 1-12
- Zhao Z, Fang LL, Johnsen R, Baillie DL (2004) ATP-binding cassette protein E is involved in gene transcription and translation in *Caenorhabditis elegans*. *Biochem Biophys Res Commun* 323: 104-11
- Zheng SQ, Palovcak E, Armache J-P, Verba KA, Cheng Y & Agard DA (2017) MotionCor2: anisotropic correction of beam-induced motion for improved singleparticle electron cryo-microscopy. *Nat Methods* 14: 331-2
- Zhou A, Hassel BA, Silverman RH (1993) Expression cloning of 2-5A-dependent RNAase: a uniquely regulated mediator of interferon action. *Cell* 72: 753-65
- Zhou A, Molinaro RJ, Malathi K, Silverman RH (2005) Mapping of the human *RNASEL* promoter and expression in cancer and normal cells. *J Interferon Cytokine Res* 25: 595-603
- Zhouravleva G, Frolova L, Le Goff X, Le Guellec R, Inge-Vechtomov S, Kisselev L, Philippe M (1995) Termination of translation in eukaryotes is governed by two interacting polypeptide chain release factors, eRF1 and eRF3. *EMBO J* 14: 4065-72
- Zimmerman C, Klein KC, Kiser PK, Singh AR, Firestein BL, Riba SC, Lingappa JR (2002) Identification of a host protein essential for assembly of immature HIV-1 capsids. *Nature* 415: 88-92
- Zinoviev A, Hellen CUT, Pestova TV (2015) Multiple mechanisms of reinitiation on bicistronic calicivirus mRNAs. *Mol Cell* 57: 1059-73

G Erklärung und Versicherung –

Declaration and author's declaration

Ich erkläre hiermit, dass ich mich bisher keiner Doktorprüfung im Mathematisch-Naturwissenschaftlichen Bereich unterzogen habe.

I herewith declare that I have not previously participated in any doctoral examination procedure in a mathematics or natural science discipline.

Frankfurt am Main,

Datum - *date*

Unterschrift - *signature*

Ich erkläre hiermit, dass ich die vorgelegte Dissertation über **“Molecular Mechanism of ABCE1 in Ribosome Recycling”** selbständig angefertigt und mich anderer Hilfsmittel als der in ihr angegebenen nicht bedient habe, insbesondere, dass alle Entlehnungen aus anderen Schriften mit Angabe der betreffenden Schrift gekennzeichnet sind.

Ich versichere, die Grundsätze der guten wissenschaftlichen Praxis beachtet, und nicht die Hilfe einer kommerziellen Promotionsvermittlung in Anspruch genommen zu haben.

*I herewith declare that I have produced my doctoral dissertation on the topic of **“Molecular Mechanism of ABCE1 in Ribosome Recycling”** independently and using only the tools indicated therein. In particular, all references borrowed from external sources are clearly acknowledged and identified.*

I confirm that I have respected the principles of good scientific practice and have not made use of the services of any commercial agency in respect of my doctorate.

Frankfurt am Main,

Datum - *date*

Unterschrift - *signature*

H Curriculum vitae

Milan Gerovac

date of birth 22.10.1988
place of birth Osijek, Croatia
citizenship German and Croatian

education

2013-2018 PhD Thesis in the lab of Prof. Dr. Robert Tampé
Goethe University, Institute of Biochemistry,
Frankfurt am Main, Germany
2007-2012 Diploma in Biochemistry
Goethe University, Frankfurt am Main, Germany
2007 Abitur (university entrance qualification)
Goetheschule, Neu-Isenburg, Germany

fellowships

2013-2016 Boehringer Ingelheim Fonds, PhD fellowship
2010-2015 Merck KGaA Student Excellence Program (STEP)
2013 Center for Membrane Proteomics,
Goethe University, PhD fellowship
2008-2015 Studienstiftung des deutschen Volkes
student & PhD fellowship

conferences, internships, workshops, and talks during the PhD thesis

- 2017 CRC 902 IRTG Symposium, Friedrichsdorf (D), talk
- 2017 EMBO Protein Synthesis and Translational Control, conference, Heidelberg (D), talk
- 2017 Summer School of the Tampé lab, Hirscheegg (A), talk
- 2017 MPI 1st Sphire Workshop, Dortmund (D), participant
- 2016 EMBO Ribosome Structure and Function, conference, Strasbourg (F), poster
- 2016 Summer School of the Tampé lab, Hirscheegg (A), talk
- 2015 EMBO Protein Synthesis and Translational Control, conference, Heidelberg (D), poster
- 2015 Summer Seminar of the Boehringer Ingelheim Fonds, Hirscheegg (A), talk
- 2015 CRC 902 Winter School, Obergurgl (A), talk
- 2015 CRC 902 Evaluation, Frankfurt/Main (D), poster
- 2014 110th International Titisee Conference of the Boehringer Ingelheim Fonds, Titisee (D), participant
- 2014 Summer Seminar of the Boehringer Ingelheim Fonds, Hirscheegg (A), talk
- 2014 Summer School of the Tampé lab, Hirscheegg (A), talk
- 2013 ZING Ribosome Conference, Napa (CA, USA), poster
- 2013 Internship in the lab of Prof. Dr. Rachel Green, Howard Hughes Medical Institute, Johns Hopkins University School of Medicine, Baltimore (USA)

